COMPUTER AIDED DESIGN AND INITIAL TESTING OF A NOVEL STEM CELL BASED THERAPY FOR ABDOMINAL AORTIC ANEURYSMS

by

Kory J. Blose

Bachelor of Science, Pennsylvania State University, 2007

Submitted to the Graduate Faculty of

The Swanson School of Engineering in partial fulfillment

of the requirements for the degree of

Doctor of Philosophy

University of Pittsburgh

2017

UNIVERSITY OF PITTSBURGH

SWANSON SCHOOL OF ENGINEERING

This dissertation was presented

by

Kory J. Blose

It was defended on

March 14th, 2017

and approved by

Sanjeev G. Shroff, Ph.D., Professor, Departments of Bioengineering and Medicine

Anne Robertson, Ph.D., Professor, Departments of Mechanical and Bioengineering

John A. Curci, MD, Professor, Departments Surgery, Vanderbilt University

Justin S. Weinbaum, Ph.D., Research Assistant Professor, Department of Bioengineering

Dissertation Director: David A. Vorp, Ph.D., Professor, Departments of Bioengineering, Cardiothoracic Surgery, and Surgery

COMPUTER AIDED DESIGN AND INITIAL TESTING OF A NOVEL STEM CELL BASED THERAPY FOR ABDOMINAL AORTIC ANEURYSMS

Kory J. Blose, Ph.D.

University of Pittsburgh, 2017

Exsanguination from abdominal aortic aneurysm (AAA) rupture is frequently fatal and is currently the 13th leading cause of death in the United States of America. AAAs can take years to progress to the point where surgical intervention is recommended (> 5.5 cm diameter). Surgical intervention does not benefit small AAAs, and management of these patients is limited to "watchful waiting" (i.e., serial imaging of the AAA progression until the threshold for surgical treatment is met).

The goal of this dissertation is to develop a novel stem cell therapy for small AAAs. Approximately 90% of patients with AAA do not meet the size criterion for intervention and could benefit from this alternative therapy.

In short, our proposed strategy is delivery of adipose-derived mesenchymal stem cells to the external surface of the AAA. In this way autologous cells can be isolated from a patient, culture-expanded if necessary, mixed in a hydrogel, and injected around that same patient's aorta in a minimally invasive procedure. The work of this dissertation represents four foundational steps towards design and initial evaluation of the proposed therapy: evaluation of the potential of SMCs to produce elastin in vitro, assessment of the effects of elastin production in silico, demonstration of efficacy in a small animal model, and fabrication of a new self-mixing injector device for human use.

TABLE OF CONTENTS

1.0 INTRODUCTION 1

1.1 ABDOMINAL AORTIC ANEURYSM ANATOMY (AAA) AND ETIOLOGY 2

1.1.1 Aneurysm Types and Etiology 2

1.1.2 Smooth Muscle Cells in Normal vs. Aneurysmal Aortas 3

1.1.3 Elastin in Normal vs. Aneurysmal Aortas 6

1.1.4 Collagen in Normal vs. Aneurysmal Aortas 7

1.1.5 Mechanical Environment in Normal vs. Aneurysmal Aortas 9

1.1.6 Other Differences in Normal vs. Aneurysmal Aortas 11

1.2 CURRENT CLINICAL TREATMENT OF AAA 12

1.2.1 Surgical Options: Open Repair and EVAR 13

1.2.2 Systemic Anti-inflammatory Drugs 14

1.3 PRECLINICAL AAA MODELS 15

1.3.1 Animal Models 15

1.3.2 Computational Models of Growth and Remodeling 16

1.4 PRECLINICAL AAA TREATMENT APPROACHES 17

1.4.1 Localized Treatments 18

1.4.2 MircoRNAs 18

1.4.3 Mesenchymal Stem Cell (MSC) Treatment 19

1.5 AAA STUDIES IN THE VASCULAR BIOENGINEERING LABORATORY 20

1.6 HYPOTHESES AND SPECIFIC AIMS 21

2.0 DESIGN AND VALIDATION OF A VACUUM ASSISTED ANCHORAGE FOR THE UNIAXIAL TENSILE TESTING OF SOFT MATERIALS 24

2.1 INTRODUCTION 24

2.2 METHODS 26

2.2.1 Design and Functional Principles of the VAA 26

2.2.2 Fibrin Gels as Testing Materials 28

2.2.3 Mechanical Testing 28

2.2.4 Material Assumption and Mechanical Properties 29

2.2.5 Statistics 33

2.3 RESULTS 33

2.3.1 Device Performance 33

2.3.2 Device Validation and Verification 35

2.4 DISCUSSION 37

2.5 CONCLUSION 40

3.0 SPECIFIC AIM 1, PART 1: ELASTIN PRODUCTION OF SMOOTH MUSCLE CELLS WHEN CO CULUTRED WITH MSCS 41

3.1 INTRODUCTION 41

3.2 METHODS 43

3.2.1 Cell Culture 43

3.2.2 Fibrin Gel Fabrication 44

3.2.3 Treatment Description 45

3.2.4 Qualitative Elastin Fiber Imaging 47

3.2.5 Quantitative Elastin Protein Detection 47

3.2.6 Tensile Testing 48
3.2.7 Statistics 48
3.3 RESULTS 49
3.3.1 Early Time Point Studies from Flexcell Culture Plates 49
3.3.2 Late Time Point Studies in Tissue Culture Plates 55
3.4 DISCUSSION 62
3.5 CONCLUSION 67
3.6 FUTURE WORK 67
4.0 SPECIFIC AIM 1, PART 2: IN-SILICO EFFECTS OF ELASTIN PRODUCTION IN THE CONTEXT OF AAA 69
4.1 INTRODUCTION 69
4.2 METHODS 73
4.2.1 FEA Stress Analysis 73
4.2.2 Elastin Production in Tissue Growth and Remodeling Models 75
4.2.3 Intervention Time Points 76
4.2.4 Monitoring Model Properties 78
4.3 RESULTS 78
4.3.1 Changes in Diameter with Elastin Production 78
4.3.2 Changes in Collagen Content with Elastin Production 84
4.3.3 Changes in Stress with Elastin Production 88
4.4 DISCUSSION 90
4.5 CONCLUSION 93
4.6 FUTURE WORK 93
5.0 SPECIFIC AIM 2: PERIADVENTITIAL ADMSC THERAPY TO SLOW AND/OR REVERSE THE PROGRESSION OF AN ELASTASE PERFUSED AAA 95

5.1 INTRODUCTION 95
5.2 METHODS 97
5.2.1 Culture of MSCs 97
5.2.2 Elastase Perfusion 98
5.2.3 ADMSC Delivery 100
5.2.4 Aorta Diameter Measurement 103
5.2.5 Histological Characterization of Aorta 103
5.2.6 Mechanical Testing and Characterization of Aorta 104
5.2.7 Statistics 104
5.3 RESULTS 105
5.3.1 Progression of AAA with Saline Delivered ADMSC Treatment 105
5.3.2 Histological Changes with Saline Delivered ADMSC Treatment 107
5.3.3 Diameter Measurements with Fibrin Delivered ADMSC Treatment 111
5.3.4 Aorta Mechanical Properties with Fibrin Delivered ADMSC Treatment 114
5.4 DISCUSSION 117
5.5 CONCLUSION 120
5.6 FUTURE WORK 120
6.0 SPECIFIC AIM 3: DEVELOP CLINICAL MSC DELIVERY SYSTEM 121
6.1 DESIGN DESCRIPTION, MOTIVATION, AND CRITERIA 121
6.1.1 Clinical MSC Delivery System Description 121
6.1.2 Minimally Invasive Delivery of MSCs 123
6.1.3 Directed Homing of MSCs 124
6.1.4 Magnetic Probe Placement Considerations 124
6.1.5 Cell Delivery Vehicle Material Considerations 127
6.1.6 FDA Regulatory Considerations 129

6.2 METHODS 130
6.2.1 Cell Culture 130
6.2.2 Iron Nanoparticle Loading Efficiency 130
6.2.3 Fibrin Gel Fabrication 131
6.2.4 Cell Viability 131
6.2.5 Magnetic Migration 132
6.2.6 Fibrin Gel Mixer Performance 134
6.2.7 Magnetic Probe Ultrasound Identification 135
6.2.8 Histology and Imaging 137
6.2.9 Statistics 137
6.3 RESULTS 137
6.3.1 Optimal Iron Nanoparticle and Fibrin Gel Parameters 137
6.3.2 In-vitro Magnetic Force Induced Cell Localization 142
6.3.3 Cell Delivery Mixer Performance 150
6.3.4 Magnetic Probe Ultrasound Identification 153
6.4 DISCUSSION 155
6.5 CONCLUSION 160
6.6 FUTURE WORK 160
7.0 STUDY SUMMARY 162
7.1 SUMMARY OF RESULTS 162
7.1.1 Specific Aim 1 162
7.1.2 Specific Aim 2 163
7.1.3 Specific Aim 3 163
7.2 SUMMARY OF ACOMPLISHMENTS 164
7.3 FUTURE WORK 165

APPENDIX A: FEAP IMPLEMENTATION OF CONSTRAINED MIXTURE MODEL OF AAA G&R..... 166

APPENDIX B: COMPARISON OF MODEL OUTPUTS FOR HOMEOSTATIC, BASELINE, AND 2X ELASTIN PRODUCTION MODELS..... 231

APPENDIX C: QUALITATIVE FIBRIN GEL MIXER ASSESTMENT..... 244

BIBLIOGRAPHY..... 246

LIST OF TABLES

Table 1. Breakdown of useful sample numbers by group. Successful tensile tests illustrate the gripping efficiency of the VAA. By utilizing the VAA during uniaxial tensile loading, we were able to collect meaningful tensile and ultimate data from samples. 35

Table 2. Fibrin gel elastic mechanical properties. Significant differences (*) in the elastic mechanical properties of the fibrin gel groups are revealed during tensile tests using the VAA. Yield stretch, yield stress, and tangent modulus values are reported as mean ± SD from each fibrin gel group. The VAA Fib_5 group had higher yield stress and tangent modulus values. 36

Table 3. Fibrin gel ultimate mechanical properties. Significant differences (*) in the ultimate mechanical properties of the fibrin gel groups are revealed during tensile tests using the VAA. Ultimate stretch and ultimate tensile strength (UTS) are reported as mean ± SD from each fibrin gel group. The VAA Fib_5 group had higher ultimate stretch and UTS values.....36

Table 4. Experimental group descriptions. Experimental groups are described by treatment, culture time, and loading condition. The number of samples for each group is shown for the ninhydrin assay.....46

Table 5. Constrained gels showed a higher yield stretch than all groups expect the stretched group and a higher tangent modulus than all groups. Measurements for yield stretch and tangent modulus are given as mean ± standard deviation. Tukey groupings identifiers “A” and “B” show which groups have significantly different means. The ADMSC group yielded useful data in 6 of 8 (75%) tests. All other groups yielded useful data in 2of 3 (67%) of tests. 51

Table 6. A number of elastin production factors were explored by modifying constrained mixture models of AAA G&R. The values listed are in units of $\mu g/mm^3/2$ weeks. The elastin production factors are multiples of the absolute value of the natural elastin degradation rate calculated at the end of the baseline model run[25]. These values are added to the existing elastin at each time step within the simulation after the elastogenic intervention. 75

Table 7. Increasing elastin production and earlier intervention slows the rate of aneurysmal enlargement. The rate of aneurysmal enlargement (outer diameter) at the end of the baseline model run (~ 10 years simulation time) is 5.340 mm/year. Intervention at 30% growth of the vessel caused the aneurysm to begin to contract at as high as 15.480 mm/year (i.e. residual tension begins to pull the artery back towards its original size) with most elastin production rates. 83

Table 8. Native aortas have a lower tangent modulus than all elastase treated groups. Measurements for tangent modulus are given as mean ± standard deviation. Tukey groupings identifiers “A” and “B” show which groups have different means. 116

Table 9. All groups show a similar average distance between nuclei. When fit with an ellipse, the average distance between centroid of each nucleus was 52.4±4.5 pixels for the control group, 49.1±12.7 pixels for the Left group, 45.2±5.7 pixels for the Center group, and 53.0±3.5 pixels for the Right group. 152

Table 10. Proforma cost of proposed interventional stem cell treatment for AAA. The projected costs of our proposed therapy are broken down by the device and the administration of the treatment. 159

LIST OF FIGURES

Figure 1. AAA "cycle of destruction". AAAs present an active inflammatory environment with multiple positive feedback loops. Figure adapted from Boddy et al.[1] 1

Figure 2. VAA Design Concept. Schematic of the VAA design is shown. A house vacuum source is directed to the testing sample and clamped by pneumatic grips 27

Figure 3. Features of Stress-Strain Behavior Captured by the VAA. The black curve shows σ_{11} vs. λ_α from a sample test using 5 mg/mL fibrinogen. The gray curve is a scaled form of the second derivative of the σ_{11} with respect to λ_α. Points A and B indicate the yield stress and yield stretch, respectively. The ultimate tensile strength (UTS) and ultimate stretch are noted by points C and D, respectively. The linear portion of the black stress-strain curve is estimated by a dotted gray line. The slope of this line is the tangent modulus. 32

Figure 4. Visual Confirmation of a Tensile Break. Three frames (captured at 30 frames per second) from a video of uniaxial tensile test are shown. The left frame shows the gel just before its tensile failure. The middle frame confirms a tensile break in the center of the fibrin gel (arrow) with the two halves of the fibrin gel recoiling back to their respective VAA grips (right frame). 34

Figure 5. There is little elastin autofluorescence in SMC seeded fibrin gels after 10 days in culture. Elastin autofluorescence images reveal low levels of emission signal in Group 2 (A), slightly higher levels of emission signal in Group 3 (B), and bright signal in Group 4 (C). 50

Figure 6. Ninhydrin assay reveals that all groups produced elastin after just 10 days in culture. Values shown as mean ± standard deviation. * indicates significant difference from all other groups. 53

Figure 7. Ninhydrin assay reveals that all groups produced elastin after just 10 days in culture. Values shown as mean ± standard deviation. Statistically different groups are indicated by * and #. 54

Figure 8. Elastin autofluorescence images reveal a developed elastin network in long term culture. Elastic fibers (red arrows) are seen in Group 8 (A) and Group 9 (B). A less developed network is seen in Group 10 (C), and no network is seen (merely glowing cell outlines) in Group 11 (D). 56

Figure 9. VVG stained images reveal a faint staining in all groups around areas of dense fiber accumulation within the gels. The orientation of the sections is shown at top (A). Group 8 is shown in (B.) Group 9 is shown in (C). Group 10 is shown in (D). Group 11 is shown in (E). ...57

Figure 10. IFC stained images reveal a vivid network at various levels of signal intensity between the experimental groups. The orientation of the sections is shown at top (A). Group 8 is shown in (B.) Group 9 is shown in (C). Group 10 is shown in (D). Group 11 is shown in (E). ...58

Figure 11. Ninhydrin assay reveals that all groups produced elastin after 28 days in culture. Values shown as mean ± standard deviation. 60

Figure 12. Ninhydrin assay reveals that all groups produced elastin after 28 days in culture. Values shown as mean ± standard deviation. 61

Figure 13. A constrained mixture model of AAA G&R is able to capture known qualities of AAA. The upper red curve represents the progression of the outer diameter of the model AAA while the lower red curve represents progression of the inner diameter of the model AAA. The vertical black, green, and blue lines reflect the time points that the outer diameter is increased by 30%, 40%, and 50%, respectively. 77

Figure 14. Elastin production at 50% increase in outer diameter moderately slows enlargement. Diameter in mm is shown on the y-axis. Model simulation time is shown on the x-axis. The outer diameters are the top curves, and the inner diameters are bottom curves. 80

Figure 15. Elastin production at 40% increase in outer diameter slows enlargement to an appreciable extent. Diameter in mm is shown on the y-axis. Model simulation time is shown on the x-axis. The outer diameters are the top curves, and the inner diameters are bottom curves. ..81

Figure 16. Elastin production at 30% increase in outer diameter greatly slows enlargement and even contracts the aneurysm at higher elastin production factors. Diameter in mm is shown on the y-axis. Model simulation time is shown on the x-axis. The outer diameters are the top curves, and the inner diameters are bottom curves. 82

Figure 17. 2x elastin production at 30% increase in outer diameter lowers the amount of collagen in the adventitia and media in constrained mixture models of AAA G&R. The ratio of remaining collagen to initial collagen content is shown on the y-axis. Model simulation time is shown on the x-axis. Average collagen content through the adventitia is shown by the top curves, and average collagen content through the media are bottom curves. The baseline model values are shown in red. The 2x elastin production factors model is shown in green.....85

Figure 18. 2x elastin production at 30% increase in outer diameter lowers the amount of collagen in the adventitia in constrained mixture models of AAA G&R. The ratio of remaining collagen to initial collagen content is shown on the y-axis. Model simulation time is shown on the x-axis. The baseline model values are shown in red. The 2x elastin production factors model is shown in green.....86

Figure 19. 2x elastin production at 30% increase in outer diameter lowers the amount of collagen in the media in constrained mixture models of AAA G&R. The ratio of remaining collagen to

initial collagen content is shown on the y-axis. Model simulation time is shown on the x-axis. The baseline model values are shown in red. The 2x elastin production factors model is shown in green. 87

Figure 20. 2x elastin production at 30% increase in outer diameter lowers the amount of collagen in the media in constrained mixture models of AAA G&R. The von Mises stress (kPA) is shown on the y-axis. Model simulation time is shown on the x-axis. The von Mises stresses on the luminal surface are the top curves, the von Mises stresses at the interface between the media and adventitia are the middle curves, and the von Mises stresses on the adventitial surface are the bottom curves. The baseline model values are shown in red. The 2x elastin production factors model is shown in green. 89

Figure 21. Elastase perfusion and localized adipose-derived mesenchymal stem cells treatment. (A) Schematic representing elastase perfusion. (B) Schematic demonstrating our delayed, localized delivery system. (C) Photograph of delayed, localized delivery system in place after elastase perfusion. (A & B) adapted with permission from Bartoli et. al[120]. 99

Figure 22. Experimental and control groups for saline delivery. Day 0 denotes elastase perfusion surgery and AAA induction. On day 5, post-elastase perfusion (D5 post-EP) animals were sacrificed in order to demonstrate successful aneurysm induction (n = 3, early aneurysm group). On D5 post-EP, treatment group animals were given stem cell therapy via port injection and were sacrificed on D14 post-EP (n = 9, seven animals survived to D14 post-EP, local ADMSCs treatment group). On D5 post-EP, untreated control group animals were given 400 µl of saline via port injection and were sacrificed on D14 post-EP (n = 6, untreated aneurysm group). 101

Figure 23. Progression of aneurysm is halted with local adipose-derived mesenchymal stem cells treatment. % increases in aortic diameter measurements (mean ± standard deviation) for early aneurysm group (93.3 ± 5.77 %, n = 3), local ADMSCs treatment group (104.29 ± 12.72 %, n = 7), and untreated aneurysm group (151.67 ± 18.35 %,, n = 6). A two-way analysis of variance revealed unequal means (*, $p < 0.001$) between groups. Tukey tests revealed which groups differed. 106

Figure 24. Qualitative examination of elastin. Images from early aneurysm (left column), untreated aneurysm (middle column) and local ADMSC treatment (right column) groups are shown after Verhoeff–Van Gieson staining (top row), elastin immunofluorescence (middle row), and elastin autofluorescence (bottom row) (n = 2 all groups). 108

Figure 25. Monocyte infiltration of the abdominal aortic aneurysm is not significantly reduced with adipose derived mesenchymal stem cells delivery. Images from early aneurysm, untreated aneurysm and local ADMSC treatment groups are shown after staining with hematoxylin and eosin (n = 2 all groups). 109

Figure 26. Local ADMSC treated aortas show no macrophages at day 14 post elastase perfusion. Images from early aneurysm (top), untreated aneurysm (middle) and local ADMSC treatment (bottom) groups are shown after macrophage immunofluorescence staining (green) (n = 1 all groups). All groups are counterstained with DAPI (blue). 110

Figure 27. Aneurysm growth is unchanged with local adipose-derived mesenchymal stem cells treatment delivered via fibrin (p=0.308). % increases in aortic diameter measurements (mean ± standard deviation) for local saline (no ADMSC) treatment group (82.14 ± 17.98 %, n = 4), local fibrin (no ADMSC) treatment group (62.60 ± 33.92 %, n = 23), and local ADMSC treatment group in fibrin (50.71 ± 22.64 %, n = 10).....112

Figure 28. Aneurysm growth is unchanged with local adipose-derived mesenchymal stem cells treatment delivered via fibrin even when accounting for injection order (p=0.239). % increases in aortic diameter measurements compared to per elastase perfusion measurements (mean ± standard deviation) for local saline (no ADMSC) treatment group (82.14 ± 17.98 %, n = 4), local fibrin (no ADMSC) treatment group (62.60 ± 33.92 %, n = 23), local ADMSC treatment injection 1 group (43.45 ± 29.14 %, n = 6), and local ADMSC second treatment injection 2 or 3 group (75.00 ± 24.40 %, n = 4). The first two bars from left to right are the same as the first two bars from left to right in Figure 27.....113

Figure 29. Elastase treatment leads to a stiffer aorta in mice. Circumferential stretch ratio is shown on the x-axis. Circumferential Cauchy stress is shown on the y-axis. The solid lines are from the following groups: Black = native aorta, blue=fibrin only treatment, orange=ADMSC treatment, red =saline treatment. The black triangle data points are native mouse aortas from Collins et al[167]. The black circle data points are elastase treated mouse aortas from Collins et al[167].....115

Figure 30. Magnetic probe designed to fit within an 18 Fr sheath. Disk magnets (1.5 mm height x 3 mm diameter) were glued to the inside of a clear PVC 5 mm outer diameter tube.....126

Figure 31. Cell delivery mixer designed to ensure gels are mixed only while injecting. A) The three inputs (top) were designed to accommodate a “Luer-Lok” syringe. Equal volumes of the fibrinogen, thrombin, and iron nanoparticle loaded ADMSCs will be loaded into three separate syringes and dispensed at the same time through the single output (bottom). B) Fibrin gel constituent components loaded into a syringe and locked in the fibrin gel mixer. From left to right, the constituents are fibrinogen solution (pink), cell suspension (yellow), and thrombin solution (blue).....128

Figure 32. Fibrin gel schematic and groups. Fibrin gels are shown in green. Cells are yellow with purple nucleus. Iron nanoparticles are shown in blue. Experimental groups from left to right are: cells with 100 nm iron nanoparticles, cells with 200 nm iron nanoparticles, 100 nm iron nanoparticles alone, 200 nm iron nanoparticles alone.....133

Figure 33. Tissue mimic used for ultrasonic identification of magnetic probe. A Plexiglas chamber houses a 2% gelatin gel and a clear PVC tube to serve as tissue and aorta mimics, respectively.....136

Figure 34. Iron nanoparticles load at the same efficiency at all tested iron nanoparticle concentrations. The percentage of cells staining positive for iron nanoparticles was 49.3±7.9, 57.2±11.9, 58.6±15.2 (mean±SD) for the low (0.25 mg/mL), medium (0.50 mg/mL), and high (1.00 mg/mL) concentration of iron nanoparticles, respectively. The percentage of cells with

positive staining for iron nanoparticles is shown on the y-axis. The iron nanoparticle concentration groups are labeled on the x-axis. 139

Figure 35. Fibrinogen concentration, starting cell number and a mixed effect term of fibrinogen concentration and starting cell number are significant predictors of ratio of viable cells to plated cells after 5 days in culture. The ratio of viable cells to plated cells after 5 days in culture is shown on the y-axis. The fibrinogen concentration (F3 = 3mg/mL, F10 = 10 mg/mL) and iron nanoparticle size groups are labeled on the x-axis. The starting cell number is labeled with blue ($2.0x10^5$), red ($1.0x10^5$) and green ($5.0x10^4$). 140

Figure 36. Fibrinogen concentration is a significant predictor of number of viable cells after 5 days in culture. The number of viable cells after 5 days in culture is shown on the y-axis. The fibrinogen concentration (F3 = 3mg/mL, F10 = 10 mg/mL) and iron nanoparticle size groups are labeled on the x-axis. The starting cell number is labeled with blue ($2.0x10^5$), red ($1.0x10^5$) and green ($5.0x10^4$). 141

Figure 37. The attractive force between iron nanoparticle and magnets can move cells and iron nanoparticles through a fibrin gel before gelation is complete. Iron nanoparticles appear brown within a fibrin gel 24 hours after plating. Columns are labeled with experimental group. Rows are labeled with time of magnet placement with respect to plating. 143

Figure 38. ADMSCs loaded with iron nanoparticles localize towards a small magnet after five days in culture. A) Schematic of how circular gels were sectioned and imaged. The circular gel was cut in half, and then sections were made across the z-radial plane. B) The gel has been stained with Prussian Blue dye to identify iron nanoparticles. The lower blue rectangle represents the relative position and size of the magnet to the gel during culture. The red box is the area that is magnified in panel C which shows the DAPI and Prussian Blue stain merged. 145

Figure 39. ADMSCs loaded with iron nanoparticles localize towards a large magnet after five days in culture. A) Schematic of how circular gels were sectioned and imaged. The circular gel was cut in half, and then sections were made across the z-radial plane. B) The gel has been stained with Prussian Blue dye to identify iron nanoparticles. The lower blue rectangle represents the relative position of the magnet to the gel during culture. The red box is the area that is magnified in panel C which shows the DAPI and Prussian Blue stain merged. 147

Figure 40. ADMSCs loaded with iron nanoparticles accumulate at the bottom of the wells after five days in culture. Prussian Blue and DAPI are shown in top and bottom pictures, respectively for the ADMSC iron nanoparticle loaded gel cultured without a magnet in place. 148

Figure 41. ADMSCs without iron nanoparticles remain dispersed throughout the gel after five days in culture. DAPI stain for ADMSCs without iron nanoparticles when cultured for five days with a large magnet in place. The lower blue rectangle represents the relative position and size of the magnet to the gel during culture. 149

Figure 42. ADMSC nuclei are distributed evenly throughout the fibrin gel. The dashed white line in the top image indicates the outline of the fibrin gel. The red dashed boxes were randomly chosen for ImageJ ellipse fitting and distance measurement analysis of the blue, DAPI stained ADMSC nuclei. 151

Figure 43. The magnetic probe is visible within tissue and aorta mimics using ultrasonic imaging. A) An ultrasonic image shows the aorta mimic within the tissue mimic. B) An ultrasonic image shows the magnetic probe within the aorta mimic. C) The same ultrasonic image from panel B is shown with the changes from panel A highlighted in red. 154

Figure 44. Diameters of computation models of AAA G&R. A homeostatic model was created that shows little change in inner and outer aortic diameters (blue). The baseline model of AAA G&R is shown in red. The model of AAA G&R with 2x elastin production at 30% increase in baseline outer diameter is shown in green. Diameter (mm) is on the y-axis. Model simulation time is shown on the x-axis. 233

Figure 45. Medial ratio of remaining elastin to initial elastin within computation models of AAA G&R. The homeostatic model is shown in blue. The baseline model of AAA G&R is shown in red. The model of AAA G&R with 2x elastin production at 30% increase in baseline outer diameter is shown in green. Ratio of elastin to initial elastin is on the y-axis. Model simulation time is shown on the x-axis. 235

Figure 46. Medial ratio of remaining collagen to initial collagen within computation models of AAA G&R. The homeostatic model is shown in blue. The baseline model of AAA G&R is shown in red. The model of AAA G&R with 2x elastin production at 30% increase in baseline outer diameter is shown in green. Ratio of collagen to initial collagen is on the y-axis. Model simulation time is shown on the x-axis. 237

Figure 47. Medial ratio of remaining smooth muscle to initial smooth muscle within computation models of AAA G&R. The homeostatic model is shown in blue. The baseline model of AAA G&R is shown in red. The model of AAA G&R with 2x elastin production at 30% increase in baseline outer diameter is shown in green. Ratio of smooth muscle to initial smooth muscle is on the y-axis. Model simulation time is shown on the x-axis. 239

Figure 48. Medial ratio of smooth muscle active stress to initial smooth muscle active stress within computation models of AAA G&R. The homeostatic model is shown in blue. The baseline model of AAA G&R is shown in red. The model of AAA G&R with 2x elastin production at 30% increase in baseline outer diameter is shown in green. Ratio of smooth muscle active stress to initial smooth muscle active is on the y-axis. Model simulation time is shown on the x-axis.....241

Figure 49. Mixing colored fibrin gel constituent solutions through the fibrin gel mixer produces gels that appear similar in color to a gel mixed by manual pipetting. A) Fibrin gel constituent components loaded into a syringe and locked in the fibrin gel mixer. From left to right, the constituents are fibrinogen solution (pink), cell suspension (yellow), and thrombin solution (blue). B) Photo of a gel mixed with manual pipetting. C) Photo of gel that came out of the fibrin gel mixer. 245

1.0 INTRODUCTION

The goal of this dissertation is to develop a computationally-guided, novel therapy for abdominal aortic aneurysms (AAAs). This novel therapy is being designed to service a population of AAA patients that have a clinically defined AAA but do not meet the surgical criterion for intervention. This population, which makes up 90% of those identified with a AAA, currently has no effective treatment options, and it has been hypothesized that an effective treatment must be one the replaces lost elastin[2]. In order to develop an effective AAA treatment for subcritical AAAs that addresses current barriers, one must first understand the disease, its current treatments, and methods of studying potential treatments while considering the clinical barriers to translation for the said treatment.

The AAA treatment being investigated within this study is an adipose derived mesenchymal stem cell (ADMSC) based treatment designed to be injected and entrapped around the AAA. In this way cells can be isolated from a patient, cultured expanded, mixed in a fibrin hydrogel, and injected around that same patient's aorta in a minimally invasive procedure. The current scope of this work is to apply this therapy to those AAA patients who have a subcritical sized AAAs. The work of this dissertation is specifically meant to lay the groundwork for the development of this novel AAA treatment within the laboratory of Dr. David Vorp working towards clinical translation by evaluating the potential of smooth muscle cells (SMCs) to

produce elastin in-vitro, assessing the effects of elastin production in-silico, showing efficacy in a small animal model, and creating a new cell delivery device for human use.

The introductory chapter of this dissertation will first provide a broad overview of aneurysm types and the anatomical differences in normal and aneurysmal arteries (Section 1.1). Next, an overview of current clinical treatments will be discussed in detail (Section 1.2). Following this, an overview of current preclinical models of the disease and treatment will be discussed (Section 1.3). Then, an introduction and discussion of preclinical AAA treatment approaches will be provided (Section 1.4). Next, previous AAA studies performed in the Vorp lab are reviewed (Section 1.5). Finally, the specific aims of this dissertation are provided (Section 1.6).

1.1 ABDOMINAL AORTIC ANEURYSM ANATOMY (AAA) AND ETIOLOGY

1.1.1 Aneurysm Types and Etiology

An aneurysm is defined as a 50% increase in the diameter of an artery[3]. Aneurysms are commonly found in the aorta, and are classified according to the section where it is contained[4]. These include thoracic aortic aneurysms which are subdivided into ascending and descending, and abdominal aortic aneurysms which are divided into suprarenal and infrarenal[5]. Aneurysms can also occur in other parts of the arterial tree, most notably in the brain, called cerebral aneurysms, and in peripheral arteries such as the brachial, femoral, popliteal, and carotid arteries[4]. Regardless of the aneurysm location, all are noted by their disrupted and diminished elastic fibers[5,6].

Though the exact etiology of the disease is unknown, ultimately it is the force caused by blood pressure pushing against the walls of a mechanically compromised artery that leads to dilatation[7]. There are many factors that can cause an artery to become compromised including aging, smoking, high blood pressure, and atherosclerosis. Sex and race are also risk factors for AAA[8,9].

A family history of aneurysm and certain genetic backgrounds are also risk factors for aortic aneurysms. Genetic conditions such as Marfan's syndrome[10], Loeys-Dietz syndrome[11], Ehlers-Danlos syndrome[12], Turner syndrome[13], and having a bicuspid aortic valve[14] are associated with a relatively high incidence with thoracic aortic aneurysms. These genetic conditions weaken the body's connective tissues ultimately compromising the aorta. People who have these genetic conditions tend to develop aneurysms at a younger age and are at a higher risk for rupture and dissection.

Infections may cause aortic aneurysms[15]. Additionally, aortic aneurysms also can occur as a result of diseases that inflammatory conditions such as vasculitis[16,17]. Lastly, trauma can also damage the walls of the aorta and lead to aneurysms[18].

1.1.2 Smooth Muscle Cells in Normal vs. Aneurysmal Aortas

SMCs are, by far, the predominant cell type present within the medial layer of the normal vessel wall, and are responsible for the production of the structural proteins of the extracellular matrix (ECM) – mainly collagen and elastin[19]. The SMC also provides active stress giving the wall the ability to contract and dilate in response to blood flow demands and to regulate blood pressure[19-21].

In the non-pathological condition, SMCs remain in a mostly quiescent, contractile phenotype, having produced most of it elastic fibers in early childhood and only being tasked with collagen maintenance[22-25]. However, SMCs are highly plastic, having the ability to switch phenotypes from contractile to synthetic, allowing the SMC to proliferate, migrate, and synthesize ECM in response to injury[21]. SMC plasticity has been implicated not only in aortic aneurysms[26-29] but also other vascular diseases such as hypertension[21], atherosclerosis[19,30-32] and intimal hyperplasia[30,33,34]. A number of conditions exist within the aneurysmal state that can promote SMCs to switch from a contractile to a synthetic phenotype such as increased mechanical stress[35,36], increased substrate stiffness[37], and increased inflammation[36].

An additional phenomena characteristic of AAAs compared to normal aortas is an increase in SMC apoptosis. Most of the human studies of SMC in aneurysm disease describe a decrease in the concentration of the cells within the media. In-vitro studies of SMC lines derived from aneurysmal tissue reveal increased SMC apoptosis and poor in vitro propagation[38-41]. It has therefore been hypothesized that the matrix reduction seen in AAA results in part from a reduction in the quantity or activity of SMC[28,38,39,41,42].

SMCs in the diseased AAA also produce a plethora of factors that sustain the "cycle of destruction" which exacerbates the disease (**Figure 1**). For example, one study showed that matrix metalloproteinase-13 (MMP-13; other MMP activity is more fully discussed in *Section 1.1.6 Other Differences in Normal vs. Aneurysmal Aortas*) is localized to medial SMCs in AAA tissue and to human vascular SMC in culture, which also expressed MMP-13 mRNA thus contributing to the pathophysiologic progression of AAA[43]. Additionally, studies show that SMCs from AAA patients tend to secrete elastase[44]. Clearly, SMC contributes to the cycle of destruction in AAA.

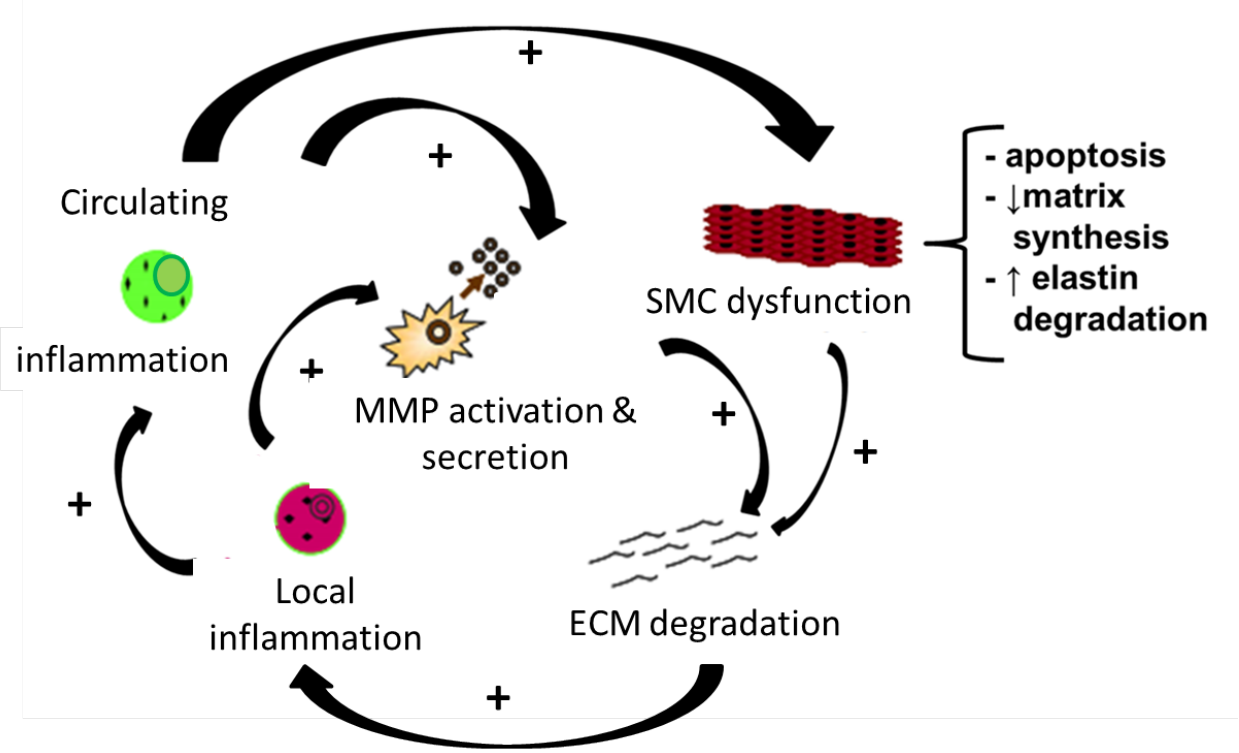

Figure 1. AAA "cycle of destruction". AAAs present an active inflammatory environment with multiple positive feedback loops. Figure adapted from Boddy et al.[1]

1.1.3 Elastin in Normal vs. Aneurysmal Aortas

One of the main extracellular structural proteins within the vascular wall is elastin which largely occurs in the form of elastic fibers/lamellae. While elastin can provide cellular signals such as maintaining SMC cell senescence[45], its primary role is to impart the biomechanical property of elasticity to the vascular wall[46-48]. This provides a direct contrast to collagen as its tensile strength is insignificant comparatively, but its elasticity is essential for arteries to recoil and recover the deformation they experience under the cyclic loading[46,48,49]. Additionally, the amount of elastic fibers present in a vessel are linearly proportional to the pressure they experience[47].

Creation of new elastic fibers is an involved, complex process that rarely happens in adulthood due to downregulation of the genes coding for elastin and elastin-related proteins postnatally[47,50] and an inherently complex elastic fiber synthesis process[51]. The down regulation of elastin-related genes in adulthood is a conserved process occurring across a variety of species[47,50].

Since adults do not normally produce elastin fibers, the loss of normal medial structure and, in particular, the near complete absence of a normal lamellar elastin is a striking feature of AAA histology compared to the non-aneurysmal aorta. The defatted dry weight of elastin is significantly lower in AAA compared to non-aneurysmal aortas[52,53].

Aortic elastin is thought to be extremely durable, with a half-life approximating the lifetime of the individual[54], thus the elastin loss characteristic of AAA is particularly remarkable. Studies of human AAA tissue demonstrate increased expression and/or activity of a variety of elastolytic matrix proteases, including MMPs[55-66], cysteine proteases[67,68] and serine proteases[69-71]. These studies back up the inverse correlation of elastin content with the elastolytic activity in

the aorta[53]. Importantly, corresponding findings in murine models of AAA have also been seen[72-77]. Additionally, elastase has been shown to come from not only the resident SMCs as discussed above, but also from leukocytes[53].

Once elastic fibers are broken down by the aforementioned proteases, a bevy of pro-inflammatory signals present in the elastin degradation products (or sometimes called elastin derived peptides) are released which recruit inflammatory cells and propagate the vicious cycle of AAA destruction[78]. Additionally, during the process of elastin fragmentation soluble elastin products can result and act as cell signaling molecules inducing negative effects such as SMC hyper-proliferation[45], inflammation[1], and calcification[79].

1.1.4 Collagen in Normal vs. Aneurysmal Aortas

Collagen is the most abundant class of proteins within the body[80] and is one of two main ECM components of the vascular wall along with elastin[47]. The primary function of collagen in the vascular wall is providing mechanical tensile strength[47,48]. The most important collagen types for the vasculature are collagens I, III, and IV[47]. Collagen types I and III are most abundant, residing in the medial and adventitial layers[19,47]. Collagen type IV is present in the basement membrane adjacent to endothelial cells and consists of a network-like structure rather than an elongated fiber like the other types[19,47].

Most of the tensile strength in the wall is provided by the fibrillar collagen network consisting principally of types I and III collagen with the extensile, or stretching, characteristics being attributed to type III collagen[81]. Ultimately, it is the progressive aneurysmal dilatation along with progressive weakening of tensile strength that causes an aneurysm to rupture.

This progressive weakening is due to the degradation of collagen. Normally, structural collagens are highly resistant to proteolytic degradation, only able to be cleaved by collagenases of the MMP family (i.e., MMP-1, -8, and -13) and selected members of the cysteine protease family[82]. However, in the aneurysmal aorta, studies in human patients have shown reduced levels of cystatin C protein expression along with increased collagen degradation products suggesting that protease inhibitor deficiency may contribute to AAA rupture[83].

While the late stages of AAA are characterized by an increase in collagen degradation, the earlier stages of the disease are quite different. There is an increase in the proportion of collagen in the aneurysmal aorta compared to non-diseased tissue (84% and 62%, respectively). In the aneurysms, collagen was increased and elastin was decreased[84,85]. Interestingly, while the ratio of type I to type III collagen remains the same in AAA and non-aneurysmal aortas[81], the turnover of type III collagen is increased in in AAA compared to non-aneurysmal aortas.[86] Additionally, there is an increase of collagen cross-links in AAA which may be attributed to old collagen accumulating cross-links while the biosynthesis of new collagen somehow defective[87].

While degradation of elastin is a hallmark of AAA and contributes to the cycle of destruction present within the disease, it is ultimately the degradation of collagen that produces the ever greater dilatation and eventual vessel rupture at the end stage of the disease[88]. To this end, collagen based interventions represent a treatment modality that may be better suited to preventing rupture of a large, critically-sized AAA, a contrast to elastin based interventions that may be more suitable for preventing the enlargement of the AAA.

1.1.5 Mechanical Environment in Normal vs. Aneurysmal Aortas

A direct consequence of the loss of elastin and temporal changes in collagen is a corresponding temporal change in the mechanical properties and stresses in the AAA compared to the non-aneurysmal aorta. One may surmise that the loss of the protein that is responsible for the elastic recoil of an artery will lead to a stiffer, less distensible tissue in AAAs compared to non-aneurysmal aortas. This is exactly the case[84,89,90].

While changes in general mechanical descriptors such as stiffness and distensibility are intuitive when one understands the function and properties of the main structural proteins, elastin and collagen, there is much more to be learned about the mechanics of AAA and the role they play in the disease. Groundbreaking studies in the Vascular Bioengineering Laboratory, headed by Dr. David Vorp, using patient specific geometries for finite element analyses (FEA) showed wall stress to be dependent on aneurysm shape and maximum diameter[91]. Subsequent studies initially built isotropic, uniaxially derived constitutive relations to perform FEA[90] before building more complex biaxial constitutive relations[92].

Determining the stress on the AAA wall is only half of the equation when understanding the effects of the disease. Understanding the strength of the tissue is also required. Again, this research was pioneered by the Vascular Bioengineering Laboratory who determined that AAA rupture is associated with aortic wall weakening, but not with wall stiffening. This wall strength (which is weaker than non-aneurysmal aortic tissue) in large aneurysms is not related to the maximum transverse diameter[93]. Further research created a regression model for estimating a patient specific strength based on the patient's age, sex, smoking status, family history, and AAA size as well as significant local predictor variables such as intraluminal thrombus (ILT) thickness and local normalized transverse diameter[94]. Importantly, the presence of ILT can alter the wall

stress distribution and reduces the peak wall stress in AAA providing a cushioning effect for the wall[95]; however, ILT has also been implicated with providing a hypoxic environment in the wall which could speed degradation of the wall[96-98].

The culmination of the Vascular Bioengineering Laboratory's work in patient specific stress and strength analysis was the creation of a way to non-invasively assess a patient's susceptibility to rupture, the rupture potential index (RPI). RPI is defined at the stress divided by the strength at each point in the finite element model of a patient's AAA. The Vascular Bioengineering Laboratory has shown that RPI could more reliably show differences in rupture vs. non-ruptured AAA when compared to maximum diameter and peak wall stress measurements[99].

While RPI may ultimately guide surgeons when determining a patient's need for interventional therapy, there is more that can be learned from the mechanics of AAA with respects to the mechanobiology of the disease. For example, mechanical and chemical cues influence the turnover rates of arterial constituents[100-103]. This is observation agrees with the theory of Y.C. Fung[104] who stated that the rate of volumetric growth is a function of a scalar measure of stress. Importantly, the ideas behind Fung's hypothesis can be traced back to at least the late 19th century[105].

Not only does the magnitude of stress seem to alter the production of ECM, but the direction of principal stress seems to influence the direction at which the ECM deposited. Research suggests that synthetic cells, such as SMCs, seem to have favorable biological functions or behaviors by affecting local anisotropy[106,107]. These mechanobiology concepts have motivated the creation of in-silico growth and remodeling models to test hypotheses. Utilizing

these models may help researchers understand such phenomena as MMP activity co-localizing with peak stresses within the AAA wall[56] and ultimately guide interventional therapies for AAA.

1.1.6 Other Differences in Normal vs. Aneurysmal Aortas

While the above sections cover the differences in the main constituents of the AAA and non-aneurysmal aortic walls, a few other differences are important enough to spell out explicitly. A particular noteworthy difference in all human abdominal aortas occurs in the number of lamellar units and the presence of vasa vasorum when compared to other mammals. The human abdominal aortic media has relatively fewer lamellar units with respect to its diameter than abdominal or thoracic aortas of other species. This elevates the mean tension per lamellar unit. Additionally, vasa vasorum are not as prevalent in human abdominal aortic media leading to avascular zones in the media[108].

Though the vasa vasorum density is sparse in humans compared to other mammals, there are also differences in the vasa vasorum of AAAs and non-aneurysmal aortas. Both tissue inhibitor of metalloproteinases (TIMPs) and gelatinases are localized to the vasa vasorum suggesting an involvement of the vasa vasorum in the maintenance and possibly the genesis of AAAs[64,65,109-111]. AAAs also have a higher density of medial neovascularization compared to non-aneurysmal aortas localizing to areas of disruption and degradation of elastin and chronic inflammation in the outer aortic wall[112].

This increase in medial neovascularization could be partially explained by the presence of the ILT which occurs in 75% of AAAs[113]. The ILT creates a physical barrier between the circulating blood and the wall, and an increase in the vasa vasorum would allow access to the wall from circulating cytokines and macrophages which are present in AAAs[83]. It's no wonder

that the process of aneurysmal enlargement is so complex, involving inflammatory cells, elastin and collagen degradation, smooth muscle apoptosis, and hypoxia mediated weakening[114], all mentioned above. Additionally, studies of human AAA tissue demonstrate increased expression and/or activity of a variety of elastolytic matrix proteases, including MMPs[55-66], cysteine proteases[67,68] and serine proteases[69-71] while lower or steady levels of TIMPs[115] when compared to non-aneurysmal aortas.

1.2 CURRENT CLINICAL TREATMENT OF AAA

The impact of AAA on the health of the nation is staggering. 7-10% of all males over the age of 55 are affected by this disease, resulting in about 1% of the annual deaths in this population[116]. Available treatments for AAA currently rely on the placement of a synthetic graft to physically exclude the aneurysmal segment of the aorta. A patient may need repair if the maximum diameter of the aneurysm surpasses 5 cm or if the growth rate of the aneurysm is greater than 0.5 cm per year, criterions that suggest the risk of rupture is greater than the risk associated with surgery. A patient may also need repair to relieve symptoms of the disease, restore blood flow, or to address emergency, life-threatening bleeding that is not due to rupture. Currently, repair is performed via two different methods, open and endovascular aneurysm repair (EVAR).

1.2.1 Surgical Options: Open Repair and EVAR

During open repair, surgeons make a large incision in the abdomen to expose the aorta. The aorta is cross clamped, and the aneurysm is cut open. A graft is sewn inside the aneurysmal portion of the aorta after removal of the ILT if present. Then, the wall is sewn back in place around the graft. Open repair is associated with a number of risks including but not limited to: heart attack, irregular heart rhythms, bleeding during or after surgery, injury to the bowel, blood clot, and infection of the graft. The 30 day mortality risk is higher with open repair, but long term problems are lower when compared to EVAR[117].

EVAR is a minimally invasive option done without a large incision. Surgeons make a small incision in the groin where a catheter is feed through an artery to access the aneurysm. Once in the aneurysm is reached, a grafting stent is deployed that can stretch from above the renal arteries down through the iliac bifurcation. EVAR is associated with a number of risks including but not limited to: damage to surrounding blood vessels, organs, or other structures, kidney damage, groin wound infection and hematoma, and endoleaks – a continual leaking of blood out of the graft and into the aneurysm sac.

While both procedures accomplish the goal of physically excluding the AAA from blood flow thus lowering the risk of a fatal rupture, neither approach has shown a benefit in the treatment of small AAA (<5.5 cm maximal diameter) which have a very low risk of rupture[118]. Currently, there are no effective treatments to offer these patients, and management is limited to "watchful waiting" (i.e., serial imaging of the AAA until the threshold for surgical treatment is met). There is also a huge healthcare cost burden associated with AAA repair which is estimated at $2.125 billion dollars per year (50,000 annual patients * $85,000 total 2 year costs[119]).

1.2.2 Systemic Anti-inflammatory Drugs

Given the problems with current AAA treatments mentioned above, researchers have sought to find alternative, interventional therapies for the disease. There is substantial pre-clinical work in aneurysm therapy which has been directed toward the inhibition of elastolytic processes with general or more specific anti-inflammatory or anti-protease agents[76,120,121]. Other studies utilizing anti-inflammatory molecules or MMP-inhibiting antibiotics (doxycycline and tetracycline) have been shown to prevent aneurysm formation or expansion in animal models of AAA[122-125].

The work cited above has, in part, led to patients currently being enrolled in a clinical trial titled "Non-Invasive Treatment of Abdominal Aortic Aneurysm Clinical Trial" (N-TA(3)CT, NCT01756833). This study aims to determine whether doxycycline (100 mg bid) will inhibit (by at least 40%) the increase in greatest transverse diameter of small abdominal aortic aneurysms (3.5-5.0 cm in men, 3.5-4.5 cm in women) over a 2 year observation period in comparison to a placebo-treated control group.

At the time of this writing, 200 patients − 179 (90%) male and 21 (10%) female – have been randomized in the clinical trial. The average age was 70.9 (SD = 7.6) for those randomized into the trial. Among these randomized patients, the average maximum transverse diameter for men was 4.3 cm (SD = 0.4) and for women 4.0 cm (SD = 0.3)[126].

1.3 PRECLINICAL AAA MODELS

Like many diseases, AAA has a number of different models that have been created in order to study disease. Large animal models are mainly used to develop novel methods to surgically treat AAAs. Small animal models are used to explore the mechanisms involved in AAA in an effort to develop new medical treatments. In-silico computational models are used to test our current understanding of the disease and also develop new hypotheses to test in the laboratory using in-vitro or in-vivo methods.

1.3.1 Animal Models

There are a number of different animals that have been used for AAA models. The most common large animal models include canine[127,128], swine[129-134], ovine[135-137], and turkey[138] models. These models tend to be useful for surgical studies; however, the high cost makes these models impractical for mechanistic research. The most common small animal models include mouse[76,139-141], rat[121,123,142-144], and rabbit[145-147] models. These models are cheaper and allow for mechanistic studies of the disease and potential treatments. The downside to small animal models is the difficulty in handling the small sized arteries.

Animal models are created in number of different methods. Broadly speaking, the method of aneurysm induction is broken down into chemical induction, surgical induction, and genetic predisposition. The chemical induction method includes elastase perfusion[140], calcium chloride application[148], and angiotensin-II infusion[149]. Surgical induction methods include poststenotic dilatation models[150], vein patches[150], and xenografts[151,152]. Genetically predisposed models are currently limited to ApoE knockout mouse models[153]. All of the induction methods can be used

on all the animals mentioned expect the angiotensin-II infusion and the ApoE knockout models. These models are usually limited mice. These models are more thoroughly reviewed by Trollope et al.[154].

The elastase perfusion (EP) model of AAA, the chosen model for the work of this dissertation, was first described in the early 1960s[155,156]. The experimental AAA is created by transient intraluminal perfusion of the abdominal aorta with pancreatic elastase. Specifically, the EP murine model was chosen because of its lower cost compared to larger animal models and its similarities to the clinical disease including the extensive loss of elastic fibers, fusiform dilatation and its anatomic localization, as well as its reproducibility[69,76,139,157]. Additionally, the EP model is preferred over the ApoE knockout/angiotensin II infusion murine AAA model due to the latter's unsustainable hallmarks of AAA[158].

1.3.2 Computational Models of Growth and Remodeling

While the insights gained from the animal models discussed above are important to the field of AAA research, they do have drawbacks including high cost, extended time for results, and the inherent variability that exists in biological studies. Due to these limitations, researchers have been motivated to develop theories of arterial growth and remodeling (G&R) which has led to frameworks for modeling G&R of soft cardiovascular tissues[159-163]. These early models focused on the consequences of G&R rather than the mechanisms driving G&R.

The first framework that was introduced to investigate G&R's governing principles was the constrained mixture model put forth by Humphrey and Rajagopal in 2002[164]. This theoretical framework utilized computational studies to clarify the complex mechanisms of sophisticated experimental techniques by narrowing the parametric spaces. These models would in turn allow

researchers to focus their experimental studies allowing more detailed and complete empirical observations. Since mixture models were first introduced in 2002, this framework has tested hypotheses of arterial G&R computationally while guiding new experiments that may back up the computationally predicted trends[22-25,96,165-181].

Other frameworks of arterial G&R have been postulated. Their mechanisms are similar to constrained mixture models in the sense that they are built on observed behaviors and that their predictions can be tested by experimentation. Many different arterial G&R hypothesis exist (see Watton et al.[182] for a detailed review); however, due to its particular strengths[183], the constrained mixture model is used in the work of this dissertation to understand the effects of a pro-elastogenic therapy on AAA.

1.4 PRECLINICAL AAA TREATMENT APPROACHES

While the ongoing N-TA(3)CT clinical trial will help determine if systemic administration of oral antibiotics can slow the enlargement of AAAs in patients, researchers continue to seek out alternative therapies. Generally speaking, these therapies are designed to be interventional. The targets of these therapies are some of the highlighted differences AAA vs. non-aneurysmal aortas highlighted in the sections above. Importantly, the treatments tend to address the causes of the disease rather than solely prevent rupture which is the goal of current treatment methods.

1.4.1 Localized Treatments

In clinical studies prior to the N-TA(3)CT clinical trial, doxycycline was found to be well tolerated by most patients with small AAAs; however, some patients developed dose-dependent side effects, such as cutaneous photosensitivity, dental discoloration, and gastrointestinal tract disturbances[184]. In response to these findings, researchers sought to localize (periaortic) administration of doxycycline in an attempt to inhibit the development of experimental AAAs as effectively as systemic treatment[120]. The results of this study by Bartoli et al. indicated that localized administration of doxycycline was a promising strategy to inhibit the progression of aortic aneurysms. The methods detailed in this study have also served as inspiration for the method of localizing the treatment described in this dissertation.

At least one other group of researchers, the Vyavahare Laboratory, has examined the localized delivery of therapeutic agents to the periadventitial wall of the aorta in AAA models. This group delivered an elastin binding polyphenol, pentagalloyl glucose (PGG), to the periadventitial wall of the aorta and found that a one-time periadventitial delivery of PGG inhibited elastin degeneration, attenuated aneurysmal expansion, and hindered AAA development in rats[185]. Local, periadventitial delivery of therapeutics shows promise in attenuating AAA progression in animal models while avoiding side effects of systemic delivery and avoiding the physical barrier presented by the ILT.

1.4.2 MircoRNAs

MicroRNAs (miRNAs) are approximately 20-nucleotide, single-stranded RNA molecules that target mRNA through partial complement binding. These molecules regulate gene

expression by inhibiting translation or degrading the transcript[186]. There is emerging evidence that miRNAs play a role in AAA pathogenesis. Unsurprisingly, a number of different miRNAs that are associated with the function of integral features of AAA disease have recently been explored.

miRNAs that affect SMC function have been explored as potential treatment options for AAA. Specifically, miRNA-21[187] and miRNA-26a[188] have been studied in the context of AAA disease because they are known to be key modulators of proliferation and apoptosis as well as differentiation, proliferation and migration, respectively. Given the deficiencies in aneurysmal SMCs noted in the sections above, it is not surprising that these miRNAs are being studied.

Other miRNAs have been shown to modulate gene expression of ECM proteins as well as MMPs and TIMPs. For example, miRNA-29b is a known target of elastin and collagen, and studies show that miRNA-29b can modulate gene expression in AAA models[189,190]. Additionally, miRNA-205 can modulate TIMP levels[191], and miRNAs 1, 21, 29a, and 133a have been shown to modulate MMP-2 and MMP-9 expression[192].

1.4.3 Mesenchymal Stem Cell (MSC) Treatment

While the aforementioned preclinical AAA therapies all have their benefits including localized treatment and treating some of the causes of the disease, none have as much potential to treat the disease as mesenchymal stem cells (MSCs). The processes that initiate and expand a AAA are heavily based on cellular activity; therefore AAAs represent an optimal target for regenerative MSC based therapy. MSCs have the ability to secrete growth factors[193,194] which suppress inflammation and MMP activity while stimulating elastin and collagen production. MSCs can also differentiate, thus providing a means to replace lost smooth muscle cells.

Furthermore, MSCs have already shown promise as a treatment for AAAs in animal models when delivered systemically which showed a reduction in the inflammatory response[195] and decreased MMP levels[196] suggesting a paracrine mechanism of action. MSCs have also shown promise when delivered by direct injection into the aortic wall which displayed MSC engraftment into the aneurysm wall allowing for the possibility of MSC differentiation[133]. Additionally, MSCs have also been delivered to the periadventitial of the experimental AAA using cell sheets[197].

In the MSC treatment studies mentioned above, the experiments delivered treatment concurrent with or prior to model initiation and demonstrated prevention of AAA development. Yet clinical therapy for AAA is unlikely to be initiated prior to measurable dilatation of the aorta. By the time an aneurysm can be clinically detected, severe matrix degradation – including near complete loss of medial elastin – has already occurred, and inhibition of further matrix degeneration alone may be insufficient. With that in mind, the delivery of MSCs to an experimental AAA should be done after the aneurysm is actively expanding. The work detailed in this dissertation which has led to published results[140] was designed with this requirement in mind.

1.5 AAA STUDIES IN THE VASCULAR BIOENGINEERING LABORATORY

The Vascular Bioengineering Laboratory has been a pioneer in AAA research, studying many different aspects of AAA biology[98,198-206], modeling[89,92-95,114,168,207-240], stress analysis[90,91,95,203,230,234,236,241-243], mechanobiology[206,233,244-246], and index modeling[94,99,247,248]. The Vascular Bioengineering Laboratory has also performed studies on thoracic aneurysms

including stress analysis[201,217-221,230,249] and microstructure analysis[250-255]. For most of the life of the laboratory, the Vascular Bioengineering Laboratory has sought out understanding of the disease. The work of this dissertation represents a step into the direction of an interventional therapy for AAA and has resulted in two peer reviewed publications[140,256] as well as funding from the National Institutes of Health (HL129066) and the University of Pittsburgh Center for Medical Innovation (F_168-2016, PI: Blose).

1.6 HYPOTHESES AND SPECIFIC AIMS

The work of this dissertation will lay the groundwork for an interventional MSC based AAA therapy. The subsequent chapters will cover pre-clinical, experimental in-vitro, in-silico, and in-vivo work as well as pre-clinical, experimental product development work. This study includes the three following Specific Aims and Hypotheses:

Specific Aim 1: *Establish the ability of SMCs to produce elastin when co-cultured with ADMSCs in-vitro and determine the utility of elastin production in in-silico models of AAA.* We seek to establish a method of inducing adult, human, SMCs to produce mature, mechanically functional elastic fibers. We hypothesize adult, human, SMCs grown in 3-D fibrin gels will produce elastic fibers when co-cultured with ADMSCs. We anticipate that co-culture of SMCs with ADMSCs will have positive impact on elastin production showing elastin that is formed into fibers.

Not stopping at just this elastogenic proof of concept, we will also try to understand any potential benefits of elastin production in the context of AAA. We hypothesize that elastin production within computational models of AAA G&R will alter the mechanical state of AAA to

the point where growth of the maximum diameter slows. We expect the results of the computational study to show that elastin production in the computational model with have an inverse relation to the enlargement rate of the AAA.

Specific Aim 2: *Demonstrate that a periadventitial cell therapy approach halts and/or reverses the progression of a AAA in a mouse model.* We hypothesize that the periadventitial delivery of ADMSCs to an established, expanding murine AAA model will acutely halt the progression of the disease within the model. We will assess the effects of treatment on infrarenal aortic diameter, tensile properties, elastin architecture, and collagen architecture.

We expect a significant reduction in aortic dilation, the primary measure of success for this aim. Should elastin be produced in our therapeutic model, we would expect our treatment to lower the tangent modulus of the vessel.

Specific Aim 3: *Development of a preclinical periadventitial cell therapy delivery system.* Our proposed therapy for treating subcritical AAAs (<5.5 cm), is the localized delivery of therapeutic cells to the periadventitial wall encapsulated in a fibrin gel. The system for accomplishing the localized delivery consists of 4 parts: (1) iron nanoparticle loaded therapeutic cells; (2) a mixing and delivery apparatus that ensures proper mixing and dispensing of cells, fibrinogen, and thrombin; (3) ultrasonic needle guidance; and an (4) endoluminal magnetic catheter.

We expect that when combined, the resulting therapy will be capable of delivering therapeutic cells to the periadventitial surface of the AAA with a fibrin gel holding the cells in place.

This research project was designed to build an interventional, MSC based AAA therapy. Much of the preclinical work involved with this idea is contained in the following chapters. First,

a novel method for testing soft materials is described (Chapter 2). This work is used in the evaluation of the elastogenic potential of MSCs when co-cultured with ADMSCs. The elastogenic potential of these SMCs is evaluated mechanically, histologically, and biochemically (Chapter 3). This analysis is followed by in-silico experiment determining the effect of elastin production in computational models of AAA G&R (Chapter 4). After exploring elastin production in the context of AAA, our ADMSC therapy is tested in-vivo using a murine elastase perfusion model of AAA (Chapter 5). Next, the development of a cellular delivery system for use in patients in detailed (Chapter 6). Finally, a summary of results and thoughts on future directions is provided (Chapter 7).

2.0 DESIGN AND VALIDATION OF A VACUUM ASSISTED ANCHORAGE FOR THE UNIAXIAL TENSILE TESTING OF SOFT MATERIALS

Due to the limitations of current uniaxial tensile testing methods, we sought to design an alternative gripping mechanism for soft materials such as the gels created in Section 3.2.3. Mechanically testing these gels will allow us to verify the production of mechanically functional elastin fibers and networks by SMCs within our 3D fibrin hydrogel culture system, an important step in showing proper elastogenesis. The gripping mechanism, a vacuum assisted anchor, is detailed and verified in this chapter and was published in Soft Materials[256].

2.1 INTRODUCTION

Tensile testing systems are commonly used to impart mechanical load to materials in order to experimentally evaluate mechanical properties including stiffness and tensile strength. Current commercial tensile testing systems rely on spring-loaded or other compression-based grips to clamp tissues in place to avoid slipping during uniaxial extension. For robust and mature tissues or materials, the clamping force is typically not a problem. However, when attempting to clamp soft materials (which we define as tissue or materials with a tangent modulus ~15 kPA), the clamping force can cause catastrophic damage to the sample. This also poses a problem when studying the mechanobiology of soft materials when loading is desired.

For instance, cell-seeded fibrin gels are used to create tissue engineered constructs, such as vascular grafts[257-259] and heart valve leaflets[260,261], and as three dimensional (3D) in-vitro culture systems[262-264]. Unless these gels are polymerized around a grippable post[265] or integrated into a stronger material[266], they cannot be secured in conventional uniaxial tensile loading systems until significant remodeling has occurred. Attempts to mechanically test or load purely gel-based tissue constructs have been limited to ring tests on sections of tubular cell-seeded constructs[267-269]. While ring tests represent a valuable tool for determining mechanical properties, the method has inherent deficiencies including non-constant strain rates, compression at the pulling posts, and convoluting edge effects[270]. Using either ring tests or custom molds restricts the geometry and possibly the material of samples that can be used for testing. Performing uniaxial tensile tests mitigates the problems surrounding ring tests and will allow researchers to gather meaningful tensile data that might reveal the role of the mechanical environment during the initiation of tissue remodeling in these experimental systems.

Drawing inspiration from micro-aspiration techniques that are used for membrane mechanics studies[271], we designed a vacuum-based anchorage system to grip a soft material subjected to uniaxial tensile loading. Here we present our solution: a novel vacuum-assisted anchor (VAA). Our design was validated by using the VAA to grip and mechanically test two soft materials (fibrin gels) that were previously unable to withstand uniaxial tensile testing using conventional methods.

2.2 METHODS

2.2.1 Design and Functional Principles of the VAA

The VAA design is shown in **Figure 2**. The prototype uses a typical house vacuum source (approximately 45 kPa gauge pressure) to secure a sample against an in-line filter via a 90 degree plastic elbow. The elbow (1/4" outer diameter) fits inside the pneumatic clamps of a commercial tensile testing system and can therefore be moved up and down. The open end of the elbow is connected to a truncated, aerosol-resistant micropipette tip, allowing the sample to be secured without being pulled into the vacuum line.

Our prototype was designed to be used within a specific commercial uniaxial tensile testing system (Instron, #5543a, Norwood, MA) although vacuum supply line sizes can also be altered to fit inside a wide variety of commercial testing systems. All components of the prototype VAA are readily available in most laboratory settings.

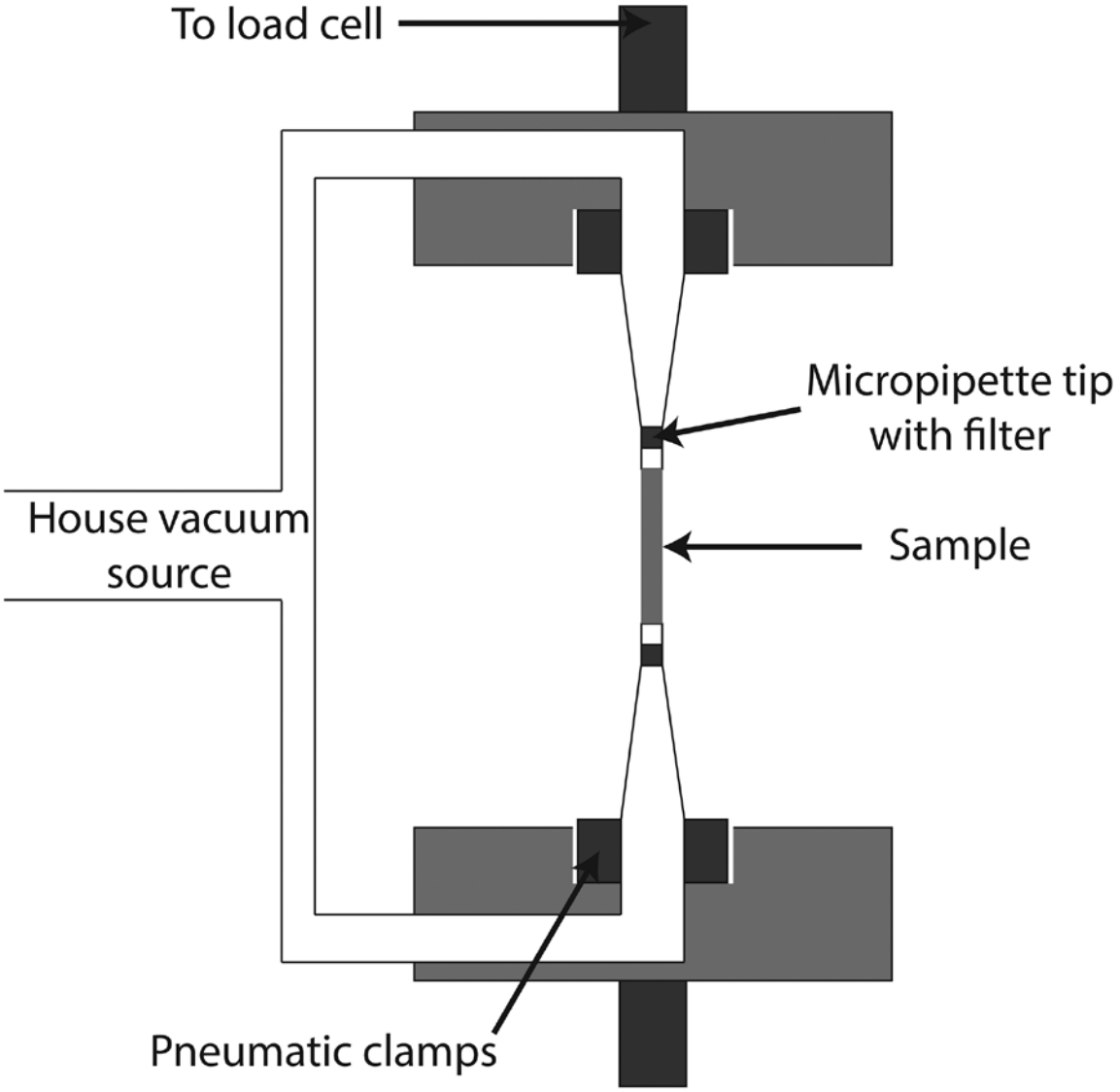

Figure 2. VAA Design Concept. Schematic of the VAA design is shown. A house vacuum source is directed to the testing sample and clamped by pneumatic grips

2.2.2 Fibrin Gels as Testing Materials

Fibrin gel was used as a sample material to demonstrate proof-of-concept of the VAA for tensile testing. Two densities of fibrin gels were fabricated by mixing bovine fibrinogen type I at different concentrations (VAA Fib_5 [5 mg/mL] and VAA Fib_10 [10 mg/mL], Sigma-Aldrich, St. Louis MO) with bovine thrombin (1 NIHU/mL, Sigma-Aldrich, St. Louis, MO) within the troughs of Flexcell™ Tissue-Train™ plates (Flexcell Int., Hillsborough, NC). Gels were allowed to polymerize for at least 2 hours in incubator conditions (37^{o} C, 5% CO_2).

Additional gels were fabricated using the same concentrations of fibrinogen (Ver. Fib_5 [5 mg/mL] and Ver. Fib_10 [10 mg/mL]) and thrombin mentioned above, and these gels were formed between two strips of polyvinyl alcohol (PVA) sponge material that served as anchorage points for mechanical testing. These gels served to verify the VAA compared to alternative testing methods.

2.2.3 Mechanical Testing

The VAA was clamped into an Instron uniaxial tensile testing system (Instron, #5543a, Norwood, MA,) and fibrin gels were gently placed next to the open ends of the VAA while the vacuum was turned on. Samples were stretched to initial, unloaded lengths by moving the crosshead until force readings were present. A constant crosshead speed of 0.1 mm/sec was used to pull on the samples, and the applied load and resulting displacement (d) were recorded continuously using the Instron-packaged software (Bluehill, Version 2, Instron, Norwood, MA). The axial component of the First Piola Kirchhoff Stress (the P_{11} component of the full First Piola Kirchhoff Stress Tensor, **P**) was calculated using the force measurement (f) from a 25 N load cell

(MDB-25, Transducer Techniques, Temecula, CA) and the initial measured area (A_o, diameter measured from pictures of stress free samples held in VAA), as follows:

$$P_{11} = \frac{f}{A_o} \tag{2-1}$$

The fibrin gels that were formed between the PVA-sponge strips were tested in the same manner as described above. The PVA-sponge served as the anchor point for clamping.

2.2.4 Material Assumption and Mechanical Properties

We assumed that all fibrin gels displayed transverse isotropy for a rod-like material. A Poisson's Ratio (ν) of 0.25 was assumed which was consistent with previously reported values for fibrin[268]. The deformation gradient tensor, ***F***, is described as:

$$\boldsymbol{F} = \begin{bmatrix} \lambda_a & 0 & 0 \\ 0 & \lambda_t & 0 \\ 0 & 0 & \lambda_t \end{bmatrix} \tag{2-2}$$

The axial stretch (λ_a) is calculated from the initial length measurement (L_0) and the displacement (d) measured during testing as follows:

$$\lambda_a = \frac{L_0 + d}{L_0} \tag{2-3}$$

The transverse stretch (λ_t) was calculated from the exact relation for finite stretch values as follows[272]:

$$\lambda_t = \lambda_a^{-v} \tag{2-4}$$

The Cauchy stress is defined as:

$$\boldsymbol{\sigma} = J^{-1}\mathbf{P}\mathbf{F}^T \tag{2-5}$$

where the Jacobian, J, is defined as the determinant of **F**

$$J = \det(\mathbf{F}) \tag{2-6}$$

For uniaxial loading, we will consider the axial component of the Cauchy stress (σ_{11}):

$$\sigma_{11} = P_{11}\lambda_a^{2v} \tag{2-7}$$

We defined the experimentally determined elastic limit as the stretch ratio where the second derivative of the axial component of Cauchy stress (σ_{11}) with respect to λ_a is a maxima[273] (see **Figure 3**.) The "yield stress" was defined as the value of σ_{11} at the experimentally determined elastic limit; i.e. the "yield stretch." The tangent modulus is defined as the slope of the linear portion of the σ_{11} vs. λ_a curve. The ultimate tensile strength (UTS) is defined as the maximum value of the σ_{11} vs. λ_a curve, and the ultimate stretch is the value of λ_a where the UTS is defined. The ultimate properties were only calculated for samples that had a confirmed tensile failure. Any samples that demonstrated slipping behavior were corrected by analyzing the tangent modulus of the sample.

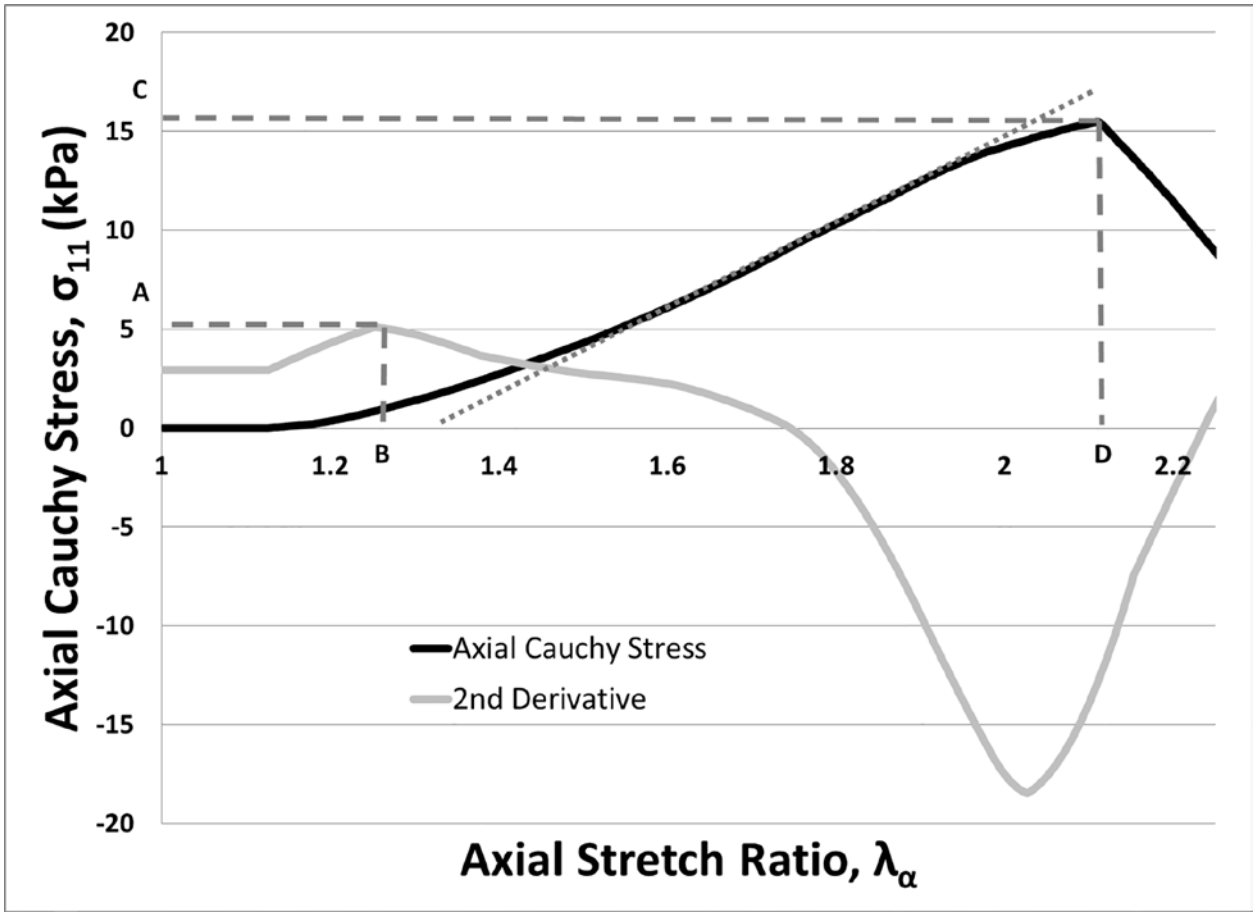

Figure 3. Features of Stress-Strain Behavior Captured by the VAA. The black curve shows σ_{11} vs. λ_α from a sample test using 5 mg/mL fibrinogen. The gray curve is a scaled form of the second derivative of the σ_{11} with respect to λ_α. Points A and B indicate the yield stress and yield stretch, respectively. The ultimate tensile strength (UTS) and ultimate stretch are noted by points C and D, respectively. The linear portion of the black stress-strain curve is estimated by a dotted gray line. The slope of this line is the tangent modulus.

2.2.5 Statistics

Student t-tests were used to compare mechanical properties (yield stretch, yield stress, tangent modulus, ultimate stretch, ultimate tensile strength) between material groups. Statistical significance was assigned to p-values < 0.05. Data given as mean ± SD.

2.3 RESULTS

2.3.1 Device Performance

The VAA was able to successfully grip soft, delicate fibrin gels subjected to uniaxial tensile testing leading to tensile failures (confirmed with frames from slow-motion video in **Figure 4**). By using regulated vacuum, the VAA does not damage the sample at the gripped location and creates a highly tunable method of delivering anchoring force to soft materials. The use of the VAA yielded true tensile breaks in 47% of all tests (compared to a 0% success rate we experienced in our lab using conventional gripping methods). A total of 59% of samples provided useful yielding data (i.e. stress-strain data through stretch ratios up to the yield stretch, see **Table 1**).

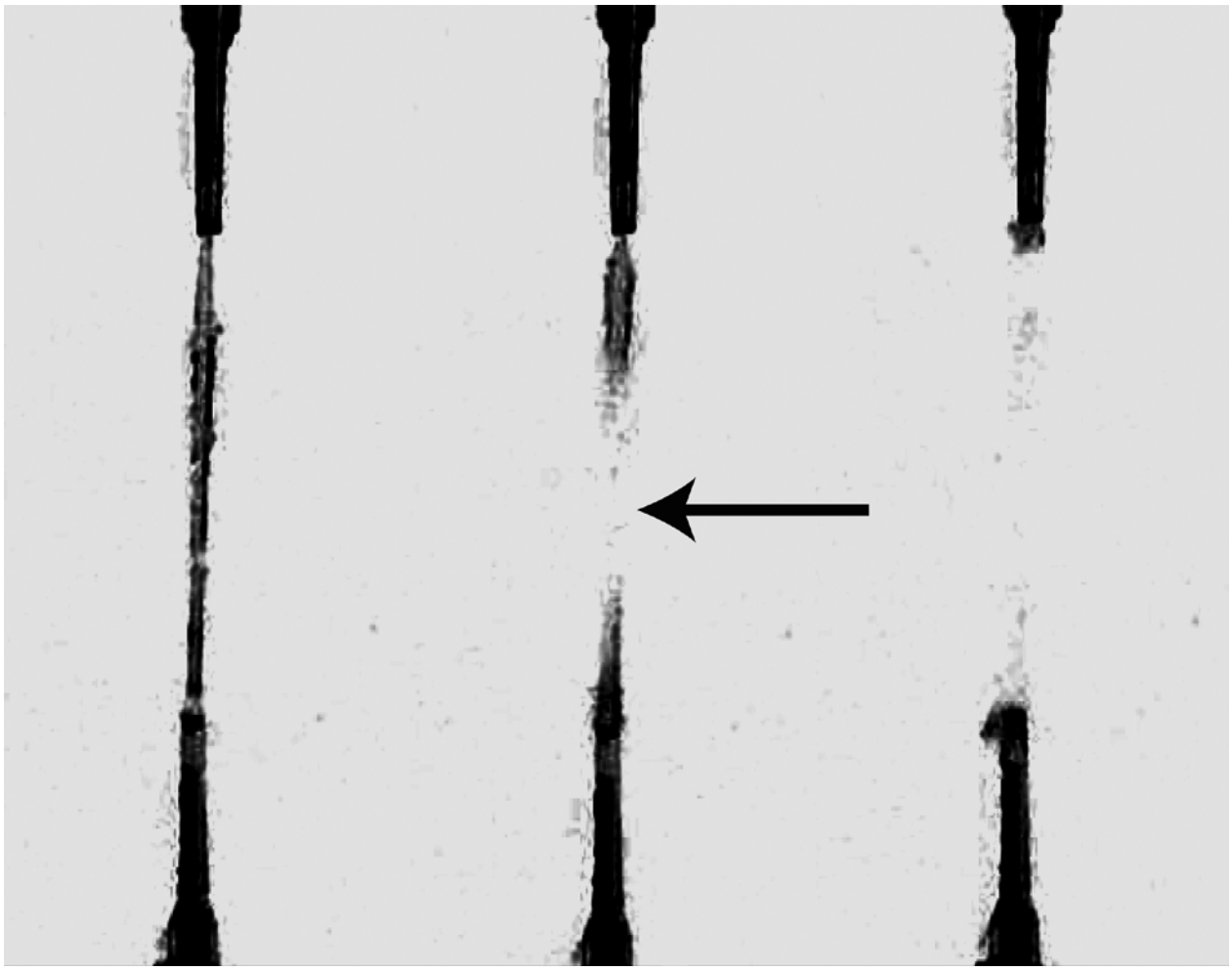

Figure 4. Visual Confirmation of a Tensile Break. Three frames (captured at 30 frames per second) from a video of uniaxial tensile test are shown. The left frame shows the gel just before its tensile failure. The middle frame confirms a tensile break in the center of the fibrin gel (arrow) with the two halves of the fibrin gel recoiling back to their respective VAA grips (right frame).

Table 1. Breakdown of useful sample numbers by group. Successful tensile tests illustrate the gripping efficiency of the VAA. By utilizing the VAA during uniaxial tensile loading, we were able to collect meaningful tensile and ultimate data from samples.

Group	Total Samples	Useful Yield Data	Useful Ultimate Data
VAA Fib_5	n=29	n=20 (69%)	n=18 (62%)
VAA Fib_10	n=29	n=14 (48%)	n=9 (31%)
VAA Total	n=58	n=34 (59%)	n=27 (47%)
Ver. Fib_5	n=10	n=7 (70%)	n=6 (60%)
Ver. Fib_10	n=10	n=7 (70%)	n=5 (50%)
Ver. Total	n=20	n=14 (70%)	n=11 (55%)

2.3.2 Device Validation and Verification

The VAA was validated by determining the mechanical properties of fibrin gels made from two different concentrations of fibrinogen that were previously unable to be evaluated using conventional methods for uniaxial tensile testing. A summary of the elastic mechanical properties of the fibrin gels made with two different concentrations of fibrinogen (VAA Fib_5 = 5 mg/ml, or VAA Fib_10 = 10 mg/ml) is provided in

Table 2. The VAA Fib_5 group had a higher yield stress (2.74±1.62 vs. 1.53±0.74 kPa; p=0.014) and tangent modulus (12.94±4.85 vs. 9.64±3.77 kPa; p=0.033). A summary of the ultimate mechanical properties is provided in

Table 3. The VAA Fib_5 group also had a higher UTS (8.18±3.97 vs. 4.12±1.55 kPa; p=0.001) and ultimate stretch (2.00±0.23 vs. 1.76±0.25; p=0.031).

Table 2. Fibrin gel elastic mechanical properties. Significant differences (*) in the elastic mechanical properties of the fibrin gel groups are revealed during tensile tests using the VAA. Yield stretch, yield stress, and tangent modulus values are reported as mean ± SD from each fibrin gel group. The VAA Fib_5 group had higher yield stress and tangent modulus values.

Group	Yield Stretch	Yield Stress (kPa)	Tangent Modulus (kPa)
VAA Fib_5 (n=20)	1.20 ± 0.11	2.74 ± 1.62	12.94 ± 4.85
VAA Fib_10 (n=14)	1.24 ± 0.12	1.53 ± 0.74	9.64 ± 3.77
p-value	0.322	0.014 *	0.033 *

Table 3. Fibrin gel ultimate mechanical properties. Significant differences (*) in the ultimate mechanical properties of the fibrin gel groups are revealed during tensile tests using the VAA. Ultimate stretch and ultimate tensile strength (UTS) are reported as mean ± SD from each fibrin gel group. The VAA Fib_5 group had higher ultimate stretch and UTS values.

Group	Ultimate Stretch	UTS (kPa)
VAA Fib_5 (n=18)	2.00 ± 0.23	8.18 ± 3.97
VAA Fib_10 (n=9)	1.76 ± 0.25	4.12 ± 1.55
p-value	0.031 *	0.001 *

The VAA Fib_5 group had a similar yield stress and tangent modulus when compared to the Ver. Fib_5 group [yield stress: (2.74±1.62 vs. 3.95±1.88 kPa, respectively; p=0.20), tangent modulus: (12.94±4.85 vs. 12.1±2.97 kPa, respectively; p=0.72)]. The VAA Fib_10 group also had a similar yield stress and tangent modulus when compared to the Ver. Fib_10 group [yield stress: (1.53±0.74 vs. 1.97±0.58 kPa; p=0.29), tangent modulus: (9.64±3.77 vs. 10.40±1.69 kPa; p=0.69)].

2.4 DISCUSSION

In this study, we developed a device for uniaxial tensile loading of soft materials such as gels. Previous attempts to do so using conventional mechanical grips consistently resulted in failures at the gripped location. We designed our vacuum-based gripping mechanism to provide a means to adequately grip the sample during tensile loading – even to true tensile failures – while avoiding the edge effects associated with ring tests. Our novel grip described here could be used to evaluate the uniaxial mechanical properties of a wide array of soft, gelatinous-like tissues and materials, both biological and non-biological. Further, it could be used to impart uniaxial loading on materials, such as cell-seeded gels for mechanobiology studies.

Analysis of our mechanical tests revealed differences in the mechanical properties between two groups of soft fibrin gel strips, which could not be achieved using other conventional testing systems. Our results are similar to a previously published study by Cummings et al.[267], which performed ring tests of tubular fibrin constructs, and calculated a tangential modulus of 19 kPa for gels created with 4 mg/mL fibrinogen and 0.4 NIHU/mL thrombin. We calculated a mean tangent modulus of ~13 kPa for our VAA Fib_5 group, which

was a similar fibrinogen concentration (5 mg/mL) to the Cummings et al. study. The VAA was also verified through our own testing using alternative means.

The VAA will allow for uniaxial tensile testing of soft materials that were previously limited to other mechanical testing methods such as compressive testing and atomic force microscopy (AFM) to determine mechanical properties. For example, Kirchmajer et al.[274] have developed a degradable genipin cross-linked gelatin hydrogel to be used as a scaffold for tissue engineering purposes. The mechanical characterization of this soft material was limited to compression and rheological studies - sufficient for researchers looking to use this hydrogel scaffold for creating tissue engineered cartilage or other compressive load bearing tissues. However, the same hydrogel might also be useful for tissues bearing tensile loads (e.g. tendon, blood vessels, skin). Evaluation of soft material tensile properties with a device such as the VAA will be a critical step towards engineering new tensile load bearing tissue equivalents[275-278].

AFM is a technique often used to investigate the mechanical properties of individual cells, fibers, or other materials that may be too delicate to undergo conventional uniaxial tensile testing where compressive grips are employed. Equipment cost considerations and availability can make using AFM impractical; however the desire to know tensile properties of cells, their substrates, and the effects of the substrate's mechanical properties has left researchers with no other options for very soft materials. For example, Solon et al.[279] used AFM to examine the functional effect of polyacrylamide gel stiffness on cultured fibroblasts, revealing important insights into how substrate stiffness can affect cell stiffness and f-actin organization. The VAA provides an alternative tool for performing uniaxial tensile tests on soft materials like polyacrylamide gels that is more affordable and readily available than AFM.

The VAA is inherently limited by the strength of the vacuum source, the normal area of the sample in contact with the device, and the integrity of the seal between the sample and the device. A quality seal will ultimately lead to higher success rates during mechanical testing. This is demonstrated in the differences in the success rates between the VAA Fib_5 and VAA Fib_10 groups. The VAA Fib_10 group will have more dense fibers [280] and less water in the sample. As the sample is pulled, water will be squeezed out, thus eventually compromising the quality of the seal. This phenomenon would partially explain the differences in success rates between the two testing groups. The theoretical maximum gripping force is limited to the product of atmospheric pressure and the normal area of the sample in contact with the VAA. A practical limit to maximum gripping force is dependent upon the strength of vacuum source (house source or commonly available vacuum pumps). In order to extend this technology to hydrated samples, improvements in the quality and repeatability of the seal would need to be made.

Our mechanical analysis has limitations inherent to the material fabrication and assumptions made regarding our test materials (fibrin gels). When fabricating our gels, we only varied the fibrinogen concentration. The amount of thrombin used was held constant. This meant that the ratio of fibrinogen to thrombin in each sample was also different and may have introduced convoluting effects such as changing relative fiber diameters, lengths and branchpoint densities[280]. Indeed, this work by Ryan et al. shows that decreasing ratios of fibrinogen to thrombin leads to increased fiber density and branchpoint density. The higher tensile and ultimate properties exhibited by the VAA Fib_5 could be due to the lower ratio of fibrinogen to thrombin which leads to increased fiber density and branchpoint density. Additionally, we assumed a Poisson's Ratio of 0.25 for both groups based on previously published values[268] although the actual value is likely to change when changing the concentration of fibrinogen in

the sample groups. Lastly, we assumed a uniform strain across the length of the sample though this may not be the case. Future studies should determine any convoluting effects of non-constant fibrinogen to thrombin ratios by testing additional samples where this ratio is kept constant. Future studies should also focus on measuring transverse stretch in order to calculate an experimental Poisson's Ratio and determining the axial strain distribution through video analysis and ink spattering of the samples. These analyses will also help determine if the VAA affects the strain conditions near the seal. These considerations were beyond the scope of the current study.

2.5 CONCLUSION

Our VAA design was validated through the successful mechanical tests of two groups of fibrin gels made from two different concentrations of fibrinogen that were previously unable to withstand uniaxial tensile testing using conventional methods. This anchorage method will allow new studies into the uniaxial mechanics and/or mechanobiology of soft materials. Specifically, this tool will now allow mechanical testing of our SMC seeded fibrin gels that will ultimately allow us to determine the mechanical quality of any elastin produced in the experiments described in Chapter 3.

3.0 SPECIFIC AIM 1, PART 1: ELASTIN PRODUCTION OF SMOOTH MUSCLE CELLS WHEN CO CULUTRED WITH MSCS

The first part of Aim 1 is showing that elastin fibers can be produced by adult, human SMCs when co-cultured with ADMSCs. We employed 3D cell culture by utilizing fibrin gels. Our gels were then subjected to qualitative imaging, a quantitative biochemical assay, and mechanical tensile testing all chosen due to the experiments' ability to detect mature - fully assembled and cross-linked by lysyl oxidase (LOX) - elastic fibers.

3.1 INTRODUCTION

Elastic recoil is a necessary quality of many tissues in the body, including skin, lung, ligaments, and large diameter arteries[19]. This recoil is provided primarily by elastic fibers made up of elastin and a supporting microfibrillar network. In the context of the abdominal aorta, most elastic fibers are created primarily during development[281] and then slowly degrade. The half-life for this process has been disputed as either ~40[282] or ~80[54] years.

The critical hallmark of AAA is a noted loss of elastic fibers in the medial layer of the vessel. This loss of elastic fibers is thought to lead to a host of downstream effects that exacerbate the disease, such as higher circumferential stretch and stress in the vessel wall, marked increase in the circulating inflammatory environment, and increased elastolytic activity

by resident SMCs among others. Notably, researchers hypothesize that in order to ever fully reverse the disease, production of new, mechanically functional elastic fibers will be necessary[2].

The physiological process of cellular elastin synthesis and matrix assembly is a highly complex process involving coordinated intracellular and extracellular activities directed by SMCs (described in detail elsewhere[283,284]). The elastin production process begins when elastin protein is secreted by SMCs as a tropoelastin precursor molecule. This molecule is then moved into the extracellular space and binds to a chaperone elastin binding protein (EBP) which protects the tropoelastin from degradation[283]. Arrays of microfibrillar glycoproteins made up of fibrillins (particularly 1, 3 and 5), microfibril associated glycoproteins (MAGPs 1 and 2), and fibulins (1,2, and 5)[45,46,285,286] in the extracellular space reduce binding affinity of the EBP for tropoelastin and the cell membrane facilitating the release of bound tropoelastin and the dissociation of the EBP from the cell membrane. The tropoelastin collects on the microfibrillar scaffold as amorphous elastin and then undergoes crosslinking by oxidation of lysine amino acid side chains on the elastin molecules via LOX[287]. This results in mature fibers (~300 nm-1 μm in diameter), containing a core of crosslinked, amorphous elastin, surrounded by microfibrils[288,289]. Mature fibers are then linked by desmosine and isodesmosine moieties providing the ability to stretch and recoil as a single unit thus providing a portion of a vessel's mechanical properties. The contributions of elastic fibers (compared to collagen fibers) to vessel mechanics have been quantified from the different regions of the stress–strain curve[290].

Given that elastogenesis is a complex, multistep process, it isn't surprising that it has been the subject of research in the context of aneurysms and regenerative medicine. Broadly speaking, elastogenesis efforts can be classified into two groups: elastin synthesis inhibitors (e.g., ascorbic acid[291], basic fibroblast growth factor[292], cyclic AMP[293], and monensin[294]) and elastin

synthesis stimulators (e.g., cyclic GMP[293], fetal calf serum[295], insulin-like growth factor 1 [IGF-1][296,297], and transforming growth factor β1 [TGF-β1][298]).

In this chapter, we too seek to establish a method of inducing adult, human, SMCs to produce mature, mechanically functional elastic fibers. We chose to seed SMCs in fibrin gels in various states of mechanical loading before stimulating the SMCs with ADMSC co-culture, TGF-β1 stimulation, or conditioned media (CM) collected from ADMSCs in an attempt to induce SMC elastogenesis.

3.2 METHODS

3.2.1 Cell Culture

Commercially sourced ADMSCs (Thermo Fisher Scientific, #R7788110) were cultured in 75-cm^2 or 175-cm^2 tissue culture flasks (Corning) and grown under defined culture media [1:1 Dulbecco's modified Eagle's medium (DMEM; Gibco #11965) to DMEM/F12 (Gibco #113300) with 10% fetal bovine serum (Atlanta Biologics #S11550), antibiotics (1% Pen/Strep, 0.5% Fungizone, 0.1% Gentamycin), and 10 μL of 10 mM dexamethasone] mixed with 25% Preadipocyte Growth Medium (#C-27410, #C-39425; PromoCell). Culture media was changed every 2-3 days and when ADMSCs were expanded to near confluence, they were passage expanded utilizing 0.25% trypsin-EDTA (#25200-056; Gibco) or utilized for subsequent experimentation.

To obtain conditioned media, culture media was replenished in near confluent flasks of ADMSCs (~80%) and cultured for an additional two days upon which it was collected. The

conditioned media was then centrifuged (#Sorvall Legend RT, 1200 rpm, 5 min) to remove any cellular material or debris. It was stored at –80°C until use.

Additionally, human aortic SMCs were purchased from ATCC (#PCS-100-012) and grown in a similar manner to ADMSCs but in their own culture media (Cell Applications, #311-500, #311-GS).

3.2.2 Fibrin Gel Fabrication

SMC-seeded fibrin constructs were fabricated by mixing bovine fibrinogen type I (3 mg/mL, Sigma-Aldrich, St. Louis MO) with bovine thrombin (1 NIHU/mL, Sigma-Aldrich, St. Louis, MO) and SMC cell suspension ($3x10^5$ cells/gel). The gels were plated in the troughs of Flexcell(Flexcell Int.™ Tissue-Train™ plates, Hillsborough, NC) for the early time point studies and within 24-well plates (Corning) that had been imprinted with custom circular molds for the late time point studies. Gels were allowed to polymerize for at least 2 hours in incubator conditions (37°C, 5% CO2) before adding SMC culture media. The gels were allowed to compact for 2 days before being subjected to treatments.

ADMSC-seeded fibrin constructs were fabricated by mixing bovine fibrinogen type I (3 mg/mL, Sigma-Aldrich, St. Louis MO) with bovine thrombin (1 NIHU/mL, Sigma-Aldrich, St. Louis, MO) and ADMSC cell suspension ($4.5x10^6$ cells/gel). The gels were plated on top of SMC gels within the Flexcell™ Tissue-Train™ plates (Flexcell Int., Hillsborough, NC) for the early time point studies and on top of SMC gels within the 24-well plates (Corning) for the late time point studies. Gels were allowed to polymerize for at least 2 hours in incubator conditions (37°C, 5% CO2) before adding SMC culture media. The gels were then cultured in incubator conditions according to the treatment condition.

3.2.3 Treatment Description

The experimental groups are summarized in **Table 4**. The groups are broken down by treatment delivered to the SMC-seeded fibrin gel, the length of the treatment, and the loading condition imposed. In order to understand the final experimental groups, a note should be made about the ideas behind the formation of these groups.

Originally, we intended to only use the Flexcell Tissue-Train system in our studies due to its ability to mechanically stimulate our fibrin gels. This mechanical stimulation would mimic the conditions we imagined an MSC-seeded fibrin gel therapeutic and resident SMCs would experience when the therapeutic was delivered to the periadventitial surface of a AAA. However, after seeing some of the results that are shown in Section 3.3.1, we realized that our experimental design would need to be altered. We moved away from using the Flexcell Tissue-Train system due to the cost involved while troubleshooting the co-culture system. Ultimately, we found that extended culture of the co-culture system in the 24-well plates was sufficient for elastin production. It was this pivot in approach that led to using two different culture times and two different culture substrates and loading conditions.

The experimental groups and controls were as follows: A control group received normal SMC culture media in the early time point group (10 days) and normal SMC culture media along with 200 μL of fibrin gel (fabricated in the same concentrations as the SMC gels) in the late time point group (28 days). Another control group received normal SMC culture media supplemented with 3ng/ml TGF-β1 in the early time point group (10 days) and normal SMC culture media culture media supplemented with 3ng/ml TGF-β1 along with 200 μL of fibrin gel (fabricated in the same concentrations as the SMC gels) in the late time point group (28 days). An

experimental ADMSC co-culture group received a 200 μL fibrin gel containing $4.5x10^6$ ADMSCs on top of the SMC-seeded fibrin gels. An experimental CM group received a mix of culture media containing 50% normal SMC culture media and 50% CM from $9.0x10^6$ ADMSCs in the early time point group (10 days) and the same mixture of media along with 200 μL of fibrin gel (fabricated in the same concentrations as the SMC gels) in the late time point group (28 days).

Treatments lasted for 10 and 28 days for the early and late time points, respectively. Lastly, the early time point gels were all cultured in of Flexcell™ Tissue-Train™ plates (Flexcell Int., Hillsborough, NC) and subjected to 10% stretch at 1 Hz in the stretched loading condition and static, uniaxial constrainment in the constrained loading condition. The constrained loading condition for the late time point consisted on static, radially constrained gels.

Table 4. Experimental group descriptions. Experimental groups are described by treatment, culture time, and loading condition. The number of samples for each group is shown for the ninhydrin assay.

Experimental Group #	Treatment Description	Culture Time	Loading Condition
Group 1	No Treatment (n=3)	10 days	Constrained
Group 2	No Treatment (n=3)	10 days	Stretched
Group 3	TGFβ-1 (n=3)	10 days	Stretched
Group 4	ADMSC Co-culture (n=8)	10 days	Stretched
Group 5	CM (n=8)	10 days	Stretched
Group 6	Fibrin Only (n=2)	10 days	Stretched
Group 7	Rat Aorta (n=1)	N/A	N/A
Group 8	ADMSC Co-culture (n=5)	28 days	Constrained
Group 9	TGFβ-1 (n=5)	28 days	Constrained
Group 10	CM (n=5)	28 days	Constrained
Group 11	No Treatment (n=5)	28 days	Constrained

3.2.4 Qualitative Elastin Fiber Imaging

After culture, the fibrin tissue constructs were prepared for imaging using three modalities. Tissue constructs were lifted from culture plates and put onto glass slides for multiphoton imaging. Additional samples from the late time point group were fixed in 4% paraformaldehyde for 30 minutes before being embedded in paraffin wax and sectioned (5μm) for Verhoeff's Van Gieson and immunofluorescence staining.

An Olympus multi-photon microscope (Model FV10, ASW software) was used to observe elastin. Elastin was automatically detected and visualized based on intrinsic fluorescence (excitation wavelength 780 nm, emission wavelength 525±25 nm).

Paraffin embedded sections were deparaffinized by 3 minute washes in xylene, xylene/ethanol mix, and ever decreasing dilutions of ethanol before being rinsed in tap water. Sections were then stained with Verhoeff's Van Gieson (VVG) stain. Additional sections were labeled for elastin using a standard immunofluorescence (IFC) protocol staining for BA4 (1:200, Sigma #E4013) and a Cy3 conjugated goat anti-mouse (GAM) secondary (1:1000, Sigma #AP124C) with counterstains for DAPI. All sectioned samples were imaged using NIS Elements software (version 4.0).

3.2.5 Quantitative Elastin Protein Detection

After multi-photon microscopy, tissue constructs were analyzed for elastin content using previously published protocols[299,300]. Briefly, basic hydrolysis (0.1 M NaOH, 1 hour at 98°C) and centrifugation will separate insoluble elastin from other tissue construct components. Each fraction will then be fully hydrolyzed in acidic conditions (6 M HCl, 24 hours at 110°C) and then

dried. Total protein and elastin content are determined by a ninhydrin assay compared to standards of known amounts of bovine serum albumen (BSA) and elastin.

3.2.6 Tensile Testing

The VAA described in Chapter 2 and developed specifically for this purpose was clamped into an Instron uniaxial tensile testing system (Instron, #5543a, Norwood, MA,) and tissue constructs from the early time point gels were gently placed next to the open ends of the VAA while the vacuum was turned on. Samples were stretched to initial, unloaded lengths by moving the crosshead until force readings were present. A constant crosshead speed of 0.1 mm/sec was used to pull on the samples, and the applied load and resulting displacement were recorded continuously using the Instron-packaged software (Bluehill, Version 2, Instron, Norwood, MA). Stress, stretch, and other mechanical properties were calculated as described in Sections 2.2.3 and 2.2.4.

3.2.7 Statistics

All statistical analysis was done utilizing Minitab software (version 16) to perform either t-tests or ANOVA. Statistical significance was accepted at $p<0.05$. All data were verified for parametric tests by confirming normality and homogeneity of variance (not shown). Appropriate post-hoc tests when using ANOVA analyses were performed (Fisher's LSD, Tukey).

3.3 RESULTS

3.3.1 Early Time Point Studies from Flexcell Culture Plates

To assess whether ADMSCs could induce adult, human SMCs to produce elastic fibers detectable using common imaging modalities, SMC-seeded fibrin gels were imaged via multiphoton imaging for early time point studies (**Figure 5**). While emission signal was detected at a higher level in Group 4 (**Figure 5, C**) when compared to Group 2 (**Figure 5, A**) and Group 3 (**Figure 5, B**) in the early time point group, the signal was localized to the cell bodies and lacked any fibers or network appearance.

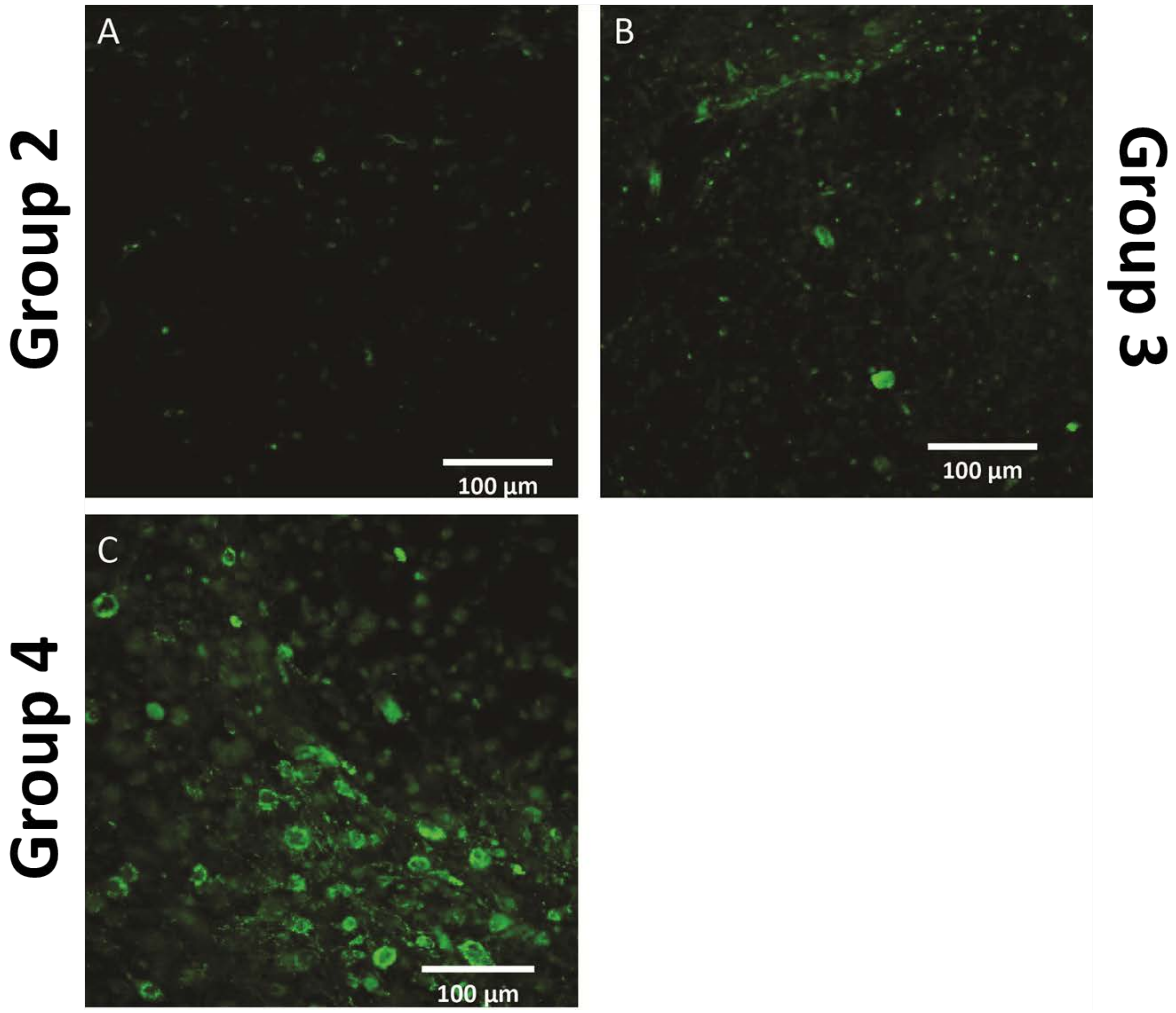

Figure 5. There is little elastin autofluorescence in SMC seeded fibrin gels after 10 days in culture. Elastin autofluorescence images reveal low levels of emission signal in Group 2 (A), slightly higher levels of emission signal in Group 3 (B), and bright signal in Group 4 (C).

To assess whether ADMSCs could induce adult, human SMCs to produce mechanically functional elastic fibers, SMC-seeded fibrin gels from the early time point group were uniaxially tensile tested using the VAA described in Chapter 2. **Table 5** summarizes the results for yield stretch and tangent modulus for all tested groups. One-way ANOVA reveal statistically significant differences in the groups for both yield stretch (p=0.017) and tangent modulus (p=0.003). Subsequent Tukey tests, an ANOVA post-hoc analysis which finds means that are significantly different from each other, revealed that Group 1 had a higher yield stretch than Groups 3, 4, & 5. Tukey test also revealed that Group 1 had a higher tangent modulus than all other tested groups.

Table 5. Constrained gels showed a higher yield stretch than all groups expect the stretched group and a higher tangent modulus than all groups. Measurements for yield stretch and tangent modulus are given as mean ± standard deviation. Tukey groupings identifiers "A" and "B" show which groups have significantly different means. The ADMSC group yielded useful data in 6 of 8 (75%) tests. All other groups yielded useful data in 2of 3 (67%) of tests.

Experimental Group #	Yield Stretch	Tukey Groupings	Tangent Mod. (kPa)	Tukey Groupings
Group 1 (n=2)	2.2±0.5	A	135.5±51.2	A
Group 2 (n=2)	1.3±0.1	A B	24.1±5.8	B
Group 3 (n=2)	1.4±0.1	B	16.2±13.0	B
Group 4 (n=6)	1.4±0.2	B	25.1±19.7	B
Group 5 (n=2)	1.2±0.3	B	18.3±10.7	B
One way ANOVA	p=0.017		p=0.003	

To assess whether ADMSCs could induce adult, human SMCs to produce detectable amounts of insoluble elastic fibers, SMC-seeded fibrin gels were separated into soluble and insoluble components after NaOH boil. The resultant supernatant and pellet were further processed before being measured in a ninhydrin assay. The total amount of insoluble elastin measured in the early time points (**Figure 6**) was statistically different for Group 6 (ANOVA, $p=0.023$). The assay did show detectable amounts of elastin for all other groups. For a better comparison between the groups in the early time point, percentage of elastin was calculated with respect to total protein content (**Figure 7**). The only statistical differences noted were between Group 7 and Groups 1, 2, 4, 5, & 6 (ANOVA, $p=0.042$).

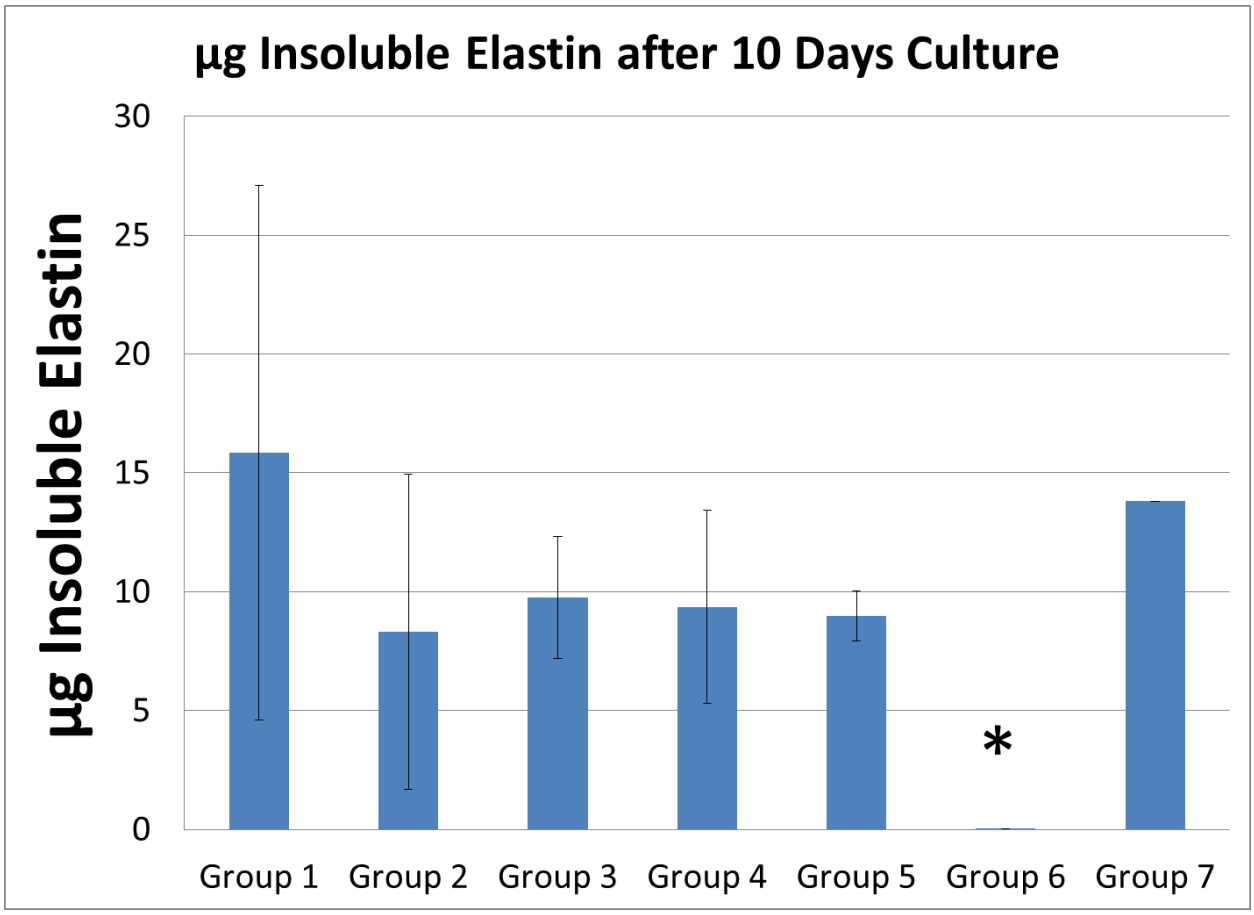

Figure 6. Ninhydrin assay reveals that all groups produced elastin after just 10 days in culture. Values shown as mean ± standard deviation. * indicates significant difference from all other groups.

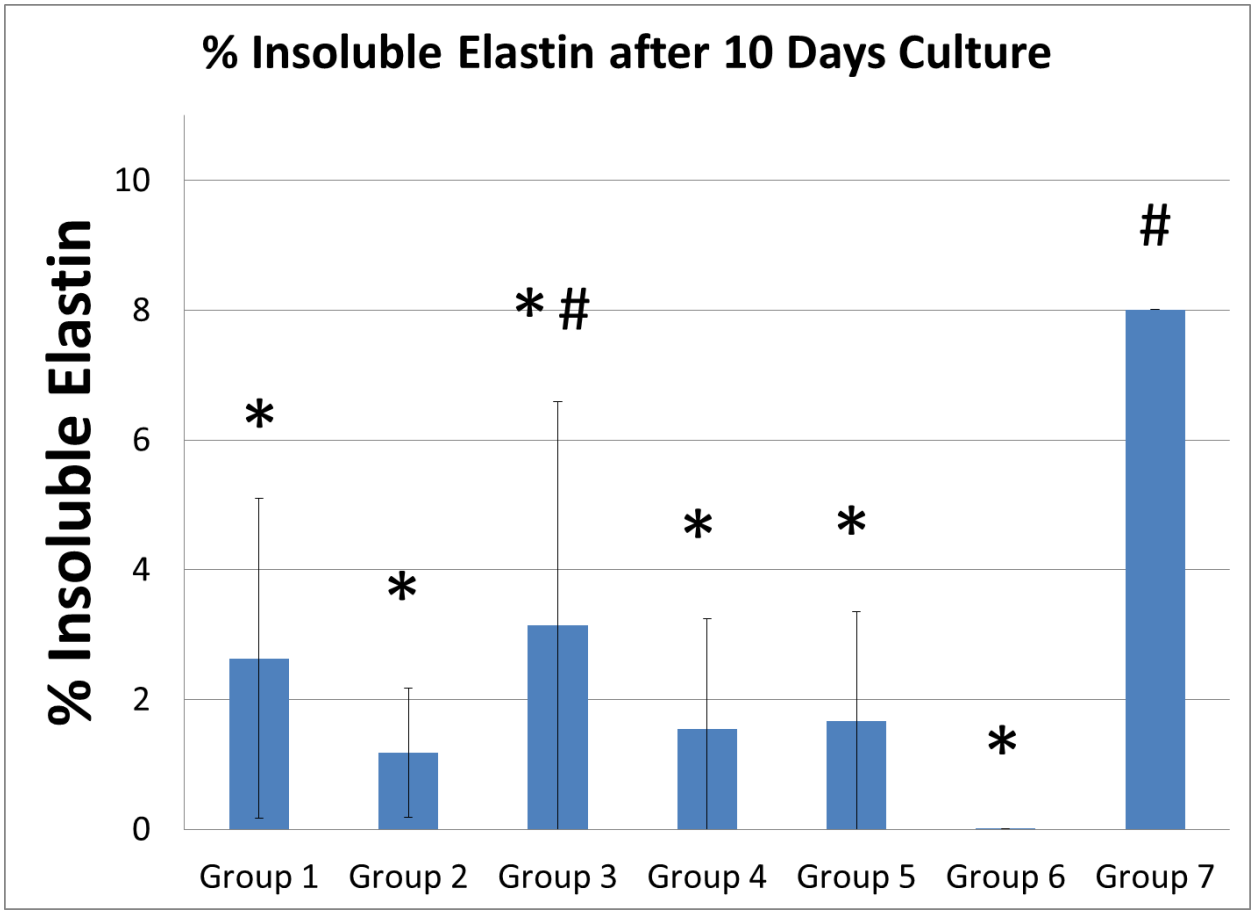

Figure 7. Ninhydrin assay reveals that all groups produced elastin after just 10 days in culture. Values shown as mean ± standard deviation. Statistically different groups are indicated by * and #.

3.3.2 Late Time Point Studies in Tissue Culture Plates

To assess whether ADMSCs could induce adult, human SMCs to produce elastic fibers detectable using common imaging modalities, SMC-seeded fibrin gels were imaged via multiphoton imaging for late time points (**Figure 8**). There seems to be fibers located in Groups 8 & 9 (**Figure 8, A and B,** respectively). The network is far more developed when compared to Group 10 (**Figure 8, C**). Lastly, Group 11 (**Figure 8, D**) merely shows glowing cell bodies.

Additional samples from the late time point groups were stained with VVG (**Figure 9**) and via IFC (**Figure 10**) to reveal elastic fibers and networks. All groups showed faint VVG staining especially noticeable in parts of the gels that seems to have undergone fiber compaction. The IFC stain reveals a much more intense signal that is seen unbroken throughout the gels in Groups 8 & 9 (**Figure 10, B and C,** respectively). This unbroken signal reflects the results shown by the multiphoton imaging and is far more developed when compared to Groups 10 & 11 (**Figure 10, D and E,** respectively) though both groups show small amount of network development.

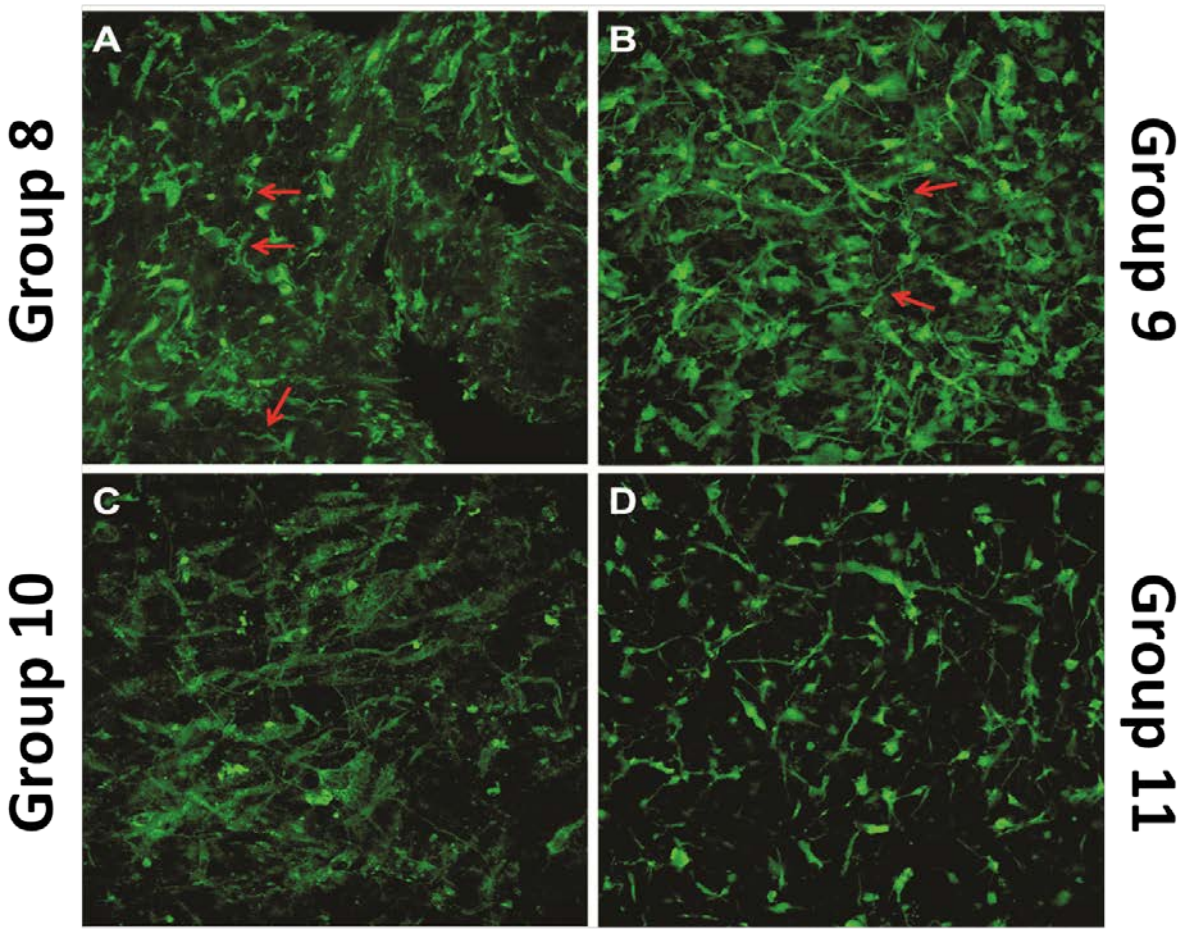

Figure 8. Elastin autofluorescence images reveal a developed elastin network in long term culture. Elastic fibers (red arrows) are seen in Group 8 (A) and Group 9 (B). A less developed network is seen in Group 10 (C), and no network is seen (merely glowing cell outlines) in Group 11 (D).

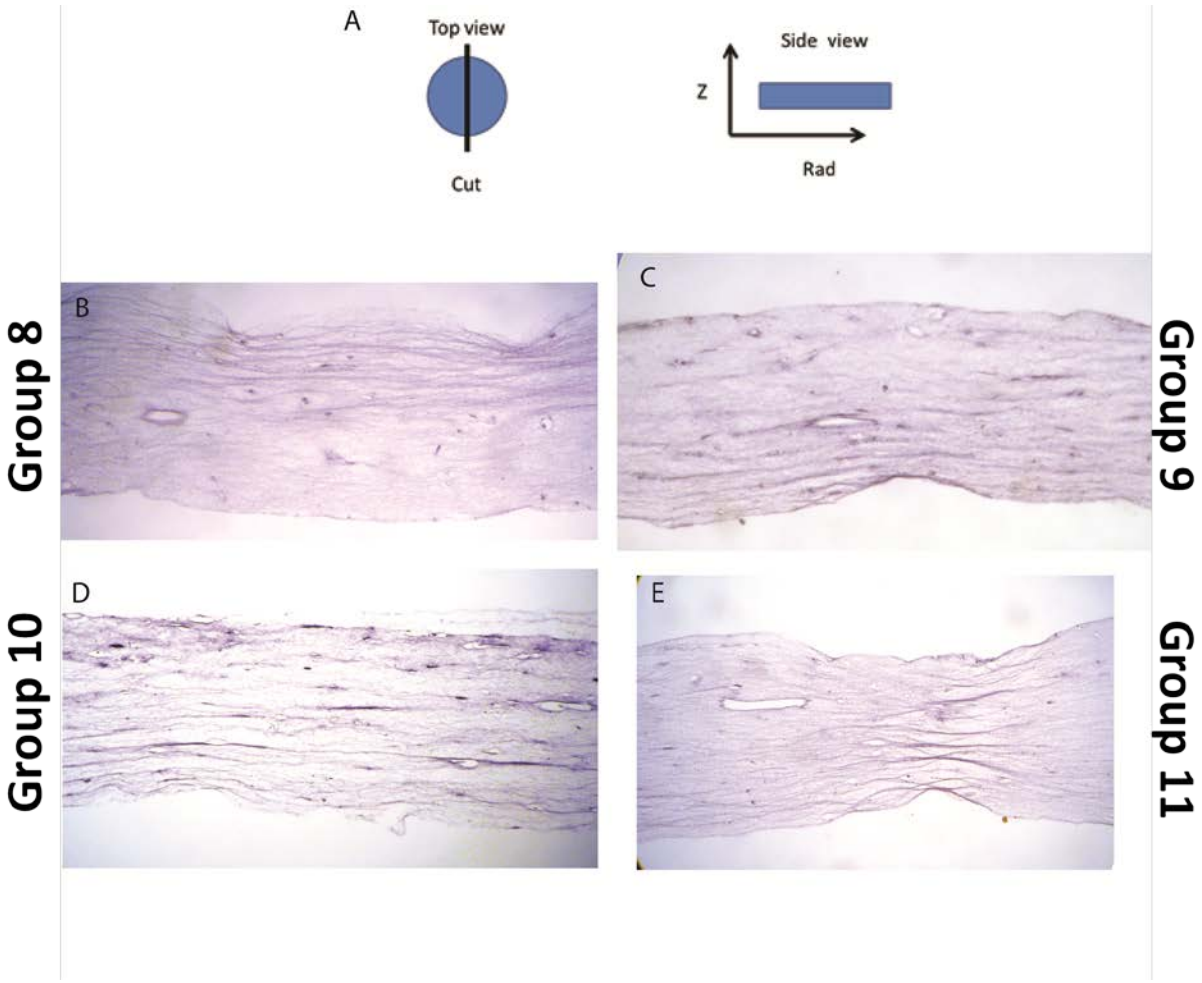

Figure 9. VVG stained images reveal a faint staining in all groups around areas of dense fiber accumulation within the gels. The orientation of the sections is shown at top (A). Group 8 is shown in (B.) Group 9 is shown in (C). Group 10 is shown in (D). Group 11 is shown in (E).

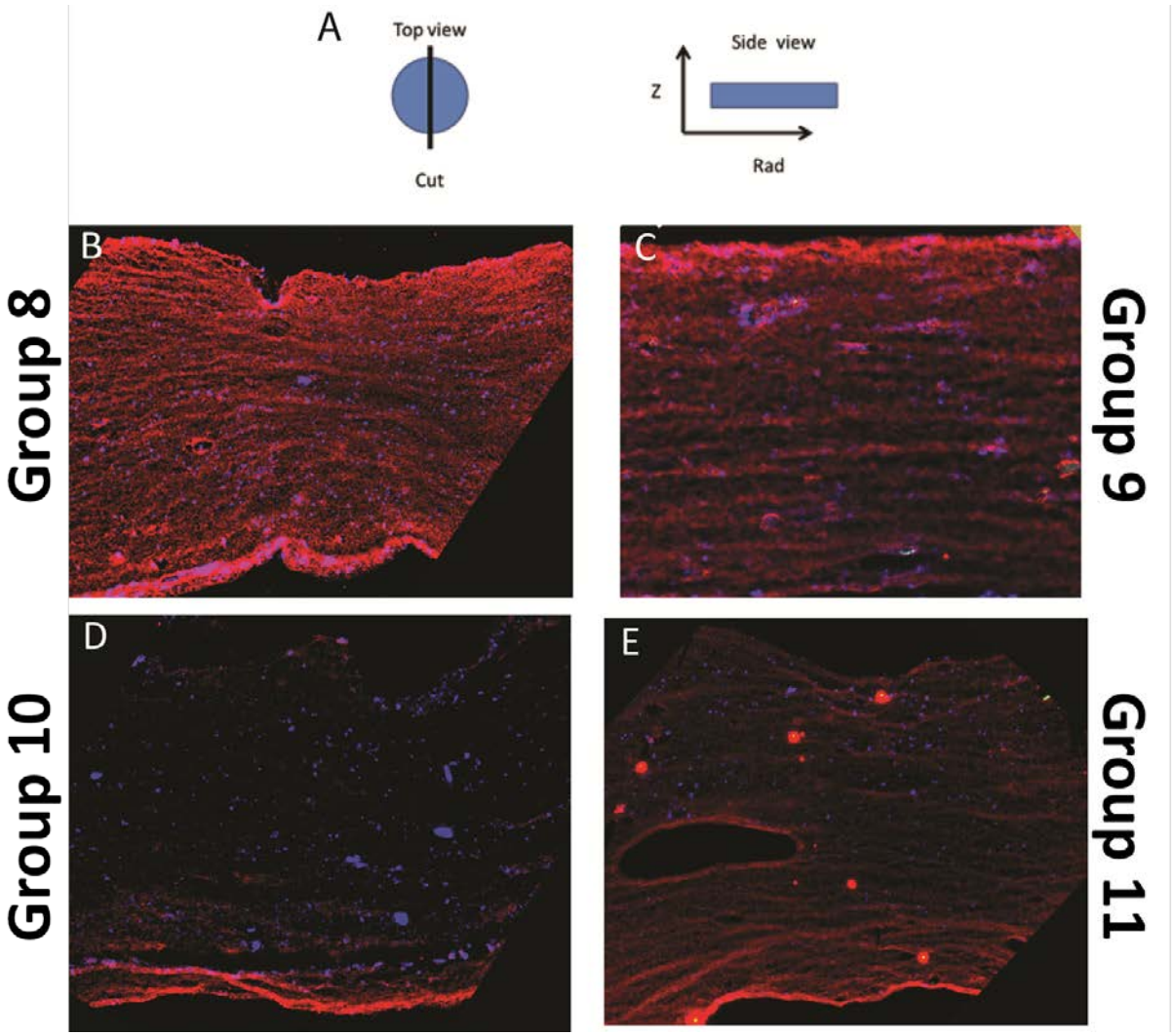

Figure 10. IFC stained images reveal a vivid network at various levels of signal intensity between the experimental groups. The orientation of the sections is shown at top (A). Group 8 is shown in (B.) Group 9 is shown in (C). Group 10 is shown in (D). Group 11 is shown in (E).

The same ninhydrin assay was carried out for the late time point groups. While no statistical difference was shown between any of the groups (ANOVA, p=0.472) when looking at the percent elastin of total protein (**Figure 11**), the assay did reveal that the samples were producing insoluble elastic fibers. The percentage of elastin was calculated with respect to total protein content (**Figure 12**). No statistical difference was shown between any of the groups (ANOVA, p=0.554).

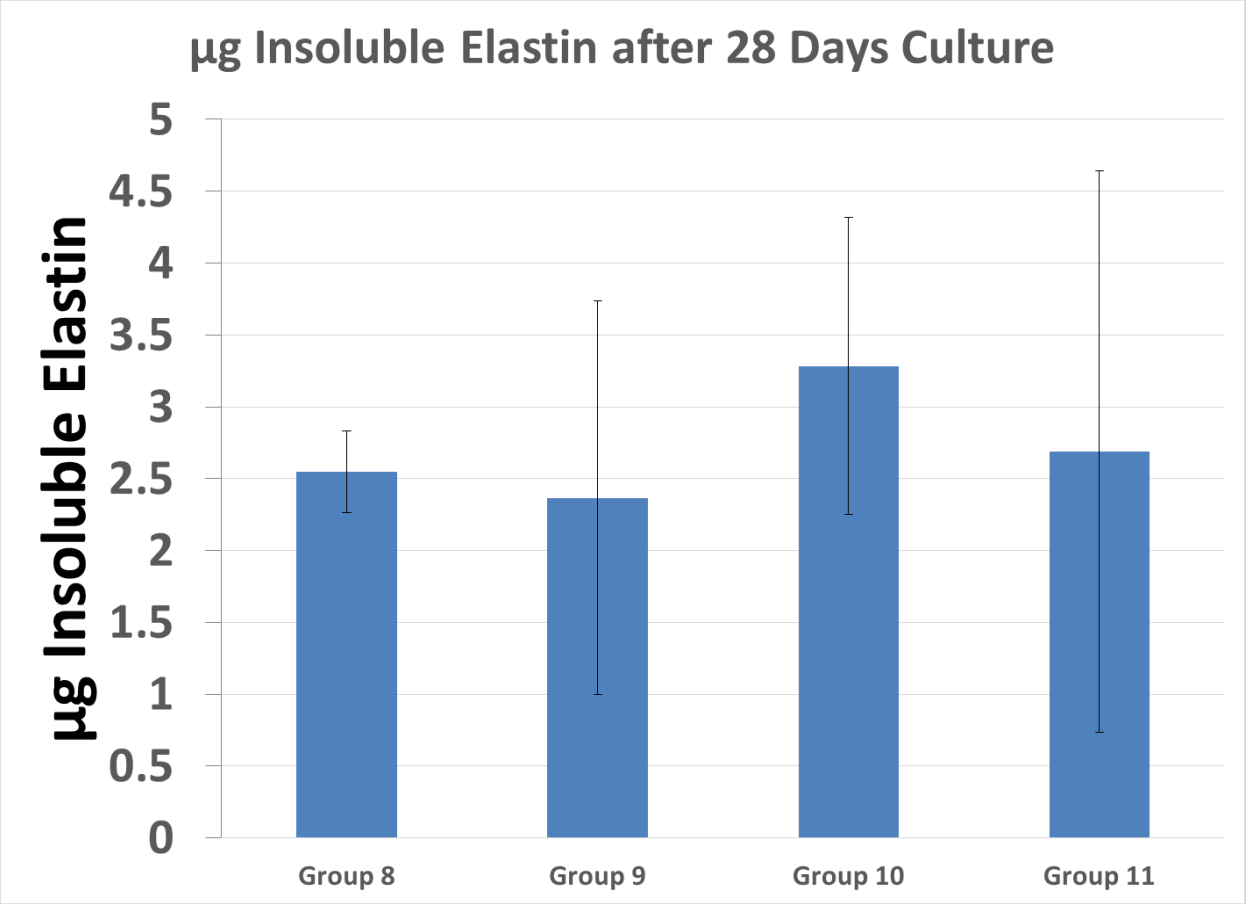

Figure 11. Ninhydrin assay reveals that all groups produced elastin after 28 days in culture. Values shown as mean ± standard deviation.

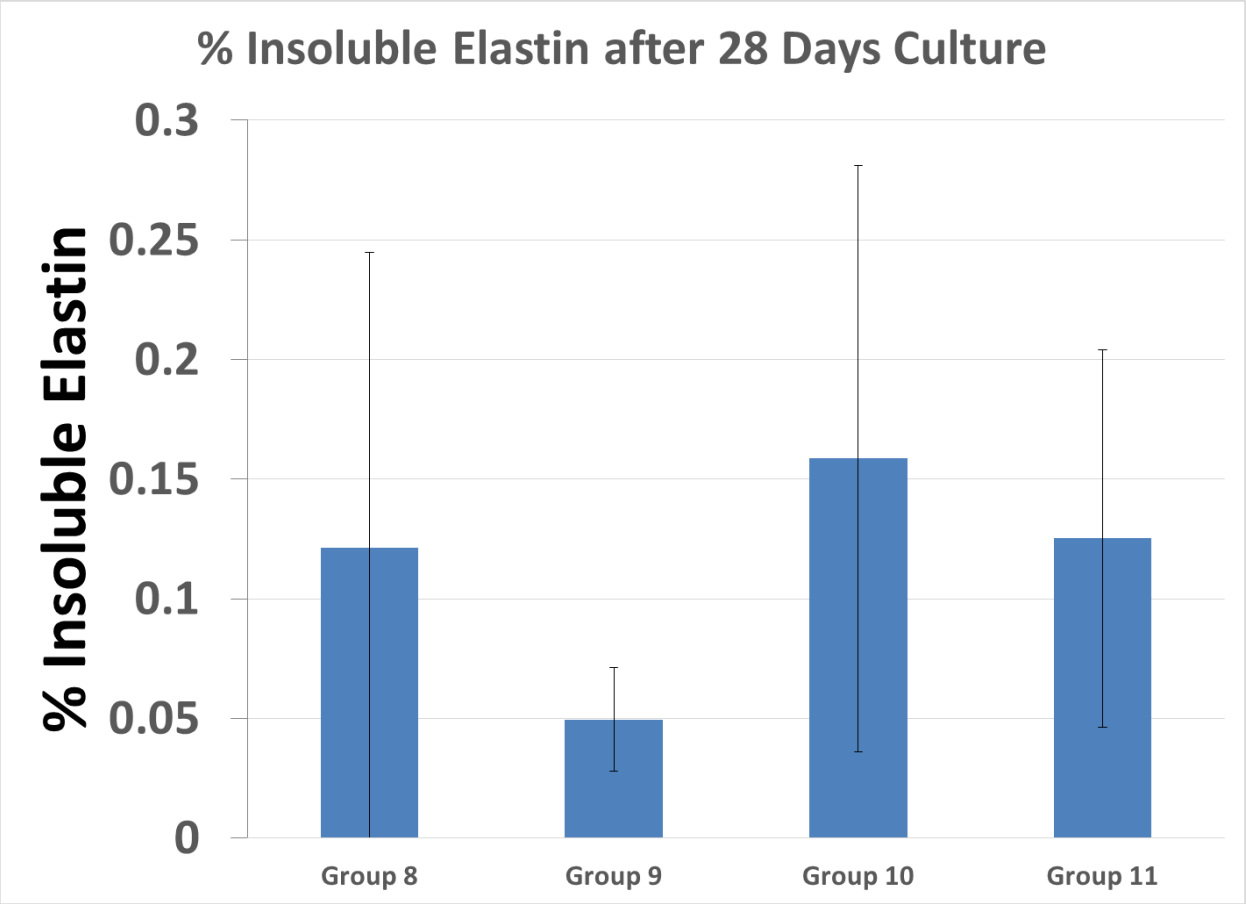

Figure 12. Ninhydrin assay reveals that all groups produced elastin after 28 days in culture. Values shown as mean ± standard deviation.

3.4 DISCUSSION

The gradual breakdown of elastic fibers is seen in a wide variety of tissues such as skin, lung, and arteries. As elastic fibers break down, the resultant elastin degradation products have been shown to upregulate the inflammatory response[78,301-303] and inhibit the switch from M1 macrophages to M2 macrophages[304]. The damage done to adult elastic fiber rich tissue is often repaired with unorganized material that does not function properly[281]. Diseases such as atherosclerosis cause SMCs to deposit amorphous amyloid elastic fibers[305]; however, these easily degraded pseudo-fibers displaying limited crosslinking, are disorganized, and contribute to the pathology. AAAs present an even more complex prospect of regenerating elastic fibers and matrix within an active proteolytic environment featuring local production and activity of elastolytic enzymes by both recruited inflammatory cells and SMCs[306].

Given the complexity of elastic matrix assembly described at the beginning of this chapter, one appreciates the challenges faced when trying to regenerate natural elastic matrix structures by adult SMCs[307] or even less elastogenic, diseased SMCs[305,308,309]. Particularly in the case of AAAs, the challenges described above ultimately reduce the net accumulation of new elastin deposits while disrupting new and pre-existing elastic matrix structures[46]. Knowledge and methods of promoting assembly of precursors into mature, structural, and functional elastic fibers[310] remains fleeting.

The ability of adult SMCs to produce mechanically functional elastic fibers is thought to be necessary for an interventional therapy to work for treating AAAs[2]. Though the resident SMCs within a AAA are synthetic[311] and producing elastin mRNA[52], adults do not normally produce mechanically functional elastic fibers. In this aim we have induced elastic fiber production in adult SMCs as shown by biochemical (**Figure 6, Figure 7, Figure 11, & Figure**

12) and imaging (**Figure 8 & Figure 10**) means which is in line with other published studies stimulating SMCs with TGF-β1[312-314]. This study adds to the field showing that elastic fiber production is also possible by co-culturing SMCs with ADMSCs in a 3D fibrin gel (**Figure 8A & Figure 10B**), and the effect is present but somewhat subdued when treating the same SMCs with CM. This reduced effect is apparent in the multiphoton and IFC imaging of that group showing a less developed elastic network (**Figure 8C & Figure 10D,** respectively). This may be due to the inability of CM to increase LOX expression in SMCs as shown by Swamin et al.[315].

Our working hypothesis is that the ADMSCs are acting in a paracrine manner, producing growth factors that are ultimately responsible for the SMC elastogenesis. The most studied elastogenic factors to date for SMCs are TGF-β1 and IGF-1, which have been shown to increase elastin synthesis both transcriptional and post-translational means. TGF-β1 improves matrix assembly via LOX mRNA expression upregulation and enzyme activity[316] while preventing proteolysis of existing matrix by tipping the balance of MMPs (2 and 9) and TIMPs (1,2,3) in favor of TIMPs[317,318]. Elastogenic effects are enhanced synergistically when TGF-β1 and IGF-1 were provided to healthy SMCs together with the hyaluronan oligomers[319,320]. Exogenous LOX supplemented to rat aortic SMC cultures improves tropoelastin crosslinking significantly, enhancing elastic matrix deposition above what is capable by endogenous LOX enzymes alone[321]. The extracellular transport of endogenous LOX and functional activity of endogenous and exogenous LOX can be further enhanced by copper ions which enable electron transfer from oxygen to facilitate oxidative deamination of lysyl groups in elastin and collagen[287].

Additionally, elastin production has been shown in human vascular smooth muscle cells embedded in 3D scaffolds when stimulated with TGF-β1[313], and TGF-β1 has a dose dependent

effect on elastin production[312,314]. Clearly, the growth factors above have a profound elastogenic effect on adult, human SMCs.

Rather than using growth factors as therapeutic agents directly, MSCs could be used for paracrine effects as they secrete TGF-β1, IFG-1 and other growth factors[194]. This treatment modality could remove concerns about off target effects from treating with supraphysiological concentrations of growth factors, provide a renewable source of growth factors, and allow for synergic effects that could happen when different growth factors are combined[312].

In fact, paracrine factors secreted by MSCs have been shown to evoke in vivo wound healing, tissue repair, and regeneration in different tissue types[322,323]. CM collected from in vitro MSC cultures in real time, or collected and then concentrated, has also been shown to improve cellular health in diseased cells in vitro[324,325], restore tissue/organ state and function in vivo[322,323], and stimulate SMC migration[326,327]. SMC migration is a feature of a synthetic phenotype[21]. Removing SMCs from their native environment likely switches the phenotype from contractile to synthetic, and our paracrine treatment is likely encouraging the cells to remain synthetic while in the 3D fibrin gel. In the context of aneurysm disease, Swamin et al.[315] investigated whether and how exposing diseased SMCs to trophic factors generated by co-cultured BMMSC-derived smooth muscle like cells impacts their matrix synthesis potential. These cultures displayed upregulation of elastin, fibrillin-1, and fibulin-5 expression thus providing the cells with the essential building blocks for elastic fiber and network synthesis.

In light of the published literature regarding elastogenesis, we explored using MSCs - specifically ADMSCs - as therapeutic agents in the treatment of AAA. We believe that these ADMSCs will act as growth factor factories, secreting TGF-β1 as well as other growth factors[194]. Using ADMSCs instead of the factors they produce allows for communication

between the therapeutic cells and the target cells which could in turn produce a more desirable result. In the context of this chapter, the purpose of the ADMSCs is to stimulate the SMCs to produce mature elastic fibers; however, in the overall context of treating AAA, MSCs also attenuate the circulating inflammatory environment[195,328].

While MSCs have been isolated from a variety of tissues and basically everywhere blood vessels are found[329,330], adipose tissue makes for an attractive source of MSCs due to its growing abundance in the western population. ADMSCs express classic mesodermal markers used to classify MSCs (CD44, CD73, CD90, CD105[331]), but ADMSCs also express CD34[332,333], a marked distinct from bone marrow MSCs[334]. Upon definition as a multipotent stem cell in 2001[335] and recent characterization of surface marker profile, genome, and composition[336-340], ADMSC research has extended to fields ranging from regenerative medicine[341-351] to cancer[352-354]. Here we employ the ADMSC as a therapeutic cell to treat AAA with the ultimate goal of stimulating new elastic fiber production.

Since Group 10 (**Figure 8C & Figure 10D**) did not perform as well from a qualitative standpoint as Group 8 (**Figure 8A & Figure 10B**), the ADMSC co-culture may be producing different growth factors due to the culture environment (gel vs. stiff substrate) or in response to signals received from the SMCs. In this regard, the co-culture may be necessary to produce meaningful quantities of mature, fully crosslinked elastic fibers in the context of AAA. While we were unable to quantify differences in the amount of elastin produced from the ninhydrin assay (**Figure 12**), we were able to show that measurable amounts of mature, crosslinked elastin were present in our biochemical assay (**Figure 11**). It should be noted that while the ninhydrin assay is a standard method of detecting insoluble elastin, the method itself is a highly involved process which could explain the high variance seen in the data.

Additionally, during the elastic fiber assembly process, a number of naturally occurring fluorophores such as pyridolamine crosslinks[355] as well as desmosine and isodesmosine[356] elastin crosslinks are trapped within the fiber. Exciting these fluorophores using multiphoton microscopy allows researchers to visualize elastin with intrinsic confocal resolution with great depth penetration due to the use of near-infrared excitation wavelengths. This imaging modality can be used on fresh tissue without sectioning, staining or other preparation. Collagen can also be detected alongside elastin due to its second harmonic (SHG) signal[357]. This technique has been used to investigate the collagen and elastin fiber networks in arteries[217,250,252-254,358,359], heart valves[360,361], and changes in the collagen matrix of porcine cartilage[362]. The multiphoton images from the long term culture ADMSC and TGF-β1 experimental groups clearly show signal in the form of fibers.

Interestingly, the mechanical analysis shows a much higher yield stretch and tangent modulus for Group 1 when compared to the Groups 2-5 (**Table 5**). This means that the resultant gel was stiffer and more distensible which could be explained by an increase in the amount of collagen produced relative to the other groups. Collagen production by SMCs when cultured in fibrin gels has been shown before[267,269,363] and these conditions are somewhat similar to the constrained group. This mechanical analysis has limitations inherent to the material fabrication and assumptions made regarding fibrin gels. We assumed a Poisson's Ratio of 0.25 for all groups although the actual value is likely to change between each group and evolve as ECM is produced. Lastly, we assumed a uniform strain across the length of the sample though this may not be the case.

One of the requirements for a lasting, interventional AAA therapy is the replacement of lost elastic fibers in the aortic wall. While others have shown that MSC treatment can modulate

the circulating inflammatory AAA environment[195,328], another important aspect of interventional AAA therapies, this study is the first to show that ADMSCs are capable of inducing SMCs to produce mature, elastic fibers in an in-vitro analog to our proposed in-vivo treatment.

3.5 CONCLUSION

In conclusion, when co-cultured with adult SMCs in a 3D fibrin gel, ADMSCs stimulate elastic fiber production. This novel finding lends credence to using ADMSCs as a pro-elastogenic therapy for treating AAAs.

3.6 FUTURE WORK

The work presented in this chapter represents an exciting new finding, and will be constructed into a manuscript in combination with the results of Chapter 4. While this Aim makes clear progress in showing that ADMSCs can stimulate elastic fiber production in adult SMCs, future work needs to focus on understanding the mechanism of action as well as improving quantification efforts. Future studies should also focus on extended culture times as we have shown that elastic fiber production seems to take longer than 10 days and appears, qualitatively, by 28 days. Longer time points need to be investigated for this co-culture system in order to understand the time course of elastic fiber production. Lastly, the elastogenic ability of diseased SMCs needs to be compared to the healthy SMCs used in this study. Treating SMCs

with elastase in culture could serve as an intermediate step to using SMCs harvested from aneurysmal tissue.

4.0 SPECIFIC AIM 1, PART 2:

IN-SILICO EFFECTS OF ELASTIN PRODUCTION IN THE CONTEXT OF AAA

The second part of Aim 1 is understanding the potential effects, mechanics, and mechanobiology of elastin production in an expanding AAA. After seeing that elastic fibers are produced by SMCs when co-cultured with ADMSCs in the first part of Aim 1, we introduced elastin production in a constrained mixture model of AAA G&R[25]. By understanding the effects and potential benefits of a pro-elastogenic therapy within the context of a constrained mixture model of AAA G&R, we will be better prepared to carry out future experiments to refine and optimize a pro-elastogenic therapy.

4.1 INTRODUCTION

As discussed in the introduction to this dissertation (Section 1.2.5), models of soft tissue G&R have been around for some time. Specifically, the framework posed by Humphrey and Rajagopal[164] has been refined and proven useful for explaining the processes and trends associated with arterial G&R since its introduction[22-25,96,165,169-171,174-176,178,179,181]. The resulting numerical experiments have predicted trends and behaviors which were then compared to experimental observations. Though not the focus of this dissertation, it is important to

understand the three fundamental hypotheses on which these frameworks rely: constitutive turnover, depositional prestretches, and vasoactivity[22].

The constitutive turnover hypothesis states that synthesizing cells, SMCs in the context of AAAs and relevant to this work, respond to their changing chemo-mechanical environment by turning over the extracellular matrix and via cell proliferation and apoptosis. This hypothesis is based upon experimental observations[100-103], and Fung proposed a conceptual mathematical relation stating that the volumetric growth rate is a function of stress[104]. Fung arrived at this concept while trying to understand the function of residual stress residing in blood vessels. He saw a correlation between the arterial stresses and the change in residual strain. Fung's explanation for this relation was a biological law that related the rate of growth or resorption of tissue with the stress in the tissue. This implied that residual stresses are related to the remodeling of the blood vessel wall (i.e. blood vessels remodel when stresses change). Fung's insight provided a stress-growth relationship which has become a biomechanical foundation for tissue engineering and regenerative medicine. For its use in this chapter, this constitutive turnover hypothesis is governed by **Equation 4-1**:

$$\boldsymbol{m}^{\alpha}(s) = \boldsymbol{m}_0^{\alpha}\left(\frac{\sigma^{\alpha}(s)}{\sigma^{\alpha}(0)} - 1\right) \tag{4-1}$$

In **Equation 4-1**, $\boldsymbol{m}^{\alpha}(s)$ is the net mass production for the α constituent (collagen and smooth muscle) at simulation time, s. The net mass production rate is dependent on $\boldsymbol{m}^{\alpha}_{0,}$ a defined

homeostatic mass production rate, and a scaling factor dependent upon the ratio of the Cauchy stress at time s, $\sigma^{\alpha}(s)$, and the initial homeostatic Cauchy stress, $\sigma^{\alpha}(s)$, for each constituent.

In addition to the stress-volumetric growth rate relation, the constitutive turnover hypothesis also governs the direction in which fibrillar proteins such as collagen are deposited. The local, principal stresses or stretches define the directions of fiber alignment for newly deposited material which affects local anisotropy[106,107]. These concepts can be tested in arterial G&R models by comparing predicted responses to evolved arteries.

Experimental observations[47,364,365] also reveal that cells achieve such G&R by actively manipulating structural proteins during and following deposition. The mechanical forces exerted by synthetic cells during deposition or reorganization are contributing to the mechanical properties exhibited by the extracellular matrix, which can lead to residual stresses in unloaded tissues and thus optimal states of stress in vivo[366].

The next fundamental hypothesis, depositional prestretches, captures the mechanobiology of the cells and states that newly produced constituents are deposited under a state of prestretch. The experimental evidence suggests that synthetic cells are capable of depositing material in varying quantities, in different directions, and in a state of mechanical prestretch[281,364]. This hypothesis covers related phenomena, such as spatial variations in prestretches resulting from differential deposition and cross-linking over specific temporal intervals during development[367,368]. This hypothesis also suggests that constituents possess a potentially unique prestretch[104,369,370]. The depositional prestretch concept is closely related to the constitutive turnover hypothesis with interesting complementary effects. In this chapter, the depositional prestretches for collagen, elastin, and smooth muscle are 1.08, 1.3, and 1.2, respectively.

The last fundamental hypothesis, vasoactivity, is related to smooth muscle contractility. Murray[371] first proposed, through deductive physiology, that the body minimizes metabolic costs by maintaining an optimal volume of blood. This conclusion implied luminal shear stresses must be maintained by arteries actively adjusting their diameter[372,373]. Two separate mechanisms governing smooth muscle activity have been identified[374]: actin–myosin fiber overlap[375] and chemical dosage-response (e.g. acetylcholine and endothelin-1). For example, when subjected to increased shear stresses arteries dilate in response to upregulation of nitric oxide by endothelial cells. Vasoactivity is coupled to matrix remodelling in two phases: acute changes in vascular tone followed by long-term entrenchment[372].

Acutely, activated SMCs allow arteries to rapidly respond to changes in blood flow. Contractile SMCs minimize the metabolic costs associated with maintaining caliber while maintaining the ability to adapt to altered hemodynamic conditions[375]. Though SMCs can accommodate these acute effects (e.g. brief physical exertion), SMCs can also shift its vasoactive response under sustained hemodynamic changes[376] ultimately resetting the artery's caliber. The vasoactive hypothesis has since been demonstrated by numerous observations[377]. For its use in this chapter, this vasoactivity hypothesis is governed by **Equation 4-2**:

$$f_{act}(s) = \frac{\rho^m(s)}{\rho(s)} T_{max} \left(1 - exp\left\{\left[C_b - C_s\left(\frac{\tau_w(s)}{\tau_w(0)} - 1\right)\right]^2\right\}\right) \quad (4\text{-}2)$$

where f_{act}(s) is the active stress generated by the smooth muscle at any simulation time, s. This stress is dependent upon the ratio of smooth muscle density, ρ^m(s), to total density of the

constituents, $\rho(s)$, the maximum force capable of being generated by smooth muscle, T_{max}, the ratio of vasoconstrictors and vasodilators (C_b is the homeostatic ratio and C_s is a scaled factor based on the shear stress), and ratio of the shear stress at time s, $\tau_w(s)$ and the initial homeostatic shear stress, $\tau_w(0)$.

In summary, constrained mixture models of AAA G&R are designed to account for biological features and processes that are essential to both tissue maintenance and adaptation: constitutive turnover, depositional prestretches, and vasoactivity. Moreover, said models are well suited for basic hypothesis generation and testing, such as the one under investigation here – if elastin is produced in a AAA, then the growth of the AAA will slow. The biological appropriateness of these fundamental hypotheses enables the implementation of the model to capture and predict relevant features of the complex time-varying changes in dilatation, composition, and biomechanics of the AAA.

4.2 METHODS

4.2.1 FEA Stress Analysis

Generally speaking, FEA is numerical technique that discretizes and approximates boundary value problems or partial differential equations. As employed in this chapter, FEA is used to solve the solid mechanics problem posed in our study – a vessel experiencing loading on the lumen due to blood pressure. In order to utilize FEA, we must know some prescribed quantities such as displacements or tractions that occur at the boundary, or enclosing geometry. These prescribed quantities are called boundary conditions. The geometry of the object in

question must also be discretized, or meshed, and mechanical properties must be prescribed to discretized element. The mechanical properties describe how each element will deform in response to a force, and the coordinates of each element, or nodes, determine where the linear approximations to the differential equations governing the body's movement will be made.

The implementation of the FEA utilized a two-layered model of AAA with separate mechanical properties for the medial (inner 2/3 of vessel) and adventitial (outer 1/3 of vessel) layers. These mechanical properties are updated based on the growth laws contained within the G&R model which have a time step of two weeks. Boundary conditions were employed such that only radial nodal displacements were permitted, and a pressure of 93 mmHg was prescribed over the lumen of the vessel defined by set of 2D surface elements. When utilizing these assumptions, the problem is reduced to a single-dimensional analysis of the inflation of a thick-walled tube with fixed axial length.

The finite element model was employed with user-specified material properties within FEAP[378] and using a Q1-P0 'mixed' element, based on the three-field variational approach described by Hu and Washizu[379-381]. This element uses linear shape functions for deformations and is appropriate for modeling incompressible materials. The eigenvectors and corresponding eigenvalues were computed using LAPACK[382], and temporal integrations were performed using trapezoidal rule quadrature. All time constants were updated with a temporal resolution of 2 weeks per time step. Results were calculated at the element Gauss points. The mesh utilized 400 eight-noded hexahedral elements (820 nodes in total).

4.2.2 Elastin Production in Tissue Growth and Remodeling Models

An existing constrained mixture model of G&R[25] was modified to allow for elastin production. The existing models do not allow for elastin production as adult cells do not normally produce elastin in its mechanically functional fiber form. The existing model[25] only allows for elastin degradation modeled as exponential decay with a half-life of 40 years which accounts for the only form of elastin degradation within the AAA model. To modify this model for studying an elastogenic therapy, the change in elastin mass parameter (which is negative in the baseline model) was modified to add new elastin to the remaining elastin (making it a net accumulation of elastin). We explored a range of elastin mass production rates (**Table 6**) within the growth and remodeling simulations at various points in the growth history of the AAA. The FEAP input model and custom material property codes can be found in Error! Bookmark not defined..

Table 6. A number of elastin production factors were explored by modifying constrained mixture models of AAA G&R. The values listed are in units of $\mu g/mm^3/2$ weeks. The elastin production factors are multiples of the absolute value of the natural elastin degradation rate calculated at the end of the baseline model run[25]. These values are added to the existing elastin at each time step within the simulation after the elastogenic intervention.

Normal elastin degration rate	-0.675
Elastin Production Factor	
2x	1.350
3x	2.025
4x	2.700
8x	5.400
16x	10.800

4.2.3 Intervention Time Points

A constrained mixture model of G&R was run in order to establish a baseline model for AAA G&R. The implementation was similar to a previously published study by Valentin et al.[25]. The resulting output from this baseline model, the inner and outer diameters of the modeled AAA, is shown in **Figure 13**. The input that starts this model down the path of becoming a AAA is the loss of a predefined, critical amount of elastin (~65% of initial content) and a small amount of collagen and smooth muscle (~3.5% for each). As shown, the model captures characteristic features of AAA such as dilation (increase in both inner and outer diameters) and wall thinning (decrease in difference between outer and inner diameters, shown at least in some AAA cases[383]). Three "time points" are identified in the simulation: the time point when a 30% increase in outer diameter is reached, the time point when a 40% increase in outer diameter is reached, and the time point when a 50% increase in outer diameter is reached, the latter representing the clinical definition of a AAA.

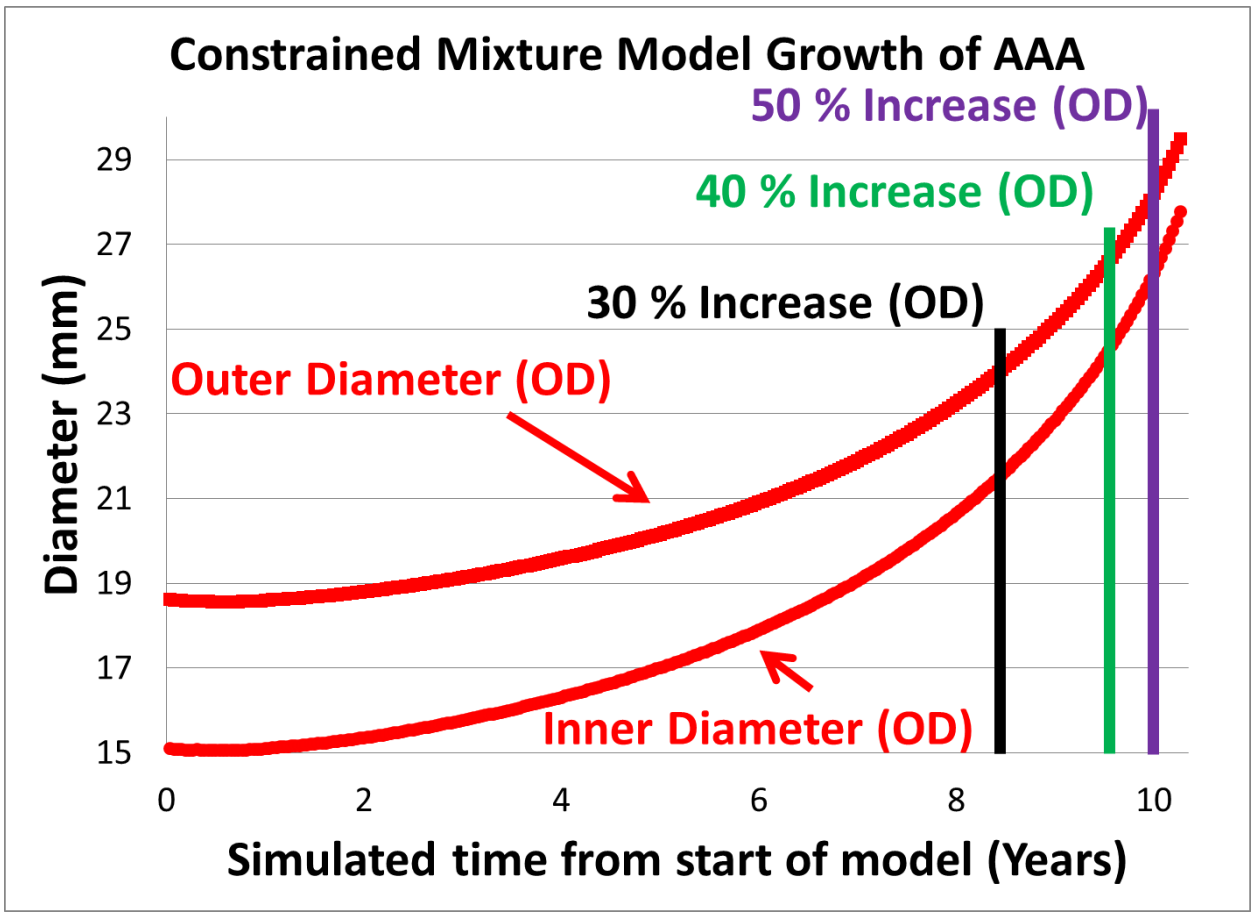

Figure 13. A constrained mixture model of AAA G&R is able to capture known qualities of AAA. The upper red curve represents the progression of the outer diameter of the model AAA while the lower red curve represents progression of the inner diameter of the model AAA. The vertical black, green, and blue lines reflect the time points that the outer diameter is increased by 30%, 40%, and 50%, respectively.

4.2.4 Monitoring Model Properties

In order to understand how elastin production within a constrained mixture model of AAA G&R affects the progression of the disease, the displacement and stress tensor were tracked within the output of the FEA, and the relative amount of collagen in the model was tracked within the custom material property codes. The enlargement rate of the AAA was also calculated for all 15 parameter combinations (5 elastin production factors and 3 intervention time points) at the end of the model run.

A full set of model outputs is provided in **Appendix B**. Here three models are employed: a model that recovers vessel homeostasis, a baseline model without elastogenic intervention, and a model with 2x elastin production at 30% increase in outer diameter. The aortic diameters and changes in collagen, elastin, smooth muscle, and smooth muscle active stress are shown.

4.3 RESULTS

4.3.1 Changes in Diameter with Elastin Production

The inner and outer diameters from the constrained mixture models of AAA G&R featuring elastin production at 50% increase in outer diameter are shown in **Figure 14**. While elastin production does decrease the rate at which the diameter is expanding, the effects are small even at the greatest elastin production factors tested. In **Figure 15**, diameter vs. model simulation time is shown at the various elastin production factors tested for the 40% increase in outer diameter intervention time point. Elastin production slows the dilatation of the AAA more than

the 50% increase time point. In **Figure 16**, again, diameter vs. model simulation time is shown at the various elastin production factors tested but this time for the 30% increase in outer diameter intervention time point. Elastin production slows the dilatation of the AAA to a greater degree than both the 40% and 50% increase time points. The effect is so dramatic at the highest elastin production factors that the both the inner and outer diameter begin to decrease, signifying a contraction of the AAA within the model space. Lastly, **Table 7** shows the calculated rate of outer diameter increase at the end of simulation time for selected model intervention time points and elastin production factors. The rate of aneurysmal enlargement at the end of the baseline model run (~ 10 years simulation time) is 5.340 mm/year.

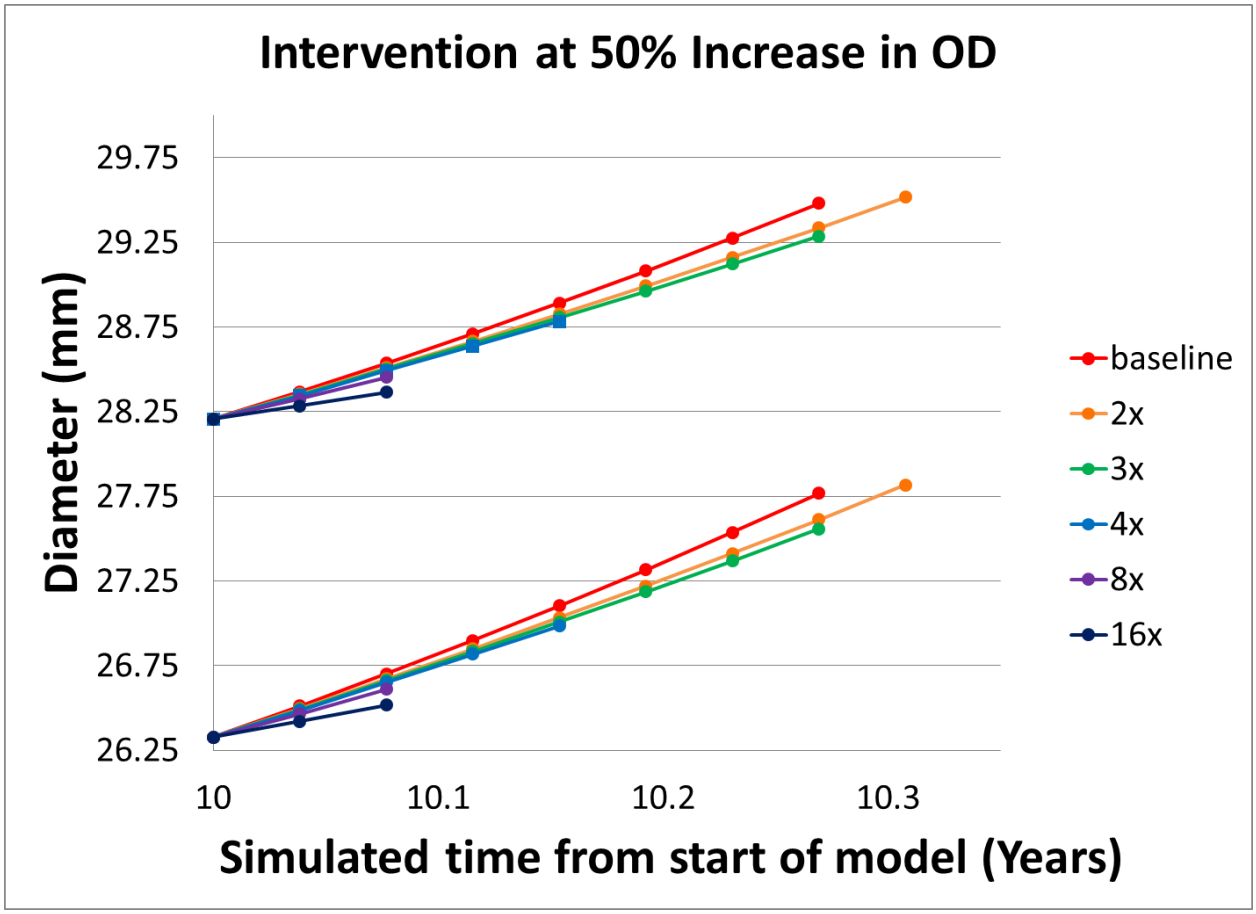

Figure 14. Elastin production at 50% increase in outer diameter moderately slows enlargement. Diameter in mm is shown on the y-axis. Model simulation time is shown on the x-axis. The outer diameters are the top curves, and the inner diameters are bottom curves.

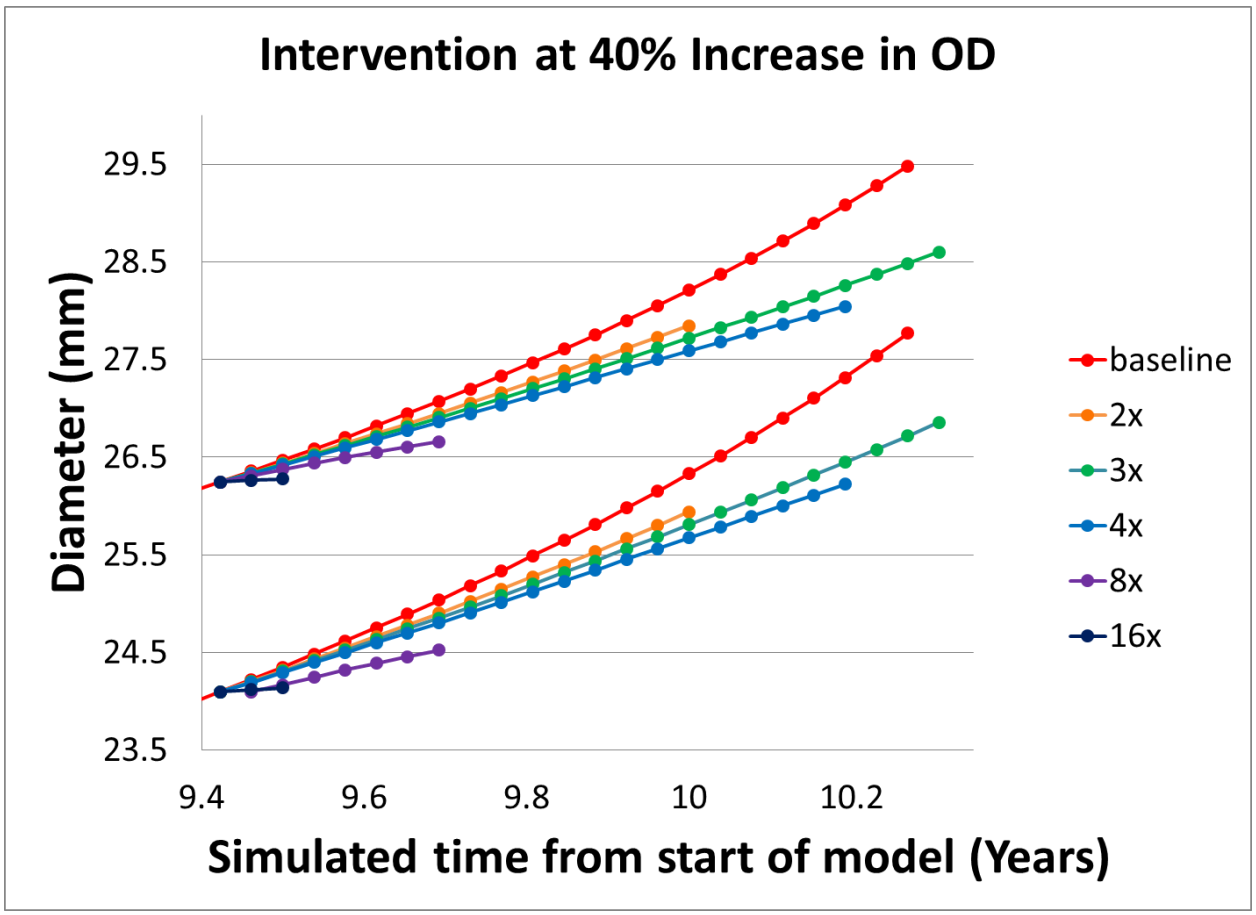

Figure 15. Elastin production at 40% increase in outer diameter slows enlargement to an appreciable extent. Diameter in mm is shown on the y-axis. Model simulation time is shown on the x-axis. The outer diameters are the top curves, and the inner diameters are bottom curves.

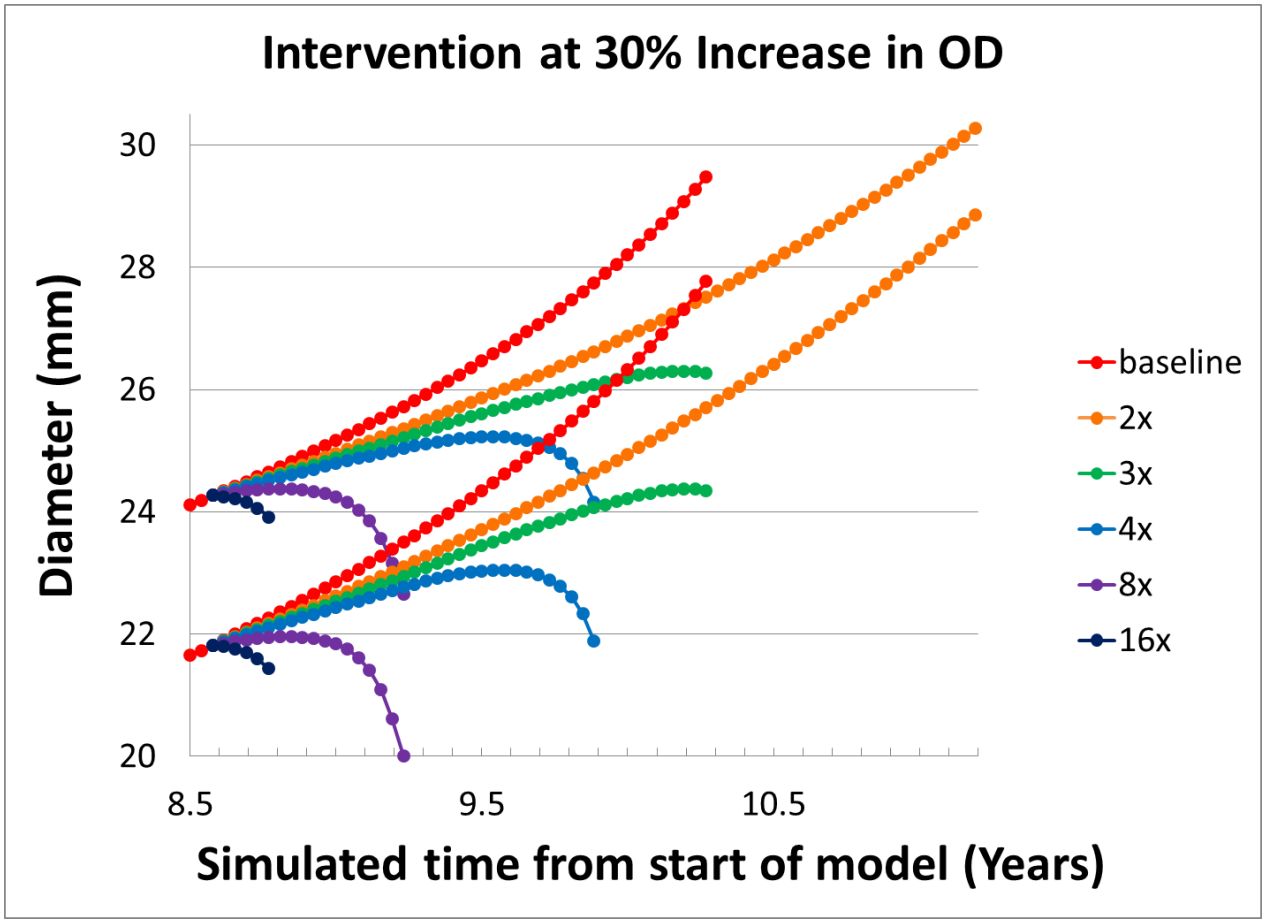

Figure 16. Elastin production at 30% increase in outer diameter greatly slows enlargement and even contracts the aneurysm at higher elastin production factors. Diameter in mm is shown on the y-axis. Model simulation time is shown on the x-axis. The outer diameters are the top curves, and the inner diameters are bottom curves.

Table 7. Increasing elastin production and earlier intervention slows the rate of aneurysmal enlargement. The rate of aneurysmal enlargement (outer diameter) at the end of the baseline model run (~ 10 years simulation time) is 5.340 mm/year. Intervention at 30% growth of the vessel caused the aneurysm to begin to contract at as high as 15.480 mm/year (i.e. residual tension begins to pull the artery back towards its original size) with most elastin production rates.

		Rate of Aneurysm growth (mm/year)		
		Point of Intervention		
		30%	40%	50%
Elastin Production Factor	2x	3.338	3.110	4.711
	3x	-0.692	3.172	4.274
	4x	-13.302	2.356	3.791
	8x	-15.480	1.352	3.302
No Intervention		5.340		

4.3.2 Changes in Collagen Content with Elastin Production

Moving forward, all results shown are from the 30% increase time point featuring the 2x elastin production factor. This model was chosen because the model was able to complete the most time steps in the G&R simulation and thus would provide the most data to compare with the baseline G&R model run. **Figure 17** shows the changes in collagen content over simulated time from the constrained mixture models of AAA G&R featuring 2x elastin production with intervention at 30% increase in outer diameter and the baseline model for the adventitial (top curves) and medial (bottom curves) layers. In **Figure 18 & Figure 19**, we zoom in on the adventitia and media, respectively, to more easily see the differences in the collagen content. The trend for both layers is clear. When elastin is produced in the G&R models, there is an initial net reduction in collagen in both layers compared to the baseline model that returns to the baseline model amounts by the end of the model run.

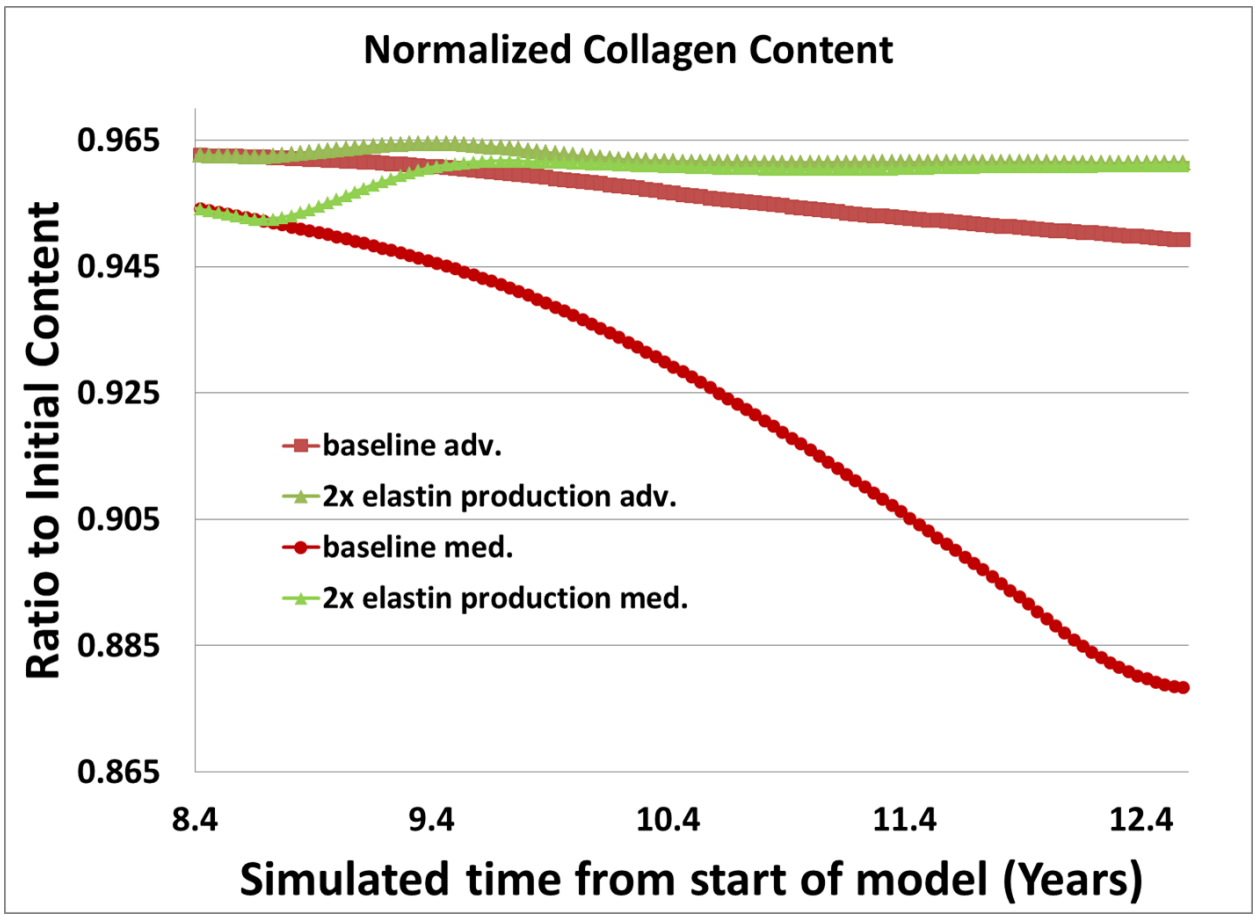

Figure 17. 2x elastin production at 30% increase in outer diameter lowers the amount of collagen in the adventitia and media in constrained mixture models of AAA G&R. The ratio of remaining collagen to initial collagen content is shown on the y-axis. Model simulation time is shown on the x-axis. Average collagen content through the adventitia is shown by the top curves, and average collagen content through the media are bottom curves. The baseline model values are shown in red. The 2x elastin production factors model is shown in green..

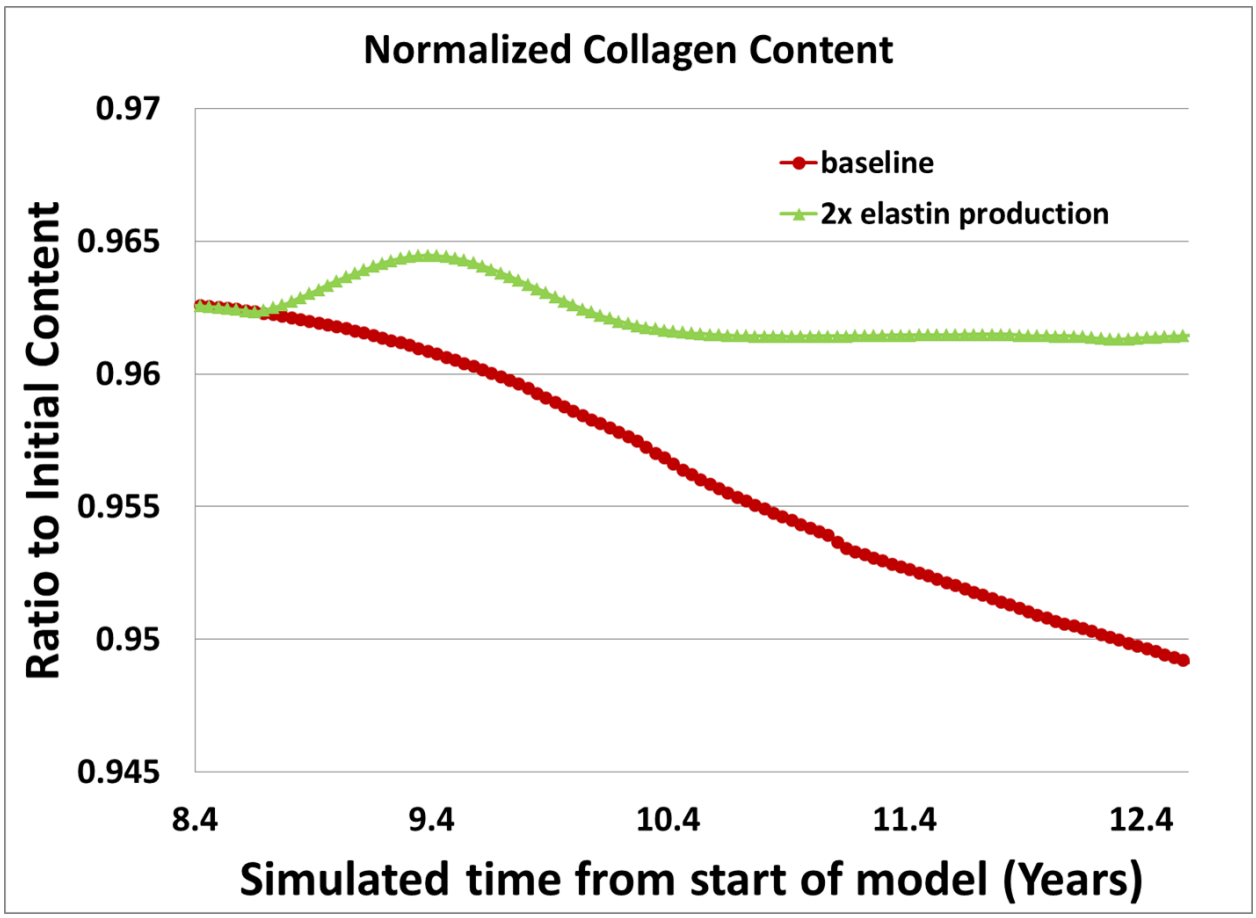

Figure 18. 2x elastin production at 30% increase in outer diameter lowers the amount of collagen in the adventitia in constrained mixture models of AAA G&R. The ratio of remaining collagen to initial collagen content is shown on the y-axis. Model simulation time is shown on the x-axis. The baseline model values are shown in red. The 2x elastin production factors model is shown in green.

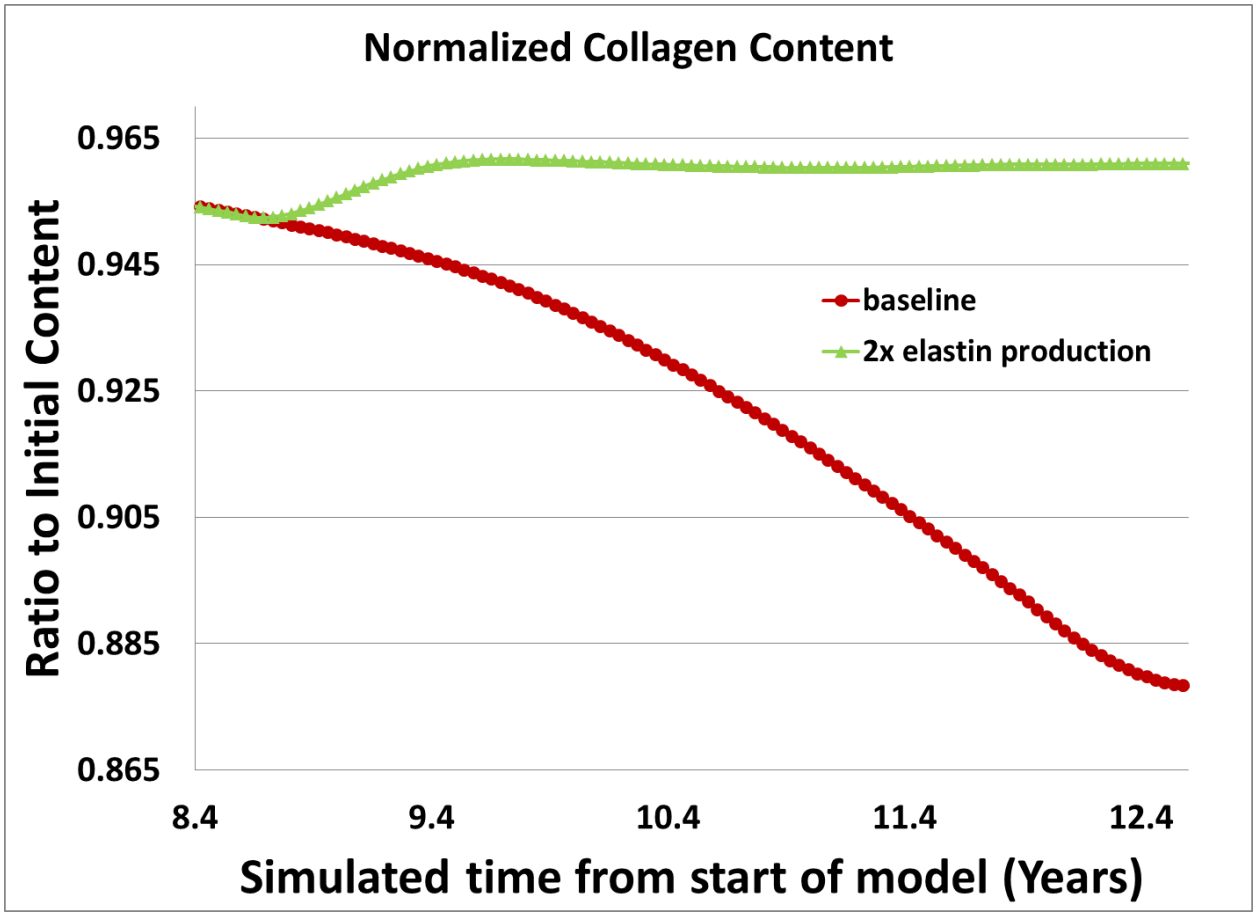

Figure 19. 2x elastin production at 30% increase in outer diameter lowers the amount of collagen in the media in constrained mixture models of AAA G&R. The ratio of remaining collagen to initial collagen content is shown on the y-axis. Model simulation time is shown on the x-axis. The baseline model values are shown in red. The 2x elastin production factors model is shown in green.

4.3.3 Changes in Stress with Elastin Production

Since stress based growth is a driver in the constrained mixture models of AAA G&R employed in this exercise, it is prudent to examine the changes in stress when elastin production is allowed. **Figure 20** shows the calculated von Mises stresses from the constrained mixture models of AAA G&R featuring elastin production at 30% increase in outer diameter and the baseline model for the luminal surface (top curves), the medial-adventitial interface (middle curves), and adventitial surface (bottom curves). The von Mises stress is reduced when elastin is produced in the G&R models through the thickness of the vessel.

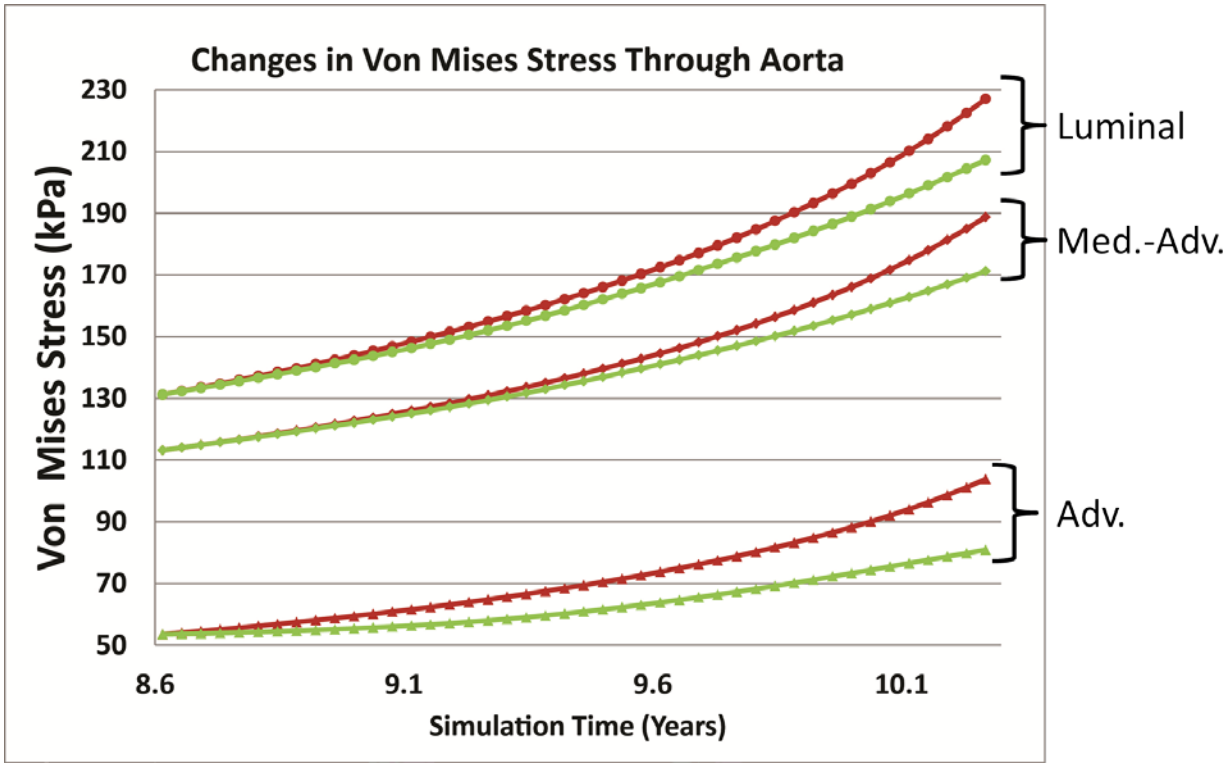

Figure 20. 2x elastin production at 30% increase in outer diameter lowers the amount of collagen in the media in constrained mixture models of AAA G&R. The von Mises stress (kPA) is shown on the y-axis. Model simulation time is shown on the x-axis. The von Mises stresses on the luminal surface are the top curves, the von Mises stresses at the interface between the media and adventitia are the middle curves, and the von Mises stresses on the adventitial surface are the bottom curves. The baseline model values are shown in red. The 2x elastin production factors model is shown in green.

4.4 DISCUSSION

In this study, we modified an existing constrained mixture model of AAA G&R within a 3D finite element framework, a tool that utilizes constrained mixture models that account for chemical and stress based changes in masses and orientations of arterial constituents. Our FEA included physiologically relevant geometry and boundary conditions. Embedded within the custom material properties codes were the key G&R postulates: constitutive turnover, depositional prestretches, and vasoactivity.

The modification of the constrained mixture model of AAA G&R was to allow for elastin production in the material properties codes. This modification was done to mimic a pro-elastogenic therapy for the treatment of an existing and expanding AAA such as the ADMSC treatment explored in-vitro in Chapter 3 and explored in-vivo in Chapter 5. When elastin is allowed to be produced, we are able to capture and predict relevant features of the complex time-varying changes in dilatation, composition, and biomechanics of the AAA.

Some important distinctions should be made between the computational AAA G&R model and what is actually happening in physical AAAs. In the AAA G&R model, elastin is slowly degraded, but this degradation in the G&R model is a degradation of mechanically functional elastin. This would be analogous to breaks in the elastic fibers in a physical AAAs and less insoluble elastin in the tissue. Tissue from AAA patients has been shown to contain less insoluble elastin that non-aneurysmal tissue even though mRNA levels are similar[52]. The amount of insoluble elastin has also been shown to decrease with increasing AAA diameters[384] which is similar to what we see in the baseline AAA G&R models.

In all experimental cases examined, the rate of diameter enlargement of the AAA was slowed. We speculated that this would be the case due to the distensibility and recoil properties

of elastin which is akin to adding stretched rubber bands around an inflated rubber tube. A question we sought to answer with respect to the dilatation of the AAA was how much newly produced elastin would be necessary to produce a desired result (i.e., a reduction of the enlargement rate by 50%). This figure was selected because it has been postulated that reducing the enlargement rate by 50% would remove the need for surgery by ten years[385]. A number of experimental cases met or came close to this desired result which can be seen in **Table 7**. Less elastin production is necessary the sooner the intervention is initiated.

After seeing that the 50% reduction in enlargement rate is obtainable, we turned our focus to the collagen composition of the artery. Focusing on the 30% intervention time point with the 2x elastin production factor, we examined the collagen content relative to the amount of collagen at the start of the simulation. Compared to the baseline AAA G&R model, the amount of collagen is lower in the adventitia and media when elastin is produced. In both layers, there is an initial net increase in collagen when the elastin production is turned on, but by the end of the simulation, the amount of collagen is largely unchanging. The adventitia is particularly interesting as seen in **Figure 18**. The amount of collagen in the elastin production model is increased initially and then starts to decrease before leveling off. There seems to be competing interests between the stress based collagen production and the vasoactivity which is being influenced by the changes in diameter due to elastin production. Smaller diameters are leading to less stretch on the existing SMCs thus allowing the SMCs to produce more active stress.

The overall lower reduction in relative amounts of collagen production in the elastin production model compared to the baseline model can partially be explained by the lower von Mises stress shown in **Figure 20**. The lower von Mises stress leads to less collagen production with the material properties codes which is one of the fundamental hypothesis built into the G&R

models, stress based constitutive turnover. Additionally, part of the stress is being shifted to the newly produced elastin, and some is being shifted to SMCs that are able to produce more active stress when they are stretched less.

The chosen constrained mixture model of AAA G&R is an 'integral-based' approach where the total history of the arterial constituents is accounted for over a finite model simulation time. There are other G&R models such as the 'rate-based' approach introduced by Watton et al. [386] where physiologically determined remodelling rates for constituents are used to predicted dilations of the aneurysm. The integral approach can account for time-varying mass production and degradation rates while retaining their biological interpretations, an advantage over the rate-based approaches. However, an integral-based formulation is computationally demanding requiring mass amounts of memory. In contrast, the rate-based approach used by Watton above and others[387,388] is more computationally expedient.

There are other inherent limitations to the general framework of the constrained mixture model of AAA G&R used in this study. Due to the discretization of the results, error can arise in slight deviations from the desired loaded geometry which changes the initial conditions for the time-dependent G&R simulation. While these differences are initially small, these errors manifest as compounding errors in the kinetics modeling. Some of the accumulation of error can be reduced by variable temporal resolutions. Additionally, variable temporal resolutions may be necessary and useful to investigate some of the more peculiar observations such as the amount of collagen found in the adventitia in **Figure 18**.

Lastly, it should be noted that in this implementation, newly formed fibers are deposited in a constant direction. This is because our simplified case produces a first principal stresses in a constant, circumferential direction. However, the principal stress directions are not necessarily

constant, and non-constant principal stresses will be seen in irregularly shaped aneurysms that are not captured in this implementation.

In the baseline AAA G&R models, the loss of elastin leads to luminal expansion and ineffective vasoactivity due to stretched SMCs, behaviors that are consistent with the physical manifestation of AAAs. One of the inherent compensation mechanisms on display in the model is the local stiffening of collagen shown in the increases von Mises stresses in the model. In contrast, when elastin production is allowed in our simulations, three things are clear: a decrease in diameter enlargement, a decrease in short term collagen deposition, and a decrease in von Mises stress.

4.5 CONCLUSION

The results of this study show that elastin production within an aneurysm could relieve the maladaptive mechanical environment to an extent that slows aneurysmal enlargement. Early intervention can reduce the enlargement rate by more than 50%, potentially delaying the need for surgical intervention by 10 years[385]. These findings also confirm our thoughts that regeneration of functional elastic fibers in a AAA can help slow the progression of the disease.

4.6 FUTURE WORK

These exciting results can be used to guide future experiments that study elastin production. They can also be used as a starting point for optimizing treatment protocols for AAA

therapies such as MSC therapy. Additional work needs to be devoted towards addressing computational limitations through creative problem posing such as changing the temporal resolution of the time step, creative coding that optimizes the problem for parallel computing, and upgrades in computational hardware. Studies should also be devoted to some of the more interesting changes in collagen content that are displayed in **Figure 18**.

5.0 SPECIFIC AIM 2: PERIADVENTITIAL ADMSC THERAPY TO SLOW AND/OR REVERSE THE PROGRESSION OF AN ELASTASE PERFUSED AAA

In Aim 2 we tested an ADMSC based therapy in a mouse elastase perfusion model of AAA. We tested two ADMSC delivery methods: in saline suspension and within a fibrin gel. We then evaluated the treatment using physical measurements, histological characterization, and mechanical testing. The work presented in Aim 2 that utilized the saline suspension cell delivery has been previously published[140].

5.1 INTRODUCTION

AAA rupture was the cause of mortality in over 11,000 cases in 2008 in the US[116]. Large AAAs (>6.0 cm diameter) expand more rapidly than small AAAs (<4.0 cm diameter) with the former expanding 7 to 8 mm annually while the latter only expand 1 to 4 mm annually. As demonstrated by the slow growth rate of small AAAs, the disease can take years to reach a size when surgical intervention is recommended (> 5.5 cm diameter) which is the endovascular placement of a synthetic graft to physically exclude the aneurysmal aorta. Surgical intervention does not benefit small AAAs[118], and management of these patients is limited to "watchful waiting" (i.e., serial imaging of the AAA progression until the threshold for surgical treatment is

met.) Additionally, the use of pharmaceutical treatment to alter the progression of small AAAs has been proven ineffective[184,389,390].

The process of aneurysmal enlargement is complex, involving inflammatory cells, increased MMP activity leading to elastin and collagen degradation, smooth muscle apoptosis, and hypoxia mediated weakening[114]. These processes are heavily based on cellular activity, therefore AAAs represent an optimal target for regenerative MSC based therapy. MSCs have the ability to secrete growth factors[193,194] which could suppress inflammation and MMP activity while stimulating elastin and collagen production. MSCs can also differentiate, thus providing a potential means to replace lost smooth muscle cells. Furthermore, MSCs have already shown promise as a treatment for AAAs in animal models when delivered systemically[195] and by direct injection into the aortic wall[133] immediately after an elastase insult. Though the former study showed a reduction in the inflammatory response suggesting a paracrine mechanism of action, systemic delivery of cells may encounter physical barriers such as atherosclerotic plaques and ILT. The latter showed displayed MSC engraftment into the aneurysmal wall allowing for the possibility of MSC differentiation, but this delivery method which would require puncturing a weakened AAA wall could be troublesome to a vascular surgeon in a clinical setting.

These approaches have proven useful in evaluating the effects of MSCs on the diseased condition showing a proof of concept for the stem cell treatment of AAA. However, AAA is a complex disease that takes years to fully develop to the stage where medical intervention is necessary. In humans, the exact moment when sufficient elastin is lost and the disease is initiated is unknown. Therefore, any clinical stem cell based therapy would be delivered well into the disease progression. The lapse between disease onset and diagnosis presents the need for an alternate therapeutic model. The objective of this study was to explore an alternative therapeutic

model using localized, delayed delivery of MSCs to an established and expanding aneurysm in an animal model.

5.2 METHODS

5.2.1 Culture of MSCs

OriCell™ C57BL/6 green fluorescent protein (GFP) labeled murine ADMSCs were purchased commercially (Cyagen Biosciences Inc., Santa Clara, CA.) The ADMSCs were cultured according to the manufacturer's protocols. Briefly, the ADMSCs were cultured at 37°C and 5.0% CO2 with OriCell™ Adipose-derived Stem Cell Growth Medium (10% fetal bovine serum, 1% penicillin-streptomycin, 1% glutamine; Cyagen Biosciences Inc., Santa Clara, CA.) The ADMSCs were used between passages 6–10. Media changes were performed every 2-3 days. Once the ADMSCs were approximately 80-90% confluent, the ADMSCs were washed three times in phosphate-buffered saline and then incubated with Trypsin-EDTA (Gibco, Life Technologies, Grand Island, NY) solution for 5 min to remove them from the flasks. These cells were used in the saline suspension delivery method.

Commercially sourced human ADMSCs (Thermo Fisher Scientific, #R7788110) were cultured in 75-cm^2 or 175-cm^2 tissue culture flasks (Corning) and grown under defined culture media [1:1 Dulbecco's modified Eagle's medium (DMEM; Gibco #11965) to DMEM/F12 (Gibco #113300) with 10% fetal bovine serum (Atlanta Biologics #S11550), antibiotics (1% Pen/Strep, 0.5% Fungizone, 0.1% Gentamycin), and 10 µL of 10 mM dexamethasone] mixed with 25% Preadipocyte Growth Medium (#C-27410, #C-39425; PromoCell). Culture media was

changed every 2-3 days and when ADMSCs were expanded to near confluence, they were passage expanded utilizing 0.25% trypsin-EDTA (#25200-056; Gibco) or utilized for subsequent experimentation. These cells were used in the fibrin gel delivery method.

5.2.2 Elastase Perfusion

Adult male mice were subjected to transient elastase perfusion of the abdominal aorta as described previously[69,76,139,157,391]. Briefly, after sedation and sterile preparation, a midline laparotomy was made to expose the peritoneum. Once abdominal contents were displaced in moistened gauze, a small incision was made in the mouse's right retroperitoneal muscle. Forceps created a subcutaneous space, and then a subcutaneous microport (Instech, Plymouth Meeting, PA) connected to a polyurethane catheter tubing (Braintree Scientific, Braintree, MA) was attached and placed in the retroperitoneal space. The exposed tubing was set aside to proceed with dissection of the infrarenal aorta. The surrounding tissues were cleaned peri-aortically, and the diameter was measured under magnification with a micrometer. A segment of infrarenal aorta was isolated, and a 5-minute perfusion was performed through an arteriotomy at 100 mm Hg with a solution containing type I porcine pancreatic elastase (PPE, 0.16 U/mL; Sigma-Aldrich, St. Louis, MO). All of the experiments were performed with a single PPE preparation derived from the same commercial source and lot. Following aortic perfusion the arteriotomy was repaired, an Ivalon sponge (5mm x 8mm) was connected to the end of the set aside tubing, and the sponge was tacked in place over the aorta (for schematic see **Figure 21**). The incision was closed, and the animal was allowed to completely recover before returning to standard housing. The animals were maintained in standard housing with ad libitum access to standard food and water for 14 days.

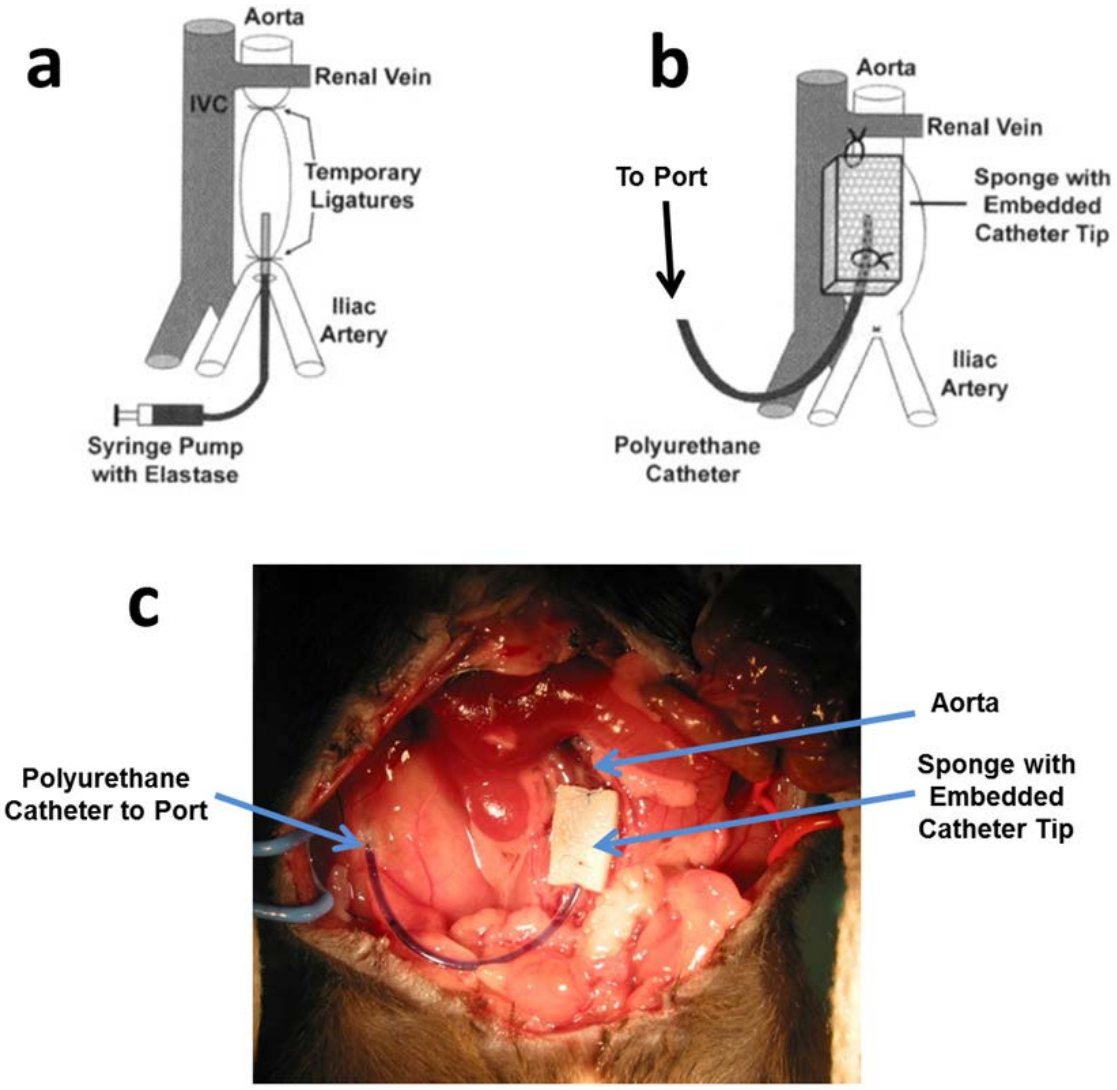

Figure 21. Elastase perfusion and localized adipose-derived mesenchymal stem cells treatment. (A) Schematic representing elastase perfusion. (B) Schematic demonstrating our delayed, localized delivery system. (C) Photograph of delayed, localized delivery system in place after elastase perfusion. (A & B) adapted with permission from Bartoli et. al[120].

5.2.3 ADMSC Delivery

For experimental consistency, all groups had the local delivery sponge in place, and the elastase perfusion surgery (denoting day 0) was performed on all groups. Two ADMSC delivery methods were tested: in saline suspension and within a fibrin gel. The saline suspension delivery method was the first method explored as a proof-of-concept study. The fibrin gel delivery method was added in an attempt to improve ADMSC retention. In the saline suspension delivery, the groups were as follows (**Figure 22**): 1) An early aneurysm group that was sacrificed on day 5 prior to any injection in order to demonstrate successful aneurysm induction (n=3.) 2) An untreated aneurysm group was given 400 μl of saline via port injection on day 5. The mice were sacrificed on day 14 (n=6.) 3) A local ADMSC delivery group was given $1x10^5$ ADMSCs suspended in 400 μl of saline via port injection on day 5. The mice were sacrificed on day 14 (n=9, 7 animals survived to day 14; cell concentration = $2.5x10^5$ cells/mL.) All saline delivered ADMSC experiments were performed at Washington University in St. Louis in the laboratory of Dr. John Curci.

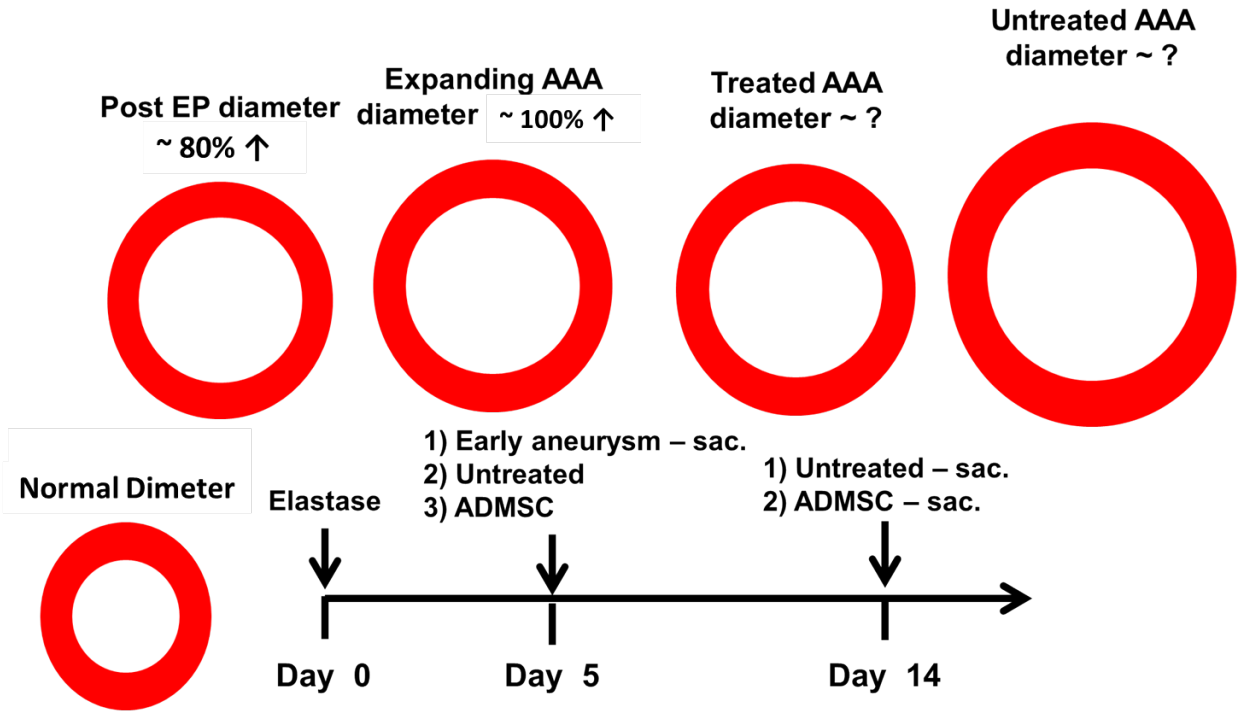

Figure 22. Experimental and control groups for saline delivery. Day 0 denotes elastase perfusion surgery and AAA induction. On day 5, post-elastase perfusion (D5 post-EP) animals were sacrificed in order to demonstrate successful aneurysm induction (n = 3, early aneurysm group). On D5 post-EP, treatment group animals were given stem cell therapy via port injection and were sacrificed on D14 post-EP (n = 9, seven animals survived to D14 post-EP, local ADMSCs treatment group). On D5 post-EP, untreated control group animals were given 400 µl of saline via port injection and were sacrificed on D14 post-EP (n = 6, untreated aneurysm group).

When using fibrin as a delivery vehicle for the ADMSCs to allow for the potential increase in ADMSC engraftment to the periadventitial AAA wall, the groups were as follows: 1) An untreated control group where saline was delivered via port injection on day 6. The mice were sacrificed on day 15 (n=4.) 2) A local ADMSC delivery group was given $1x10^5$ ADMSCs suspended in 250 μl of fibrin gel via port injection on day 6. The mice were sacrificed on day 15 (n=10; fibrinogen concentration = 3 mg/mL, thrombin concentration = 1 NIHU/mL, cell concentration = $4.0x10^5$ cells/mL.). 3) A local, acellular fibrin delivery group was given 250 μl of fibrin gel via port injection on day 6. The mice were sacrificed on day 15 (n=23; fibrinogen concentration = 3 mg/mL, thrombin concentration = 1 NIHU/mL). ADMSC-seeded fibrin gels were mixed from constituent solutions as a single batch for delivery. Up to three mice at a time were injected for the cell based treatments. These mice were further grouped by the order in which they were injected from the single batch of ADMSC-seeded fibrin gel for diameter analysis. The group labeled "injection 1" consisted of animals that received the first injection from the single batch of ADMSC-seeded fibrin gel. The group labeled "injection 2 or 3" consisted of animals that received the second or third injection from the single batch of ADMSC-seeded fibrin gel. It should be noted that the treatment delivery and harvest occurred at days 6 and 15, respectively. These values are each one day later than the saline delivery counterparts described in Section 5.2.3. All fibrin delivered ADMSC experiments were performed at Vanderbilt University in the laboratory of Dr. John Curci.

5.2.4 Aorta Diameter Measurement

Two weeks following elastase perfusion, the mice were again anesthetized, and the laparotomy incision was reopened. Final aortic diameter was measured in vivo with an ocular grid prior to sacrifice. Animals were euthanized, and the entire perfused segment of aorta was harvested for further analysis. The diameter data are presented as a % increase in diameter defined as the difference in final and initial diameters divided by the initial diameter and multiplied by 100 to be expressed as a percentage.

5.2.5 Histological Characterization of Aorta

Aortic specimens were formalin fixed for 24 hours before being preserved via paraffin embedding. Paraffin embedded tissue blocks were sectioned using a microtome at 5 μm thickness. Before staining, sections were deparaffinized and rehydrated by consecutive washes in xylene, alcohol, and de-ionized water. Cross sections of the aortic wall were stained with Verhoeff-Van Gieson (VVG) stain for elastin as well as hematoxylin and eosin to identify cellular composition.

Rehydrated sections were blocked with 5% goat serum and incubated with primary mouse specific recombinant tropoelastin antibody (1:1000, generous gift from R.P. Mecham, Washington University in St. Louis[392]) overnight. Sections were then incubated with Alexa 647-conjugated goat anti-rabbit antibody (Molecular Probes, Life Technologies, Grand Island, NY) followed by counterstaining with 4',6-diamidino-2-phenylindole (DAPI) and imaged on a fluorescent microscope (Olympus, Provis 1, Center Valley, PA, Center for Biological Imaging, University of Pittsburgh).

Additional samples were also stained with a mouse F4/80 antibody (BioRad, MCA497A488) as pan macrophage marker in a similar manner as described above. A 1:50 dilution was used as well as a proteinase K antigen retrieval step. The antibody was preconjugated with Alexa 488.

Unstained specimens were imaged using a multi-photon microscope (Olympus, Model FV10, Center Valley, PA, Center for Biological Imaging, University of Pittsburgh) to observe elastin fiber arrangement. Samples were excited at 790 nm wavelength, and elastin was detected according to intrinsic fluorescence wavelength (525 ± 25 nm).

5.2.6 Mechanical Testing and Characterization of Aorta

Ring sections were cut from the murine aortas (shipped cold overnight from Vanderbilt University) at the midpoint between the renal arteries and the iliac-tail-aortic trifurcation. The rings were threaded with stiff metal wire which was clamped in an Instron tensile testing device described in Section 2.2.3. The mechanical analysis was performed in the same manner as described in Section 2.2.4 with the notable exception of using a Poisson's ratio of 0.5 which indicates an incompressible material.

5.2.7 Statistics

All statistics were performed in a similar manner to Section 3.2.7 ("Statistics").

5.3 RESULTS

5.3.1 Progression of AAA with Saline Delivered ADMSC Treatment

Five days after elastase perfusion, the artery dilated to approximately double the original diameter (**Figure 23**). At this point, when the aneurysm has already been established, either saline or ADMSCs were delivered through the treatment port. The untreated (saline) aneurysm group had a larger diameter than the early aneurysm group indicating that the untreated aneurysm continued to enlarge. By contrast, the group treated with ADMSCs demonstrated an aortic diameter equivalent to the early aneurysm group (and smaller than the untreated group) indicating that the expansion of the AAA had essentially been halted at the time of ADMSC treatment.

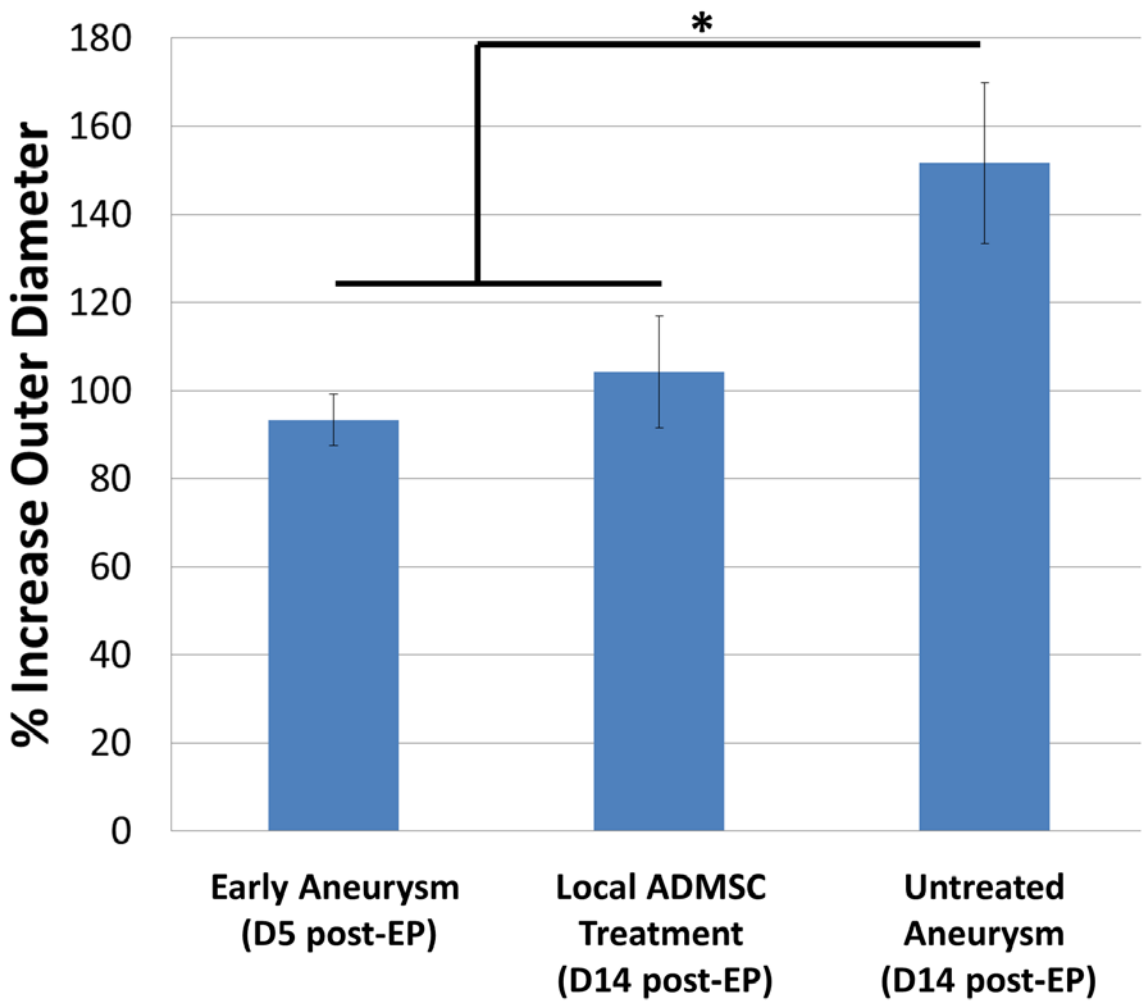

Figure 23. Progression of aneurysm is halted with local adipose-derived mesenchymal stem cells treatment. % increases in aortic diameter measurements (mean ± standard deviation) for early aneurysm group (93.3 ± 5.77 %, n = 3), local ADMSCs treatment group (104.29 ± 12.72 %, n = 7), and untreated aneurysm group (151.67 ± 18.35 %,, n = 6). A two-way analysis of variance revealed unequal means (*, $p < 0.001$) between groups. Tukey tests revealed which groups differed.

5.3.2 Histological Changes with Saline Delivered ADMSC Treatment

VVG, elastin autofluorescence, and immunofluorescent staining are shown in **Figure 24**. Qualitative examination of the imaged sections revealed less disruption of the elastic lamella in the local ADMSC treatment group when compared with the untreated aneurysm group. This is most apparent with VVG staining where elastin fiber breaks are highlighted by red arrows. The elastic fibers look similar between the early aneurysm group and the local ADMSC treatment group indicating that the delivery of ADSMCs is associated with preserved elastin integrity at the time of ADMSC treatment. Immunofluorescent staining (**Figure 24B**) and elastin autofluorescence (**Figure 24C**) confirmed the VVG results (**Figure 24A**).

Aneurysm progression in this model is mediated by inflammation – inflammatory cells are recruited by elastin degradation peptides and actively contribute to further matrix degradation[393]. In our study, moderately severe inflammation was apparent at day 5 (note the presence of mononuclear cells in **Figure 25**). At day 14, the presence of mononuclear cells decreased, but no significant difference was seen between treatment groups. Additionally, at day 14, there are no detectable macrophages in the local ADMSC treatment group compared to the early aneurysm and untreated aneurysm groups which display positive staining for macrophages (**Figure 26**).

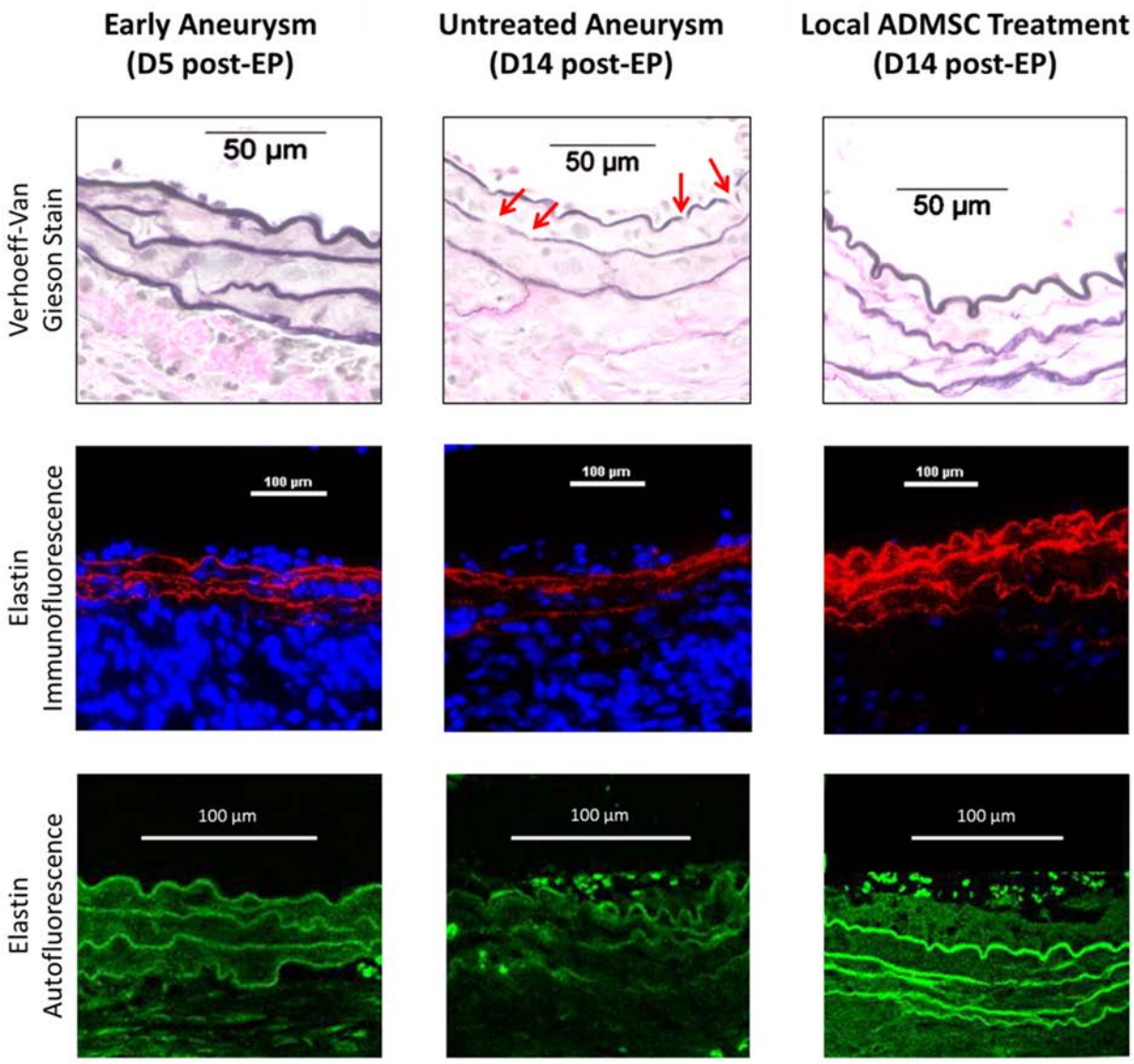

Figure 24. Qualitative examination of elastin. Images from early aneurysm (left column), untreated aneurysm (middle column) and local ADMSC treatment (right column) groups are shown after Verhoeff–Van Gieson staining (top row), elastin immunofluorescence (middle row), and elastin autofluorescence (bottom row) (n = 2 all groups).

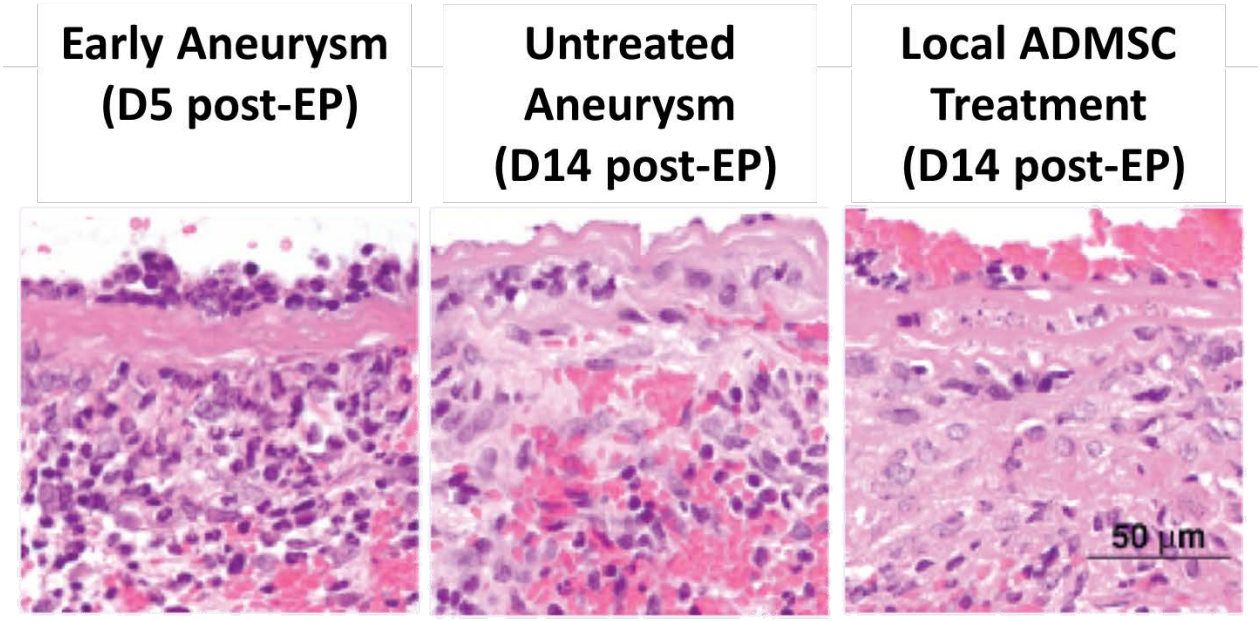

Figure 25. Monocyte infiltration of the abdominal aortic aneurysm is not significantly reduced with adipose derived mesenchymal stem cells delivery. Images from early aneurysm, untreated aneurysm and local ADMSC treatment groups are shown after staining with hematoxylin and eosin (n = 2 all groups).

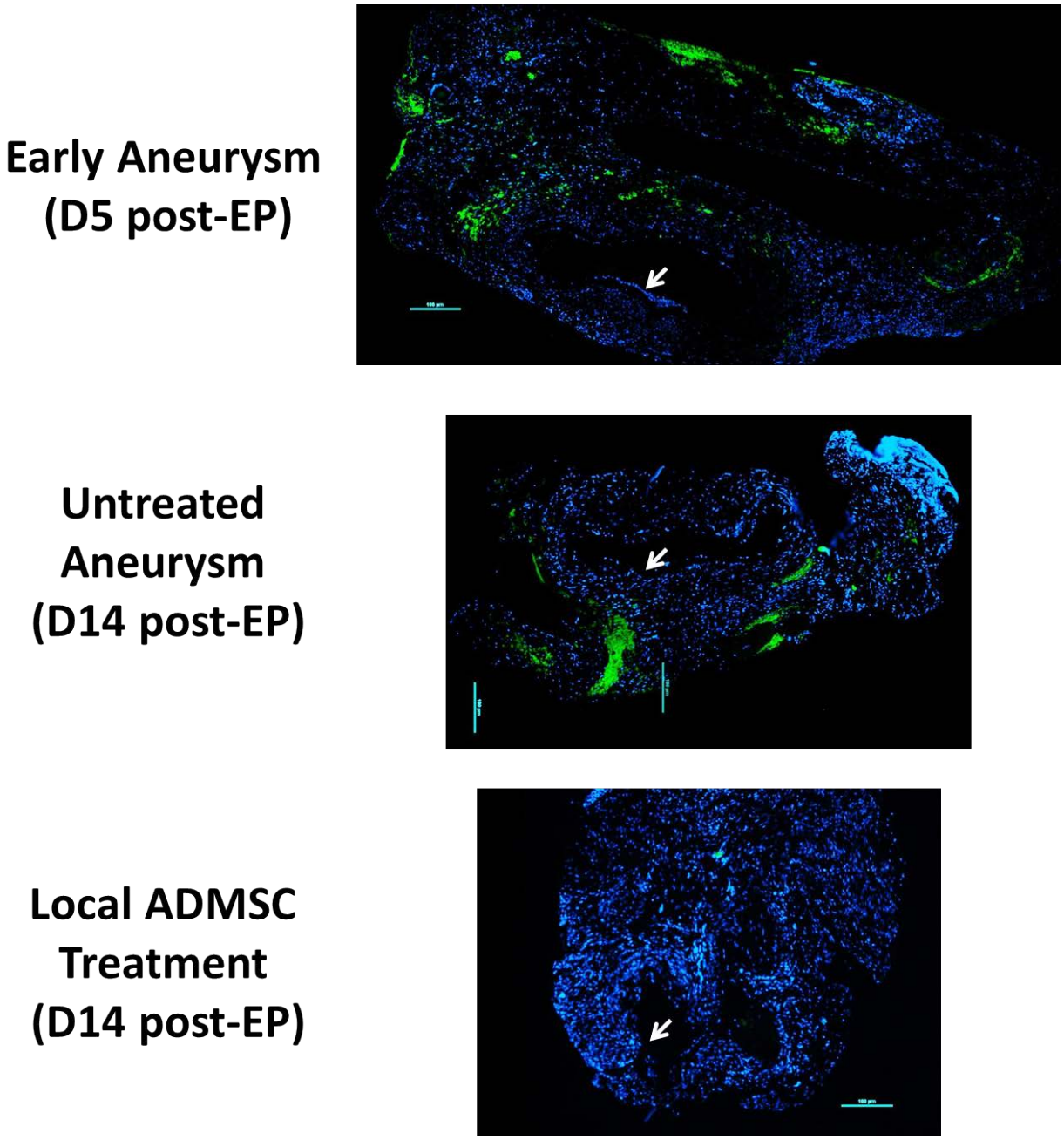

Figure 26. Local ADMSC treated aortas show no macrophages at day 14 post elastase perfusion. Images from early aneurysm (top), untreated aneurysm (middle) and local ADMSC treatment (bottom) groups are shown after macrophage immunofluorescence staining (green) (n = 1 all groups). All groups are counterstained with DAPI (blue).

Diameter Measurements with Fibrin Delivered ADMSC Treatment

Six days after elastase perfusion, saline (no ADMSCs), fibrin(no ADMSCs), or ADMSC seeded fibrin treatments were delivered through the treatment port. Upon harvest at day 15, there was no statistical differences in the % increase in outer aortic dimeter (p=0.308). **Figure 27** shows the mean and standard deviation for each group. The untreated saline controls harvested at day 15 were smaller than the equivalent untreated saline controls harvested at day 14 shown in **Figure 23** (p=0.0004).

The ADMSC seeded fibrin delivery group was further broken down according to the timing of the injections. Since there is a temporal aspect to fibrin gelling, mice that were injected at a later gelation time were separated from mice that received the first injection from the batch mixing of fibrin. This breakdown is shown in **Figure 28**. The groups are not statistically different when including this further breakdown (p=0.239).

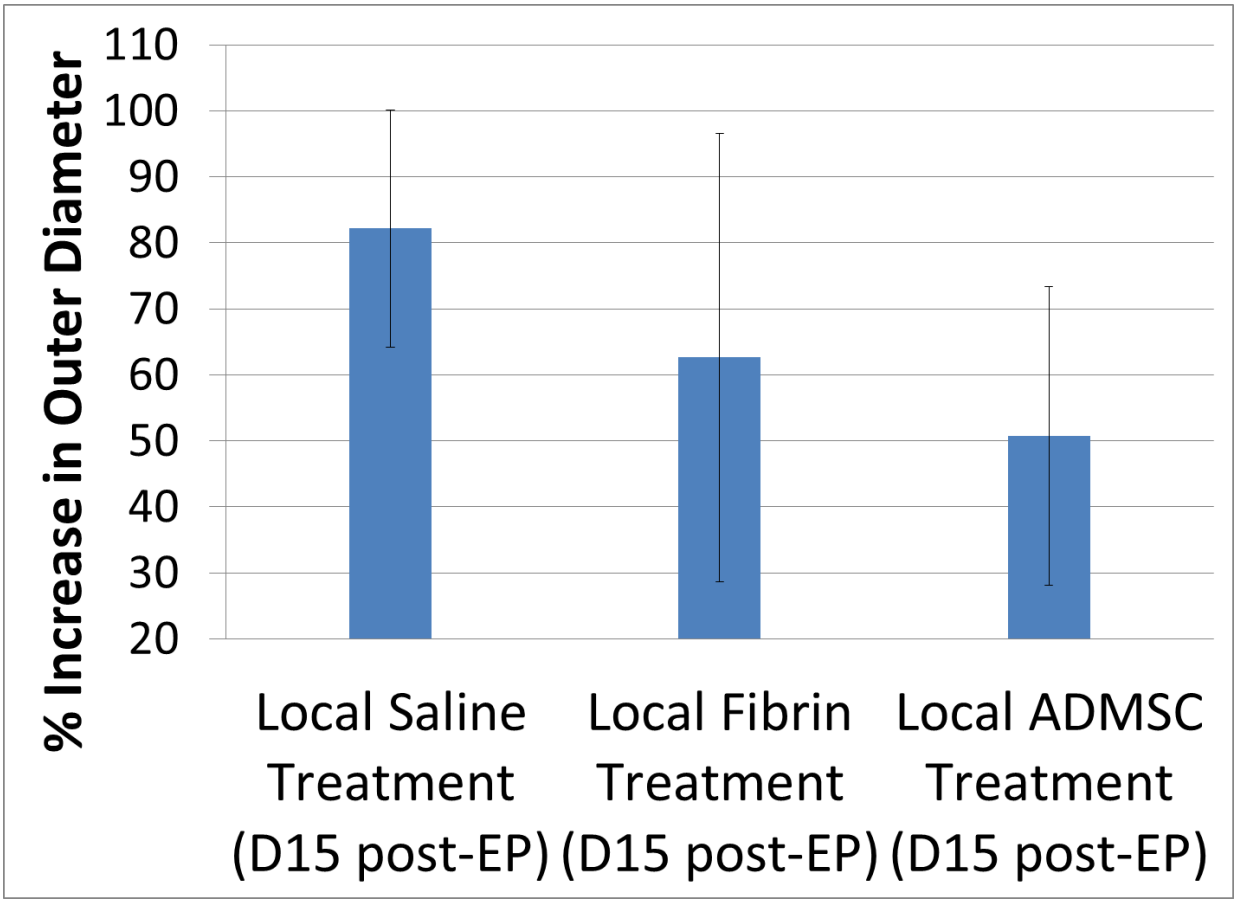

Figure 27. Aneurysm growth is unchanged with local adipose-derived mesenchymal stem cells treatment delivered via fibrin (p=0.308). % increases in aortic diameter measurements (mean ± standard deviation) for local saline (no ADMSC) treatment group (82.14 ± 17.98 %, n = 4), local fibrin (no ADMSC) treatment group (62.60 ± 33.92 %, n = 23), and local ADMSC treatment group in fibrin (50.71 ± 22.64 %, n = 10).

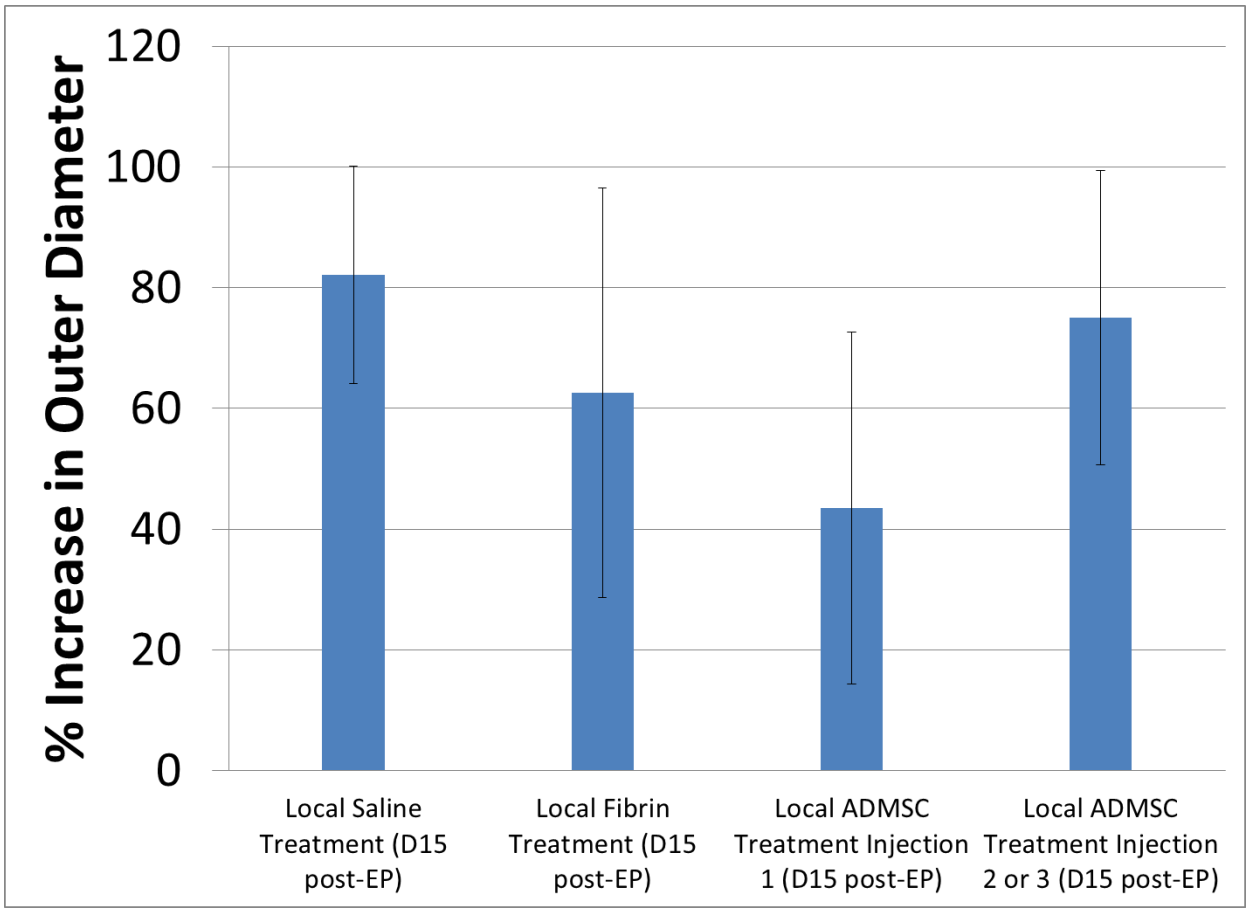

Figure 28. Aneurysm growth is unchanged with local adipose-derived mesenchymal stem cells treatment delivered via fibrin even when accounting for injection order (p=0.239). % increases in aortic diameter measurements compared to per elastase perfusion measurements (mean ± standard deviation) for local saline (no ADMSC) treatment group (82.14 ± 17.98 %, n = 4), local fibrin (no ADMSC) treatment group (62.60 ± 33.92 %, n = 23), local ADMSC treatment injection 1 group (43.45 ± 29.14 %, n = 6), and local ADMSC second treatment injection 2 or 3 group (75.00 ± 24.40 %, n = 4). The first two bars from left to right are the same as the first two bars from left to right in Figure 27.

5.3.4 Aorta Mechanical Properties with Fibrin Delivered ADMSC Treatment

In order to determine the tangent modulus of the aortas, the circumferential Cauchy stress was calculated and plotted against the circumferential stretch ratio is shown in **Figure 29** (along with similar data from Collins et al.[167]). One-way ANOVA reveals differences in the tangent modulus, seen visually as the higher slope of the second linear portions of the curves in **Figure 29**, between the groups ($p=0.014$). Subsequent Tukey tests revealed that the native aortas have a lower tangent modulus than the acellular fibrin treated and ADMSC-seeded fibrin treated groups (**Table 8**).

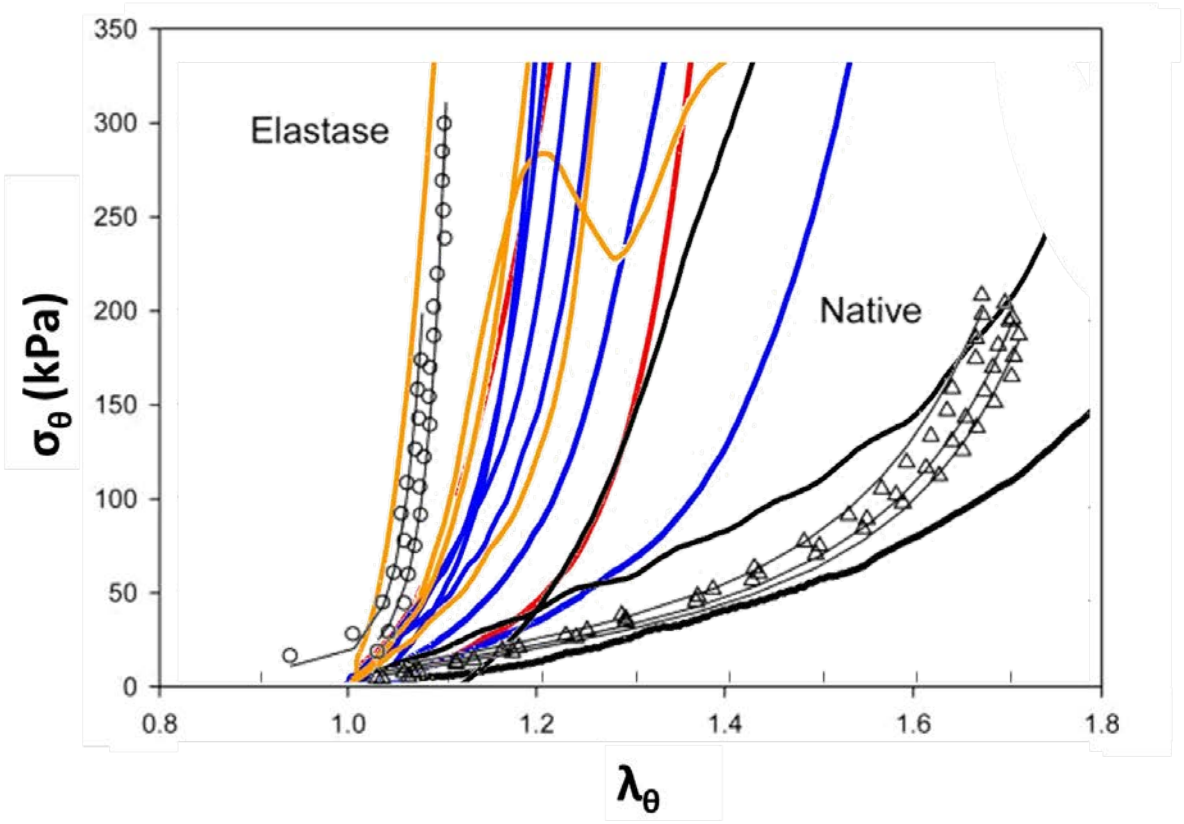

Figure 29. Elastase treatment leads to a stiffer aorta in mice. Circumferential stretch ratio is shown on the x-axis. Circumferential Cauchy stress is shown on the y-axis. The solid lines are from the following groups: Black = native aorta, blue=fibrin only treatment, orange=ADMSC treatment, red =saline treatment. The black triangle data points are native mouse aortas from Collins et al[167]. The black circle data points are elastase treated mouse aortas from Collins et al[167].

Table 8. Native aortas have a lower tangent modulus than all elastase treated groups. Measurements for tangent modulus are given as mean ± standard deviation. Tukey groupings identifiers "A" and "B" show which groups have different means.

Group	Tangent Mod. (MPa)	Tukey Groupings
Native aorta (n=3)	0.6±0.3	A
Saline (n=2)	2.9±0.3	A B
Fibrin Only (n=6)	3.3±1.4	B
ADMSC (n=4)	4.2±1.2	B
One way ANOVA	p=0.014	

5.4 DISCUSSION

Local ADMSC treatment delivered by saline suspension halted aortic diameter enlargement at the time of cell delivery (**Figure 23**). It has been estimated that if enlargement rates of small aneurysms (<4.0 cm diameter in humans) could be reduced by even 50%, the need for surgical intervention could be delayed by 10 years, thus preventing the need for intervention in many patients[385]. From a qualitative perspective, ADMSC treatment preserved the structure of elastic lamellae at levels comparable to the time of cell delivery, although quantitative analysis has not been performed. This could indicate a role for ADMSC in preventing elastin degradation and/or promoting elastic fiber production. Elastin degradation is both a hallmark of a developed AAA and an active recruiter of inflammatory cells[394] that continues the AAA destructive cycle. Preserving elastin integrity, and thus decreasing inflammation, could halt AAA progression. In our study, we cannot conclusively state that ADMSC diminished the inflammatory response, but they could theoretically have offset any monocyte-derived elastase activity. Our study also showed a decrease in the presence of macrophages when treated locally with ADMSCs (**Figure 25**).

Alternately, and not exclusive, to preventing degradation, therapeutic cells could stimulate elastin production. Elastic fibers can be produced by human vascular SMCs in vitro when stimulated with TGF-β1[313] which is secreted by ADMSCs[194]. Therefore, ADMSCs could stimulate repair by native vascular SMCs.

When considering the increase in aortic diameter and elastin structure, our periadventitial stem cell delivery method produced results similar to those shown by Sharma et al.[195] where the

systemic delivery of MSCs reduced the rate of AAA progression and preserved elastin lamella integrity in elastase-perfused mice. Our study extends the work of Sharma et al. by demonstrating that the macroscopic benefits of stem cell therapy are accessible to established and expanding aneurysms and not limited to attenuating the inflammation response immediately following elastase perfusion. Our study also shows that periadventitial delivery of a stem cell therapy is effective and may avoid potential problems of systemic delivery such as unintended stem cell migration and engraftment. It also focuses the cells on the anatomically defined segment of the aorta affected by the disease and circumvents the physical barriers presented by endothelium, atherosclerotic plaque and/or ILT. This an important finding in the development of treatments for patients with an identified AAA, of which 90% are smaller than the size recommended for surgical repair (5.5 cm)[395].

Although this study yielded exciting results, it does have limitations. This proof-of-concept study was designed to be a short-term study. While the murine elastase-perfused aneurysm does not expand after our chosen end point of 14 days[120], the human aneurysm expands progressively. Longer studies will need to be completed in order to understand the long term effects of our treatment. Additionally, future studies will investigate the progression of the disease in real-time by sacrificing animals at more frequent intervals and utilizing noninvasive imaging, such as ultrasound or micro-CT/micro-MRI.

In this study of local ADMSC treatment delivered via saline suspension, we had sought to develop and show proof-of-concept for an alternative therapeutic model for AAAs. A localized, periadventitial route of stem cell therapy administration avoids the drawbacks of both systemic delivery (e.g., uncertain destination of cells and presence of ILT) and local delivery via direct injection into a weakened aneurysmal wall. The placement of the port, catheter, and

sponge (**Figure 21**) allows for initiation of therapy at any point in the development of the model aneurysm. A final advantage of our approach is the use of MSCs sourced from adipose tissue. ADMSCs are a very attractive clinical source of stem cells due to the ease of obtaining adipose tissue from donors seeking liposuction treatment and the high yield of MSCs from adipose tissue[351,396]. Our study revealed how ADMSCs can alter the progression of an already established and expanding aneurysm while others have shown the ADMSCs have immunomodulatory properties[397].

In contrast to the results when ADMSCs were delivered with saline, ADMSCs delivered via a fibrin hydrogel had no significant effect on aneurysm in terms of % increase in outer diameter and tangent modulus of the vessel. There are a number of confounding factors that could be influencing our results. First, the size of the aneurysm in terms of % increase in outer diameter is smaller when comparing the untreated aneurysm controls between the saline suspension delivery experiments performed at Washington University in St. Louis and the fibrin gel delivery experiments performed at Vanderbilt University. Though following the same protocols, the change in location has also meant a change in animal technician performing the surgeries, different lots of elastase, and potential differences in food and water given to the animals. Since the aneurysm we were treating is small overall, the ADMSC therapy may not be able to have a large enough effect to be seen in a macroscopic measurement such as diameter.

Another confounding factor could be the timing of the delivery using fibrin gels as a delivery vehicle. Once the constituents of the fibrin gel are mixed, gelation begins. Should gelation proceed too rapidly, the cells may not be able to get close enough to the aorta to have a positive effect. This is partially shown in the trend of lower diameters for the aortas treated with the first injection from the fibrin-cell mixture compared to the second and third injections from

the fibrin-cell mixture which are highlighted in **Figure 28**. Gelation may have been nearing completion by the time the second and third injections from the fibrin-cell mixture were delivered to the animals thus inhibiting the cells from reaching the periadventitial AAA wall.

5.5 CONCLUSION

We have developed an animal model for delayed, periadventitial delivery of ADMSCs to ameliorate elastase-induced AAA. Delayed, periadventitial delivery of ADMSCs halted two aspects of aneurysm progression – expansion of the aortic diameter and fragmentation of the elastic lamella. This work represents an important step towards developing clinically realistic stem cell therapies for AAA patients.

5.6 FUTURE WORK

Future work should concentrate on generating larger aneurysms in the fibrin based delivery of ADMSCs experiments. Once this technique is refined, work needs to be dedicated to improving ADMSC delivery to the periadventitial surface of the aorta. Once improved and shown to be effective, the ADMSC's mechanisms of action need to be determined to fully understand why the therapy is effective. Lastly, these studies need to be extended to longer time points in order to determine the lasting effect of the treatment.

6.0 SPECIFIC AIM 3: DEVELOP CLINICAL MSC DELIVERY SYSTEM

The third Specific Aim of this dissertation is the early developmental work towards creating a clinical delivery system for our MSC therapy (which is thoroughly described in Section 6.1.1). Critical aspects of this clinical delivery system were evaluated four ways: 1) we evaluated the loading efficiency of iron nanoparticles into ADMSCs, 2) we determined cell viability with respect to fibrin gelling parameters and iron nanoparticle size, 3) we examined whether a magnetic force between the iron nanoparticles and an external magnet could induced movement of ADMSCs through a fibrin gel, and 4) we created and evaluated a cell delivery prototype. But, before detailing the experimental methods, it is important to understand the motivation and design criteria of our MSC delivery system as well as an overall description of the system.

6.1 DESIGN DESCRIPTION, MOTIVATION, AND CRITERIA

6.1.1 Clinical MSC Delivery System Description

We wish to deliver our proposed MSC therapy to the periadventitial surface of a AAA in a minimally invasive manner. This will be accomplished by gaining access to the peri-aortic space through the use of image-guided needles or retroperitoneoscopic techniques, and directing

the transmural migration of MSCs by incorporating iron nanoparticles within the MSCs along with the placement of an intra-aortic magnet. The iron nanoparticle loaded MSCs will be delivered along with a fibrin gel which will entrap the cells on the periadventitial surface of the AAA. Local delivery of therapeutic agents should overcome noted inefficiencies of systemic delivery (i.e., poor homing[398], compromised vasa[64,65,109-111], and physical barriers like the ILT[113]). Our approach also has the potential intrinsic benefit of reduced systemic effects/toxicities.

When combined, the resulting therapy is the delivery of therapeutic cells to the periadventitial surface of the AAA with a fibrin gel holding the cells in place. The practical implementation of this system will occur as follows: (1) the endoluminal magnetic probe will be placed in the AAA lumen through femoral artery catheterization, and placement will be confirmed via ultrasound, (2) prescribed volumes of iron nanoparticle loaded therapeutic cells, fibrinogen, and thrombin solutions will be loaded into syringes and attached to a mixing and dispensing device that is designed to ensure that the solutions are mixed at the exact ratio and only upon injection, and (3) up to two translumbar injections can be made on either side of the spine to the periadventitial side of the AAA, and the solutions of iron nanoparticle loaded therapeutic cells, fibrinogen, and thrombin will be dispensed and mixed simultaneously.

This system is designed to ensure delivery of the therapeutic cells to the periadventitial surface of the AAA. The magnetic force between the iron nanoparticles and the endoluminal magnetic probe pull the therapeutic cells to the periadventitial surface of the AAA. The fibrin gel forms around the cells, restricting cell movement after withdrawal of the endoluminal magnetic probe. The mixing and dispensing system is designed to ensure the iron nanoparticle loaded therapeutic cells, fibrinogen, and thrombin solutions do not begin mixing until the time of

dispensing and are mixed in the appropriate ratios. While novel technology is being developed for this therapeutic cellular delivery system, the parts are designed to leverage existing technologies such as syringes, surgical needles, and ultrasonic probing systems. In our small animal studies, described in Chapter 5, we have been successful at delivering a fibrin gel to the area immediately surrounding the aorta in an elastase perfused AAA mouse model[140]. The insights gained from our small animal studies combined with the development and testing of the proposed system will ensure a quality and effective end product. It is important to note that some of the work detailed below has been put into a successfully funded development grant through the University of Pittsburgh Center for Medical Innovation (F_168-2016, PI: Blose) and is the subject of an invention disclosure submitted to the University's Office of Technology Management (Disclosure #03490).

6.1.2 Minimally Invasive Delivery of MSCs

We sought to make our therapeutic delivery of MSCs as minimally invasive as possible for two reasons. First, the advanced age of most patients makes open surgery a risky proposition with respect to mortality and extends hospital stays. Both problems are currently manifested with open repair of AAA. Secondly, the cost of an invasive surgery would be higher requiring more skilled healthcare providers, sterile rooms, and longer in-hospital recovery times. We have designed the delivery system to distribute a chosen therapeutic, MSC-seeded fibrin gels, to the periadventitial surface of the AAA. This will be accomplished through an ultrasonic guided translumbar injection.

6.1.3 Directed Homing of MSCs

Upon injection, the MSC-seeded fibrin gel is still a cell suspension in a viscous liquid. Gelation takes some time to complete and is tunable[280]. During the interval of time between injection and gelation, there is an opportunity, and possibly a necessity, to direct the injected cells to the periadventitial surface. Should the therapeutic MSCs become locked in the fibrin gel, any potential paracrine mechanism of action, which is demonstrated in Chapters 3 and 5, could be hindered if the MSCs are too far from the AAA wall.

Our proposed solution to this problem was to use magnetic attraction to concentrate the cells in a desired location. We borrowed a technique pioneered in imaging modalities using iron nanoparticles[399-401]. Loading cells with iron nanoparticles has since been used in the magnetic guidance of stem cells for preclinical testing of therapies for myocardial infarction[402] and retinal degeneration[403], and we will adapt this approach for AAAs by loading iron nanoparticles inside our therapeutic cells. A magnetic probe can be introduced into the lumen of the AAA via femoral artery access. The magnetic attraction force between the magnetic probe and the iron nanoparticles will pull the iron nanoparticle loaded cells through the fibrin hydrogel to the periadventitial surface of the AAA.

6.1.4 Magnetic Probe Placement Considerations

The endoluminal magnetic probe needs adequate femoral access which is influenced by aortic and iliac tortuosity posing a challenge to accessing the AAA[404] The concept of tortuosity, an estimate of the arc to chord ratio, is often left to qualitative and subjective characterizations. Historically, there was no consensus on the best method of quantifying tortuosity and therefore

was not commonly done. Advances in computerized measurement techniques have led to an adoption of femoral artery tortuosity measurements which have demonstrated an increased rate of asymptomatic femoral dissections in more tortuous arteries[405-408].

Though tortuosity measurements are helpful in determining the best course of therapy for a AAA patient[409], the tortuosity of the femoral artery is often mitigated for EVAR patients by using an extra stiff guide wire, a "pull down" maneuver, and occasional implantation of a temporary graft sutured to the common iliac artery via a retroperitoneal approach. The "pull down" maneuver consists of dissecting the common femoral and external iliac arteries and pulling these arteries inferiorly to straighten the tortuosity[410]. Once straightened, a sheath (15-18 Fr [3Fr = 1mm]) is inserted to allow the graft probe to reach the desired location. We will borrow this technique and size our probe to fit inside a 15-18 Fr sheath.

The magnetic probe was designed to fit within an 18 Fr sheath in order to utilize the “pull down” technique when necessary. Additionally, the magnetic probe was designed such that it can be visualized using ultrasonic imaging by using solid metallic magnets. A prototype of the magnetic probe is shown in **Figure 30**.

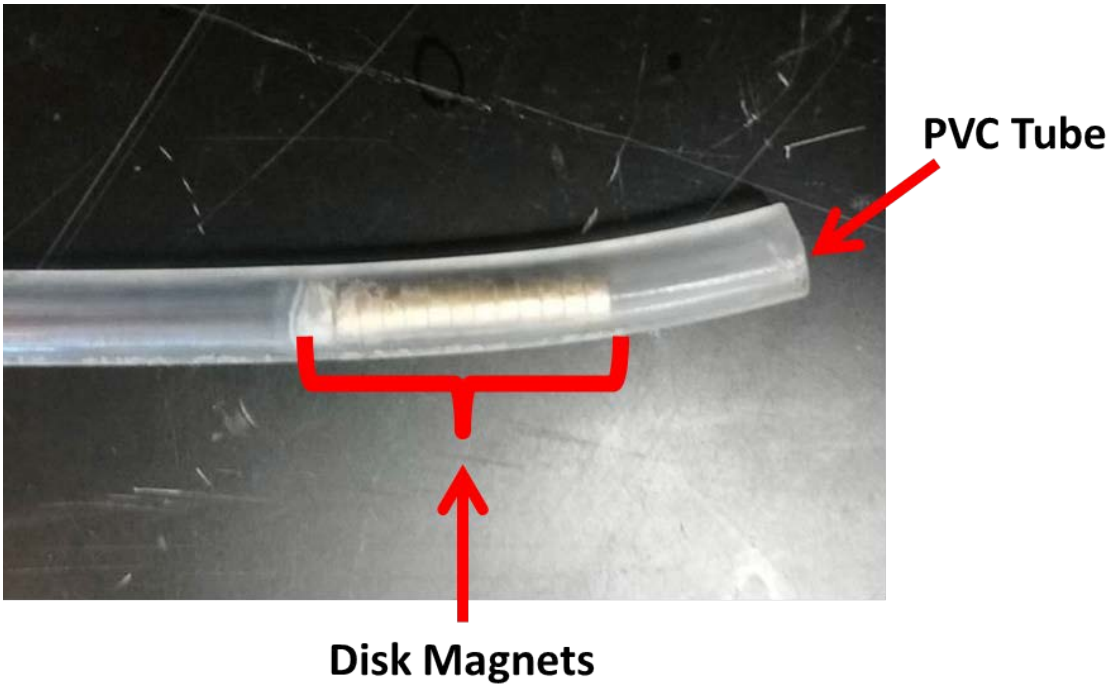

Figure 30. Magnetic probe designed to fit within an 18 Fr sheath. Disk magnets (1.5 mm height x 3 mm diameter) were glued to the inside of a clear PVC 5 mm outer diameter tube.

6.1.5 Cell Delivery Vehicle Material Considerations

We chose fibrin as our vehicle for cell delivery due to its ease of gelation and extensive track record of cell compatibility[299,411-414]. The use of a hydrogel will restrict the cells to the local aneurysmal aorta (providing a decreased risk of cells ending up in remote tissue beds compared to systemic delivery). Also, because of its temporal and thermal gelation properties, fibrin can be injected while still a liquid and gel inside the body at our desired location. Fibrin has already been approved by the Food and Drug Administration (FDA) in a number of applications under the tradenames TISSEEL, EVARREST, etc. However, it is important to note that the FDA does not broadly approve a specific material; rather they approve a material for a specific application.

The gelling nature of the fibrin requires that the constituents of the gel be mixed as close to injection as possible. Once mixed, the fibrin begins to gel, and the cells will have a harder time localizing to the periadventitial surface of the AAA as the gelation process proceeds even in the presence of a magnetic attraction force. In order to delay the gelation as long as possible and to remove any user error with respect to gelation, a delivery device needed to be designed such that the prescribed volumes of iron nanoparticle loaded therapeutic cells, fibrinogen, and thrombin solutions can only be mixed as the injection is occurring.

A cell delivery mixer was designed to accommodate three separate “Luer-Lok” syringes as inputs and a single “Luer-Lok” as output. The diameters of the tubes from each input “Luer-Lok” were also designed to ensure that the volumetric flow rate is constant for all three inputs. A 3D rendering of the cell delivery mixer is shown in **Figure 31**.

A

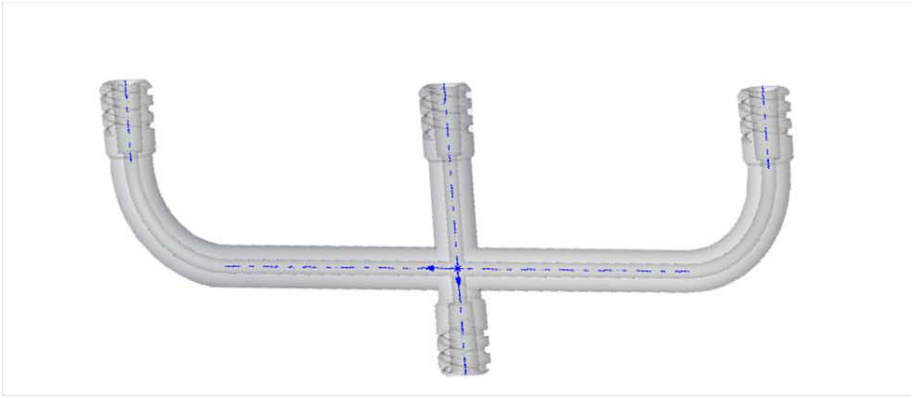

B

Figure 31. Cell delivery mixer designed to ensure gels are mixed only while injecting. A) The three inputs (top) were designed to accommodate a "Luer-Lok" syringe. Equal volumes of the fibrinogen, thrombin, and iron nanoparticle loaded ADMSCs will be loaded into three separate syringes and dispensed at the same time through the single output (bottom). B) Fibrin gel constituent components loaded into a syringe and locked in the fibrin gel mixer. From left to right, the constituents are fibrinogen solution (pink), cell suspension (yellow), and thrombin solution (blue).

6.1.6 FDA Regulatory Considerations

The practical application of our MSC based AAA therapeutic would fall under the FDA category "combination product" designation. A combination product is defined by the FDA as "a product comprised of any combination of a drug and a device, a biological product and a device, a drug and a biological product, or a drug, device, and a biological product."[415] The FDA classifies these products differently as a precautionary measure due to interactions of the products being combined that may not be readily apparent. In our specific application, the delivery of our therapeutic is to a new location. The delivery location may make it "necessary to develop new methods to determine the effect of such localized/targeted delivery, particularly when it results in higher exposure to that target than when the drug is systemically administered."[415]

Additionally, the FDA would consider our product a cellular therapy (CT) which is grouped with gene therapy (GT) products and referred to collectively as CGT. The FDA is rightfully worried about the risks of CGT products. A previous trial showed tumors in the brain and spinal cord when a patient was treated with intrathecal allogeneic stem cells for ataxia telangiectasia[416]. This tragic outcome highlights the risky nature of CGT products.

It is their very nature that we are trying to harness for a therapeutic that makes CT products a unique, dynamic, and complex problem to address. The ADMSCs used in our therapy produce a number of beneficial growth factors such as TGF-β1[194] in the context of treating AAA, but the ADSMC may also produce other undesirable growth factors that negatively affect the patient such as interluekin-6[417], a pro-inflammatory cytokine. Additionally, the therapeutic cells, such as the ADMSCs used or our studies or MSCs in general, could also develop undesired functions such as a CT that was delivered to the heart which produced cardiomyocytes that were

beating out of sync[418]. Clearly, the FDA understands the risks associated with CT, and our AAA therapy will need to address those concerns.

6.2 METHODS

6.2.1 Cell Culture

For all cell-based experiments, commercially sourced human ADMSCs (Thermo Fisher Scientific, #R7788110) were cultured in 75-cm^2 or 175-cm^2 tissue culture flasks (Corning) and grown under defined culture media [1:1 Dulbecco's modified Eagle's medium (DMEM; Gibco #11965) to DMEM/F12 (Gibco #113300) with 10% fetal bovine serum (Atlanta Biologics #S11550), antibiotics (1% Pen/Strep, 0.5% Fungizone, 0.1% Gentamycin), and 10 µL of 10 mM dexamethasone] mixed with 25% Preadipocyte Growth Medium (#C-27410, #C-39425; PromoCell). Culture media was changed every 2-3 days, and when ADMSCs were expanded to near confluence, they were passage expanded utilizing 0.25% trypsin-EDTA (#25200-056; Gibco) or utilized for subsequent experimentation. Cells were used between passages 6-10.

6.2.2 Iron Nanoparticle Loading Efficiency

Cell loading with iron nanoparticles (fluidMAG-D, Chemicell) was performed according to published protocols[419,420]. Briefly, ADMSCs were incubated overnight with 0.5 mg/mL nanoparticles (100 or 200 nm diameter) in growth medium. Cells were also loaded with a 0.25 mg/mL and 1.00 mg/mL iron nanoparticles, and loading efficiency was calculated as the total

number of cells containing iron nanoparticles (identified by staining described in Section 6.2.8) per view divided by the total number of cells per view (n=3 per group, 3 images per n).

6.2.3 Fibrin Gel Fabrication

All experiments using ADMSC-seeded fibrin constructs were fabricated by mixing bovine fibrinogen type I (3 mg/mL or 10 mg/mL, Sigma-Aldrich, St. Louis MO) with bovine thrombin (1 NIHU/mL, Sigma-Aldrich, St. Louis, MO) and ADMSC cell suspension ($5.0x10^4$ cells/gel, $1.0x10^5$ cells/gel, and $2.0x10^5$ cells/gel). The gels were plated within 24-well plates (Corning). Gels were either allowed to polymerize for at least 2 hours in incubator conditions (37°C, 5% CO2) or handled immediately before adding ADMSC culture media for the viability (Section 6.2.4) and migration assays (Section 6.2.5), respectively. The gels were then cultured in incubator conditions according to the treatment condition.

6.2.4 Cell Viability

In order to determine the optimal fibrin gelation parameters for ADMSC viability, the ADMSC viability of ADMSC-seeded fibrin constructs was evaluated using an MTT assay. After 5 days in culture, 200 mL of serum-free α-MEM and 20 mL of Thyazolyl Blue Tetrazolium Bromide (Sigma–Aldrich, St. Louis, MO) was added to each sample. Samples were then incubated at 37°C for four hours to allow crystal formation. The supernatant volume was then carefully removed and 200 μL of 0.04N HCl in 2-propanol solution was added to dissolve the crystals. Samples were kept in the dark at 4°C for 24 hours. Lastly, absorbance readings were taken for 100 μL of the solution for each condition at 550 nm wavelength using a microplate

reader (BioTek, Winooski, VT). The final number of cells was calculated using a standard curve generated for known cell concentrations.

6.2.5 Magnetic Migration

In order to determine the localization effects of short term magnetic stimulation, ADMSCs were loaded with iron nanoparticles (100 and 200 nm diameter) and seeded in a fibrin gel. Fibrin gels were also formed with iron nanoparticles only (100 and 200 nm diameter). The gels were plated in a 24-well plate. A magnet (0.3T) was placed under the 24-well plate in the center of each well. In order to determine the temporal effects of magnetic stimulation of an actively gelling construct, a magnet was put in place at three different time points: at the beginning of gelation (prior to gel plating), mid gelation (20 seconds after gel plating), and after complete gelation (10 minutes after gel plating). Gels were also plated without magnet placement as a control. A side view schematic of the experimental groups is shown in **Figure 32**. The gels were cultured in incubator conditions (37 C, 5% CO2) for 24 hours. The gels were then imaged from above to qualitatively assess the localization of the iron nanoparticles.

In order to determine the localization effects of long term magnetic stimulation, gels made from cells loaded with 200 nm iron nanoparticles and magnet placement at mid gelation were cultured for 5 days. We added an additional magnet size to the longer term culture experiments. The larger magnet had a greater pull strength (12 lbs. vs. 4 oz.), but the same magnetic field surface strength (0.3 T).

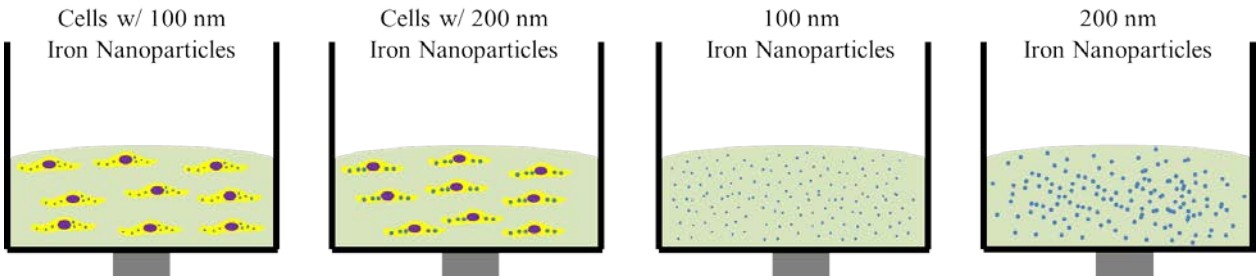

Figure 32. Fibrin gel schematic and groups. Fibrin gels are shown in green. Cells are yellow with purple nucleus. Iron nanoparticles are shown in blue. Experimental groups from left to right are: cells with 100 nm iron nanoparticles, cells with 200 nm iron nanoparticles, 100 nm iron nanoparticles alone, 200 nm iron nanoparticles alone.

6.2.6 Fibrin Gel Mixer Performance

In order to determine how effectively our fibrin gel mixer was able to create a uniform distribution of cells within an ADMSC-seeded fibrin construct, ADMSC-seeded fibrin constructs were made by utilizing the fibrin gel mixer described in Section 6.1.5. Equal volumes of a fibrinogen solution (9 mg/mL), thrombin solution (3 NIHU/mL), and ADMSC cell suspension ($7.5x10^5$ cells/mL), were loaded into separate 3mL syringes and attached to the fibrin gel mixer. 400 μL gels were plated in 24-well plates using the fibrin gel mixer. Three groups of gels were made by rotating the fibrin gel component solutions (fibrinogen, thrombin, and cell suspension) syringes through the three fibrin gel mixer inputs. The three groups (n=3 per group) were named as follows: 1) Left – cell suspension in the left input, fibrinogen solution in the center input, and thrombin solution in the right input, 2) Center - cell suspension in the center input, fibrinogen solution in the right input, and thrombin solution in the left input, and 3) Right - cell suspension in the right input, fibrinogen solution in the left input, and thrombin solution in the center input. A control group was also made by mixing the components thoroughly by manual pipetting before plating. Samples were allowed to gel for 2 hours before being processed for nuclei imaging as described in Section 6.2.8. Three random square views (~thickness of gel x thickness of gel) of each gel were processed in ImageJ by fitting ellipses to nuclei. The average distance from each nucleus to all other nuclei is each image was calculated for each group. An additional qualitative mixing experiment is described and results are shown in **231**.

6.2.7 Magnetic Probe Ultrasound Identification

In order to show that the magnetic probe portion of the cell delivery system described in Section 6.1.4 is visible by ultrasonic imaging, the magnetic probe prototype was imaged within a tissue mimic using a 21 MHz ultrasound linear probe (MS 250) connected to a high frequency imaging system (Vevo2100, Visualsonics, Canada) in B-scan mode. The tissue mimic, shown in **Figure 33**, was made from a 2% gelatin solution contained within a Plexiglas chamber with a clear PVC tube running the length of the chamber to serve as an aorta mimic. The tube was approximately 3 inches from the top of the tissue mimic. Ultrasound images of the aorta mimic were captured with and without the magnetic probe in place and processed to highlight the magnetic probe.

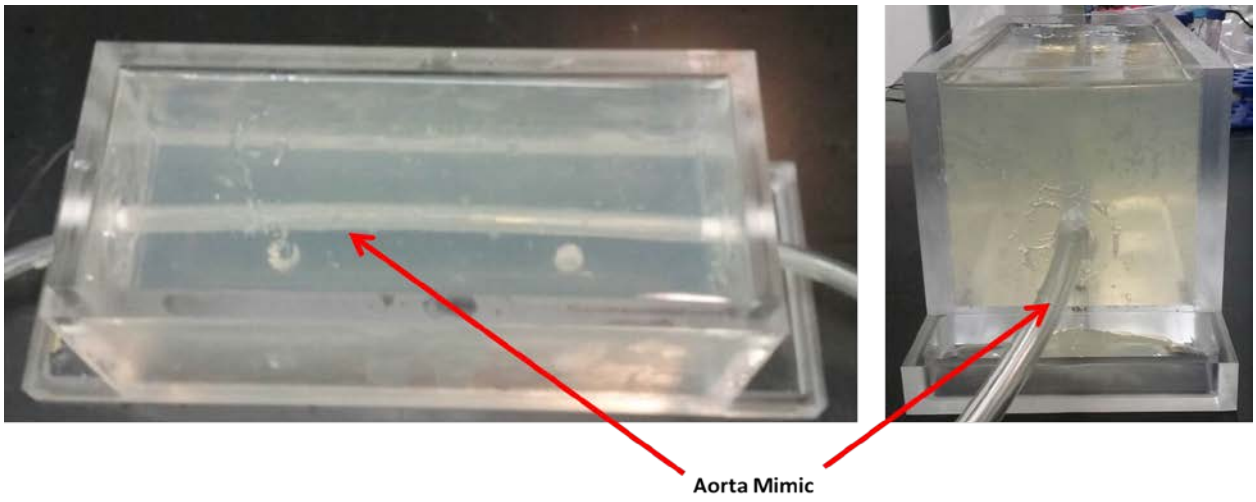

Figure 33. Tissue mimic used for ultrasonic identification of magnetic probe. A Plexiglas chamber houses a 2% gelatin gel and a clear PVC tube to serve as tissue and aorta mimics, respectively.

6.2.8 Histology and Imaging

All samples collected for imaging were fixed in 4% paraformaldehyde, frozen, and sectioned. Sections were stained with Prussian Blue stain for iron and DAPI to show nuclei. Images of sections were taken looking at the z-radial plane and taken from the middle of the gel. All sectioned samples were imaged using NIS Elements software (version 4.0).

6.2.9 Statistics

A linear regression model was used to determine significant predictors for the cell viability experiments. All other statistics were performed in a similar manner to Section 3.2.7 ("Statistics").

6.3 RESULTS

6.3.1 Optimal Iron Nanoparticle and Fibrin Gel Parameters

When preforming the iron nanoparticle loading efficiency experiments, we found that ~52% of cells had iron nanoparticles (**Figure 34**), and a one-way ANOVA revealed that the tested concentrations of iron nanoparticles had no effect on loading efficiency ($p=0.495$). A linear egression revealed that fibrinogen concentration ($p<0.001$), starting cell number ($p<0.001$), and a mixed effect term of fibrinogen concentration and starting cell number

($p=0.006$) to be significant predictors of the ratio of viable cells to initial cells plated. These results are shown in **Figure 35**. Lower fibrinogen and plated cell concentrations lead to higher ratios of viable cells to initial cells plated. However, only fibrinogen concentration is a significant predictor ($p<0.001$) of total number of cells after 5 days in culture (**Figure 36**).

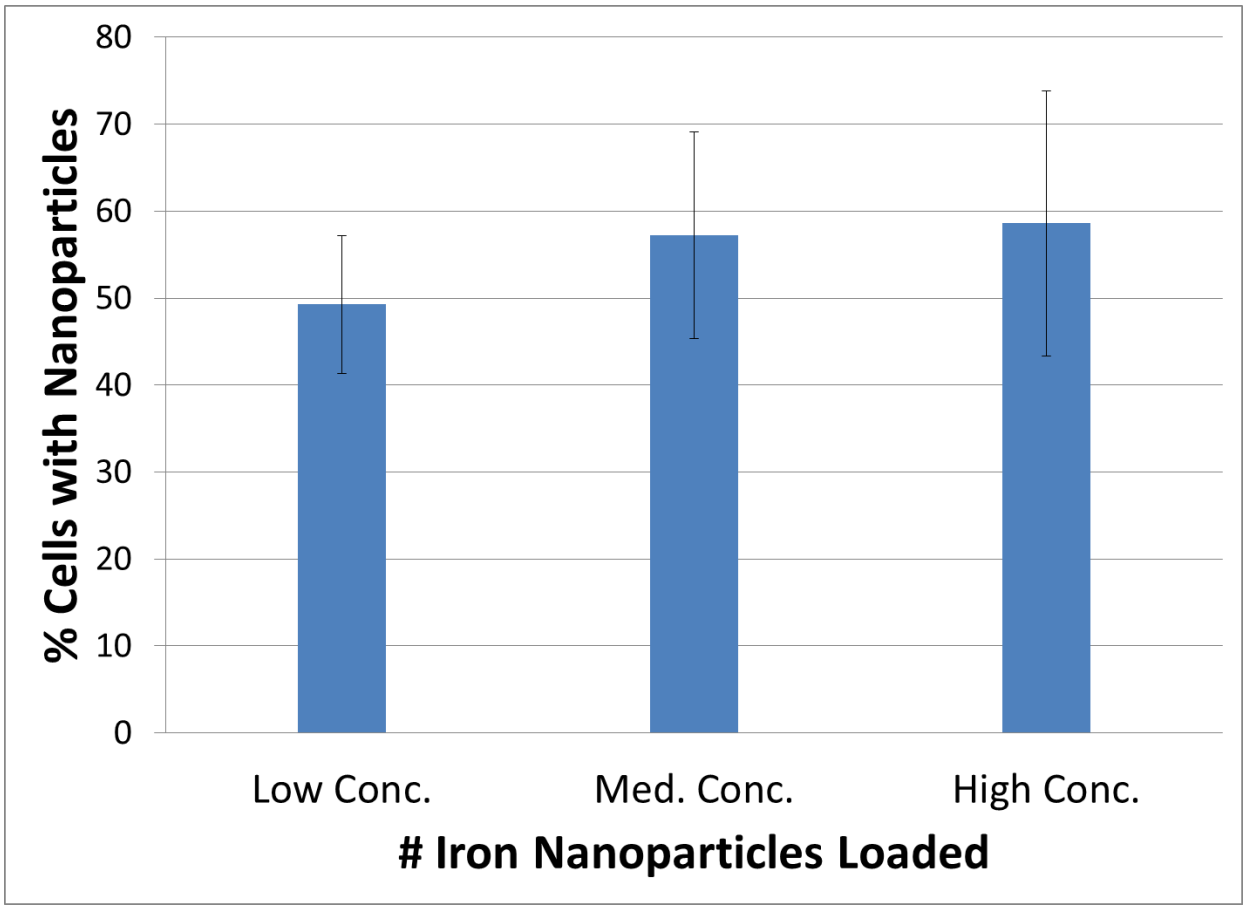

Figure 34. Iron nanoparticles load at the same efficiency at all tested iron nanoparticle concentrations. The percentage of cells staining positive for iron nanoparticles was 49.3±7.9, 57.2±11.9, 58.6±15.2 (mean±SD) for the low (0.25 mg/mL), medium (0.50 mg/mL), and high (1.00 mg/mL) concentration of iron nanoparticles, respectively. The percentage of cells with positive staining for iron nanoparticles is shown on the y-axis. The iron nanoparticle concentration groups are labeled on the x-axis.

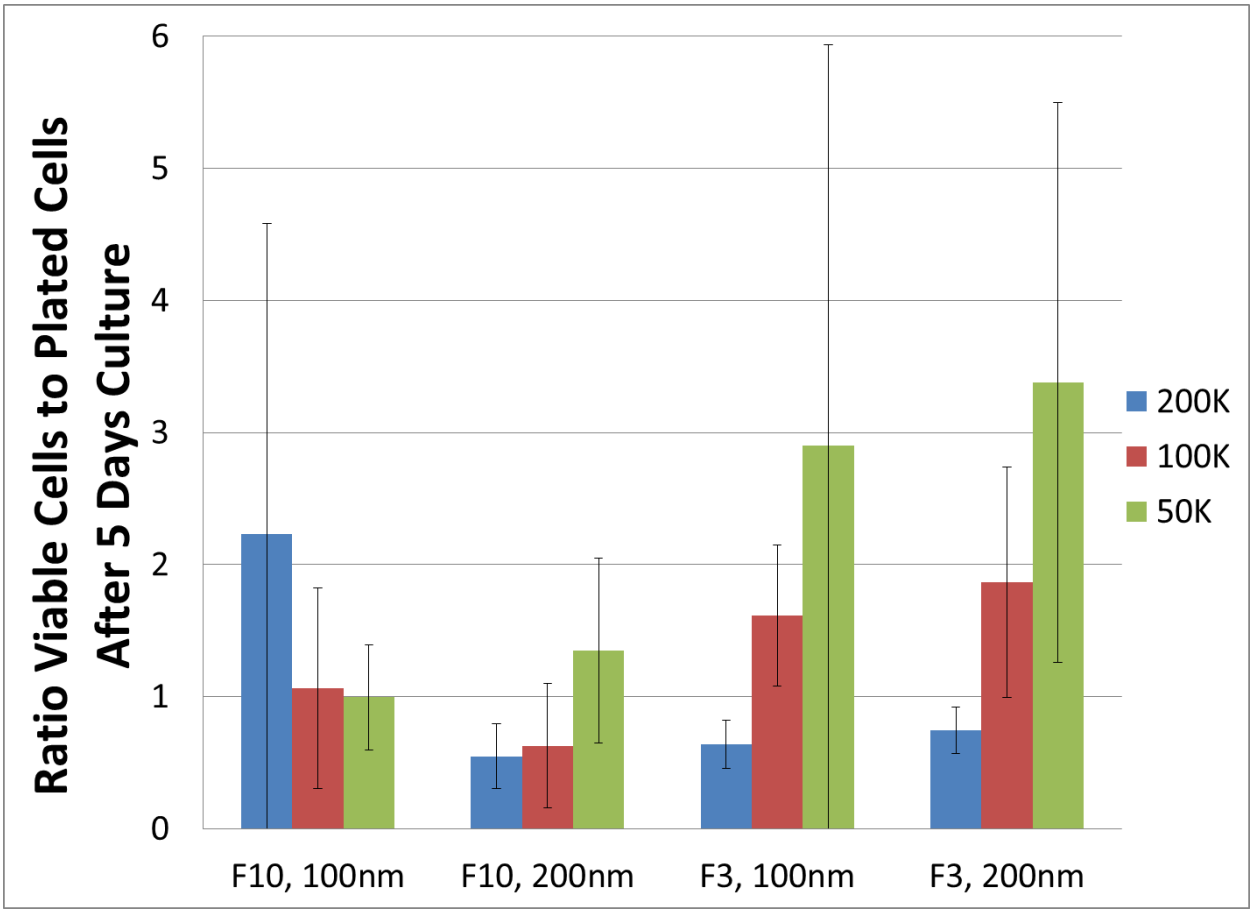

Figure 35. Fibrinogen concentration, starting cell number and a mixed effect term of fibrinogen concentration and starting cell number are significant predictors of ratio of viable cells to plated cells after 5 days in culture. The ratio of viable cells to plated cells after 5 days in culture is shown on the y-axis. The fibrinogen concentration (F3 = 3mg/mL, F10 = 10 mg/mL) and iron nanoparticle size groups are labeled on the x-axis. The starting cell number is labeled with blue ($2.0x10^5$), red ($1.0x10^5$) and green ($5.0x10^4$).

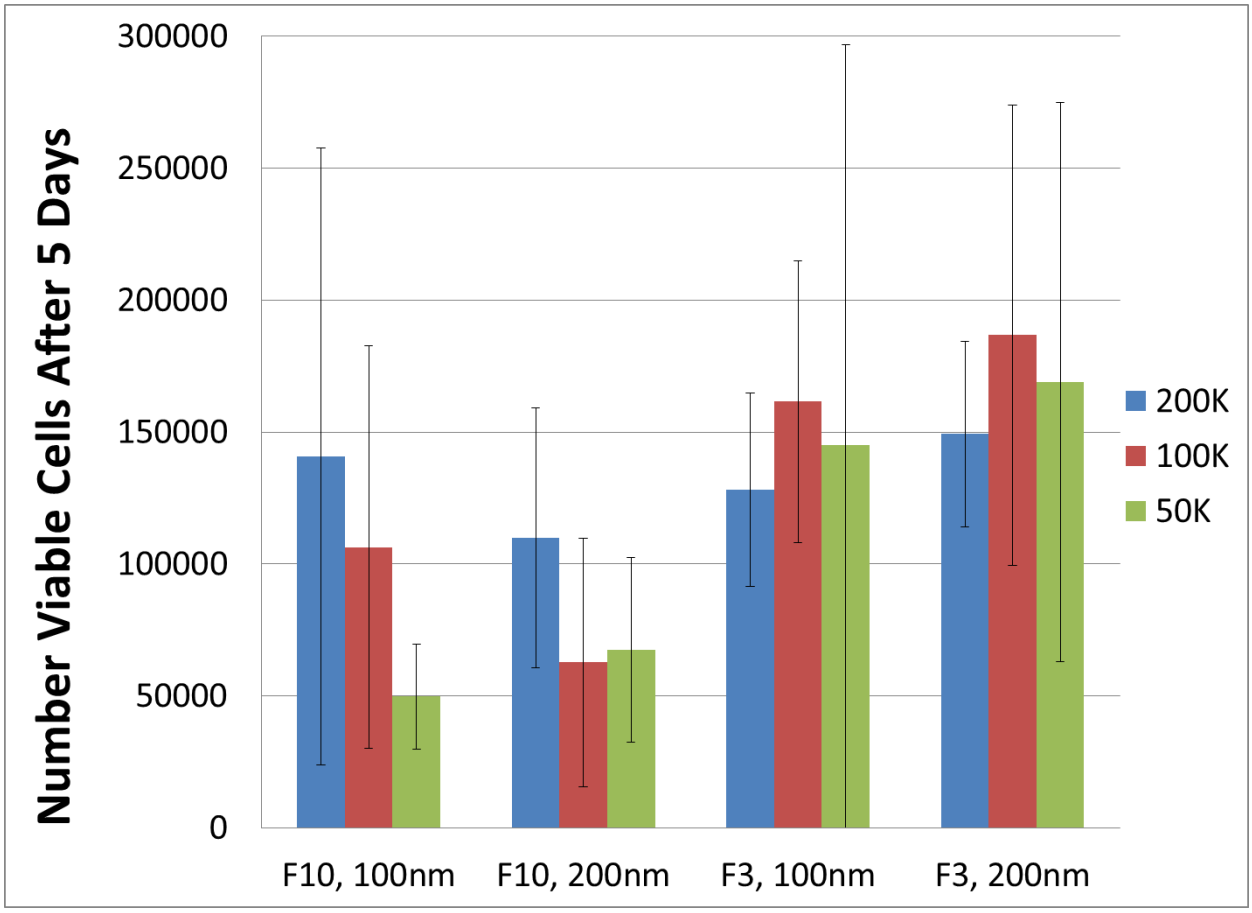

Figure 36. Fibrinogen concentration is a significant predictor of number of viable cells after 5 days in culture. The number of viable cells after 5 days in culture is shown on the y-axis. The fibrinogen concentration (F3 = 3mg/mL, F10 = 10 mg/mL) and iron nanoparticle size groups are labeled on the x-axis. The starting cell number is labeled with blue ($2.0x10^5$), red ($1.0x10^5$) and green ($5.0x10^4$).

6.3.2 In-vitro Magnetic Force Induced Cell Localization

We assessed the ability of magnetic attractive forces between a magnet and iron nanoparticles to move cells through a fibrin hydrogel. This ability was tested in short and long term studies. The results of the short term study are shown in **Figure 37**. We found that cells loaded with iron nanoparticles were unable to be pulled through a fibrin hydrogel when the localizing magnetic field was introduced 20 seconds after plating the gel. This was not the case in the experimental group that did not include cells as iron nanoparticles were still able to localize over the magnet at the 20 second time point but were unable to localize at the 10 minute time point. Though the pictures shown in **Figure 37** were taken one day after plating the gels, all groups looked the same shortly after placement of the magnet.

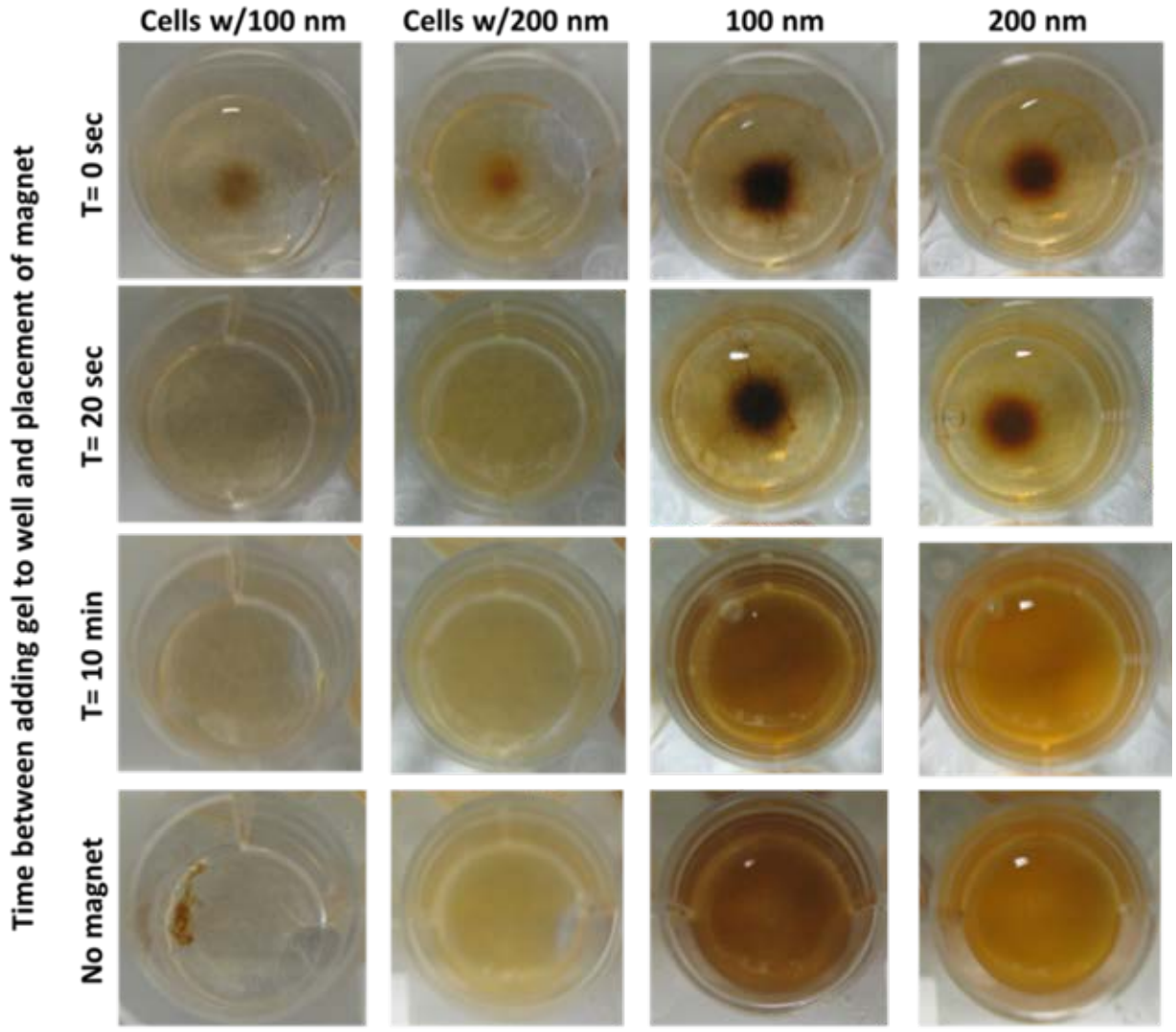

Figure 37. The attractive force between iron nanoparticle and magnets can move cells and iron nanoparticles through a fibrin gel before gelation is complete. Iron nanoparticles appear brown within a fibrin gel 24 hours after plating. Columns are labeled with experimental group. Rows are labeled with time of magnet placement with respect to plating.

Since we determined that acute magnetic exposure was unable to localize the cells within the fibrin hydrogel, we wanted to determine whether long term magnetic exposure could accomplish the task. When exposed to a magnetic field for five days in culture, cells loaded with iron nanoparticles localized over the source of the magnetic field. **Figure 38B** shows a cross section of a fibrin gel exposed to a small diameter magnet for five days that has been stained with Prussian Blue and DAPI. There is compression of the fibrin gel in the area directly over the magnet. **Figure 38C** shows a blowup of the red rectangle in **Figure 38B** for the Prussian Blue stain, DAPI and merged channels from top to bottom respectively.

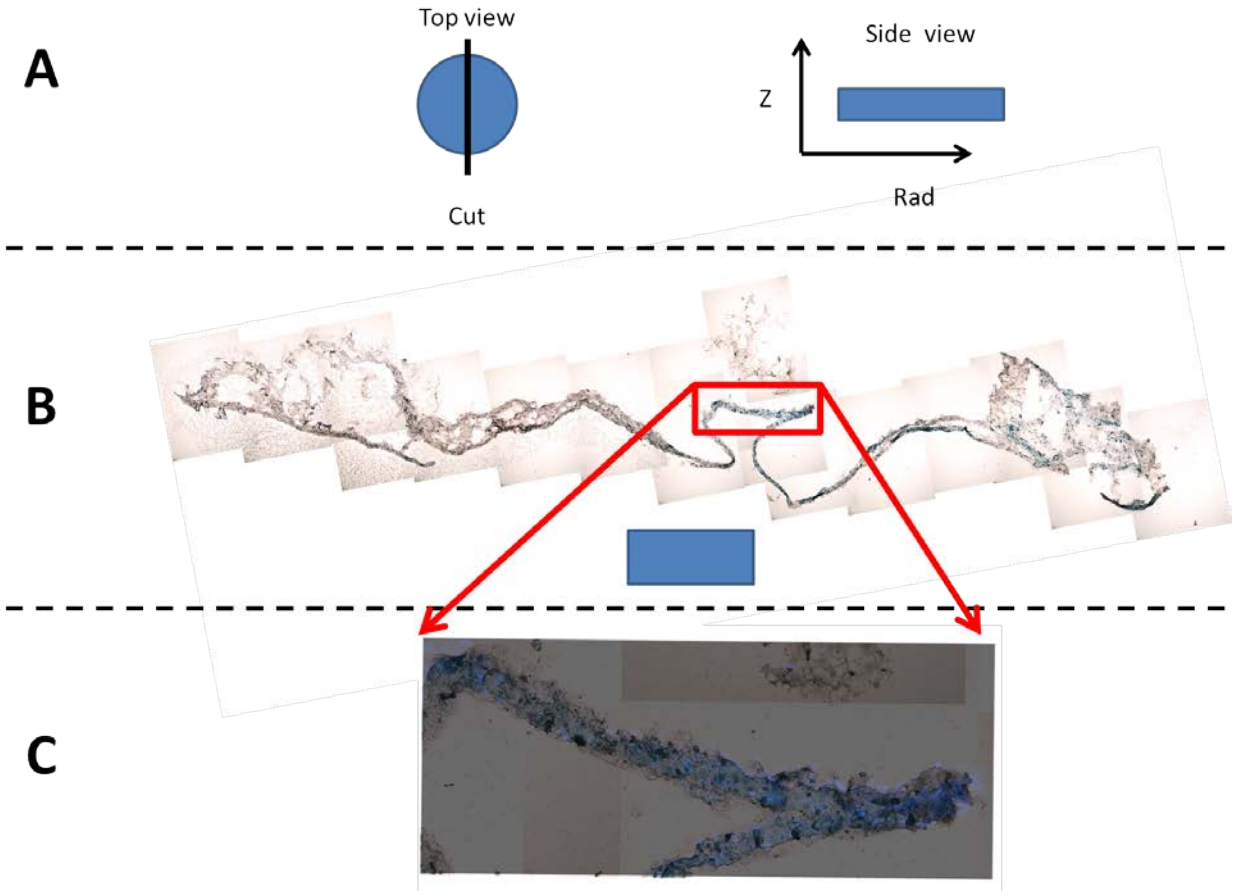

Figure 38. ADMSCs loaded with iron nanoparticles localize towards a small magnet after five days in culture. A) Schematic of how circular gels were sectioned and imaged. The circular gel was cut in half, and then sections were made across the z-radial plane. B) The gel has been stained with Prussian Blue dye to identify iron nanoparticles. The lower blue rectangle represents the relative position and size of the magnet to the gel during culture. The red box is the area that is magnified in panel C which shows the DAPI and Prussian Blue stain merged.

Figure 39B shows a cross section of a fibrin gel exposed to a large diameter magnet for five days that has been stained with Prussian Blue and DAPI. There is a compression of the fibrin gel over nearly the entire gel which is approximately the same size as the large magnet. **Figure 39C** shows a blowup of the red rectangle in **Figure 39B** for the merged Prussian Blue and DAPI channels.

Figure 40 shows a Prussian Blue and DAPI stain of an ADMSC seeded gel loaded with iron nanoparticles that was cultured for 5 days without any magnet in place. There is a small accumulation of cells along the bottom of the gel, but the gel remains thicker than the counterparts shown in **Figure 38 & Figure 39**. **Figure 41** shows a DAPI stain of an ADMSC seeded gel that had not been loaded with iron nanoparticles. The gel was cultured for 5 days with the large magnet in place. The gel is thicker and less dense in appearance compared to the iron nanoparticle loaded counterpart in **Figure 39**.

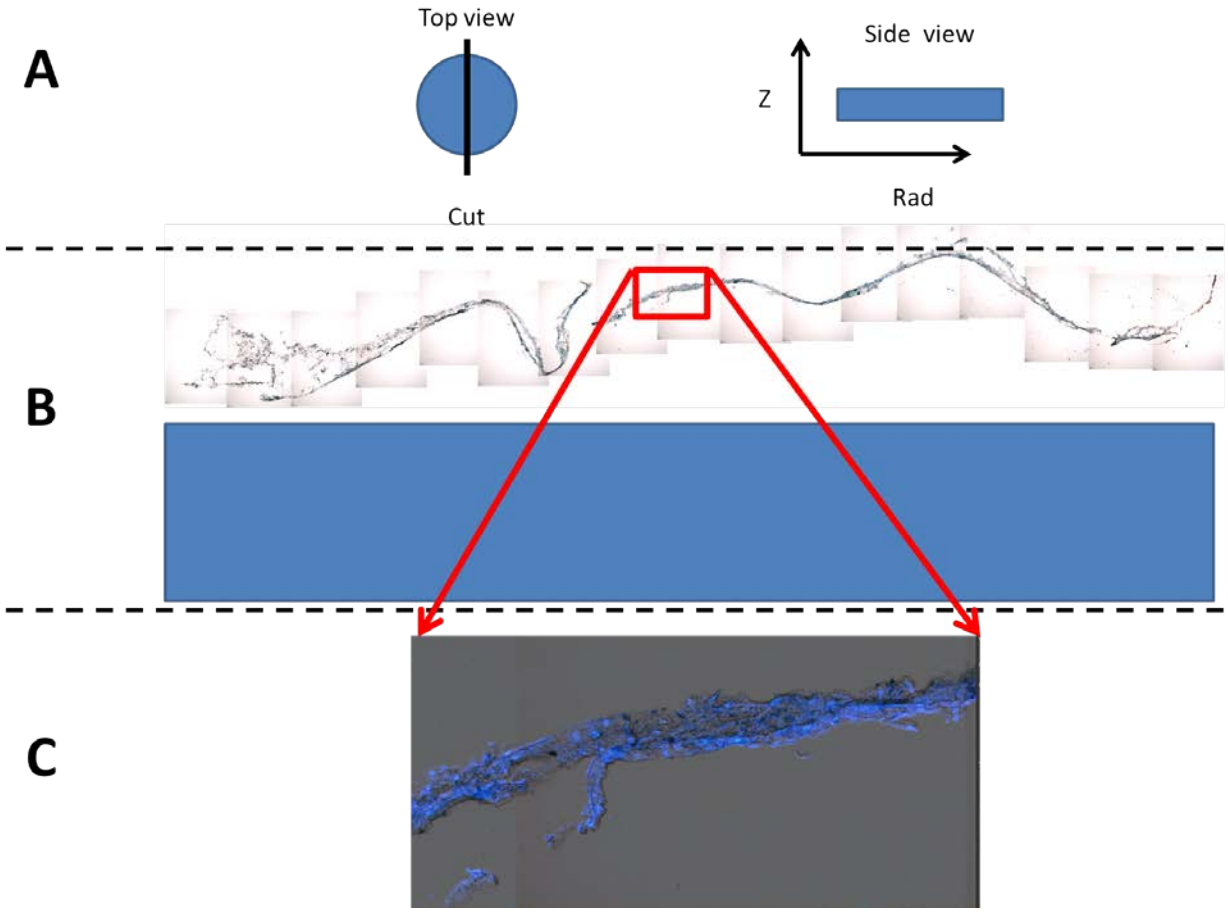

Figure 39. ADMSCs loaded with iron nanoparticles localize towards a large magnet after five days in culture. A) Schematic of how circular gels were sectioned and imaged. The circular gel was cut in half, and then sections were made across the z-radial plane. B) The gel has been stained with Prussian Blue dye to identify iron nanoparticles. The lower blue rectangle represents the relative position of the magnet to the gel during culture. The red box is the area that is magnified in panel C which shows the DAPI and Prussian Blue stain merged.

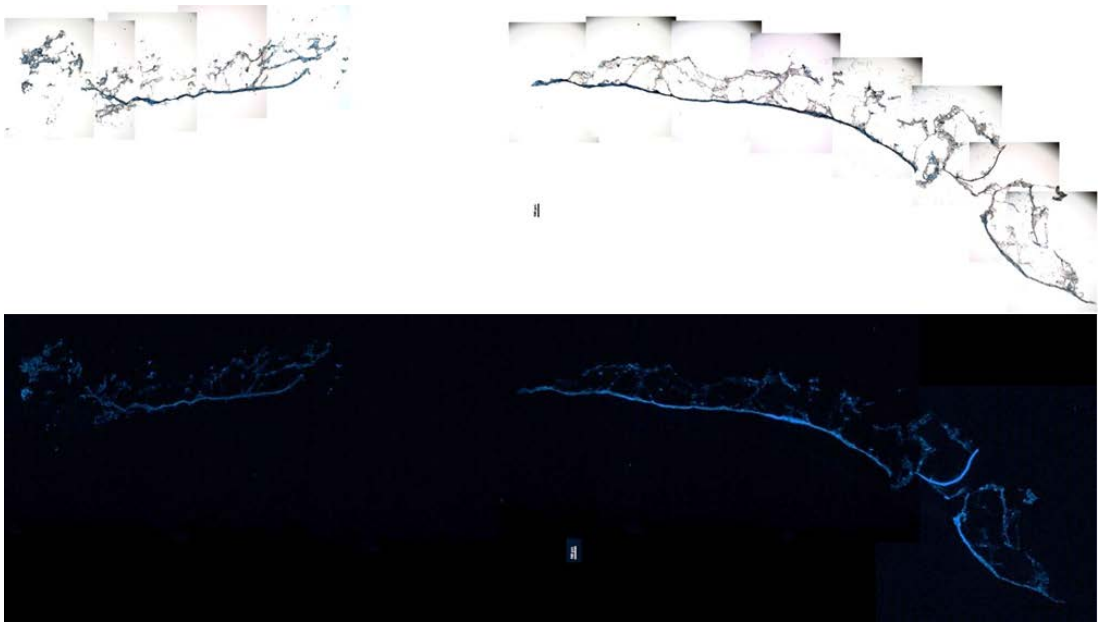

Figure 40. ADMSCs loaded with iron nanoparticles accumulate at the bottom of the wells after five days in culture. Prussian Blue and DAPI are shown in top and bottom pictures, respectively for the ADMSC iron nanoparticle loaded gel cultured without a magnet in place.

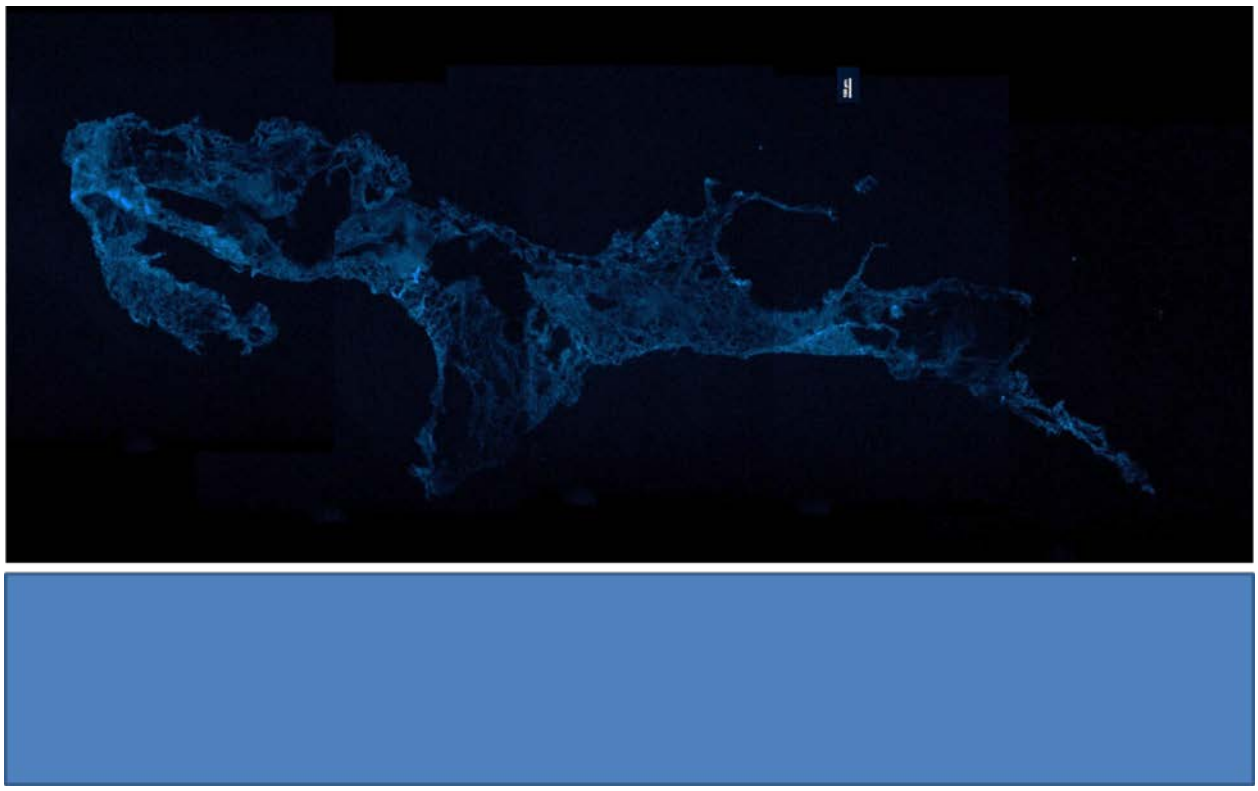

Figure 41. ADMSCs without iron nanoparticles remain dispersed throughout the gel after five days in culture. DAPI stain for ADMSCs without iron nanoparticles when cultured for five days with a large magnet in place. The lower blue rectangle represents the relative position and size of the magnet to the gel during culture.

6.3.3 Cell Delivery Mixer Performance

A one-way ANOVA revealed that there was no statistical difference ($p=0.587$) between any of the tested groups (**Table 9**). The fibrin gel mixer was able to produce fibrin gels that had a similar cell distribution throughout the gel compared to gels that were thoroughly mixed by manual pipetting. Also, the cell distribution was not dependent upon which input (Left, Center, or Right) that the cell suspension was attached to. A sample image of the DAPI stained nuclei from the control group is shown in **Figure 42**.

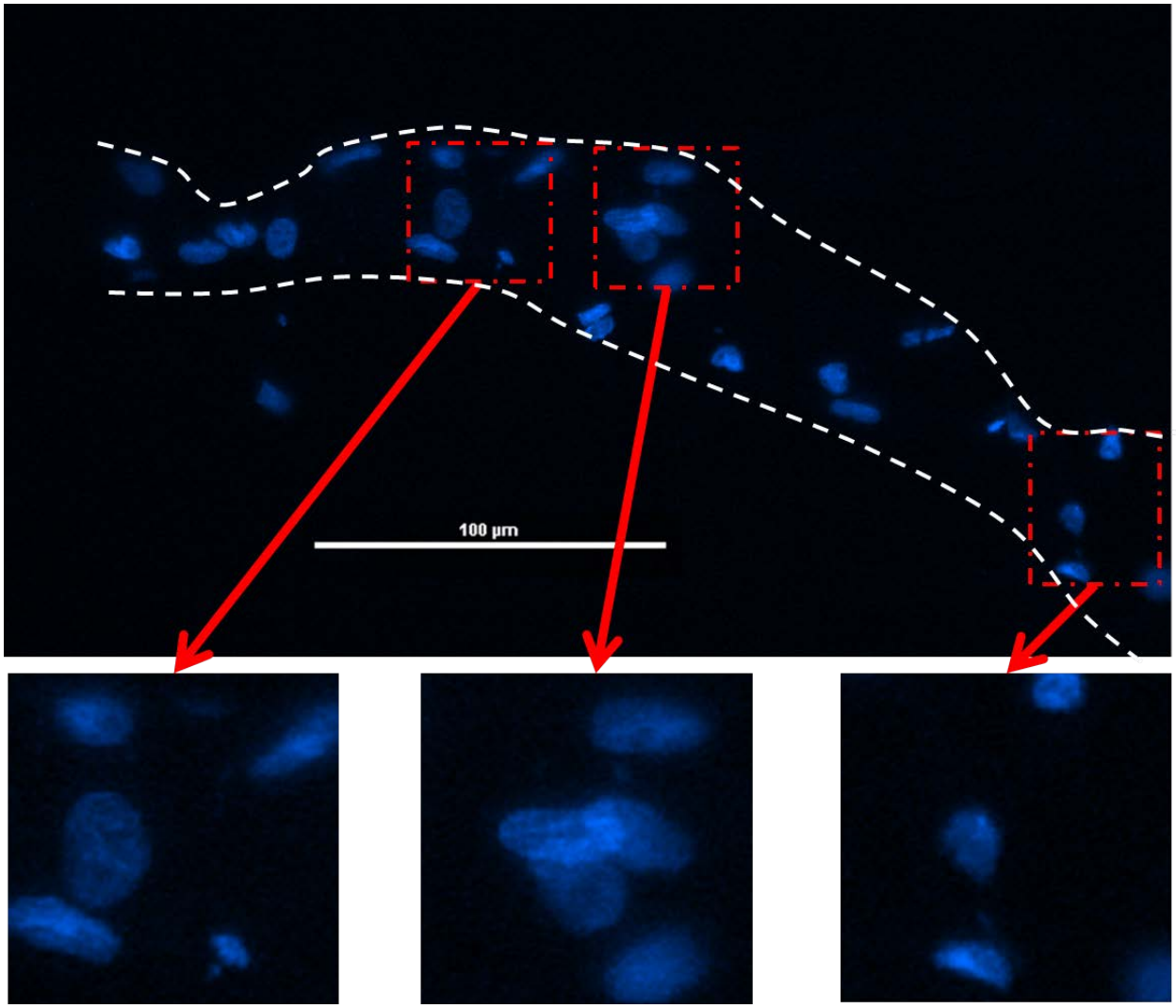

Figure 42. ADMSC nuclei are distributed evenly throughout the fibrin gel. The dashed white line in the top image indicates the outline of the fibrin gel. The red dashed boxes were randomly chosen for ImageJ ellipse fitting and distance measurement analysis of the blue, DAPI stained ADMSC nuclei.

Table 9. All groups show a similar average distance between nuclei. When fit with an ellipse, the average distance between centroid of each nucleus was 52.4±4.5 pixels for the control group, 49.1±12.7 pixels for the Left group, 45.2±5.7 pixels for the Center group, and 53.0±3.5 pixels for the Right group.

	Distance Between Nuclei (mean ±SD, pixels)
Control	52.4±4.5
Left	49.1±12.7
Center	45.2±5.7
Right	53.0±3.5
	p=0.587

6.3.4 Magnetic Probe Ultrasound Identification

The ultrasonic images of the magnetic probe are shown in **Figure 43**. In **Figure 43A** the image was captured without the magnetic probe in place, and the anterior aortic mimic outer and inner diameters can be seen in the image. The posterior outer diameter can also be seen. In **Figure 43B**, the magnetic probe was brought into the field of view, and the anterior portion of the catheter and the magnets can be seen. The magnetic probe is highlighted in **Figure 43C** in red.

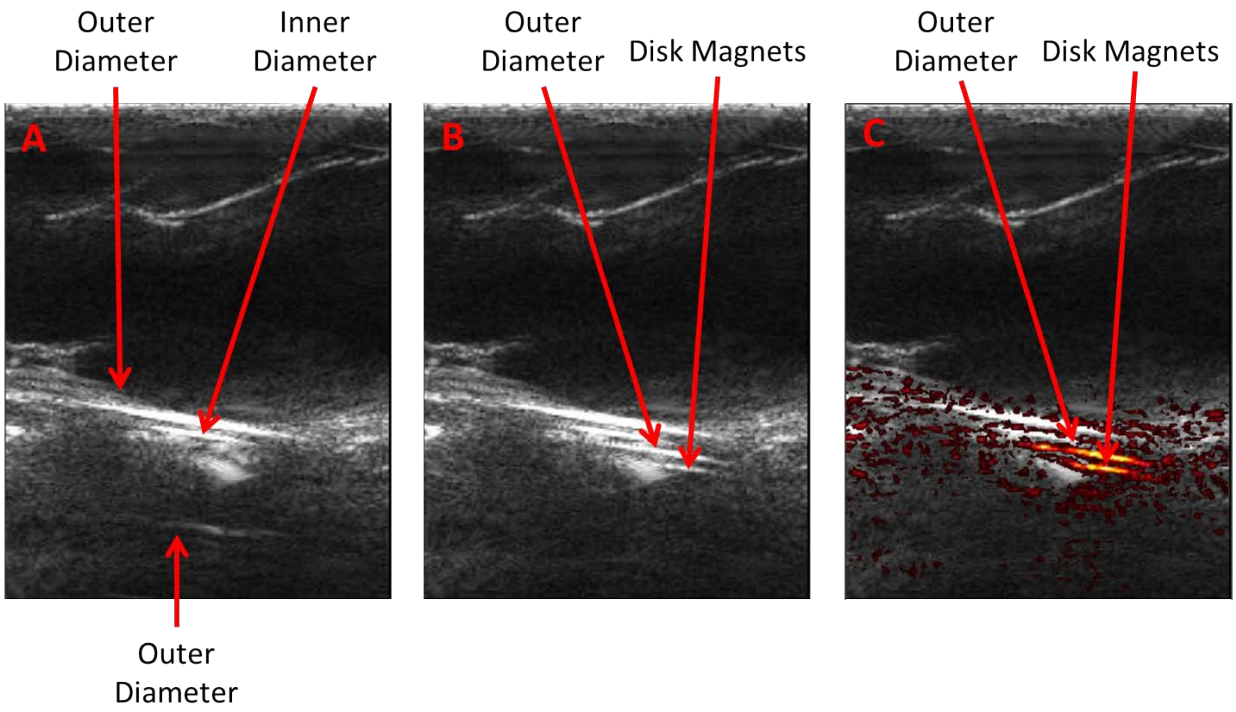

Figure 43. The magnetic probe is visible within tissue and aorta mimics using ultrasonic imaging. A) An ultrasonic image shows the aorta mimic within the tissue mimic. B) An ultrasonic image shows the magnetic probe within the aorta mimic. C) The same ultrasonic image from panel B is shown with the changes from panel A highlighted in red.

6.4 DISCUSSION

We saw no statistical difference in iron nanoparticle loading efficiency amongst the tested concentrations. This result was not so surprising considering the manufacturer's recommended concentration is a general value to be used for all cell types, and conversations with the manufacturer revealed that loading efficiency will be dependent on cell type. While the lowest concentration tested may seem to be the best choice from a cost perspective, the middle concentration was chosen for all remaining experiments due to other groups maintaining good viability and differentiation potential using a similar concentration[403,419,420].

Our own viability studies of cells within fibrin gels after five days in culture showed that total cell number and ratio of cells after five days in culture to plated cells were not dependent on the size of iron nanoparticle used which is in agreement with other published studies[403,419-421]. Our viability experiments did show fibrinogen concentration to be a significant predictor of both total cell number and ratio of cells after five days in culture to plated cells, and our total cell numbers are consistent with other published studies[267,269,411]. Starting cell concentration and a cross talk term between starting cell concentration and fibrinogen concentration were also significant predictors of ratio of cells after five days in culture to plated cells. When taken together, the increases in cell number are largely dependent on the amount of free space within the fibrin gels. This can partially explain the difference in starting cell concentration being a significant predictor of the ratio of cells after five days in culture to plated cells but not of the total cell number. This knowledge can also be used to manipulate a potential cell therapy. The fibrinogen concentration should be kept high if cell division is undesired. Conversely, if cell division is desired, then fibrinogen and starting cell concentration should be kept low. In our application, cell division is undesirable since we want the ADMSCs producing the growth factor

profile shown at confluence[194]. However, we also desire a lower fibrinogen concentration so that the cells can more easily move towards the magnet. A compromise for our application would be using a high cell concentration with a low fibrinogen concentration.

Using the combination of fibrin gels and iron nanoparticles seem to have no negative effects on our therapeutic ADMSCs in terms of viability. However, we still needed to determine if using the fibrin and iron nanoparticles would allow for the migration or movement of the therapeutic ADMSCs through the fibrin gel to the periadventitial surface of the AAA. Our short term experiments show that ADMSCs loaded with iron nanoparticles contained in a fibrin gel will move through the fibrin gel solution to a magnetic field source if the fibrin has not completely gelled. It is important to note that forming fibrin gels in the presence of an external magnetic field will produce an anisotropic gel that is aligned in the direction of the magnetic field[422-424]. This effect may be partially responsible for the increased localization of cells and iron nanoparticles near the magnet in the gels which were plated in the presence of a magnetic field.

Our long term experiments show that ADMSCs loaded with iron nanoparticles contained in a fibrin gel will move to a magnetic field source even after the fibrin has gelled to an appreciable amount. The movement in the long term experiments seems to be due to compression of the fibrin gel rather than movement of the cells through the gel. This is apparent in **Figure 38 & Figure 39** which shows compacted gels directly over the external magnet while **Figure 41** shows that ADMSCs without iron nanoparticles within a fibrin gel do not compact over an external magnet. The gel remains "fluffy" in this case. Others have had success when using externally applied magnetic fields in attempts to localize cells or drugs that have incorporated iron nanoparticles[402,403].

The hardware elements of the cell delivery system, the fibrin gel mixer and the magnetic probe, achieve the design criteria goals. The fibrin gel mixer was able to produce fibrin gels with a uniform ADMSC distribution as shown in **Table 9**. The magnetic probe prototype was successfully imaged through tissue and aorta mimics using ultrasonic imaging.

While we largely saw movement of iron nanoparticle loaded ADMSCs toward our magnet, we must evaluate our product through the lens of the FDA, and there are important questions the FDA raises when considering CTs. For example, the FDA has explicitly expressed concerns[425] about cell migration. When delivered systemically, CTs could end up in a variety of tissues. This has been seen even when cells delivered to a specific tissue or organ eventually migrate to unintended locations[426]. Our system has been designed to localize our CT and keep it in place. The FDA also highlights that concerns about autologous vs. allogeneic cells. We also share this concern. While using autologous cells is certainly possible in our therapy, we have concerns about the efficacy of cells derived from older patients[326,327,427].

The FDA also highlights concerns regarding combination products[415] recommending that researchers consider the scientific and technical issues raised by the combination product and its constituents. Once considered, the study design to address these concerns should be performed using proper statistical consideration to evaluate the combination product without duplication or redundancy so that development is streamlined. Careful attention should be paid when constituents are mixed and produced as a single entity because there could now be a broader range of potential, unintended interactions. The FDA has additional concerns that particularly apply to our system. “A new device used to deliver a drug/biologic to a new area of the body that was previously inaccessible might make it necessary to develop new methods to determine the effect of such localized/targeted delivery, particularly when it results in higher exposure to that

target than when the drug is systemically administered. Likewise, innovative technologies such as nanotechnology or live cellular products may lead to the development of new manufacturing methodologies or unique safety issues not associated with products manufactured in other ways."[415] The nature of our system, a combination product and CT, does present additional hurdles to clear before gaining FDA approval. However, the current design and subsequent design iterations are made with the FDA guidelines in mind.

Utilizing our therapeutic cell delivery system, patients could avoid the mortality risks associated with open AAA repair and avoid the secondary complications associated with endovascular repair. Our therapy may lower the total number of MRI or CT scans that surgeons use to monitor the growth rate and size of AAAs.

Treating the disease early may also have other intangible quality-of-life benefits. When patients are diagnosed with the disease and told how the disease progresses, they (as well as their families) can feel stressed about having a "ticking time bomb" in their abdomen. Providing a viable therapy shortly after diagnosis should alleviate anxiety over the disease.

In addition to these non-tangible benefits, we have provided a pro forma cost analysis of our proposed therapy in **Table 10** that highlights the potential cost savings benefits. Our therapy will attempt to carve out a space in the huge healthcare cost burden that is AAA repair. The burden is over $2.125 billion dollars per year (50,000 annual patients * $85,000 total 2 year costs[119]). If only a third of patients gained enough therapeutic benefit through our treatment to avoid the need for surgical repair, $458 million dollars could be removed from the US healthcare burden each year ($2.125 billion /3 – 50,000 patients * $5,000 per patient for our therapy).

Table 10. Proforma cost of proposed interventional stem cell treatment for AAA. The projected costs of our proposed therapy are broken down by the device and the administration of the treatment.

Proposed Production Costs Cell Delivery System	
Cells	$1,000
Licensed fibrin product (EVARREST)	$500
Syringes	$10
Solution mixer & dispenser	$20
Delivery needle	$40
Magnetic catheter	$100
Nanoparticles	$30
Subtotal	$1,700
Location and Administration Costs	
Hospital room	$2,500
Medical technician (catheter)	$400
Ultrasound technician	$400
Subtotal	$3,300
Total	$5,000

6.5 CONCLUSION

Individual aspects of the cell delivery system were tested with respect to their promise for the future clinical translation of the technology. Iron nanoparticle loading efficiency in ADMSCs was approximately 52% when loading the manufacturer recommended amount of iron nanoparticles and ±50% of manufacturer recommended amount of iron nanoparticles. Fibrinogen concentration was a significant predictor of cell viability in iron nanoparticle loaded, ADMSC-seeded, fibrin gels. Acute magnetic mediated movement of iron nanoparticle loaded cells only happened before complete gelation of fibrin gels. Longer term exposure to a magnet caused the iron nanoparticle loaded ADMSCs to compress fibrin gels locally over a magnetic field source. The fibrin gel mixer was able to produce gels with uniformly distributed ADMSCs. The magnetic probe was able to be detected using ultrasonic imaging.

6.6 FUTURE WORK

Iterative prototyping of the cell delivery mixer and bench side testing of the device needs to be performed and is currently underway. These experiments will precede large animal studies testing the efficacy of the system.

The FDA pathway for approval of this system will likely be either an Investigational New Drug (IND) or an Investigational Device Exemption (IDE). Trial design, sample size, statistical methods, clinical endpoints, appropriate number of clinical studies, and appropriate indications/claims will all need to be determined. Since our system has a device constituent part, we will need to evaluate the human factors of device use on the safety and effectiveness of the

combination product. These studies will help us understand how users operate the system in realistic, stressful conditions. Lastly, manufacturing, scale-up, and quality management need to be considered and studied with respect to both premarket development and postmarket regulation.

7.0 STUDY SUMMARY

The following sections will summarize the key findings presented within this dissertation, discuss the future directions of each Aim, and present my scientific accomplishments achieved through this work.

7.1 SUMMARY OF RESULTS

7.1.1 Specific Aim 1

In Aim 1, we sought to prove that adult, human SMCs could produce elastin fibers when co-cultured with ADMSCs and that elastin production was able to slow the expansion of a AAA in a computational model. In Aim 1-1 we showed that ADMSCs in co-culture in with adult SMCs stimulate elastic fiber production in a 3D fibrin gels. This novel finding lends credence to using ADMSCs as a pro-elastogenic therapy for treating AAAs.

In Aim 1-2 we showed that elastin production within an aneurysm could relieve the maladaptive mechanical environment to an extent that slows aneurysmal enlargement within a computational model of AAA G&R. Early intervention can reduce the enlargement rate by more than 50%, delaying delay the need for surgical intervention by 10 years[385]. These findings also

confirm our thoughts that regeneration of functional elastic fibers in a AAA could help slow the progression of the disease.

7.1.2 Specific Aim 2

In Aim 2, we sought to prove that periadventitial ADMSC treatment to an established, expanding, murine elastase perfused AAA could halt dilation of the artery. Indeed, we have developed an animal model for delayed, periadventitial delivery of ADMSCs to ameliorate elastase-induced AAA. Delayed, periadventitial delivery of ADMSCs halted two aspects of aneurysm progression – expansion of the aortic diameter and fragmentation of the elastic lamella. This work represents an important step towards developing clinically realistic stem cell therapies for AAA patients.

7.1.3 Specific Aim 3

In Aim 3 we sought to design and test key aspects of a cell delivery system for treating AAAs. We utilized iron nanoparticles, magnets, and fibrin hydrogel to localize the delivery of therapeutic cells to a desired location. We found the following: 1) Iron nanoparticle loading efficiency in ADMSCs is approximately 52% when loading the manufacturer recommended amount of iron nanoparticles and ±50% of manufacturer recommended amount of iron nanoparticles. 2) Fibrinogen concentration is a significant predictor of cell viability in iron nanoparticle loaded, ADMSC seeded, fibrin gels. 3) Acute magnetic mediated movement of iron nanoparticle loaded cells only happens before complete gelation of fibrin gels. 4) Longer term

exposure to a magnet will cause the iron nanoparticle loaded ADMSCs to compress fibrin gels locally over a magnetic field source. 5) Our fibrin gel mixer was able to make gels with a uniform distribution of ADMSCs. 6) Our magnetic probe was able to be imaged through tissue and aorta mimics via ultrasound.

7.2 SUMMARY OF ACCOMPLISHMENTS

The work of this dissertation has led to the generation of the following scientific manuscripts:

1. **Blose KJ**, Pichamuthu JE, Weinbaum JS, Vorp DA. "Design and validation of a vacuum assisted anchorage for the uniaxial tensile testing of soft materials." Soft Materials 14.2 (2016)
2. **Blose KJ**, Ennis TL, Arif B, Weinbaum JS, Curci JA, Vorp DA. "Periadventitial adipose-derived stem cell treatment halts elastase-induced abdominal aortic aneurysm progression." Regenerative medicine 9.6 (2014)
3. **Blose KJ**, Weinbaum JS, Robertson AM, Vorp DA. "Stem Cell-Induced Elastin Production by Smooth Cells: In-Vitro Assessment and In-Silico Implications for Abdominal Aortic Aneurysm." [in preparation]

Additionally, a book chapter was written pertaining to the background material utilized in this dissertation:

1. **Blose KJ**, Krawiec JT, Weinbaum JS, Vorp DA. "Chapter 15: Bioreactors for Tissue Engineering Purposes," *Regenerative Medicine Applications in Organ Transplantation, 1st Edition*. Giuseppe Orlando, ed. Academic Press, 2013.

Finally, multiple individual fellowships or grants were obtained by the author of this dissertation or by undergraduates who were mentored by the author:

1. **F_168-2016**, "Minimally invasive delivery of therapeutic cells to abdominal aortic aneurysm" University of Pittsburgh Center for Medical Innovation Early-Stage Medical Technology Research and Development 2016 Pilot Funding Program [PI: Kory Blose]

2. **NIH T32 EB000392**, "Computationally Guided Development of Therapies for Abdominal Aortic Aneurysms", 9/2014-8/2016 [Training fellowship to Kory Blose]
3. **NIH T32 HL076124**, "Computational Simulation Model for Biomechanically-Guided Growth and Differentiation of Tissue Engineered Vascular Grafts", 2/2012-1/2014 [Training fellowship to Kory Blose]
4. **Undergraduate Summer Research Internship Scholarship**, Swanson School of Engineering (SSOE), University of Pittsburgh, 6/2011-8/2011 [Summer Fellowship to Huong Tran]

7.3 FUTURE WORK

The future directions of this dissertation are discussed within each Aim due to the independent nature of those projects. For the discussion of future directions in Aim 1-1 see **Section 3.6**, for Aim 1-2 see **Section 4.5**, for Aim 2 see **Section 5.6**, and for Aim 3 see **Section 6.6**.

APPENDIX A

FEAP IMPLEMENTATION OF CONSTRAINED MIXTURE MODEL OF AAA G&R

FEAP Implementation:

```
!====================
! Parenthetical citations refer to a page number within the FEAP version 8.2 User Manual.

! batch mode.

! Control data (pg 24)
! All FEAP input files must begin with "FEAP" in either upper or lower case (here in lower
case).
! The remaining characters are used for the problem title in the output file.
! The second record contains problem size information:
! (a) NUMNP number of nodal point
! (b) NUMEL number of elements
! (c) NUMMAP number of material property sets
! (d) NDM space dimension of mesh
! (e) NDF maximum number of unknowns per node
! (f) NEN maximum number of nodes per element
! NOTE that for the first 3 items are specified as ZERO (0) since FEAP can determine
appropriate values
! from the data provided below (pg 25).
feap ** aortic aging
0 0 0 3 3 8

! We define the material as an elastic solid with a neo-Hookean strain energy function
! NOTE that this is not an incompressible material
material 1                      ! 1st material (adventitia)
  solid                         ! Solid material
  finite                !,volume,2
  mixed                         ! Use Q1-P0 element
  uconst adve 1.0e8 1.25e5
  augment off
```

```
material 2                      ! 2nd material (media)
  solid                         ! Solid material
  finite                !,volume,2
  mixed                         ! Use Q1-P0 element
  uconst medi 1.0e8 1.25e5
  augment off

material 3                      ! 3rd material (luminal surface)
  pressure                      ! "pressure" elements
  load,pr                       ! Loaded by parameter pr
  follower                      ! Load pr "follows" the moving lumen
  finite
  augment off

! Set a parameter pr. This is the transmural pressure (Pa).
PARAmeter
pr = -1.239898026e4
! parameter for % baseline elastin degradation
pe = 7.5e-1
! Set parameter d. This is a displacement.
!d = 0.0

! Nodal coordinates in the global coordinate system (pg 26)
! N NG X_N Y_N Z_N
! N number of nodal point
! NG generation increment to next node
!   when no coordinate generation is required, set to ZERO (0) (pg 28)
! X_N value of x_1 coordinate
! Y_N value of x_2 coordinate
! Z_N value of x_3 coordinate
COORdinates
1       0       0.000000E+00 7.500000E-03  -3.000000E-02
2       0       0.000000E+00 7.700000E-03  -3.000000E-02
3       0       0.000000E+00 7.900000E-03  -3.000000E-02
4       0       0.000000E+00 8.100000E-03  -3.000000E-02
5       0       0.000000E+00 8.300000E-03  -3.000000E-02
6       0       0.000000E+00 8.500000E-03  -3.000000E-02
7       0       0.000000E+00 8.700000E-03  -3.000000E-02
8       0       0.000000E+00 8.900000E-03  -3.000000E-02
9       0       0.000000E+00 9.100000E-03  -3.000000E-02
10      0       0.000000E+00 9.300000E-03  -3.000000E-02
11      0       0.000000E+00 7.500000E-03  -2.623803E-02
12      0       0.000000E+00 7.700000E-03  -2.623803E-02
13      0       0.000000E+00 7.900000E-03  -2.623803E-02
14      0       0.000000E+00 8.100000E-03  -2.623803E-02
```

15	0	0.000000E+00	8.300000E-03	-2.623803E-02
16	0	0.000000E+00	8.500000E-03	-2.623803E-02
17	0	0.000000E+00	8.700000E-03	-2.623803E-02
18	0	0.000000E+00	8.900000E-03	-2.623803E-02
19	0	0.000000E+00	9.100000E-03	-2.623803E-02
20	0	0.000000E+00	9.300000E-03	-2.623803E-02
21	0	0.000000E+00	7.500000E-03	-2.268899E-02
22	0	0.000000E+00	7.700000E-03	-2.268899E-02
23	0	0.000000E+00	7.900000E-03	-2.268899E-02
24	0	0.000000E+00	8.100000E-03	-2.268899E-02
25	0	0.000000E+00	8.300000E-03	-2.268899E-02
26	0	0.000000E+00	8.500000E-03	-2.268899E-02
27	0	0.000000E+00	8.700000E-03	-2.268899E-02
28	0	0.000000E+00	8.900000E-03	-2.268899E-02
29	0	0.000000E+00	9.100000E-03	-2.268899E-02
30	0	0.000000E+00	9.300000E-03	-2.268899E-02
31	0	0.000000E+00	7.500000E-03	-1.934085E-02
32	0	0.000000E+00	7.700000E-03	-1.934085E-02
33	0	0.000000E+00	7.900000E-03	-1.934085E-02
34	0	0.000000E+00	8.100000E-03	-1.934085E-02
35	0	0.000000E+00	8.300000E-03	-1.934085E-02
36	0	0.000000E+00	8.500000E-03	-1.934085E-02
37	0	0.000000E+00	8.700000E-03	-1.934085E-02
38	0	0.000000E+00	8.900000E-03	-1.934085E-02
39	0	0.000000E+00	9.100000E-03	-1.934085E-02
40	0	0.000000E+00	9.300000E-03	-1.934085E-02
41	0	0.000000E+00	7.500000E-03	-1.618223E-02
42	0	0.000000E+00	7.700000E-03	-1.618223E-02
43	0	0.000000E+00	7.900000E-03	-1.618223E-02
44	0	0.000000E+00	8.100000E-03	-1.618223E-02
45	0	0.000000E+00	8.300000E-03	-1.618223E-02
46	0	0.000000E+00	8.500000E-03	-1.618223E-02
47	0	0.000000E+00	8.700000E-03	-1.618223E-02
48	0	0.000000E+00	8.900000E-03	-1.618223E-02
49	0	0.000000E+00	9.100000E-03	-1.618223E-02
50	0	0.000000E+00	9.300000E-03	-1.618223E-02
51	0	0.000000E+00	7.500000E-03	-1.320239E-02
52	0	0.000000E+00	7.700000E-03	-1.320239E-02
53	0	0.000000E+00	7.900000E-03	-1.320239E-02
54	0	0.000000E+00	8.100000E-03	-1.320239E-02
55	0	0.000000E+00	8.300000E-03	-1.320239E-02
56	0	0.000000E+00	8.500000E-03	-1.320239E-02
57	0	0.000000E+00	8.700000E-03	-1.320239E-02
58	0	0.000000E+00	8.900000E-03	-1.320239E-02
59	0	0.000000E+00	9.100000E-03	-1.320239E-02
60	0	0.000000E+00	9.300000E-03	-1.320239E-02

61	0	0.000000E+00	7.500000E-03	-1.039122E-02
62	0	0.000000E+00	7.700000E-03	-1.039122E-02
63	0	0.000000E+00	7.900000E-03	-1.039122E-02
64	0	0.000000E+00	8.100000E-03	-1.039122E-02
65	0	0.000000E+00	8.300000E-03	-1.039122E-02
66	0	0.000000E+00	8.500000E-03	-1.039122E-02
67	0	0.000000E+00	8.700000E-03	-1.039122E-02
68	0	0.000000E+00	8.900000E-03	-1.039122E-02
69	0	0.000000E+00	9.100000E-03	-1.039122E-02
70	0	0.000000E+00	9.300000E-03	-1.039122E-02
71	0	0.000000E+00	7.500000E-03	-7.739181E-03
72	0	0.000000E+00	7.700000E-03	-7.739181E-03
73	0	0.000000E+00	7.900000E-03	-7.739181E-03
74	0	0.000000E+00	8.100000E-03	-7.739181E-03
75	0	0.000000E+00	8.300000E-03	-7.739181E-03
76	0	0.000000E+00	8.500000E-03	-7.739181E-03
77	0	0.000000E+00	8.700000E-03	-7.739181E-03
78	0	0.000000E+00	8.900000E-03	-7.739181E-03
79	0	0.000000E+00	9.100000E-03	-7.739181E-03
80	0	0.000000E+00	9.300000E-03	-7.739181E-03
81	0	0.000000E+00	7.500000E-03	-5.237254E-03
82	0	0.000000E+00	7.700000E-03	-5.237254E-03
83	0	0.000000E+00	7.900000E-03	-5.237254E-03
84	0	0.000000E+00	8.100000E-03	-5.237254E-03
85	0	0.000000E+00	8.300000E-03	-5.237254E-03
86	0	0.000000E+00	8.500000E-03	-5.237254E-03
87	0	0.000000E+00	8.700000E-03	-5.237254E-03
88	0	0.000000E+00	8.900000E-03	-5.237254E-03
89	0	0.000000E+00	9.100000E-03	-5.237254E-03
90	0	0.000000E+00	9.300000E-03	-5.237254E-03
91	0	0.000000E+00	7.500000E-03	-2.876945E-03
92	0	0.000000E+00	7.700000E-03	-2.876945E-03
93	0	0.000000E+00	7.900000E-03	-2.876945E-03
94	0	0.000000E+00	8.100000E-03	-2.876945E-03
95	0	0.000000E+00	8.300000E-03	-2.876945E-03
96	0	0.000000E+00	8.500000E-03	-2.876945E-03
97	0	0.000000E+00	8.700000E-03	-2.876945E-03
98	0	0.000000E+00	8.900000E-03	-2.876945E-03
99	0	0.000000E+00	9.100000E-03	-2.876945E-03
100	0	0.000000E+00	9.300000E-03	-2.876945E-03
101	0	0.000000E+00	7.500000E-03	-6.502386E-04
102	0	0.000000E+00	7.700000E-03	-6.502386E-04
103	0	0.000000E+00	7.900000E-03	-6.502386E-04
104	0	0.000000E+00	8.100000E-03	-6.502386E-04
105	0	0.000000E+00	8.300000E-03	-6.502386E-04
106	0	0.000000E+00	8.500000E-03	-6.502386E-04

107	0	0.000000E+00	8.700000E-03	-6.502386E-04
108	0	0.000000E+00	8.900000E-03	-6.502386E-04
109	0	0.000000E+00	9.100000E-03	-6.502386E-04
110	0	0.000000E+00	9.300000E-03	-6.502386E-04
111	0	0.000000E+00	7.500000E-03	1.450428E-03
112	0	0.000000E+00	7.700000E-03	1.450428E-03
113	0	0.000000E+00	7.900000E-03	1.450428E-03
114	0	0.000000E+00	8.100000E-03	1.450428E-03
115	0	0.000000E+00	8.300000E-03	1.450428E-03
116	0	0.000000E+00	8.500000E-03	1.450428E-03
117	0	0.000000E+00	8.700000E-03	1.450428E-03
118	0	0.000000E+00	8.900000E-03	1.450428E-03
119	0	0.000000E+00	9.100000E-03	1.450428E-03
120	0	0.000000E+00	9.300000E-03	1.450428E-03
121	0	0.000000E+00	7.500000E-03	3.432189E-03
122	0	0.000000E+00	7.700000E-03	3.432189E-03
123	0	0.000000E+00	7.900000E-03	3.432189E-03
124	0	0.000000E+00	8.100000E-03	3.432189E-03
125	0	0.000000E+00	8.300000E-03	3.432189E-03
126	0	0.000000E+00	8.500000E-03	3.432189E-03
127	0	0.000000E+00	8.700000E-03	3.432189E-03
128	0	0.000000E+00	8.900000E-03	3.432189E-03
129	0	0.000000E+00	9.100000E-03	3.432189E-03
130	0	0.000000E+00	9.300000E-03	3.432189E-03
131	0	0.000000E+00	7.500000E-03	5.301774E-03
132	0	0.000000E+00	7.700000E-03	5.301774E-03
133	0	0.000000E+00	7.900000E-03	5.301774E-03
134	0	0.000000E+00	8.100000E-03	5.301774E-03
135	0	0.000000E+00	8.300000E-03	5.301774E-03
136	0	0.000000E+00	8.500000E-03	5.301774E-03
137	0	0.000000E+00	8.700000E-03	5.301774E-03
138	0	0.000000E+00	8.900000E-03	5.301774E-03
139	0	0.000000E+00	9.100000E-03	5.301774E-03
140	0	0.000000E+00	9.300000E-03	5.301774E-03
141	0	0.000000E+00	7.500000E-03	7.065534E-03
142	0	0.000000E+00	7.700000E-03	7.065534E-03
143	0	0.000000E+00	7.900000E-03	7.065534E-03
144	0	0.000000E+00	8.100000E-03	7.065534E-03
145	0	0.000000E+00	8.300000E-03	7.065534E-03
146	0	0.000000E+00	8.500000E-03	7.065534E-03
147	0	0.000000E+00	8.700000E-03	7.065534E-03
148	0	0.000000E+00	8.900000E-03	7.065534E-03
149	0	0.000000E+00	9.100000E-03	7.065534E-03
150	0	0.000000E+00	9.300000E-03	7.065534E-03
151	0	0.000000E+00	7.500000E-03	8.729459E-03
152	0	0.000000E+00	7.700000E-03	8.729459E-03

153	0	0.000000E+00	7.900000E-03	8.729459E-03
154	0	0.000000E+00	8.100000E-03	8.729459E-03
155	0	0.000000E+00	8.300000E-03	8.729459E-03
156	0	0.000000E+00	8.500000E-03	8.729459E-03
157	0	0.000000E+00	8.700000E-03	8.729459E-03
158	0	0.000000E+00	8.900000E-03	8.729459E-03
159	0	0.000000E+00	9.100000E-03	8.729459E-03
160	0	0.000000E+00	9.300000E-03	8.729459E-03
161	0	0.000000E+00	7.500000E-03	1.029920E-02
162	0	0.000000E+00	7.700000E-03	1.029920E-02
163	0	0.000000E+00	7.900000E-03	1.029920E-02
164	0	0.000000E+00	8.100000E-03	1.029920E-02
165	0	0.000000E+00	8.300000E-03	1.029920E-02
166	0	0.000000E+00	8.500000E-03	1.029920E-02
167	0	0.000000E+00	8.700000E-03	1.029920E-02
168	0	0.000000E+00	8.900000E-03	1.029920E-02
169	0	0.000000E+00	9.100000E-03	1.029920E-02
170	0	0.000000E+00	9.300000E-03	1.029920E-02
171	0	0.000000E+00	7.500000E-03	1.178009E-02
172	0	0.000000E+00	7.700000E-03	1.178009E-02
173	0	0.000000E+00	7.900000E-03	1.178009E-02
174	0	0.000000E+00	8.100000E-03	1.178009E-02
175	0	0.000000E+00	8.300000E-03	1.178009E-02
176	0	0.000000E+00	8.500000E-03	1.178009E-02
177	0	0.000000E+00	8.700000E-03	1.178009E-02
178	0	0.000000E+00	8.900000E-03	1.178009E-02
179	0	0.000000E+00	9.100000E-03	1.178009E-02
180	0	0.000000E+00	9.300000E-03	1.178009E-02
181	0	0.000000E+00	7.500000E-03	1.317715E-02
182	0	0.000000E+00	7.700000E-03	1.317715E-02
183	0	0.000000E+00	7.900000E-03	1.317715E-02
184	0	0.000000E+00	8.100000E-03	1.317715E-02
185	0	0.000000E+00	8.300000E-03	1.317715E-02
186	0	0.000000E+00	8.500000E-03	1.317715E-02
187	0	0.000000E+00	8.700000E-03	1.317715E-02
188	0	0.000000E+00	8.900000E-03	1.317715E-02
189	0	0.000000E+00	9.100000E-03	1.317715E-02
190	0	0.000000E+00	9.300000E-03	1.317715E-02
191	0	0.000000E+00	7.500000E-03	1.449513E-02
192	0	0.000000E+00	7.700000E-03	1.449513E-02
193	0	0.000000E+00	7.900000E-03	1.449513E-02
194	0	0.000000E+00	8.100000E-03	1.449513E-02
195	0	0.000000E+00	8.300000E-03	1.449513E-02
196	0	0.000000E+00	8.500000E-03	1.449513E-02
197	0	0.000000E+00	8.700000E-03	1.449513E-02
198	0	0.000000E+00	8.900000E-03	1.449513E-02

199	0	0.000000E+00	9.100000E-03	1.449513E-02
200	0	0.000000E+00	9.300000E-03	1.449513E-02
201	0	0.000000E+00	7.500000E-03	1.573851E-02
202	0	0.000000E+00	7.700000E-03	1.573851E-02
203	0	0.000000E+00	7.900000E-03	1.573851E-02
204	0	0.000000E+00	8.100000E-03	1.573851E-02
205	0	0.000000E+00	8.300000E-03	1.573851E-02
206	0	0.000000E+00	8.500000E-03	1.573851E-02
207	0	0.000000E+00	8.700000E-03	1.573851E-02
208	0	0.000000E+00	8.900000E-03	1.573851E-02
209	0	0.000000E+00	9.100000E-03	1.573851E-02
210	0	0.000000E+00	9.300000E-03	1.573851E-02
211	0	0.000000E+00	7.500000E-03	1.691152E-02
212	0	0.000000E+00	7.700000E-03	1.691152E-02
213	0	0.000000E+00	7.900000E-03	1.691152E-02
214	0	0.000000E+00	8.100000E-03	1.691152E-02
215	0	0.000000E+00	8.300000E-03	1.691152E-02
216	0	0.000000E+00	8.500000E-03	1.691152E-02
217	0	0.000000E+00	8.700000E-03	1.691152E-02
218	0	0.000000E+00	8.900000E-03	1.691152E-02
219	0	0.000000E+00	9.100000E-03	1.691152E-02
220	0	0.000000E+00	9.300000E-03	1.691152E-02
221	0	0.000000E+00	7.500000E-03	1.801812E-02
222	0	0.000000E+00	7.700000E-03	1.801812E-02
223	0	0.000000E+00	7.900000E-03	1.801812E-02
224	0	0.000000E+00	8.100000E-03	1.801812E-02
225	0	0.000000E+00	8.300000E-03	1.801812E-02
226	0	0.000000E+00	8.500000E-03	1.801812E-02
227	0	0.000000E+00	8.700000E-03	1.801812E-02
228	0	0.000000E+00	8.900000E-03	1.801812E-02
229	0	0.000000E+00	9.100000E-03	1.801812E-02
230	0	0.000000E+00	9.300000E-03	1.801812E-02
231	0	0.000000E+00	7.500000E-03	1.906209E-02
232	0	0.000000E+00	7.700000E-03	1.906209E-02
233	0	0.000000E+00	7.900000E-03	1.906209E-02
234	0	0.000000E+00	8.100000E-03	1.906209E-02
235	0	0.000000E+00	8.300000E-03	1.906209E-02
236	0	0.000000E+00	8.500000E-03	1.906209E-02
237	0	0.000000E+00	8.700000E-03	1.906209E-02
238	0	0.000000E+00	8.900000E-03	1.906209E-02
239	0	0.000000E+00	9.100000E-03	1.906209E-02
240	0	0.000000E+00	9.300000E-03	1.906209E-02
241	0	0.000000E+00	7.500000E-03	2.004696E-02
242	0	0.000000E+00	7.700000E-03	2.004696E-02
243	0	0.000000E+00	7.900000E-03	2.004696E-02
244	0	0.000000E+00	8.100000E-03	2.004696E-02

245	0	0.000000E+00	8.300000E-03	2.004696E-02
246	0	0.000000E+00	8.500000E-03	2.004696E-02
247	0	0.000000E+00	8.700000E-03	2.004696E-02
248	0	0.000000E+00	8.900000E-03	2.004696E-02
249	0	0.000000E+00	9.100000E-03	2.004696E-02
250	0	0.000000E+00	9.300000E-03	2.004696E-02
251	0	0.000000E+00	7.500000E-03	2.097609E-02
252	0	0.000000E+00	7.700000E-03	2.097609E-02
253	0	0.000000E+00	7.900000E-03	2.097609E-02
254	0	0.000000E+00	8.100000E-03	2.097609E-02
255	0	0.000000E+00	8.300000E-03	2.097609E-02
256	0	0.000000E+00	8.500000E-03	2.097609E-02
257	0	0.000000E+00	8.700000E-03	2.097609E-02
258	0	0.000000E+00	8.900000E-03	2.097609E-02
259	0	0.000000E+00	9.100000E-03	2.097609E-02
260	0	0.000000E+00	9.300000E-03	2.097609E-02
261	0	0.000000E+00	7.500000E-03	2.185262E-02
262	0	0.000000E+00	7.700000E-03	2.185262E-02
263	0	0.000000E+00	7.900000E-03	2.185262E-02
264	0	0.000000E+00	8.100000E-03	2.185262E-02
265	0	0.000000E+00	8.300000E-03	2.185262E-02
266	0	0.000000E+00	8.500000E-03	2.185262E-02
267	0	0.000000E+00	8.700000E-03	2.185262E-02
268	0	0.000000E+00	8.900000E-03	2.185262E-02
269	0	0.000000E+00	9.100000E-03	2.185262E-02
270	0	0.000000E+00	9.300000E-03	2.185262E-02
271	0	0.000000E+00	7.500000E-03	2.267954E-02
272	0	0.000000E+00	7.700000E-03	2.267954E-02
273	0	0.000000E+00	7.900000E-03	2.267954E-02
274	0	0.000000E+00	8.100000E-03	2.267954E-02
275	0	0.000000E+00	8.300000E-03	2.267954E-02
276	0	0.000000E+00	8.500000E-03	2.267954E-02
277	0	0.000000E+00	8.700000E-03	2.267954E-02
278	0	0.000000E+00	8.900000E-03	2.267954E-02
279	0	0.000000E+00	9.100000E-03	2.267954E-02
280	0	0.000000E+00	9.300000E-03	2.267954E-02
281	0	0.000000E+00	7.500000E-03	2.345966E-02
282	0	0.000000E+00	7.700000E-03	2.345966E-02
283	0	0.000000E+00	7.900000E-03	2.345966E-02
284	0	0.000000E+00	8.100000E-03	2.345966E-02
285	0	0.000000E+00	8.300000E-03	2.345966E-02
286	0	0.000000E+00	8.500000E-03	2.345966E-02
287	0	0.000000E+00	8.700000E-03	2.345966E-02
288	0	0.000000E+00	8.900000E-03	2.345966E-02
289	0	0.000000E+00	9.100000E-03	2.345966E-02
290	0	0.000000E+00	9.300000E-03	2.345966E-02

291	0	0.000000E+00	7.500000E-03	2.419561E-02
292	0	0.000000E+00	7.700000E-03	2.419561E-02
293	0	0.000000E+00	7.900000E-03	2.419561E-02
294	0	0.000000E+00	8.100000E-03	2.419561E-02
295	0	0.000000E+00	8.300000E-03	2.419561E-02
296	0	0.000000E+00	8.500000E-03	2.419561E-02
297	0	0.000000E+00	8.700000E-03	2.419561E-02
298	0	0.000000E+00	8.900000E-03	2.419561E-02
299	0	0.000000E+00	9.100000E-03	2.419561E-02
300	0	0.000000E+00	9.300000E-03	2.419561E-02
301	0	0.000000E+00	7.500000E-03	2.488991E-02
302	0	0.000000E+00	7.700000E-03	2.488991E-02
303	0	0.000000E+00	7.900000E-03	2.488991E-02
304	0	0.000000E+00	8.100000E-03	2.488991E-02
305	0	0.000000E+00	8.300000E-03	2.488991E-02
306	0	0.000000E+00	8.500000E-03	2.488991E-02
307	0	0.000000E+00	8.700000E-03	2.488991E-02
308	0	0.000000E+00	8.900000E-03	2.488991E-02
309	0	0.000000E+00	9.100000E-03	2.488991E-02
310	0	0.000000E+00	9.300000E-03	2.488991E-02
311	0	0.000000E+00	7.500000E-03	2.554491E-02
312	0	0.000000E+00	7.700000E-03	2.554491E-02
313	0	0.000000E+00	7.900000E-03	2.554491E-02
314	0	0.000000E+00	8.100000E-03	2.554491E-02
315	0	0.000000E+00	8.300000E-03	2.554491E-02
316	0	0.000000E+00	8.500000E-03	2.554491E-02
317	0	0.000000E+00	8.700000E-03	2.554491E-02
318	0	0.000000E+00	8.900000E-03	2.554491E-02
319	0	0.000000E+00	9.100000E-03	2.554491E-02
320	0	0.000000E+00	9.300000E-03	2.554491E-02
321	0	0.000000E+00	7.500000E-03	2.616283E-02
322	0	0.000000E+00	7.700000E-03	2.616283E-02
323	0	0.000000E+00	7.900000E-03	2.616283E-02
324	0	0.000000E+00	8.100000E-03	2.616283E-02
325	0	0.000000E+00	8.300000E-03	2.616283E-02
326	0	0.000000E+00	8.500000E-03	2.616283E-02
327	0	0.000000E+00	8.700000E-03	2.616283E-02
328	0	0.000000E+00	8.900000E-03	2.616283E-02
329	0	0.000000E+00	9.100000E-03	2.616283E-02
330	0	0.000000E+00	9.300000E-03	2.616283E-02
331	0	0.000000E+00	7.500000E-03	2.674577E-02
332	0	0.000000E+00	7.700000E-03	2.674577E-02
333	0	0.000000E+00	7.900000E-03	2.674577E-02
334	0	0.000000E+00	8.100000E-03	2.674577E-02
335	0	0.000000E+00	8.300000E-03	2.674577E-02
336	0	0.000000E+00	8.500000E-03	2.674577E-02

337	0	0.000000E+00	8.700000E-03	2.674577E-02
338	0	0.000000E+00	8.900000E-03	2.674577E-02
339	0	0.000000E+00	9.100000E-03	2.674577E-02
340	0	0.000000E+00	9.300000E-03	2.674577E-02
341	0	0.000000E+00	7.500000E-03	2.729572E-02
342	0	0.000000E+00	7.700000E-03	2.729572E-02
343	0	0.000000E+00	7.900000E-03	2.729572E-02
344	0	0.000000E+00	8.100000E-03	2.729572E-02
345	0	0.000000E+00	8.300000E-03	2.729572E-02
346	0	0.000000E+00	8.500000E-03	2.729572E-02
347	0	0.000000E+00	8.700000E-03	2.729572E-02
348	0	0.000000E+00	8.900000E-03	2.729572E-02
349	0	0.000000E+00	9.100000E-03	2.729572E-02
350	0	0.000000E+00	9.300000E-03	2.729572E-02
351	0	0.000000E+00	7.500000E-03	2.781454E-02
352	0	0.000000E+00	7.700000E-03	2.781454E-02
353	0	0.000000E+00	7.900000E-03	2.781454E-02
354	0	0.000000E+00	8.100000E-03	2.781454E-02
355	0	0.000000E+00	8.300000E-03	2.781454E-02
356	0	0.000000E+00	8.500000E-03	2.781454E-02
357	0	0.000000E+00	8.700000E-03	2.781454E-02
358	0	0.000000E+00	8.900000E-03	2.781454E-02
359	0	0.000000E+00	9.100000E-03	2.781454E-02
360	0	0.000000E+00	9.300000E-03	2.781454E-02
361	0	0.000000E+00	7.500000E-03	2.830400E-02
362	0	0.000000E+00	7.700000E-03	2.830400E-02
363	0	0.000000E+00	7.900000E-03	2.830400E-02
364	0	0.000000E+00	8.100000E-03	2.830400E-02
365	0	0.000000E+00	8.300000E-03	2.830400E-02
366	0	0.000000E+00	8.500000E-03	2.830400E-02
367	0	0.000000E+00	8.700000E-03	2.830400E-02
368	0	0.000000E+00	8.900000E-03	2.830400E-02
369	0	0.000000E+00	9.100000E-03	2.830400E-02
370	0	0.000000E+00	9.300000E-03	2.830400E-02
371	0	0.000000E+00	7.500000E-03	2.876574E-02
372	0	0.000000E+00	7.700000E-03	2.876574E-02
373	0	0.000000E+00	7.900000E-03	2.876574E-02
374	0	0.000000E+00	8.100000E-03	2.876574E-02
375	0	0.000000E+00	8.300000E-03	2.876574E-02
376	0	0.000000E+00	8.500000E-03	2.876574E-02
377	0	0.000000E+00	8.700000E-03	2.876574E-02
378	0	0.000000E+00	8.900000E-03	2.876574E-02
379	0	0.000000E+00	9.100000E-03	2.876574E-02
380	0	0.000000E+00	9.300000E-03	2.876574E-02
381	0	0.000000E+00	7.500000E-03	2.920135E-02
382	0	0.000000E+00	7.700000E-03	2.920135E-02

383	0	0.000000E+00	7.900000E-03	2.920135E-02
384	0	0.000000E+00	8.100000E-03	2.920135E-02
385	0	0.000000E+00	8.300000E-03	2.920135E-02
386	0	0.000000E+00	8.500000E-03	2.920135E-02
387	0	0.000000E+00	8.700000E-03	2.920135E-02
388	0	0.000000E+00	8.900000E-03	2.920135E-02
389	0	0.000000E+00	9.100000E-03	2.920135E-02
390	0	0.000000E+00	9.300000E-03	2.920135E-02
391	0	0.000000E+00	7.500000E-03	2.961231E-02
392	0	0.000000E+00	7.700000E-03	2.961231E-02
393	0	0.000000E+00	7.900000E-03	2.961231E-02
394	0	0.000000E+00	8.100000E-03	2.961231E-02
395	0	0.000000E+00	8.300000E-03	2.961231E-02
396	0	0.000000E+00	8.500000E-03	2.961231E-02
397	0	0.000000E+00	8.700000E-03	2.961231E-02
398	0	0.000000E+00	8.900000E-03	2.961231E-02
399	0	0.000000E+00	9.100000E-03	2.961231E-02
400	0	0.000000E+00	9.300000E-03	2.961231E-02
401	0	0.000000E+00	7.500000E-03	3.000000E-02
402	0	0.000000E+00	7.700000E-03	3.000000E-02
403	0	0.000000E+00	7.900000E-03	3.000000E-02
404	0	0.000000E+00	8.100000E-03	3.000000E-02
405	0	0.000000E+00	8.300000E-03	3.000000E-02
406	0	0.000000E+00	8.500000E-03	3.000000E-02
407	0	0.000000E+00	8.700000E-03	3.000000E-02
408	0	0.000000E+00	8.900000E-03	3.000000E-02
409	0	0.000000E+00	9.100000E-03	3.000000E-02
410	0	0.000000E+00	9.300000E-03	3.000000E-02
411	0	4.709289E-04	7.485200E-03	-3.000000E-02
412	0	4.834870E-04	7.684806E-03	-3.000000E-02
413	0	4.960451E-04	7.884411E-03	-3.000000E-02
414	0	5.086032E-04	8.084017E-03	-3.000000E-02
415	0	5.211613E-04	8.283622E-03	-3.000000E-02
416	0	5.337194E-04	8.483227E-03	-3.000000E-02
417	0	5.462775E-04	8.682833E-03	-3.000000E-02
418	0	5.586429E-04	8.879375E-03	-3.000000E-02
419	0	5.712636E-04	9.079975E-03	-3.000000E-02
420	0	5.839518E-04	9.281649E-03	-3.000000E-02
421	0	4.709289E-04	7.485200E-03	-2.623803E-02
422	0	4.834870E-04	7.684806E-03	-2.623803E-02
423	0	4.960451E-04	7.884411E-03	-2.623803E-02
424	0	5.086032E-04	8.084017E-03	-2.623803E-02
425	0	5.211613E-04	8.283622E-03	-2.623803E-02
426	0	5.337194E-04	8.483227E-03	-2.623803E-02
427	0	5.462775E-04	8.682833E-03	-2.623803E-02
428	0	5.588356E-04	8.882438E-03	-2.623803E-02

429	0	5.713937E-04	9.082043E-03	-2.623803E-02
430	0	5.839518E-04	9.281649E-03	-2.623803E-02
431	0	4.709289E-04	7.485200E-03	-2.268899E-02
432	0	4.834870E-04	7.684806E-03	-2.268899E-02
433	0	4.960451E-04	7.884411E-03	-2.268899E-02
434	0	5.086032E-04	8.084017E-03	-2.268899E-02
435	0	5.211613E-04	8.283622E-03	-2.268899E-02
436	0	5.337194E-04	8.483227E-03	-2.268899E-02
437	0	5.462775E-04	8.682833E-03	-2.268899E-02
438	0	5.588356E-04	8.882438E-03	-2.268899E-02
439	0	5.713937E-04	9.082043E-03	-2.268899E-02
440	0	5.839518E-04	9.281649E-03	-2.268899E-02
441	0	4.709289E-04	7.485200E-03	-1.934085E-02
442	0	4.834870E-04	7.684806E-03	-1.934085E-02
443	0	4.960451E-04	7.884411E-03	-1.934085E-02
444	0	5.086032E-04	8.084017E-03	-1.934085E-02
445	0	5.211613E-04	8.283622E-03	-1.934085E-02
446	0	5.337194E-04	8.483227E-03	-1.934085E-02
447	0	5.462775E-04	8.682833E-03	-1.934085E-02
448	0	5.588356E-04	8.882438E-03	-1.934085E-02
449	0	5.713937E-04	9.082043E-03	-1.934085E-02
450	0	5.839518E-04	9.281649E-03	-1.934085E-02
451	0	4.709289E-04	7.485200E-03	-1.618223E-02
452	0	4.834870E-04	7.684806E-03	-1.618223E-02
453	0	4.960451E-04	7.884411E-03	-1.618223E-02
454	0	5.086032E-04	8.084017E-03	-1.618223E-02
455	0	5.211613E-04	8.283622E-03	-1.618223E-02
456	0	5.337194E-04	8.483227E-03	-1.618223E-02
457	0	5.462775E-04	8.682833E-03	-1.618223E-02
458	0	5.588356E-04	8.882438E-03	-1.618223E-02
459	0	5.713937E-04	9.082043E-03	-1.618223E-02
460	0	5.839518E-04	9.281649E-03	-1.618223E-02
461	0	4.709289E-04	7.485200E-03	-1.320239E-02
462	0	4.834870E-04	7.684806E-03	-1.320239E-02
463	0	4.960451E-04	7.884411E-03	-1.320239E-02
464	0	5.086032E-04	8.084017E-03	-1.320239E-02
465	0	5.211613E-04	8.283622E-03	-1.320239E-02
466	0	5.337194E-04	8.483227E-03	-1.320239E-02
467	0	5.462775E-04	8.682833E-03	-1.320239E-02
468	0	5.588356E-04	8.882438E-03	-1.320239E-02
469	0	5.713937E-04	9.082043E-03	-1.320239E-02
470	0	5.839518E-04	9.281649E-03	-1.320239E-02
471	0	4.709289E-04	7.485200E-03	-1.039122E-02
472	0	4.834870E-04	7.684806E-03	-1.039122E-02
473	0	4.960451E-04	7.884411E-03	-1.039122E-02
474	0	5.086032E-04	8.084017E-03	-1.039122E-02

475	0	5.211613E-04	8.283622E-03	-1.039122E-02
476	0	5.337194E-04	8.483227E-03	-1.039122E-02
477	0	5.462775E-04	8.682833E-03	-1.039122E-02
478	0	5.588356E-04	8.882438E-03	-1.039122E-02
479	0	5.713937E-04	9.082043E-03	-1.039122E-02
480	0	5.839518E-04	9.281649E-03	-1.039122E-02
481	0	4.709289E-04	7.485200E-03	-7.739181E-03
482	0	4.834870E-04	7.684806E-03	-7.739181E-03
483	0	4.960451E-04	7.884411E-03	-7.739181E-03
484	0	5.086032E-04	8.084017E-03	-7.739181E-03
485	0	5.211613E-04	8.283622E-03	-7.739181E-03
486	0	5.337194E-04	8.483227E-03	-7.739181E-03
487	0	5.462775E-04	8.682833E-03	-7.739181E-03
488	0	5.588356E-04	8.882438E-03	-7.739181E-03
489	0	5.713937E-04	9.082043E-03	-7.739181E-03
490	0	5.839518E-04	9.281649E-03	-7.739181E-03
491	0	4.709289E-04	7.485200E-03	-5.237254E-03
492	0	4.834870E-04	7.684806E-03	-5.237254E-03
493	0	4.960451E-04	7.884411E-03	-5.237254E-03
494	0	5.086032E-04	8.084017E-03	-5.237254E-03
495	0	5.211613E-04	8.283622E-03	-5.237254E-03
496	0	5.337194E-04	8.483227E-03	-5.237254E-03
497	0	5.462775E-04	8.682833E-03	-5.237254E-03
498	0	5.588356E-04	8.882438E-03	-5.237254E-03
499	0	5.713937E-04	9.082043E-03	-5.237254E-03
500	0	5.839518E-04	9.281649E-03	-5.237254E-03
501	0	4.709289E-04	7.485200E-03	-2.876945E-03
502	0	4.834870E-04	7.684806E-03	-2.876945E-03
503	0	4.960451E-04	7.884411E-03	-2.876945E-03
504	0	5.086032E-04	8.084017E-03	-2.876945E-03
505	0	5.211613E-04	8.283622E-03	-2.876945E-03
506	0	5.337194E-04	8.483227E-03	-2.876945E-03
507	0	5.462775E-04	8.682833E-03	-2.876945E-03
508	0	5.588356E-04	8.882438E-03	-2.876945E-03
509	0	5.713937E-04	9.082043E-03	-2.876945E-03
510	0	5.839518E-04	9.281649E-03	-2.876945E-03
511	0	4.709289E-04	7.485200E-03	-6.502386E-04
512	0	4.834870E-04	7.684806E-03	-6.502386E-04
513	0	4.960451E-04	7.884411E-03	-6.502386E-04
514	0	5.086032E-04	8.084017E-03	-6.502386E-04
515	0	5.211613E-04	8.283622E-03	-6.502386E-04
516	0	5.337194E-04	8.483227E-03	-6.502386E-04
517	0	5.462775E-04	8.682833E-03	-6.502386E-04
518	0	5.588356E-04	8.882438E-03	-6.502386E-04
519	0	5.713937E-04	9.082043E-03	-6.502386E-04
520	0	5.839518E-04	9.281649E-03	-6.502386E-04

521	0	4.709289E-04	7.485200E-03	1.450428E-03
522	0	4.834870E-04	7.684806E-03	1.450428E-03
523	0	4.960451E-04	7.884411E-03	1.450428E-03
524	0	5.086032E-04	8.084017E-03	1.450428E-03
525	0	5.211613E-04	8.283622E-03	1.450428E-03
526	0	5.337194E-04	8.483227E-03	1.450428E-03
527	0	5.462775E-04	8.682833E-03	1.450428E-03
528	0	5.588356E-04	8.882438E-03	1.450428E-03
529	0	5.713937E-04	9.082043E-03	1.450428E-03
530	0	5.839518E-04	9.281649E-03	1.450428E-03
531	0	4.709289E-04	7.485200E-03	3.432189E-03
532	0	4.834870E-04	7.684806E-03	3.432189E-03
533	0	4.960451E-04	7.884411E-03	3.432189E-03
534	0	5.086032E-04	8.084017E-03	3.432189E-03
535	0	5.211613E-04	8.283622E-03	3.432189E-03
536	0	5.337194E-04	8.483227E-03	3.432189E-03
537	0	5.462775E-04	8.682833E-03	3.432189E-03
538	0	5.588356E-04	8.882438E-03	3.432189E-03
539	0	5.713937E-04	9.082043E-03	3.432189E-03
540	0	5.839518E-04	9.281649E-03	3.432189E-03
541	0	4.709289E-04	7.485200E-03	5.301774E-03
542	0	4.834870E-04	7.684806E-03	5.301774E-03
543	0	4.960451E-04	7.884411E-03	5.301774E-03
544	0	5.086032E-04	8.084017E-03	5.301774E-03
545	0	5.211613E-04	8.283622E-03	5.301774E-03
546	0	5.337194E-04	8.483227E-03	5.301774E-03
547	0	5.462775E-04	8.682833E-03	5.301774E-03
548	0	5.588356E-04	8.882438E-03	5.301774E-03
549	0	5.713937E-04	9.082043E-03	5.301774E-03
550	0	5.839518E-04	9.281649E-03	5.301774E-03
551	0	4.709289E-04	7.485200E-03	7.065534E-03
552	0	4.834870E-04	7.684806E-03	7.065534E-03
553	0	4.960451E-04	7.884411E-03	7.065534E-03
554	0	5.086032E-04	8.084017E-03	7.065534E-03
555	0	5.211613E-04	8.283622E-03	7.065534E-03
556	0	5.337194E-04	8.483227E-03	7.065534E-03
557	0	5.462775E-04	8.682833E-03	7.065534E-03
558	0	5.588356E-04	8.882438E-03	7.065534E-03
559	0	5.713937E-04	9.082043E-03	7.065534E-03
560	0	5.839518E-04	9.281649E-03	7.065534E-03
561	0	4.709289E-04	7.485200E-03	8.729459E-03
562	0	4.834870E-04	7.684806E-03	8.729459E-03
563	0	4.960451E-04	7.884411E-03	8.729459E-03
564	0	5.086032E-04	8.084017E-03	8.729459E-03
565	0	5.211613E-04	8.283622E-03	8.729459E-03
566	0	5.337194E-04	8.483227E-03	8.729459E-03

567	0	5.462775E-04	8.682833E-03	8.729459E-03
568	0	5.588356E-04	8.882438E-03	8.729459E-03
569	0	5.713937E-04	9.082043E-03	8.729459E-03
570	0	5.839518E-04	9.281649E-03	8.729459E-03
571	0	4.709289E-04	7.485200E-03	1.029920E-02
572	0	4.834870E-04	7.684806E-03	1.029920E-02
573	0	4.960451E-04	7.884411E-03	1.029920E-02
574	0	5.086032E-04	8.084017E-03	1.029920E-02
575	0	5.211613E-04	8.283622E-03	1.029920E-02
576	0	5.337194E-04	8.483227E-03	1.029920E-02
577	0	5.462775E-04	8.682833E-03	1.029920E-02
578	0	5.588356E-04	8.882438E-03	1.029920E-02
579	0	5.713937E-04	9.082043E-03	1.029920E-02
580	0	5.839518E-04	9.281649E-03	1.029920E-02
581	0	4.709289E-04	7.485200E-03	1.178009E-02
582	0	4.834870E-04	7.684806E-03	1.178009E-02
583	0	4.960451E-04	7.884411E-03	1.178009E-02
584	0	5.086032E-04	8.084017E-03	1.178009E-02
585	0	5.211613E-04	8.283622E-03	1.178009E-02
586	0	5.337194E-04	8.483227E-03	1.178009E-02
587	0	5.462775E-04	8.682833E-03	1.178009E-02
588	0	5.588356E-04	8.882438E-03	1.178009E-02
589	0	5.713937E-04	9.082043E-03	1.178009E-02
590	0	5.839518E-04	9.281649E-03	1.178009E-02
591	0	4.709289E-04	7.485200E-03	1.317715E-02
592	0	4.834870E-04	7.684806E-03	1.317715E-02
593	0	4.960451E-04	7.884411E-03	1.317715E-02
594	0	5.086032E-04	8.084017E-03	1.317715E-02
595	0	5.211613E-04	8.283622E-03	1.317715E-02
596	0	5.337194E-04	8.483227E-03	1.317715E-02
597	0	5.462775E-04	8.682833E-03	1.317715E-02
598	0	5.588356E-04	8.882438E-03	1.317715E-02
599	0	5.713937E-04	9.082043E-03	1.317715E-02
600	0	5.839518E-04	9.281649E-03	1.317715E-02
601	0	4.709289E-04	7.485200E-03	1.449513E-02
602	0	4.834870E-04	7.684806E-03	1.449513E-02
603	0	4.960451E-04	7.884411E-03	1.449513E-02
604	0	5.086032E-04	8.084017E-03	1.449513E-02
605	0	5.211613E-04	8.283622E-03	1.449513E-02
606	0	5.337194E-04	8.483227E-03	1.449513E-02
607	0	5.462775E-04	8.682833E-03	1.449513E-02
608	0	5.588356E-04	8.882438E-03	1.449513E-02
609	0	5.713937E-04	9.082043E-03	1.449513E-02
610	0	5.839518E-04	9.281649E-03	1.449513E-02
611	0	4.709289E-04	7.485200E-03	1.573851E-02
612	0	4.834870E-04	7.684806E-03	1.573851E-02

613	0	4.960451E-04	7.884411E-03	1.573851E-02
614	0	5.086032E-04	8.084017E-03	1.573851E-02
615	0	5.211613E-04	8.283622E-03	1.573851E-02
616	0	5.337194E-04	8.483227E-03	1.573851E-02
617	0	5.462775E-04	8.682833E-03	1.573851E-02
618	0	5.588356E-04	8.882438E-03	1.573851E-02
619	0	5.713937E-04	9.082043E-03	1.573851E-02
620	0	5.839518E-04	9.281649E-03	1.573851E-02
621	0	4.709289E-04	7.485200E-03	1.691152E-02
622	0	4.834870E-04	7.684806E-03	1.691152E-02
623	0	4.960451E-04	7.884411E-03	1.691152E-02
624	0	5.086032E-04	8.084017E-03	1.691152E-02
625	0	5.211613E-04	8.283622E-03	1.691152E-02
626	0	5.337194E-04	8.483227E-03	1.691152E-02
627	0	5.462775E-04	8.682833E-03	1.691152E-02
628	0	5.588356E-04	8.882438E-03	1.691152E-02
629	0	5.713937E-04	9.082043E-03	1.691152E-02
630	0	5.839518E-04	9.281649E-03	1.691152E-02
631	0	4.709289E-04	7.485200E-03	1.801812E-02
632	0	4.834870E-04	7.684806E-03	1.801812E-02
633	0	4.960451E-04	7.884411E-03	1.801812E-02
634	0	5.086032E-04	8.084017E-03	1.801812E-02
635	0	5.211613E-04	8.283622E-03	1.801812E-02
636	0	5.337194E-04	8.483227E-03	1.801812E-02
637	0	5.462775E-04	8.682833E-03	1.801812E-02
638	0	5.588356E-04	8.882438E-03	1.801812E-02
639	0	5.713937E-04	9.082043E-03	1.801812E-02
640	0	5.839518E-04	9.281649E-03	1.801812E-02
641	0	4.709289E-04	7.485200E-03	1.906209E-02
642	0	4.834870E-04	7.684806E-03	1.906209E-02
643	0	4.960451E-04	7.884411E-03	1.906209E-02
644	0	5.086032E-04	8.084017E-03	1.906209E-02
645	0	5.211613E-04	8.283622E-03	1.906209E-02
646	0	5.337194E-04	8.483227E-03	1.906209E-02
647	0	5.462775E-04	8.682833E-03	1.906209E-02
648	0	5.588356E-04	8.882438E-03	1.906209E-02
649	0	5.713937E-04	9.082043E-03	1.906209E-02
650	0	5.839518E-04	9.281649E-03	1.906209E-02
651	0	4.709289E-04	7.485200E-03	2.004696E-02
652	0	4.834870E-04	7.684806E-03	2.004696E-02
653	0	4.960451E-04	7.884411E-03	2.004696E-02
654	0	5.086032E-04	8.084017E-03	2.004696E-02
655	0	5.211613E-04	8.283622E-03	2.004696E-02
656	0	5.337194E-04	8.483227E-03	2.004696E-02
657	0	5.462775E-04	8.682833E-03	2.004696E-02
658	0	5.588356E-04	8.882438E-03	2.004696E-02

659	0	5.713937E-04	9.082043E-03	2.004696E-02
660	0	5.839518E-04	9.281649E-03	2.004696E-02
661	0	4.709289E-04	7.485200E-03	2.097609E-02
662	0	4.834870E-04	7.684806E-03	2.097609E-02
663	0	4.960451E-04	7.884411E-03	2.097609E-02
664	0	5.086032E-04	8.084017E-03	2.097609E-02
665	0	5.211613E-04	8.283622E-03	2.097609E-02
666	0	5.337194E-04	8.483227E-03	2.097609E-02
667	0	5.462775E-04	8.682833E-03	2.097609E-02
668	0	5.588356E-04	8.882438E-03	2.097609E-02
669	0	5.713937E-04	9.082043E-03	2.097609E-02
670	0	5.839518E-04	9.281649E-03	2.097609E-02
671	0	4.709289E-04	7.485200E-03	2.185262E-02
672	0	4.834870E-04	7.684806E-03	2.185262E-02
673	0	4.960451E-04	7.884411E-03	2.185262E-02
674	0	5.086032E-04	8.084017E-03	2.185262E-02
675	0	5.211613E-04	8.283622E-03	2.185262E-02
676	0	5.337194E-04	8.483227E-03	2.185262E-02
677	0	5.462775E-04	8.682833E-03	2.185262E-02
678	0	5.588356E-04	8.882438E-03	2.185262E-02
679	0	5.713937E-04	9.082043E-03	2.185262E-02
680	0	5.839518E-04	9.281649E-03	2.185262E-02
681	0	4.709289E-04	7.485200E-03	2.267954E-02
682	0	4.834870E-04	7.684806E-03	2.267954E-02
683	0	4.960451E-04	7.884411E-03	2.267954E-02
684	0	5.086032E-04	8.084017E-03	2.267954E-02
685	0	5.211613E-04	8.283622E-03	2.267954E-02
686	0	5.337194E-04	8.483227E-03	2.267954E-02
687	0	5.462775E-04	8.682833E-03	2.267954E-02
688	0	5.588356E-04	8.882438E-03	2.267954E-02
689	0	5.713937E-04	9.082043E-03	2.267954E-02
690	0	5.839518E-04	9.281649E-03	2.267954E-02
691	0	4.709289E-04	7.485200E-03	2.345966E-02
692	0	4.834870E-04	7.684806E-03	2.345966E-02
693	0	4.960451E-04	7.884411E-03	2.345966E-02
694	0	5.086032E-04	8.084017E-03	2.345966E-02
695	0	5.211613E-04	8.283622E-03	2.345966E-02
696	0	5.337194E-04	8.483227E-03	2.345966E-02
697	0	5.462775E-04	8.682833E-03	2.345966E-02
698	0	5.588356E-04	8.882438E-03	2.345966E-02
699	0	5.713937E-04	9.082043E-03	2.345966E-02
700	0	5.839518E-04	9.281649E-03	2.345966E-02
701	0	4.709289E-04	7.485200E-03	2.419561E-02
702	0	4.834870E-04	7.684806E-03	2.419561E-02
703	0	4.960451E-04	7.884411E-03	2.419561E-02
704	0	5.086032E-04	8.084017E-03	2.419561E-02

705	0	5.211613E-04	8.283622E-03	2.419561E-02
706	0	5.337194E-04	8.483227E-03	2.419561E-02
707	0	5.462775E-04	8.682833E-03	2.419561E-02
708	0	5.588356E-04	8.882438E-03	2.419561E-02
709	0	5.713937E-04	9.082043E-03	2.419561E-02
710	0	5.839518E-04	9.281649E-03	2.419561E-02
711	0	4.709289E-04	7.485200E-03	2.488991E-02
712	0	4.834870E-04	7.684806E-03	2.488991E-02
713	0	4.960451E-04	7.884411E-03	2.488991E-02
714	0	5.086032E-04	8.084017E-03	2.488991E-02
715	0	5.211613E-04	8.283622E-03	2.488991E-02
716	0	5.337194E-04	8.483227E-03	2.488991E-02
717	0	5.462775E-04	8.682833E-03	2.488991E-02
718	0	5.588356E-04	8.882438E-03	2.488991E-02
719	0	5.713937E-04	9.082043E-03	2.488991E-02
720	0	5.839518E-04	9.281649E-03	2.488991E-02
721	0	4.709289E-04	7.485200E-03	2.554491E-02
722	0	4.834870E-04	7.684806E-03	2.554491E-02
723	0	4.960451E-04	7.884411E-03	2.554491E-02
724	0	5.086032E-04	8.084017E-03	2.554491E-02
725	0	5.211613E-04	8.283622E-03	2.554491E-02
726	0	5.337194E-04	8.483227E-03	2.554491E-02
727	0	5.462775E-04	8.682833E-03	2.554491E-02
728	0	5.588356E-04	8.882438E-03	2.554491E-02
729	0	5.713937E-04	9.082043E-03	2.554491E-02
730	0	5.839518E-04	9.281649E-03	2.554491E-02
731	0	4.709289E-04	7.485200E-03	2.616283E-02
732	0	4.834870E-04	7.684806E-03	2.616283E-02
733	0	4.960451E-04	7.884411E-03	2.616283E-02
734	0	5.086032E-04	8.084017E-03	2.616283E-02
735	0	5.211613E-04	8.283622E-03	2.616283E-02
736	0	5.337194E-04	8.483227E-03	2.616283E-02
737	0	5.462775E-04	8.682833E-03	2.616283E-02
738	0	5.588356E-04	8.882438E-03	2.616283E-02
739	0	5.713937E-04	9.082043E-03	2.616283E-02
740	0	5.839518E-04	9.281649E-03	2.616283E-02
741	0	4.709289E-04	7.485200E-03	2.674577E-02
742	0	4.834870E-04	7.684806E-03	2.674577E-02
743	0	4.960451E-04	7.884411E-03	2.674577E-02
744	0	5.086032E-04	8.084017E-03	2.674577E-02
745	0	5.211613E-04	8.283622E-03	2.674577E-02
746	0	5.337194E-04	8.483227E-03	2.674577E-02
747	0	5.462775E-04	8.682833E-03	2.674577E-02
748	0	5.588356E-04	8.882438E-03	2.674577E-02
749	0	5.713937E-04	9.082043E-03	2.674577E-02
750	0	5.839518E-04	9.281649E-03	2.674577E-02

751	0	4.709289E-04	7.485200E-03	2.729572E-02
752	0	4.834870E-04	7.684806E-03	2.729572E-02
753	0	4.960451E-04	7.884411E-03	2.729572E-02
754	0	5.086032E-04	8.084017E-03	2.729572E-02
755	0	5.211613E-04	8.283622E-03	2.729572E-02
756	0	5.337194E-04	8.483227E-03	2.729572E-02
757	0	5.462775E-04	8.682833E-03	2.729572E-02
758	0	5.588356E-04	8.882438E-03	2.729572E-02
759	0	5.713937E-04	9.082043E-03	2.729572E-02
760	0	5.839518E-04	9.281649E-03	2.729572E-02
761	0	4.709289E-04	7.485200E-03	2.781454E-02
762	0	4.834870E-04	7.684806E-03	2.781454E-02
763	0	4.960451E-04	7.884411E-03	2.781454E-02
764	0	5.086032E-04	8.084017E-03	2.781454E-02
765	0	5.211613E-04	8.283622E-03	2.781454E-02
766	0	5.337194E-04	8.483227E-03	2.781454E-02
767	0	5.462775E-04	8.682833E-03	2.781454E-02
768	0	5.588356E-04	8.882438E-03	2.781454E-02
769	0	5.713937E-04	9.082043E-03	2.781454E-02
770	0	5.839518E-04	9.281649E-03	2.781454E-02
771	0	4.709289E-04	7.485200E-03	2.830400E-02
772	0	4.834870E-04	7.684806E-03	2.830400E-02
773	0	4.960451E-04	7.884411E-03	2.830400E-02
774	0	5.086032E-04	8.084017E-03	2.830400E-02
775	0	5.211613E-04	8.283622E-03	2.830400E-02
776	0	5.337194E-04	8.483227E-03	2.830400E-02
777	0	5.462775E-04	8.682833E-03	2.830400E-02
778	0	5.588356E-04	8.882438E-03	2.830400E-02
779	0	5.713937E-04	9.082043E-03	2.830400E-02
780	0	5.839518E-04	9.281649E-03	2.830400E-02
781	0	4.709289E-04	7.485200E-03	2.876574E-02
782	0	4.834870E-04	7.684806E-03	2.876574E-02
783	0	4.960451E-04	7.884411E-03	2.876574E-02
784	0	5.086032E-04	8.084017E-03	2.876574E-02
785	0	5.211613E-04	8.283622E-03	2.876574E-02
786	0	5.337194E-04	8.483227E-03	2.876574E-02
787	0	5.462775E-04	8.682833E-03	2.876574E-02
788	0	5.588356E-04	8.882438E-03	2.876574E-02
789	0	5.713937E-04	9.082043E-03	2.876574E-02
790	0	5.839518E-04	9.281649E-03	2.876574E-02
791	0	4.709289E-04	7.485200E-03	2.920135E-02
792	0	4.834870E-04	7.684806E-03	2.920135E-02
793	0	4.960451E-04	7.884411E-03	2.920135E-02
794	0	5.086032E-04	8.084017E-03	2.920135E-02
795	0	5.211613E-04	8.283622E-03	2.920135E-02
796	0	5.337194E-04	8.483227E-03	2.920135E-02

797 0 5.462775E-04 8.682833E-03 2.920135E-02
798 0 5.588356E-04 8.882438E-03 2.920135E-02
799 0 5.713937E-04 9.082043E-03 2.920135E-02
800 0 5.839518E-04 9.281649E-03 2.920135E-02
801 0 4.709289E-04 7.485200E-03 2.961231E-02
802 0 4.834870E-04 7.684806E-03 2.961231E-02
803 0 4.960451E-04 7.884411E-03 2.961231E-02
804 0 5.086032E-04 8.084017E-03 2.961231E-02
805 0 5.211613E-04 8.283622E-03 2.961231E-02
806 0 5.337194E-04 8.483227E-03 2.961231E-02
807 0 5.462775E-04 8.682833E-03 2.961231E-02
808 0 5.588356E-04 8.882438E-03 2.961231E-02
809 0 5.713937E-04 9.082043E-03 2.961231E-02
810 0 5.839518E-04 9.281649E-03 2.961231E-02
811 0 4.709289E-04 7.485200E-03 3.000000E-02
812 0 4.833365E-04 7.682414E-03 3.000000E-02
813 0 4.958265E-04 7.880940E-03 3.000000E-02
814 0 5.083553E-04 8.080080E-03 3.000000E-02
815 0 5.209021E-04 8.279507E-03 3.000000E-02
816 0 5.334576E-04 8.479070E-03 3.000000E-02
817 0 5.462775E-04 8.682833E-03 3.000000E-02
818 0 5.588356E-04 8.882438E-03 3.000000E-02
819 0 5.713937E-04 9.082043E-03 3.000000E-02
820 0 5.839518E-04 9.281649E-03 3.000000E-02

! List of nodes connected to an individual element (pg 28)
! For elements where the maximum number of nodes is less or equal to 13 (i.e.,
! the NEN parameter on the control record), the records following the command are given
! as:
! N number of element.
! NG generation increment for node numbers.
! MA material identifier associated with element.
! ND-i i-Node number defining element
ELEMents
1 0 1 417 418 8 7 427 428 18 17
2 0 1 418 419 9 8 428 429 19 18
3 0 1 419 420 10 9 429 430 20 19
4 0 1 427 428 18 17 437 438 28 27
5 0 1 428 429 19 18 438 439 29 28
6 0 1 429 430 20 19 439 440 30 29
7 0 1 437 438 28 27 447 448 38 37
8 0 1 438 439 29 28 448 449 39 38
9 0 1 439 440 30 29 449 450 40 39

10	0	1	447	448	38	37	457	458	48	47
11	0	1	448	449	39	38	458	459	49	48
12	0	1	449	450	40	39	459	460	50	49
13	0	1	457	458	48	47	467	468	58	57
14	0	1	458	459	49	48	468	469	59	58
15	0	1	459	460	50	49	469	470	60	59
16	0	1	467	468	58	57	477	478	68	67
17	0	1	468	469	59	58	478	479	69	68
18	0	1	469	470	60	59	479	480	70	69
19	0	1	477	478	68	67	487	488	78	77
20	0	1	478	479	69	68	488	489	79	78
21	0	1	479	480	70	69	489	490	80	79
22	0	1	487	488	78	77	497	498	88	87
23	0	1	488	489	79	78	498	499	89	88
24	0	1	489	490	80	79	499	500	90	89
25	0	1	497	498	88	87	507	508	98	97
26	0	1	498	499	89	88	508	509	99	98
27	0	1	499	500	90	89	509	510	100	99
28	0	1	507	508	98	97	517	518	108	107
29	0	1	508	509	99	98	518	519	109	108
30	0	1	509	510	100	99	519	520	110	109
31	0	1	517	518	108	107	527	528	118	117
32	0	1	518	519	109	108	528	529	119	118
33	0	1	519	520	110	109	529	530	120	119
34	0	1	527	528	118	117	537	538	128	127
35	0	1	528	529	119	118	538	539	129	128
36	0	1	529	530	120	119	539	540	130	129
37	0	1	537	538	128	127	547	548	138	137
38	0	1	538	539	129	128	548	549	139	138
39	0	1	539	540	130	129	549	550	140	139
40	0	1	547	548	138	137	557	558	148	147
41	0	1	548	549	139	138	558	559	149	148
42	0	1	549	550	140	139	559	560	150	149
43	0	1	557	558	148	147	567	568	158	157
44	0	1	558	559	149	148	568	569	159	158
45	0	1	559	560	150	149	569	570	160	159
46	0	1	567	568	158	157	577	578	168	167
47	0	1	568	569	159	158	578	579	169	168
48	0	1	569	570	160	159	579	580	170	169
49	0	1	577	578	168	167	587	588	178	177
50	0	1	578	579	169	168	588	589	179	178
51	0	1	579	580	170	169	589	590	180	179
52	0	1	587	588	178	177	597	598	188	187
53	0	1	588	589	179	178	598	599	189	188
54	0	1	589	590	180	179	599	600	190	189
55	0	1	597	598	188	187	607	608	198	197

56	0	1	598	599	189	188	608	609	199	198
57	0	1	599	600	190	189	609	610	200	199
58	0	1	607	608	198	197	617	618	208	207
59	0	1	608	609	199	198	618	619	209	208
60	0	1	609	610	200	199	619	620	210	209
61	0	1	617	618	208	207	627	628	218	217
62	0	1	618	619	209	208	628	629	219	218
63	0	1	619	620	210	209	629	630	220	219
64	0	1	627	628	218	217	637	638	228	227
65	0	1	628	629	219	218	638	639	229	228
66	0	1	629	630	220	219	639	640	230	229
67	0	1	637	638	228	227	647	648	238	237
68	0	1	638	639	229	228	648	649	239	238
69	0	1	639	640	230	229	649	650	240	239
70	0	1	647	648	238	237	657	658	248	247
71	0	1	648	649	239	238	658	659	249	248
72	0	1	649	650	240	239	659	660	250	249
73	0	1	657	658	248	247	667	668	258	257
74	0	1	658	659	249	248	668	669	259	258
75	0	1	659	660	250	249	669	670	260	259
76	0	1	667	668	258	257	677	678	268	267
77	0	1	668	669	259	258	678	679	269	268
78	0	1	669	670	260	259	679	680	270	269
79	0	1	677	678	268	267	687	688	278	277
80	0	1	678	679	269	268	688	689	279	278
81	0	1	679	680	270	269	689	690	280	279
82	0	1	687	688	278	277	697	698	288	287
83	0	1	688	689	279	278	698	699	289	288
84	0	1	689	690	280	279	699	700	290	289
85	0	1	697	698	288	287	707	708	298	297
86	0	1	698	699	289	288	708	709	299	298
87	0	1	699	700	290	289	709	710	300	299
88	0	1	707	708	298	297	717	718	308	307
89	0	1	708	709	299	298	718	719	309	308
90	0	1	709	710	300	299	719	720	310	309
91	0	1	717	718	308	307	727	728	318	317
92	0	1	718	719	309	308	728	729	319	318
93	0	1	719	720	310	309	729	730	320	319
94	0	1	727	728	318	317	737	738	328	327
95	0	1	728	729	319	318	738	739	329	328
96	0	1	729	730	320	319	739	740	330	329
97	0	1	737	738	328	327	747	748	338	337
98	0	1	738	739	329	328	748	749	339	338
99	0	1	739	740	330	329	749	750	340	339
100	0	1	747	748	338	337	757	758	348	347
101	0	1	748	749	339	338	758	759	349	348

102	0	1	749	750	340	339	759	760	350	349
103	0	1	757	758	348	347	767	768	358	357
104	0	1	758	759	349	348	768	769	359	358
105	0	1	759	760	350	349	769	770	360	359
106	0	1	767	768	358	357	777	778	368	367
107	0	1	768	769	359	358	778	779	369	368
108	0	1	769	770	360	359	779	780	370	369
109	0	1	777	778	368	367	787	788	378	377
110	0	1	778	779	369	368	788	789	379	378
111	0	1	779	780	370	369	789	790	380	379
112	0	1	787	788	378	377	797	798	388	387
113	0	1	788	789	379	378	798	799	389	388
114	0	1	789	790	380	379	799	800	390	389
115	0	1	797	798	388	387	807	808	398	397
116	0	1	798	799	389	388	808	809	399	398
117	0	1	799	800	390	389	809	810	400	399
118	0	1	807	808	398	397	817	818	408	407
119	0	1	808	809	399	398	818	819	409	408
120	0	1	809	810	400	399	819	820	410	409
121	0	2	427	426	16	17	417	416	6	7
122	0	2	426	425	15	16	416	415	5	6
123	0	2	425	424	14	15	415	414	4	5
124	0	2	424	423	13	14	414	413	3	4
125	0	2	423	422	12	13	413	412	2	3
126	0	2	422	421	11	12	412	411	1	2
127	0	2	437	436	26	27	427	426	16	17
128	0	2	436	435	25	26	426	425	15	16
129	0	2	435	434	24	25	425	424	14	15
130	0	2	434	433	23	24	424	423	13	14
131	0	2	433	432	22	23	423	422	12	13
132	0	2	432	431	21	22	422	421	11	12
133	0	2	447	446	36	37	437	436	26	27
134	0	2	446	445	35	36	436	435	25	26
135	0	2	445	444	34	35	435	434	24	25
136	0	2	444	443	33	34	434	433	23	24
137	0	2	443	442	32	33	433	432	22	23
138	0	2	442	441	31	32	432	431	21	22
139	0	2	457	456	46	47	447	446	36	37
140	0	2	456	455	45	46	446	445	35	36
141	0	2	455	454	44	45	445	444	34	35
142	0	2	454	453	43	44	444	443	33	34
143	0	2	453	452	42	43	443	442	32	33
144	0	2	452	451	41	42	442	441	31	32
145	0	2	467	466	56	57	457	456	46	47
146	0	2	466	465	55	56	456	455	45	46
147	0	2	465	464	54	55	455	454	44	45

148	0	2	464	463	53	54	454	453	43	44
149	0	2	463	462	52	53	453	452	42	43
150	0	2	462	461	51	52	452	451	41	42
151	0	2	477	476	66	67	467	466	56	57
152	0	2	476	475	65	66	466	465	55	56
153	0	2	475	474	64	65	465	464	54	55
154	0	2	474	473	63	64	464	463	53	54
155	0	2	473	472	62	63	463	462	52	53
156	0	2	472	471	61	62	462	461	51	52
157	0	2	487	486	76	77	477	476	66	67
158	0	2	486	485	75	76	476	475	65	66
159	0	2	485	484	74	75	475	474	64	65
160	0	2	484	483	73	74	474	473	63	64
161	0	2	483	482	72	73	473	472	62	63
162	0	2	482	481	71	72	472	471	61	62
163	0	2	497	496	86	87	487	486	76	77
164	0	2	496	495	85	86	486	485	75	76
165	0	2	495	494	84	85	485	484	74	75
166	0	2	494	493	83	84	484	483	73	74
167	0	2	493	492	82	83	483	482	72	73
168	0	2	492	491	81	82	482	481	71	72
169	0	2	507	506	96	97	497	496	86	87
170	0	2	506	505	95	96	496	495	85	86
171	0	2	505	504	94	95	495	494	84	85
172	0	2	504	503	93	94	494	493	83	84
173	0	2	503	502	92	93	493	492	82	83
174	0	2	502	501	91	92	492	491	81	82
175	0	2	517	516	106	107	507	506	96	97
176	0	2	516	515	105	106	506	505	95	96
177	0	2	515	514	104	105	505	504	94	95
178	0	2	514	513	103	104	504	503	93	94
179	0	2	513	512	102	103	503	502	92	93
180	0	2	512	511	101	102	502	501	91	92
181	0	2	527	526	116	117	517	516	106	107
182	0	2	526	525	115	116	516	515	105	106
183	0	2	525	524	114	115	515	514	104	105
184	0	2	524	523	113	114	514	513	103	104
185	0	2	523	522	112	113	513	512	102	103
186	0	2	522	521	111	112	512	511	101	102
187	0	2	537	536	126	127	527	526	116	117
188	0	2	536	535	125	126	526	525	115	116
189	0	2	535	534	124	125	525	524	114	115
190	0	2	534	533	123	124	524	523	113	114
191	0	2	533	532	122	123	523	522	112	113
192	0	2	532	531	121	122	522	521	111	112
193	0	2	547	546	136	137	537	536	126	127

194	0	2	546	545	135	136	536	535	125	126
195	0	2	545	544	134	135	535	534	124	125
196	0	2	544	543	133	134	534	533	123	124
197	0	2	543	542	132	133	533	532	122	123
198	0	2	542	541	131	132	532	531	121	122
199	0	2	557	556	146	147	547	546	136	137
200	0	2	556	555	145	146	546	545	135	136
201	0	2	555	554	144	145	545	544	134	135
202	0	2	554	553	143	144	544	543	133	134
203	0	2	553	552	142	143	543	542	132	133
204	0	2	552	551	141	142	542	541	131	132
205	0	2	567	566	156	157	557	556	146	147
206	0	2	566	565	155	156	556	555	145	146
207	0	2	565	564	154	155	555	554	144	145
208	0	2	564	563	153	154	554	553	143	144
209	0	2	563	562	152	153	553	552	142	143
210	0	2	562	561	151	152	552	551	141	142
211	0	2	577	576	166	167	567	566	156	157
212	0	2	576	575	165	166	566	565	155	156
213	0	2	575	574	164	165	565	564	154	155
214	0	2	574	573	163	164	564	563	153	154
215	0	2	573	572	162	163	563	562	152	153
216	0	2	572	571	161	162	562	561	151	152
217	0	2	587	586	176	177	577	576	166	167
218	0	2	586	585	175	176	576	575	165	166
219	0	2	585	584	174	175	575	574	164	165
220	0	2	584	583	173	174	574	573	163	164
221	0	2	583	582	172	173	573	572	162	163
222	0	2	582	581	171	172	572	571	161	162
223	0	2	597	596	186	187	587	586	176	177
224	0	2	596	595	185	186	586	585	175	176
225	0	2	595	594	184	185	585	584	174	175
226	0	2	594	593	183	184	584	583	173	174
227	0	2	593	592	182	183	583	582	172	173
228	0	2	592	591	181	182	582	581	171	172
229	0	2	607	606	196	197	597	596	186	187
230	0	2	606	605	195	196	596	595	185	186
231	0	2	605	604	194	195	595	594	184	185
232	0	2	604	603	193	194	594	593	183	184
233	0	2	603	602	192	193	593	592	182	183
234	0	2	602	601	191	192	592	591	181	182
235	0	2	617	616	206	207	607	606	196	197
236	0	2	616	615	205	206	606	605	195	196
237	0	2	615	614	204	205	605	604	194	195
238	0	2	614	613	203	204	604	603	193	194
239	0	2	613	612	202	203	603	602	192	193

240	0	2	612	611	201	202	602	601	191	192
241	0	2	627	626	216	217	617	616	206	207
242	0	2	626	625	215	216	616	615	205	206
243	0	2	625	624	214	215	615	614	204	205
244	0	2	624	623	213	214	614	613	203	204
245	0	2	623	622	212	213	613	612	202	203
246	0	2	622	621	211	212	612	611	201	202
247	0	2	637	636	226	227	627	626	216	217
248	0	2	636	635	225	226	626	625	215	216
249	0	2	635	634	224	225	625	624	214	215
250	0	2	634	633	223	224	624	623	213	214
251	0	2	633	632	222	223	623	622	212	213
252	0	2	632	631	221	222	622	621	211	212
253	0	2	647	646	236	237	637	636	226	227
254	0	2	646	645	235	236	636	635	225	226
255	0	2	645	644	234	235	635	634	224	225
256	0	2	644	643	233	234	634	633	223	224
257	0	2	643	642	232	233	633	632	222	223
258	0	2	642	641	231	232	632	631	221	222
259	0	2	657	656	246	247	647	646	236	237
260	0	2	656	655	245	246	646	645	235	236
261	0	2	655	654	244	245	645	644	234	235
262	0	2	654	653	243	244	644	643	233	234
263	0	2	653	652	242	243	643	642	232	233
264	0	2	652	651	241	242	642	641	231	232
265	0	2	667	666	256	257	657	656	246	247
266	0	2	666	665	255	256	656	655	245	246
267	0	2	665	664	254	255	655	654	244	245
268	0	2	664	663	253	254	654	653	243	244
269	0	2	663	662	252	253	653	652	242	243
270	0	2	662	661	251	252	652	651	241	242
271	0	2	677	676	266	267	667	666	256	257
272	0	2	676	675	265	266	666	665	255	256
273	0	2	675	674	264	265	665	664	254	255
274	0	2	674	673	263	264	664	663	253	254
275	0	2	673	672	262	263	663	662	252	253
276	0	2	672	671	261	262	662	661	251	252
277	0	2	687	686	276	277	677	676	266	267
278	0	2	686	685	275	276	676	675	265	266
279	0	2	685	684	274	275	675	674	264	265
280	0	2	684	683	273	274	674	673	263	264
281	0	2	683	682	272	273	673	672	262	263
282	0	2	682	681	271	272	672	671	261	262
283	0	2	697	696	286	287	687	686	276	277
284	0	2	696	695	285	286	686	685	275	276
285	0	2	695	694	284	285	685	684	274	275

286	0	2	694	693	283	284	684	683	273	274
287	0	2	693	692	282	283	683	682	272	273
288	0	2	692	691	281	282	682	681	271	272
289	0	2	707	706	296	297	697	696	286	287
290	0	2	706	705	295	296	696	695	285	286
291	0	2	705	704	294	295	695	694	284	285
292	0	2	704	703	293	294	694	693	283	284
293	0	2	703	702	292	293	693	692	282	283
294	0	2	702	701	291	292	692	691	281	282
295	0	2	717	716	306	307	707	706	296	297
296	0	2	716	715	305	306	706	705	295	296
297	0	2	715	714	304	305	705	704	294	295
298	0	2	714	713	303	304	704	703	293	294
299	0	2	713	712	302	303	703	702	292	293
300	0	2	712	711	301	302	702	701	291	292
301	0	2	727	726	316	317	717	716	306	307
302	0	2	726	725	315	316	716	715	305	306
303	0	2	725	724	314	315	715	714	304	305
304	0	2	724	723	313	314	714	713	303	304
305	0	2	723	722	312	313	713	712	302	303
306	0	2	722	721	311	312	712	711	301	302
307	0	2	737	736	326	327	727	726	316	317
308	0	2	736	735	325	326	726	725	315	316
309	0	2	735	734	324	325	725	724	314	315
310	0	2	734	733	323	324	724	723	313	314
311	0	2	733	732	322	323	723	722	312	313
312	0	2	732	731	321	322	722	721	311	312
313	0	2	747	746	336	337	737	736	326	327
314	0	2	746	745	335	336	736	735	325	326
315	0	2	745	744	334	335	735	734	324	325
316	0	2	744	743	333	334	734	733	323	324
317	0	2	743	742	332	333	733	732	322	323
318	0	2	742	741	331	332	732	731	321	322
319	0	2	757	756	346	347	747	746	336	337
320	0	2	756	755	345	346	746	745	335	336
321	0	2	755	754	344	345	745	744	334	335
322	0	2	754	753	343	344	744	743	333	334
323	0	2	753	752	342	343	743	742	332	333
324	0	2	752	751	341	342	742	741	331	332
325	0	2	767	766	356	357	757	756	346	347
326	0	2	766	765	355	356	756	755	345	346
327	0	2	765	764	354	355	755	754	344	345
328	0	2	764	763	353	354	754	753	343	344
329	0	2	763	762	352	353	753	752	342	343
330	0	2	762	761	351	352	752	751	341	342
331	0	2	777	776	366	367	767	766	356	357

332	0	2	776	775	365	366	766	765	355	356
333	0	2	775	774	364	365	765	764	354	355
334	0	2	774	773	363	364	764	763	353	354
335	0	2	773	772	362	363	763	762	352	353
336	0	2	772	771	361	362	762	761	351	352
337	0	2	787	786	376	377	777	776	366	367
338	0	2	786	785	375	376	776	775	365	366
339	0	2	785	784	374	375	775	774	364	365
340	0	2	784	783	373	374	774	773	363	364
341	0	2	783	782	372	373	773	772	362	363
342	0	2	782	781	371	372	772	771	361	362
343	0	2	797	796	386	387	787	786	376	377
344	0	2	796	795	385	386	786	785	375	376
345	0	2	795	794	384	385	785	784	374	375
346	0	2	794	793	383	384	784	783	373	374
347	0	2	793	792	382	383	783	782	372	373
348	0	2	792	791	381	382	782	781	371	372
349	0	2	807	806	396	397	797	796	386	387
350	0	2	806	805	395	396	796	795	385	386
351	0	2	805	804	394	395	795	794	384	385
352	0	2	804	803	393	394	794	793	383	384
353	0	2	803	802	392	393	793	792	382	383
354	0	2	802	801	391	392	792	791	381	382
355	0	2	817	816	406	407	807	806	396	397
356	0	2	816	815	405	406	806	805	395	396
357	0	2	815	814	404	405	805	804	394	395
358	0	2	814	813	403	404	804	803	393	394
359	0	2	813	812	402	403	803	802	392	393
360	0	2	812	811	401	402	802	801	391	392
361	0	3	411	421	11	1				
362	0	3	421	431	21	11				
363	0	3	431	441	31	21				
364	0	3	441	451	41	31				
365	0	3	451	461	51	41				
366	0	3	461	471	61	51				
367	0	3	471	481	71	61				
368	0	3	481	491	81	71				
369	0	3	491	501	91	81				
370	0	3	501	511	101	91				
371	0	3	511	521	111	101				
372	0	3	521	531	121	111				
373	0	3	531	541	131	121				
374	0	3	541	551	141	131				
375	0	3	551	561	151	141				
376	0	3	561	571	161	151				
377	0	3	571	581	171	161				

378	0	3	581	591	181	171
379	0	3	591	601	191	181
380	0	3	601	611	201	191
381	0	3	611	621	211	201
382	0	3	621	631	221	211
383	0	3	631	641	231	221
384	0	3	641	651	241	231
385	0	3	651	661	251	241
386	0	3	661	671	261	251
387	0	3	671	681	271	261
388	0	3	681	691	281	271
389	0	3	691	701	291	281
390	0	3	701	711	301	291
391	0	3	711	721	311	301
392	0	3	721	731	321	311
393	0	3	731	741	331	321
394	0	3	741	751	341	331
395	0	3	751	761	351	341
396	0	3	761	771	361	351
397	0	3	771	781	371	361
398	0	3	781	791	381	371
399	0	3	791	801	391	381
400	0	3	801	811	401	391

EDAT

360

1	2.762542E-04	8.790935E-03	-2.811901E-02	1.299301E+00	2.223579E-02
	5.924147E-01				
2	2.825170E-04	8.990479E-03	-2.811901E-02	1.299301E+00	2.223517E-02
	5.924147E-01				
3	2.888201E-04	9.190664E-03	-2.811901E-02	1.299301E+00	2.223613E-02
	5.924148E-01				
4	2.762783E-04	8.791318E-03	-2.446351E-02	1.299301E+00	2.223676E-02
	5.924148E-01				
5	2.825573E-04	8.991120E-03	-2.446351E-02	1.299301E+00	2.223676E-02
	5.924148E-01				
6	2.888364E-04	9.190923E-03	-2.446351E-02	1.299301E+00	2.223676E-02
	5.924148E-01				
7	2.762783E-04	8.791318E-03	-2.101492E-02	1.299301E+00	2.223676E-02
	5.924148E-01				
8	2.825573E-04	8.991120E-03	-2.101492E-02	1.299301E+00	2.223676E-02
	5.924148E-01				
9	2.888364E-04	9.190923E-03	-2.101492E-02	1.299301E+00	2.223676E-02
	5.924148E-01				
10	2.762783E-04	8.791318E-03	-1.776154E-02	1.299301E+00	2.223676E-02
	5.924148E-01				

11	2.825573E-04	8.991120E-03	-1.776154E-02	1.299301E+00	2.223676E-02	5.924148E-01
12	2.888364E-04	9.190923E-03	-1.776154E-02	1.299301E+00	2.223676E-02	5.924148E-01
13	2.762783E-04	8.791318E-03	-1.469231E-02	1.299301E+00	2.223676E-02	5.924148E-01
14	2.825573E-04	8.991120E-03	-1.469231E-02	1.299301E+00	2.223676E-02	5.924148E-01
15	2.888364E-04	9.190923E-03	-1.469231E-02	1.299301E+00	2.223676E-02	5.924148E-01
16	2.762783E-04	8.791318E-03	-1.179681E-02	1.299301E+00	2.223676E-02	5.924148E-01
17	2.825573E-04	8.991120E-03	-1.179681E-02	1.299301E+00	2.223676E-02	5.924148E-01
18	2.888364E-04	9.190923E-03	-1.179681E-02	1.299301E+00	2.223676E-02	5.924148E-01
19	2.762783E-04	8.791318E-03	-9.065200E-03	1.299301E+00	2.223676E-02	5.924148E-01
20	2.825573E-04	8.991120E-03	-9.065200E-03	1.299301E+00	2.223676E-02	5.924148E-01
21	2.888364E-04	9.190923E-03	-9.065200E-03	1.299301E+00	2.223676E-02	5.924148E-01
22	2.762783E-04	8.791318E-03	-6.488217E-03	1.299301E+00	2.223676E-02	5.924148E-01
23	2.825573E-04	8.991120E-03	-6.488217E-03	1.299301E+00	2.223676E-02	5.924148E-01
24	2.888364E-04	9.190923E-03	-6.488217E-03	1.299301E+00	2.223676E-02	5.924148E-01
25	2.762783E-04	8.791318E-03	-4.057099E-03	1.299301E+00	2.223676E-02	5.924148E-01
26	2.825573E-04	8.991120E-03	-4.057099E-03	1.299301E+00	2.223676E-02	5.924148E-01
27	2.888364E-04	9.190923E-03	-4.057099E-03	1.299301E+00	2.223676E-02	5.924148E-01
28	2.762783E-04	8.791318E-03	-1.763592E-03	1.299301E+00	2.223676E-02	5.924148E-01
29	2.825573E-04	8.991120E-03	-1.763592E-03	1.299301E+00	2.223676E-02	5.924148E-01
30	2.888364E-04	9.190923E-03	-1.763592E-03	1.299301E+00	2.223676E-02	5.924148E-01
31	2.762783E-04	8.791318E-03	4.000947E-04	1.299301E+00	2.223676E-02	5.924148E-01
32	2.825573E-04	8.991120E-03	4.000947E-04	1.299301E+00	2.223676E-02	5.924148E-01
33	2.888364E-04	9.190923E-03	4.000947E-04	1.299301E+00	2.223676E-02	5.924148E-01
34	2.762783E-04	8.791318E-03	2.441308E-03	1.299301E+00	2.223676E-02	5.924148E-01
35	2.825573E-04	8.991120E-03	2.441308E-03	1.299301E+00	2.223676E-02	5.924148E-01
36	2.888364E-04	9.190923E-03	2.441308E-03	1.299301E+00	2.223676E-02	5.924148E-01

37	2.762783E-04	8.791318E-03	4.366982E-03	1.299301E+00	2.223676E-02	5.924148E-01
38	2.825573E-04	8.991120E-03	4.366982E-03	1.299301E+00	2.223676E-02	5.924148E-01
39	2.888364E-04	9.190923E-03	4.366982E-03	1.299301E+00	2.223676E-02	5.924148E-01
40	2.762783E-04	8.791318E-03	6.183654E-03	1.299301E+00	2.223676E-02	5.924148E-01
41	2.825573E-04	8.991120E-03	6.183654E-03	1.299301E+00	2.223676E-02	5.924148E-01
42	2.888364E-04	9.190923E-03	6.183654E-03	1.299301E+00	2.223676E-02	5.924148E-01
43	2.762783E-04	8.791318E-03	7.897497E-03	1.299301E+00	2.223676E-02	5.924148E-01
44	2.825573E-04	8.991120E-03	7.897497E-03	1.299301E+00	2.223676E-02	5.924148E-01
45	2.888364E-04	9.190923E-03	7.897497E-03	1.299301E+00	2.223676E-02	5.924148E-01
46	2.762783E-04	8.791318E-03	9.514329E-03	1.299301E+00	2.223676E-02	5.924148E-01
47	2.825573E-04	8.991120E-03	9.514329E-03	1.299301E+00	2.223676E-02	5.924148E-01
48	2.888364E-04	9.190923E-03	9.514329E-03	1.299301E+00	2.223676E-02	5.924148E-01
49	2.762783E-04	8.791318E-03	1.103964E-02	1.299301E+00	2.223676E-02	5.924148E-01
50	2.825573E-04	8.991120E-03	1.103964E-02	1.299301E+00	2.223676E-02	5.924148E-01
51	2.888364E-04	9.190923E-03	1.103964E-02	1.299301E+00	2.223676E-02	5.924148E-01
52	2.762783E-04	8.791318E-03	1.247862E-02	1.299301E+00	2.223676E-02	5.924148E-01
53	2.825573E-04	8.991120E-03	1.247862E-02	1.299301E+00	2.223676E-02	5.924148E-01
54	2.888364E-04	9.190923E-03	1.247862E-02	1.299301E+00	2.223676E-02	5.924148E-01
55	2.762783E-04	8.791318E-03	1.383614E-02	1.299301E+00	2.223676E-02	5.924148E-01
56	2.825573E-04	8.991120E-03	1.383614E-02	1.299301E+00	2.223676E-02	5.924148E-01
57	2.888364E-04	9.190923E-03	1.383614E-02	1.299301E+00	2.223676E-02	5.924148E-01
58	2.762783E-04	8.791318E-03	1.511682E-02	1.299301E+00	2.223676E-02	5.924148E-01
59	2.825573E-04	8.991120E-03	1.511682E-02	1.299301E+00	2.223676E-02	5.924148E-01
60	2.888364E-04	9.190923E-03	1.511682E-02	1.299301E+00	2.223676E-02	5.924148E-01
61	2.762783E-04	8.791318E-03	1.632501E-02	1.299301E+00	2.223676E-02	5.924148E-01
62	2.825573E-04	8.991120E-03	1.632501E-02	1.299301E+00	2.223676E-02	5.924148E-01
63	2.888364E-04	9.190923E-03	1.632501E-02	1.299301E+00	2.223676E-02	5.924148E-01
64	2.762783E-04	8.791318E-03	1.746482E-02	1.299301E+00	2.223676E-02	5.924148E-01
65	2.825573E-04	8.991120E-03	1.746482E-02	1.299301E+00	2.223676E-02	5.924148E-01
66	2.888364E-04	9.190923E-03	1.746482E-02	1.299301E+00	2.223676E-02	5.924148E-01
67	2.762783E-04	8.791318E-03	1.854011E-02	1.299301E+00	2.223676E-02	5.924148E-01
68	2.825573E-04	8.991120E-03	1.854011E-02	1.299301E+00	2.223676E-02	5.924148E-01
69	2.888364E-04	9.190923E-03	1.854011E-02	1.299301E+00	2.223676E-02	5.924148E-01
70	2.762783E-04	8.791318E-03	1.955452E-02	1.299301E+00	2.223676E-02	5.924148E-01
71	2.825573E-04	8.991120E-03	1.955452E-02	1.299301E+00	2.223676E-02	5.924148E-01
72	2.888364E-04	9.190923E-03	1.955452E-02	1.299301E+00	2.223676E-02	5.924148E-01
73	2.762783E-04	8.791318E-03	2.051152E-02	1.299301E+00	2.223676E-02	5.924148E-01
74	2.825573E-04	8.991120E-03	2.051152E-02	1.299301E+00	2.223676E-02	5.924148E-01
75	2.888364E-04	9.190923E-03	2.051152E-02	1.299301E+00	2.223676E-02	5.924148E-01
76	2.762783E-04	8.791318E-03	2.141435E-02	1.299301E+00	2.223676E-02	5.924148E-01
77	2.825573E-04	8.991120E-03	2.141435E-02	1.299301E+00	2.223676E-02	5.924148E-01
78	2.888364E-04	9.190923E-03	2.141435E-02	1.299301E+00	2.223676E-02	5.924148E-01
79	2.762783E-04	8.791318E-03	2.226608E-02	1.299301E+00	2.223676E-02	5.924148E-01
80	2.825573E-04	8.991120E-03	2.226608E-02	1.299301E+00	2.223676E-02	5.924148E-01
81	2.888364E-04	9.190923E-03	2.226608E-02	1.299301E+00	2.223676E-02	5.924148E-01
82	2.762783E-04	8.791318E-03	2.306960E-02	1.299301E+00	2.223676E-02	5.924148E-01

83	2.825573E-04	8.991120E-03	2.306960E-02	1.299301E+00	2.223676E-02	5.924148E-01
84	2.888364E-04	9.190923E-03	2.306960E-02	1.299301E+00	2.223676E-02	5.924148E-01
85	2.762783E-04	8.791318E-03	2.382764E-02	1.299301E+00	2.223676E-02	5.924148E-01
86	2.825573E-04	8.991120E-03	2.382764E-02	1.299301E+00	2.223676E-02	5.924148E-01
87	2.888364E-04	9.190923E-03	2.382764E-02	1.299301E+00	2.223676E-02	5.924148E-01
88	2.762783E-04	8.791318E-03	2.454276E-02	1.299301E+00	2.223676E-02	5.924148E-01
89	2.825573E-04	8.991120E-03	2.454276E-02	1.299301E+00	2.223676E-02	5.924148E-01
90	2.888364E-04	9.190923E-03	2.454276E-02	1.299301E+00	2.223676E-02	5.924148E-01
91	2.762783E-04	8.791318E-03	2.521741E-02	1.299301E+00	2.223676E-02	5.924148E-01
92	2.825573E-04	8.991120E-03	2.521741E-02	1.299301E+00	2.223676E-02	5.924148E-01
93	2.888364E-04	9.190923E-03	2.521741E-02	1.299301E+00	2.223676E-02	5.924148E-01
94	2.762783E-04	8.791318E-03	2.585387E-02	1.299301E+00	2.223676E-02	5.924148E-01
95	2.825573E-04	8.991120E-03	2.585387E-02	1.299301E+00	2.223676E-02	5.924148E-01
96	2.888364E-04	9.190923E-03	2.585387E-02	1.299301E+00	2.223676E-02	5.924148E-01
97	2.762783E-04	8.791318E-03	2.645430E-02	1.299301E+00	2.223676E-02	5.924148E-01
98	2.825573E-04	8.991120E-03	2.645430E-02	1.299301E+00	2.223676E-02	5.924148E-01
99	2.888364E-04	9.190923E-03	2.645430E-02	1.299301E+00	2.223676E-02	5.924148E-01
100	2.762783E-04	8.791318E-03	2.702074E-02	1.299301E+00	2.223676E-02	5.924148E-01
101	2.825573E-04	8.991120E-03	2.702074E-02	1.299301E+00	2.223676E-02	5.924148E-01
102	2.888364E-04	9.190923E-03	2.702074E-02	1.299301E+00	2.223676E-02	5.924148E-01
103	2.762783E-04	8.791318E-03	2.755513E-02	1.299301E+00	2.223676E-02	5.924148E-01
104	2.825573E-04	8.991120E-03	2.755513E-02	1.299301E+00	2.223676E-02	5.924148E-01
105	2.888364E-04	9.190923E-03	2.755513E-02	1.299301E+00	2.223676E-02	5.924148E-01
106	2.762783E-04	8.791318E-03	2.805927E-02	1.299301E+00	2.223676E-02	5.924148E-01
107	2.825573E-04	8.991120E-03	2.805927E-02	1.299301E+00	2.223676E-02	5.924148E-01
108	2.888364E-04	9.190923E-03	2.805927E-02	1.299301E+00	2.223676E-02	5.924148E-01
109	2.762783E-04	8.791318E-03	2.853487E-02	1.299301E+00	2.223676E-02	5.924148E-01
110	2.825573E-04	8.991120E-03	2.853487E-02	1.299301E+00	2.223676E-02	5.924148E-01
111	2.888364E-04	9.190923E-03	2.853487E-02	1.299301E+00	2.223676E-02	5.924148E-01
112	2.762783E-04	8.791318E-03	2.898355E-02	1.299301E+00	2.223676E-02	5.924148E-01
113	2.825573E-04	8.991120E-03	2.898355E-02	1.299301E+00	2.223676E-02	5.924148E-01
114	2.888364E-04	9.190923E-03	2.898355E-02	1.299301E+00	2.223676E-02	5.924148E-01
115	2.762783E-04	8.791318E-03	2.940683E-02	1.299301E+00	2.223676E-02	5.924148E-01
116	2.825573E-04	8.991120E-03	2.940683E-02	1.299301E+00	2.223676E-02	5.924148E-01
117	2.888364E-04	9.190923E-03	2.940683E-02	1.299301E+00	2.223676E-02	5.924148E-01
118	2.762783E-04	8.791318E-03	2.980616E-02	1.299301E+00	2.223676E-02	5.924148E-01
119	2.825573E-04	8.991120E-03	2.980616E-02	1.299301E+00	2.223676E-02	5.924148E-01
120	2.888364E-04	9.190923E-03	2.980616E-02	1.299301E+00	2.223676E-02	5.924148E-01
121	2.699992E-04	8.591515E-03	-2.811902E-02	1.299301E+00	2.223676E-02	5.924148E-01
122	2.637202E-04	8.391712E-03	-2.811902E-02	1.299301E+00	2.223676E-02	5.924148E-01
123	2.574411E-04	8.191910E-03	-2.811902E-02	1.299301E+00	2.223676E-02	5.924148E-01
124	2.511621E-04	7.992107E-03	-2.811902E-02	1.299301E+00	2.223676E-02	5.924148E-01

125	2.448830E-04	7.792304E-03	-2.811902E-02	1.299301E+00	2.223676E-02
	5.924148E-01				
126	2.386040E-04	7.592501E-03	-2.811902E-02	1.299301E+00	2.223676E-02
	5.924148E-01				
127	2.699992E-04	8.591515E-03	-2.446351E-02	1.299301E+00	2.223676E-02
	5.924148E-01				
128	2.637202E-04	8.391712E-03	-2.446351E-02	1.299301E+00	2.223676E-02
	5.924148E-01				
129	2.574411E-04	8.191910E-03	-2.446351E-02	1.299301E+00	2.223676E-02
	5.924148E-01				
130	2.511621E-04	7.992107E-03	-2.446351E-02	1.299301E+00	2.223676E-02
	5.924148E-01				
131	2.448830E-04	7.792304E-03	-2.446351E-02	1.299301E+00	2.223676E-02
	5.924148E-01				
132	2.386040E-04	7.592501E-03	-2.446351E-02	1.299301E+00	2.223676E-02
	5.924148E-01				
133	2.699992E-04	8.591515E-03	-2.101492E-02	1.299301E+00	2.223676E-02
	5.924148E-01				
134	2.637202E-04	8.391712E-03	-2.101492E-02	1.299301E+00	2.223676E-02
	5.924148E-01				
135	2.574411E-04	8.191910E-03	-2.101492E-02	1.299301E+00	2.223676E-02
	5.924148E-01				
136	2.511621E-04	7.992107E-03	-2.101492E-02	1.299301E+00	2.223676E-02
	5.924148E-01				
137	2.448830E-04	7.792304E-03	-2.101492E-02	1.299301E+00	2.223676E-02
	5.924148E-01				
138	2.386040E-04	7.592501E-03	-2.101492E-02	1.299301E+00	2.223676E-02
	5.924148E-01				
139	2.699992E-04	8.591515E-03	-1.776154E-02	1.299301E+00	2.223676E-02
	5.924148E-01				
140	2.637202E-04	8.391712E-03	-1.776154E-02	1.299301E+00	2.223676E-02
	5.924148E-01				
141	2.574411E-04	8.191910E-03	-1.776154E-02	1.299301E+00	2.223676E-02
	5.924148E-01				
142	2.511621E-04	7.992107E-03	-1.776154E-02	1.299301E+00	2.223676E-02
	5.924148E-01				
143	2.448830E-04	7.792304E-03	-1.776154E-02	1.299301E+00	2.223676E-02
	5.924148E-01				
144	2.386040E-04	7.592501E-03	-1.776154E-02	1.299301E+00	2.223676E-02
	5.924148E-01				
145	2.699992E-04	8.591515E-03	-1.469231E-02	1.299301E+00	2.223676E-02
	5.924148E-01				
146	2.637202E-04	8.391712E-03	-1.469231E-02	1.299301E+00	2.223676E-02
	5.924148E-01				
147	2.574411E-04	8.191910E-03	-1.469231E-02	1.299301E+00	2.223676E-02
	5.924148E-01				

148	2.511621E-04	7.992107E-03	-1.469231E-02	1.299301E+00	2.223676E-02
	5.924148E-01				
149	2.448830E-04	7.792304E-03	-1.469231E-02	1.299301E+00	2.223676E-02
	5.924148E-01				
150	2.386040E-04	7.592501E-03	-1.469231E-02	1.299301E+00	2.223676E-02
	5.924148E-01				
151	2.699992E-04	8.591515E-03	-1.179680E-02	1.299301E+00	2.223676E-02
	5.924148E-01				
152	2.637202E-04	8.391712E-03	-1.179680E-02	1.299301E+00	2.223676E-02
	5.924148E-01				
153	2.574411E-04	8.191910E-03	-1.179680E-02	1.299301E+00	2.223676E-02
	5.924148E-01				
154	2.511621E-04	7.992107E-03	-1.179680E-02	1.299301E+00	2.223676E-02
	5.924148E-01				
155	2.448830E-04	7.792304E-03	-1.179680E-02	1.299301E+00	2.223676E-02
	5.924148E-01				
156	2.386040E-04	7.592501E-03	-1.179680E-02	1.299301E+00	2.223676E-02
	5.924148E-01				
157	2.699992E-04	8.591515E-03	-9.065200E-03	1.299301E+00	2.223676E-02
	5.924148E-01				
158	2.637202E-04	8.391712E-03	-9.065200E-03	1.299301E+00	2.223676E-02
	5.924148E-01				
159	2.574411E-04	8.191910E-03	-9.065200E-03	1.299301E+00	2.223676E-02
	5.924148E-01				
160	2.511621E-04	7.992107E-03	-9.065200E-03	1.299301E+00	2.223676E-02
	5.924148E-01				
161	2.448830E-04	7.792304E-03	-9.065200E-03	1.299301E+00	2.223676E-02
	5.924148E-01				
162	2.386040E-04	7.592501E-03	-9.065200E-03	1.299301E+00	2.223676E-02
	5.924148E-01				
163	2.699992E-04	8.591515E-03	-6.488217E-03	1.299301E+00	2.223676E-02
	5.924148E-01				
164	2.637202E-04	8.391712E-03	-6.488217E-03	1.299301E+00	2.223676E-02
	5.924148E-01				
165	2.574411E-04	8.191910E-03	-6.488217E-03	1.299301E+00	2.223676E-02
	5.924148E-01				
166	2.511621E-04	7.992107E-03	-6.488217E-03	1.299301E+00	2.223676E-02
	5.924148E-01				
167	2.448830E-04	7.792304E-03	-6.488217E-03	1.299301E+00	2.223676E-02
	5.924148E-01				
168	2.386040E-04	7.592501E-03	-6.488217E-03	1.299301E+00	2.223676E-02
	5.924148E-01				
169	2.699992E-04	8.591515E-03	-4.057099E-03	1.299301E+00	2.223676E-02
	5.924148E-01				
170	2.637202E-04	8.391712E-03	-4.057099E-03	1.299301E+00	2.223676E-02
	5.924148E-01				

171	2.574411E-04	8.191910E-03	-4.057099E-03	1.299301E+00	2.223676E-02	5.924148E-01
172	2.511621E-04	7.992107E-03	-4.057099E-03	1.299301E+00	2.223676E-02	5.924148E-01
173	2.448830E-04	7.792304E-03	-4.057099E-03	1.299301E+00	2.223676E-02	5.924148E-01
174	2.386040E-04	7.592501E-03	-4.057099E-03	1.299301E+00	2.223676E-02	5.924148E-01
175	2.699992E-04	8.591515E-03	-1.763592E-03	1.299301E+00	2.223676E-02	5.924148E-01
176	2.637202E-04	8.391712E-03	-1.763592E-03	1.299301E+00	2.223676E-02	5.924148E-01
177	2.574411E-04	8.191910E-03	-1.763592E-03	1.299301E+00	2.223676E-02	5.924148E-01
178	2.511621E-04	7.992107E-03	-1.763592E-03	1.299301E+00	2.223676E-02	5.924148E-01
179	2.448830E-04	7.792304E-03	-1.763592E-03	1.299301E+00	2.223676E-02	5.924148E-01
180	2.386040E-04	7.592501E-03	-1.763592E-03	1.299301E+00	2.223676E-02	5.924148E-01
181	2.699992E-04	8.591515E-03	4.000947E-04	1.299301E+00	2.223676E-02	5.924148E-01
182	2.637202E-04	8.391712E-03	4.000947E-04	1.299301E+00	2.223676E-02	5.924148E-01
183	2.574411E-04	8.191910E-03	4.000947E-04	1.299301E+00	2.223676E-02	5.924148E-01
184	2.511621E-04	7.992107E-03	4.000947E-04	1.299301E+00	2.223676E-02	5.924148E-01
185	2.448830E-04	7.792304E-03	4.000947E-04	1.299301E+00	2.223676E-02	5.924148E-01
186	2.386040E-04	7.592501E-03	4.000947E-04	1.299301E+00	2.223676E-02	5.924148E-01
187	2.699992E-04	8.591515E-03	2.441309E-03	1.299301E+00	2.223676E-02	5.924148E-01
188	2.637202E-04	8.391712E-03	2.441309E-03	1.299301E+00	2.223676E-02	5.924148E-01
189	2.574411E-04	8.191910E-03	2.441309E-03	1.299301E+00	2.223676E-02	5.924148E-01
190	2.511621E-04	7.992107E-03	2.441309E-03	1.299301E+00	2.223676E-02	5.924148E-01
191	2.448830E-04	7.792304E-03	2.441309E-03	1.299301E+00	2.223676E-02	5.924148E-01
192	2.386040E-04	7.592501E-03	2.441309E-03	1.299301E+00	2.223676E-02	5.924148E-01
193	2.699992E-04	8.591515E-03	4.366982E-03	1.299301E+00	2.223676E-02	5.924148E-01
194	2.637202E-04	8.391712E-03	4.366982E-03	1.299301E+00	2.223676E-02	5.924148E-01
195	2.574411E-04	8.191910E-03	4.366982E-03	1.299301E+00	2.223676E-02	5.924148E-01
196	2.511621E-04	7.992107E-03	4.366982E-03	1.299301E+00	2.223676E-02	5.924148E-01
197	2.448830E-04	7.792304E-03	4.366982E-03	1.299301E+00	2.223676E-02	5.924148E-01
198	2.386040E-04	7.592501E-03	4.366982E-03	1.299301E+00	2.223676E-02	5.924148E-01
199	2.699992E-04	8.591515E-03	6.183654E-03	1.299301E+00	2.223676E-02	5.924148E-01
200	2.637202E-04	8.391712E-03	6.183654E-03	1.299301E+00	2.223676E-02	5.924148E-01
201	2.574411E-04	8.191910E-03	6.183654E-03	1.299301E+00	2.223676E-02	5.924148E-01
202	2.511621E-04	7.992107E-03	6.183654E-03	1.299301E+00	2.223676E-02	5.924148E-01
203	2.448830E-04	7.792304E-03	6.183654E-03	1.299301E+00	2.223676E-02	5.924148E-01
204	2.386040E-04	7.592501E-03	6.183654E-03	1.299301E+00	2.223676E-02	5.924148E-01
205	2.699992E-04	8.591515E-03	7.897497E-03	1.299301E+00	2.223676E-02	5.924148E-01
206	2.637202E-04	8.391712E-03	7.897497E-03	1.299301E+00	2.223676E-02	5.924148E-01

207	2.574411E-04	8.191910E-03	7.897497E-03	1.299301E+00	2.223676E-02	5.924148E-01
208	2.511621E-04	7.992107E-03	7.897497E-03	1.299301E+00	2.223676E-02	5.924148E-01
209	2.448830E-04	7.792304E-03	7.897497E-03	1.299301E+00	2.223676E-02	5.924148E-01
210	2.386040E-04	7.592501E-03	7.897497E-03	1.299301E+00	2.223676E-02	5.924148E-01
211	2.699992E-04	8.591515E-03	9.514329E-03	1.299301E+00	2.223676E-02	5.924148E-01
212	2.637202E-04	8.391712E-03	9.514329E-03	1.299301E+00	2.223676E-02	5.924148E-01
213	2.574411E-04	8.191910E-03	9.514329E-03	1.299301E+00	2.223676E-02	5.924148E-01
214	2.511621E-04	7.992107E-03	9.514329E-03	1.299301E+00	2.223676E-02	5.924148E-01
215	2.448830E-04	7.792304E-03	9.514329E-03	1.299301E+00	2.223676E-02	5.924148E-01
216	2.386040E-04	7.592501E-03	9.514329E-03	1.299301E+00	2.223676E-02	5.924148E-01
217	2.699992E-04	8.591515E-03	1.103964E-02	1.299301E+00	2.223676E-02	5.924148E-01
218	2.637202E-04	8.391712E-03	1.103964E-02	1.299301E+00	2.223676E-02	5.924148E-01
219	2.574411E-04	8.191910E-03	1.103964E-02	1.299301E+00	2.223676E-02	5.924148E-01
220	2.511621E-04	7.992107E-03	1.103964E-02	1.299301E+00	2.223676E-02	5.924148E-01
221	2.448830E-04	7.792304E-03	1.103964E-02	1.299301E+00	2.223676E-02	5.924148E-01
222	2.386040E-04	7.592501E-03	1.103964E-02	1.299301E+00	2.223676E-02	5.924148E-01
223	2.699992E-04	8.591515E-03	1.247862E-02	1.299301E+00	2.223676E-02	5.924148E-01
224	2.637202E-04	8.391712E-03	1.247862E-02	1.299301E+00	2.223676E-02	5.924148E-01
225	2.574411E-04	8.191910E-03	1.247862E-02	1.299301E+00	2.223676E-02	5.924148E-01
226	2.511621E-04	7.992107E-03	1.247862E-02	1.299301E+00	2.223676E-02	5.924148E-01
227	2.448830E-04	7.792304E-03	1.247862E-02	1.299301E+00	2.223676E-02	5.924148E-01
228	2.386040E-04	7.592501E-03	1.247862E-02	1.299301E+00	2.223676E-02	5.924148E-01
229	2.699992E-04	8.591515E-03	1.383614E-02	1.299301E+00	2.223676E-02	5.924148E-01
230	2.637202E-04	8.391712E-03	1.383614E-02	1.299301E+00	2.223676E-02	5.924148E-01
231	2.574411E-04	8.191910E-03	1.383614E-02	1.299301E+00	2.223676E-02	5.924148E-01
232	2.511621E-04	7.992107E-03	1.383614E-02	1.299301E+00	2.223676E-02	5.924148E-01
233	2.448830E-04	7.792304E-03	1.383614E-02	1.299301E+00	2.223676E-02	5.924148E-01
234	2.386040E-04	7.592501E-03	1.383614E-02	1.299301E+00	2.223676E-02	5.924148E-01
235	2.699992E-04	8.591515E-03	1.511682E-02	1.299301E+00	2.223676E-02	5.924148E-01
236	2.637202E-04	8.391712E-03	1.511682E-02	1.299301E+00	2.223676E-02	5.924148E-01
237	2.574411E-04	8.191910E-03	1.511682E-02	1.299301E+00	2.223676E-02	5.924148E-01
238	2.511621E-04	7.992107E-03	1.511682E-02	1.299301E+00	2.223676E-02	5.924148E-01
239	2.448830E-04	7.792304E-03	1.511682E-02	1.299301E+00	2.223676E-02	5.924148E-01
240	2.386040E-04	7.592501E-03	1.511682E-02	1.299301E+00	2.223676E-02	5.924148E-01
241	2.699992E-04	8.591515E-03	1.632501E-02	1.299301E+00	2.223676E-02	5.924148E-01
242	2.637202E-04	8.391712E-03	1.632501E-02	1.299301E+00	2.223676E-02	5.924148E-01
243	2.574411E-04	8.191910E-03	1.632501E-02	1.299301E+00	2.223676E-02	5.924148E-01
244	2.511621E-04	7.992107E-03	1.632501E-02	1.299301E+00	2.223676E-02	5.924148E-01
245	2.448830E-04	7.792304E-03	1.632501E-02	1.299301E+00	2.223676E-02	5.924148E-01
246	2.386040E-04	7.592501E-03	1.632501E-02	1.299301E+00	2.223676E-02	5.924148E-01
247	2.699992E-04	8.591515E-03	1.746482E-02	1.299301E+00	2.223676E-02	5.924148E-01
248	2.637202E-04	8.391712E-03	1.746482E-02	1.299301E+00	2.223676E-02	5.924148E-01
249	2.574411E-04	8.191910E-03	1.746482E-02	1.299301E+00	2.223676E-02	5.924148E-01
250	2.511621E-04	7.992107E-03	1.746482E-02	1.299301E+00	2.223676E-02	5.924148E-01
251	2.448830E-04	7.792304E-03	1.746482E-02	1.299301E+00	2.223676E-02	5.924148E-01
252	2.386040E-04	7.592501E-03	1.746482E-02	1.299301E+00	2.223676E-02	5.924148E-01

253	2.699992E-04	8.591515E-03	1.854010E-02	1.299301E+00	2.223676E-02	5.924148E-01
254	2.637202E-04	8.391712E-03	1.854010E-02	1.299301E+00	2.223676E-02	5.924148E-01
255	2.574411E-04	8.191910E-03	1.854010E-02	1.299301E+00	2.223676E-02	5.924148E-01
256	2.511621E-04	7.992107E-03	1.854010E-02	1.299301E+00	2.223676E-02	5.924148E-01
257	2.448830E-04	7.792304E-03	1.854010E-02	1.299301E+00	2.223676E-02	5.924148E-01
258	2.386040E-04	7.592501E-03	1.854010E-02	1.299301E+00	2.223676E-02	5.924148E-01
259	2.699992E-04	8.591515E-03	1.955452E-02	1.299301E+00	2.223676E-02	5.924148E-01
260	2.637202E-04	8.391712E-03	1.955452E-02	1.299301E+00	2.223676E-02	5.924148E-01
261	2.574411E-04	8.191910E-03	1.955452E-02	1.299301E+00	2.223676E-02	5.924148E-01
262	2.511621E-04	7.992107E-03	1.955452E-02	1.299301E+00	2.223676E-02	5.924148E-01
263	2.448830E-04	7.792304E-03	1.955452E-02	1.299301E+00	2.223676E-02	5.924148E-01
264	2.386040E-04	7.592501E-03	1.955452E-02	1.299301E+00	2.223676E-02	5.924148E-01
265	2.699992E-04	8.591515E-03	2.051152E-02	1.299301E+00	2.223676E-02	5.924148E-01
266	2.637202E-04	8.391712E-03	2.051152E-02	1.299301E+00	2.223676E-02	5.924148E-01
267	2.574411E-04	8.191910E-03	2.051152E-02	1.299301E+00	2.223676E-02	5.924148E-01
268	2.511621E-04	7.992107E-03	2.051152E-02	1.299301E+00	2.223676E-02	5.924148E-01
269	2.448830E-04	7.792304E-03	2.051152E-02	1.299301E+00	2.223676E-02	5.924148E-01
270	2.386040E-04	7.592501E-03	2.051152E-02	1.299301E+00	2.223676E-02	5.924148E-01
271	2.699992E-04	8.591515E-03	2.141435E-02	1.299301E+00	2.223676E-02	5.924148E-01
272	2.637202E-04	8.391712E-03	2.141435E-02	1.299301E+00	2.223676E-02	5.924148E-01
273	2.574411E-04	8.191910E-03	2.141435E-02	1.299301E+00	2.223676E-02	5.924148E-01
274	2.511621E-04	7.992107E-03	2.141435E-02	1.299301E+00	2.223676E-02	5.924148E-01
275	2.448830E-04	7.792304E-03	2.141435E-02	1.299301E+00	2.223676E-02	5.924148E-01
276	2.386040E-04	7.592501E-03	2.141435E-02	1.299301E+00	2.223676E-02	5.924148E-01
277	2.699992E-04	8.591515E-03	2.226608E-02	1.299301E+00	2.223676E-02	5.924148E-01
278	2.637202E-04	8.391712E-03	2.226608E-02	1.299301E+00	2.223676E-02	5.924148E-01
279	2.574411E-04	8.191910E-03	2.226608E-02	1.299301E+00	2.223676E-02	5.924148E-01
280	2.511621E-04	7.992107E-03	2.226608E-02	1.299301E+00	2.223676E-02	5.924148E-01
281	2.448830E-04	7.792304E-03	2.226608E-02	1.299301E+00	2.223676E-02	5.924148E-01
282	2.386040E-04	7.592501E-03	2.226608E-02	1.299301E+00	2.223676E-02	5.924148E-01
283	2.699992E-04	8.591515E-03	2.306960E-02	1.299301E+00	2.223676E-02	5.924148E-01
284	2.637202E-04	8.391712E-03	2.306960E-02	1.299301E+00	2.223676E-02	5.924148E-01
285	2.574411E-04	8.191910E-03	2.306960E-02	1.299301E+00	2.223676E-02	5.924148E-01
286	2.511621E-04	7.992107E-03	2.306960E-02	1.299301E+00	2.223676E-02	5.924148E-01
287	2.448830E-04	7.792304E-03	2.306960E-02	1.299301E+00	2.223676E-02	5.924148E-01
288	2.386040E-04	7.592501E-03	2.306960E-02	1.299301E+00	2.223676E-02	5.924148E-01
289	2.699992E-04	8.591515E-03	2.382763E-02	1.299301E+00	2.223676E-02	5.924148E-01
290	2.637202E-04	8.391712E-03	2.382763E-02	1.299301E+00	2.223676E-02	5.924148E-01
291	2.574411E-04	8.191910E-03	2.382763E-02	1.299301E+00	2.223676E-02	5.924148E-01
292	2.511621E-04	7.992107E-03	2.382763E-02	1.299301E+00	2.223676E-02	5.924148E-01
293	2.448830E-04	7.792304E-03	2.382763E-02	1.299301E+00	2.223676E-02	5.924148E-01
294	2.386040E-04	7.592501E-03	2.382763E-02	1.299301E+00	2.223676E-02	5.924148E-01
295	2.699992E-04	8.591515E-03	2.454276E-02	1.299301E+00	2.223676E-02	5.924148E-01
296	2.637202E-04	8.391712E-03	2.454276E-02	1.299301E+00	2.223676E-02	5.924148E-01
297	2.574411E-04	8.191910E-03	2.454276E-02	1.299301E+00	2.223676E-02	5.924148E-01
298	2.511621E-04	7.992107E-03	2.454276E-02	1.299301E+00	2.223676E-02	5.924148E-01

299	2.448830E-04	7.792304E-03	2.454276E-02	1.299301E+00	2.223676E-02	5.924148E-01
300	2.386040E-04	7.592501E-03	2.454276E-02	1.299301E+00	2.223676E-02	5.924148E-01
301	2.699992E-04	8.591515E-03	2.521741E-02	1.299301E+00	2.223676E-02	5.924148E-01
302	2.637202E-04	8.391712E-03	2.521741E-02	1.299301E+00	2.223676E-02	5.924148E-01
303	2.574411E-04	8.191910E-03	2.521741E-02	1.299301E+00	2.223676E-02	5.924148E-01
304	2.511621E-04	7.992107E-03	2.521741E-02	1.299301E+00	2.223676E-02	5.924148E-01
305	2.448830E-04	7.792304E-03	2.521741E-02	1.299301E+00	2.223676E-02	5.924148E-01
306	2.386040E-04	7.592501E-03	2.521741E-02	1.299301E+00	2.223676E-02	5.924148E-01
307	2.699992E-04	8.591515E-03	2.585387E-02	1.299301E+00	2.223676E-02	5.924148E-01
308	2.637202E-04	8.391712E-03	2.585387E-02	1.299301E+00	2.223676E-02	5.924148E-01
309	2.574411E-04	8.191910E-03	2.585387E-02	1.299301E+00	2.223676E-02	5.924148E-01
310	2.511621E-04	7.992107E-03	2.585387E-02	1.299301E+00	2.223676E-02	5.924148E-01
311	2.448830E-04	7.792304E-03	2.585387E-02	1.299301E+00	2.223676E-02	5.924148E-01
312	2.386040E-04	7.592501E-03	2.585387E-02	1.299301E+00	2.223676E-02	5.924148E-01
313	2.699992E-04	8.591515E-03	2.645430E-02	1.299301E+00	2.223676E-02	5.924148E-01
314	2.637202E-04	8.391712E-03	2.645430E-02	1.299301E+00	2.223676E-02	5.924148E-01
315	2.574411E-04	8.191910E-03	2.645430E-02	1.299301E+00	2.223676E-02	5.924148E-01
316	2.511621E-04	7.992107E-03	2.645430E-02	1.299301E+00	2.223676E-02	5.924148E-01
317	2.448830E-04	7.792304E-03	2.645430E-02	1.299301E+00	2.223676E-02	5.924148E-01
318	2.386040E-04	7.592501E-03	2.645430E-02	1.299301E+00	2.223676E-02	5.924148E-01
319	2.699992E-04	8.591515E-03	2.702075E-02	1.299301E+00	2.223676E-02	5.924148E-01
320	2.637202E-04	8.391712E-03	2.702075E-02	1.299301E+00	2.223676E-02	5.924148E-01
321	2.574411E-04	8.191910E-03	2.702075E-02	1.299301E+00	2.223676E-02	5.924148E-01
322	2.511621E-04	7.992107E-03	2.702075E-02	1.299301E+00	2.223676E-02	5.924148E-01
323	2.448830E-04	7.792304E-03	2.702075E-02	1.299301E+00	2.223676E-02	5.924148E-01
324	2.386040E-04	7.592501E-03	2.702075E-02	1.299301E+00	2.223676E-02	5.924148E-01
325	2.699992E-04	8.591515E-03	2.755513E-02	1.299301E+00	2.223676E-02	5.924148E-01
326	2.637202E-04	8.391712E-03	2.755513E-02	1.299301E+00	2.223676E-02	5.924148E-01
327	2.574411E-04	8.191910E-03	2.755513E-02	1.299301E+00	2.223676E-02	5.924148E-01
328	2.511621E-04	7.992107E-03	2.755513E-02	1.299301E+00	2.223676E-02	5.924148E-01
329	2.448830E-04	7.792304E-03	2.755513E-02	1.299301E+00	2.223676E-02	5.924148E-01
330	2.386040E-04	7.592501E-03	2.755513E-02	1.299301E+00	2.223676E-02	5.924148E-01
331	2.699992E-04	8.591515E-03	2.805927E-02	1.299301E+00	2.223676E-02	5.924148E-01
332	2.637202E-04	8.391712E-03	2.805927E-02	1.299301E+00	2.223676E-02	5.924148E-01
333	2.574411E-04	8.191910E-03	2.805927E-02	1.299301E+00	2.223676E-02	5.924148E-01
334	2.511621E-04	7.992107E-03	2.805927E-02	1.299301E+00	2.223676E-02	5.924148E-01
335	2.448830E-04	7.792304E-03	2.805927E-02	1.299301E+00	2.223676E-02	5.924148E-01
336	2.386040E-04	7.592501E-03	2.805927E-02	1.299301E+00	2.223676E-02	5.924148E-01
337	2.699992E-04	8.591515E-03	2.853487E-02	1.299301E+00	2.223676E-02	5.924148E-01
338	2.637202E-04	8.391712E-03	2.853487E-02	1.299301E+00	2.223676E-02	5.924148E-01
339	2.574411E-04	8.191910E-03	2.853487E-02	1.299301E+00	2.223676E-02	5.924148E-01
340	2.511621E-04	7.992107E-03	2.853487E-02	1.299301E+00	2.223676E-02	5.924148E-01
341	2.448830E-04	7.792304E-03	2.853487E-02	1.299301E+00	2.223676E-02	5.924148E-01
342	2.386040E-04	7.592501E-03	2.853487E-02	1.299301E+00	2.223676E-02	5.924148E-01
343	2.699992E-04	8.591515E-03	2.898354E-02	1.299301E+00	2.223676E-02	5.924148E-01
344	2.637202E-04	8.391712E-03	2.898354E-02	1.299301E+00	2.223676E-02	5.924148E-01

345 2.574411E-04 8.191910E-03 2.898354E-02 1.299301E+00 2.223676E-02 5.924148E-01
346 2.511621E-04 7.992107E-03 2.898354E-02 1.299301E+00 2.223676E-02 5.924148E-01
347 2.448830E-04 7.792304E-03 2.898354E-02 1.299301E+00 2.223676E-02 5.924148E-01
348 2.386040E-04 7.592501E-03 2.898354E-02 1.299301E+00 2.223676E-02 5.924148E-01
349 2.699992E-04 8.591515E-03 2.940683E-02 1.299301E+00 2.223676E-02 5.924148E-01
350 2.637202E-04 8.391712E-03 2.940683E-02 1.299301E+00 2.223676E-02 5.924148E-01
351 2.574411E-04 8.191910E-03 2.940683E-02 1.299301E+00 2.223676E-02 5.924148E-01
352 2.511621E-04 7.992107E-03 2.940683E-02 1.299301E+00 2.223676E-02 5.924148E-01
353 2.448830E-04 7.792304E-03 2.940683E-02 1.299301E+00 2.223676E-02 5.924148E-01
354 2.386040E-04 7.592501E-03 2.940683E-02 1.299301E+00 2.223676E-02 5.924148E-01
355 2.699665E-04 8.590995E-03 2.980616E-02 1.299301E+00 2.223541E-02 5.924147E-01
356 2.636551E-04 8.390678E-03 2.980616E-02 1.299301E+00 2.223401E-02 5.924146E-01
357 2.573777E-04 8.190903E-03 2.980616E-02 1.299301E+00 2.223402E-02 5.924146E-01
358 2.511038E-04 7.991181E-03 2.980616E-02 1.299301E+00 2.223418E-02 5.924146E-01
359 2.448369E-04 7.791571E-03 2.980616E-02 1.299301E+00 2.223467E-02 5.924147E-01
360 2.385852E-04 7.592202E-03 2.980616E-02 1.299301E+00 2.223589E-02 5.924147E-01

! Perturbed elements
PERTurbations
9

118
119
120
355
356
357
358
359
360

! Edge BOUndary conditions
! i-coord x_i value, (ibc(j), j = 1...NDF) (pg. 257)
! example: 1 0 1 0 0
! means that if the x-value of the node is 0, restrain displacements in the x-direction
EBOUndary
! 1 0.0 1 0 1
! 2 0.0 0 1 1
! 3 -5.0E-05 0 0 1
! 3 5.0E-05 0 0 1

! Edge DISplacement conditions
! i-coord x_i value, (d(j), j = 1...NDF)

```
! example: 1 10    d 0 0
!         means that if the x-value of the node is 10, displace by d units in the x-direction
EDISplacement
!  1 0   0 0 0
!  1 10  d 0 0
!  2 0   0 0 0
!  2 10  0 d 0
!  3 0   0 0 0

! BOUNdary restraint conditions
! node1 ngen1 (id(i, node1), i = 1...NDF) (pg. 229)
! if id(i,node) = 0 a force will be an applied load to dof (default).
! if id(i,node) != 0 a displacement will be imposed to dof.
BOUNdary
1       0       0       1       1                       33      0       0       1       0
2       0       0       1       1                       34      0       0       1       0
3       0       0       1       1                       35      0       0       1       0
4       0       0       1       1                       36      0       0       1       0
5       0       0       1       1                       37      0       0       1       0
6       0       0       1       1                       38      0       0       1       0
7       0       0       1       1                       39      0       0       1       0
8       0       0       1       1                       40      0       0       1       0
9       0       0       1       1                       41      0       0       1       0
10      0       0       1       1                       42      0       0       1       0
11      0       0       1       0                       43      0       0       1       0
12      0       0       1       0                       44      0       0       1       0
13      0       0       1       0                       45      0       0       1       0
14      0       0       1       0                       46      0       0       1       0
15      0       0       1       0                       47      0       0       1       0
16      0       0       1       0                       48      0       0       1       0
17      0       0       1       0                       49      0       0       1       0
18      0       0       1       0                       50      0       0       1       0
19      0       0       1       0                       51      0       0       1       0
20      0       0       1       0                       52      0       0       1       0
21      0       0       1       0                       53      0       0       1       0
22      0       0       1       0                       54      0       0       1       0
23      0       0       1       0                       55      0       0       1       0
24      0       0       1       0                       56      0       0       1       0
25      0       0       1       0                       57      0       0       1       0
26      0       0       1       0                       58      0       0       1       0
27      0       0       1       0                       59      0       0       1       0
28      0       0       1       0                       60      0       0       1       0
29      0       0       1       0                       61      0       0       1       0
30      0       0       1       0                       62      0       0       1       0
31      0       0       1       0                       63      0       0       1       0
32      0       0       1       0                       64      0       0       1       0
```

65	0	0	1	0	111	0	0	1	0
66	0	0	1	0	112	0	0	1	0
67	0	0	1	0	113	0	0	1	0
68	0	0	1	0	114	0	0	1	0
69	0	0	1	0	115	0	0	1	0
70	0	0	1	0	116	0	0	1	0
71	0	0	1	0	117	0	0	1	0
72	0	0	1	0	118	0	0	1	0
73	0	0	1	0	119	0	0	1	0
74	0	0	1	0	120	0	0	1	0
75	0	0	1	0	121	0	0	1	0
76	0	0	1	0	122	0	0	1	0
77	0	0	1	0	123	0	0	1	0
78	0	0	1	0	124	0	0	1	0
79	0	0	1	0	125	0	0	1	0
80	0	0	1	0	126	0	0	1	0
81	0	0	1	0	127	0	0	1	0
82	0	0	1	0	128	0	0	1	0
83	0	0	1	0	129	0	0	1	0
84	0	0	1	0	130	0	0	1	0
85	0	0	1	0	131	0	0	1	0
86	0	0	1	0	132	0	0	1	0
87	0	0	1	0	133	0	0	1	0
88	0	0	1	0	134	0	0	1	0
89	0	0	1	0	135	0	0	1	0
90	0	0	1	0	136	0	0	1	0
91	0	0	1	0	137	0	0	1	0
92	0	0	1	0	138	0	0	1	0
93	0	0	1	0	139	0	0	1	0
94	0	0	1	0	140	0	0	1	0
95	0	0	1	0	141	0	0	1	0
96	0	0	1	0	142	0	0	1	0
97	0	0	1	0	143	0	0	1	0
98	0	0	1	0	144	0	0	1	0
99	0	0	1	0	145	0	0	1	0
100	0	0	1	0	146	0	0	1	0
101	0	0	1	0	147	0	0	1	0
102	0	0	1	0	148	0	0	1	0
103	0	0	1	0	149	0	0	1	0
104	0	0	1	0	150	0	0	1	0
105	0	0	1	0	151	0	0	1	0
106	0	0	1	0	152	0	0	1	0
107	0	0	1	0	153	0	0	1	0
108	0	0	1	0	154	0	0	1	0
109	0	0	1	0	155	0	0	1	0
110	0	0	1	0	156	0	0	1	0

157	0	0	1	0	203	0	0	1	0
158	0	0	1	0	204	0	0	1	0
159	0	0	1	0	205	0	0	1	0
160	0	0	1	0	206	0	0	1	0
161	0	0	1	0	207	0	0	1	0
162	0	0	1	0	208	0	0	1	0
163	0	0	1	0	209	0	0	1	0
164	0	0	1	0	210	0	0	1	0
165	0	0	1	0	211	0	0	1	0
166	0	0	1	0	212	0	0	1	0
167	0	0	1	0	213	0	0	1	0
168	0	0	1	0	214	0	0	1	0
169	0	0	1	0	215	0	0	1	0
170	0	0	1	0	216	0	0	1	0
171	0	0	1	0	217	0	0	1	0
172	0	0	1	0	218	0	0	1	0
173	0	0	1	0	219	0	0	1	0
174	0	0	1	0	220	0	0	1	0
175	0	0	1	0	221	0	0	1	0
176	0	0	1	0	222	0	0	1	0
177	0	0	1	0	223	0	0	1	0
178	0	0	1	0	224	0	0	1	0
179	0	0	1	0	225	0	0	1	0
180	0	0	1	0	226	0	0	1	0
181	0	0	1	0	227	0	0	1	0
182	0	0	1	0	228	0	0	1	0
183	0	0	1	0	229	0	0	1	0
184	0	0	1	0	230	0	0	1	0
185	0	0	1	0	231	0	0	1	0
186	0	0	1	0	232	0	0	1	0
187	0	0	1	0	233	0	0	1	0
188	0	0	1	0	234	0	0	1	0
189	0	0	1	0	235	0	0	1	0
190	0	0	1	0	236	0	0	1	0
191	0	0	1	0	237	0	0	1	0
192	0	0	1	0	238	0	0	1	0
193	0	0	1	0	239	0	0	1	0
194	0	0	1	0	240	0	0	1	0
195	0	0	1	0	241	0	0	1	0
196	0	0	1	0	242	0	0	1	0
197	0	0	1	0	243	0	0	1	0
198	0	0	1	0	244	0	0	1	0
199	0	0	1	0	245	0	0	1	0
200	0	0	1	0	246	0	0	1	0
201	0	0	1	0	247	0	0	1	0
202	0	0	1	0	248	0	0	1	0

249	0	0	1	0	295	0	0	1	0
250	0	0	1	0	296	0	0	1	0
251	0	0	1	0	297	0	0	1	0
252	0	0	1	0	298	0	0	1	0
253	0	0	1	0	299	0	0	1	0
254	0	0	1	0	300	0	0	1	0
255	0	0	1	0	301	0	0	1	0
256	0	0	1	0	302	0	0	1	0
257	0	0	1	0	303	0	0	1	0
258	0	0	1	0	304	0	0	1	0
259	0	0	1	0	305	0	0	1	0
260	0	0	1	0	306	0	0	1	0
261	0	0	1	0	307	0	0	1	0
262	0	0	1	0	308	0	0	1	0
263	0	0	1	0	309	0	0	1	0
264	0	0	1	0	310	0	0	1	0
265	0	0	1	0	311	0	0	1	0
266	0	0	1	0	312	0	0	1	0
267	0	0	1	0	313	0	0	1	0
268	0	0	1	0	314	0	0	1	0
269	0	0	1	0	315	0	0	1	0
270	0	0	1	0	316	0	0	1	0
271	0	0	1	0	317	0	0	1	0
272	0	0	1	0	318	0	0	1	0
273	0	0	1	0	319	0	0	1	0
274	0	0	1	0	320	0	0	1	0
275	0	0	1	0	321	0	0	1	0
276	0	0	1	0	322	0	0	1	0
277	0	0	1	0	323	0	0	1	0
278	0	0	1	0	324	0	0	1	0
279	0	0	1	0	325	0	0	1	0
280	0	0	1	0	326	0	0	1	0
281	0	0	1	0	327	0	0	1	0
282	0	0	1	0	328	0	0	1	0
283	0	0	1	0	329	0	0	1	0
284	0	0	1	0	330	0	0	1	0
285	0	0	1	0	331	0	0	1	0
286	0	0	1	0	332	0	0	1	0
287	0	0	1	0	333	0	0	1	0
288	0	0	1	0	334	0	0	1	0
289	0	0	1	0	335	0	0	1	0
290	0	0	1	0	336	0	0	1	0
291	0	0	1	0	337	0	0	1	0
292	0	0	1	0	338	0	0	1	0
293	0	0	1	0	339	0	0	1	0
294	0	0	1	0	340	0	0	1	0

341	0	0	1	0	387	0	0	1	0
342	0	0	1	0	388	0	0	1	0
343	0	0	1	0	389	0	0	1	0
344	0	0	1	0	390	0	0	1	0
345	0	0	1	0	391	0	0	1	0
346	0	0	1	0	392	0	0	1	0
347	0	0	1	0	393	0	0	1	0
348	0	0	1	0	394	0	0	1	0
349	0	0	1	0	395	0	0	1	0
350	0	0	1	0	396	0	0	1	0
351	0	0	1	0	397	0	0	1	0
352	0	0	1	0	398	0	0	1	0
353	0	0	1	0	399	0	0	1	0
354	0	0	1	0	400	0	0	1	0
355	0	0	1	0	401	0	0	1	1
356	0	0	1	0	402	0	0	1	1
357	0	0	1	0	403	0	0	1	1
358	0	0	1	0	404	0	0	1	1
359	0	0	1	0	405	0	0	1	1
360	0	0	1	0	406	0	0	1	1
361	0	0	1	0	407	0	0	1	1
362	0	0	1	0	408	0	0	1	1
363	0	0	1	0	409	0	0	1	1
364	0	0	1	0	410	0	0	1	1
365	0	0	1	0	411	0	0	1	1
366	0	0	1	0	412	0	0	1	1
367	0	0	1	0	413	0	0	1	1
368	0	0	1	0	414	0	0	1	1
369	0	0	1	0	415	0	0	1	1
370	0	0	1	0	416	0	0	1	1
371	0	0	1	0	417	0	0	1	1
372	0	0	1	0	418	0	0	1	1
373	0	0	1	0	419	0	0	1	1
374	0	0	1	0	420	0	0	1	1
375	0	0	1	0	421	0	0	1	0
376	0	0	1	0	422	0	0	1	0
377	0	0	1	0	423	0	0	1	0
378	0	0	1	0	424	0	0	1	0
379	0	0	1	0	425	0	0	1	0
380	0	0	1	0	426	0	0	1	0
381	0	0	1	0	427	0	0	1	0
382	0	0	1	0	428	0	0	1	0
383	0	0	1	0	429	0	0	1	0
384	0	0	1	0	430	0	0	1	0
385	0	0	1	0	431	0	0	1	0
386	0	0	1	0	432	0	0	1	0

433	0	0	1	0	479	0	0	1	0
434	0	0	1	0	480	0	0	1	0
435	0	0	1	0	481	0	0	1	0
436	0	0	1	0	482	0	0	1	0
437	0	0	1	0	483	0	0	1	0
438	0	0	1	0	484	0	0	1	0
439	0	0	1	0	485	0	0	1	0
440	0	0	1	0	486	0	0	1	0
441	0	0	1	0	487	0	0	1	0
442	0	0	1	0	488	0	0	1	0
443	0	0	1	0	489	0	0	1	0
444	0	0	1	0	490	0	0	1	0
445	0	0	1	0	491	0	0	1	0
446	0	0	1	0	492	0	0	1	0
447	0	0	1	0	493	0	0	1	0
448	0	0	1	0	494	0	0	1	0
449	0	0	1	0	495	0	0	1	0
450	0	0	1	0	496	0	0	1	0
451	0	0	1	0	497	0	0	1	0
452	0	0	1	0	498	0	0	1	0
453	0	0	1	0	499	0	0	1	0
454	0	0	1	0	500	0	0	1	0
455	0	0	1	0	501	0	0	1	0
456	0	0	1	0	502	0	0	1	0
457	0	0	1	0	503	0	0	1	0
458	0	0	1	0	504	0	0	1	0
459	0	0	1	0	505	0	0	1	0
460	0	0	1	0	506	0	0	1	0
461	0	0	1	0	507	0	0	1	0
462	0	0	1	0	508	0	0	1	0
463	0	0	1	0	509	0	0	1	0
464	0	0	1	0	510	0	0	1	0
465	0	0	1	0	511	0	0	1	0
466	0	0	1	0	512	0	0	1	0
467	0	0	1	0	513	0	0	1	0
468	0	0	1	0	514	0	0	1	0
469	0	0	1	0	515	0	0	1	0
470	0	0	1	0	516	0	0	1	0
471	0	0	1	0	517	0	0	1	0
472	0	0	1	0	518	0	0	1	0
473	0	0	1	0	519	0	0	1	0
474	0	0	1	0	520	0	0	1	0
475	0	0	1	0	521	0	0	1	0
476	0	0	1	0	522	0	0	1	0
477	0	0	1	0	523	0	0	1	0
478	0	0	1	0	524	0	0	1	0

525	0	0	1	0	571	0	0	1	0
526	0	0	1	0	572	0	0	1	0
527	0	0	1	0	573	0	0	1	0
528	0	0	1	0	574	0	0	1	0
529	0	0	1	0	575	0	0	1	0
530	0	0	1	0	576	0	0	1	0
531	0	0	1	0	577	0	0	1	0
532	0	0	1	0	578	0	0	1	0
533	0	0	1	0	579	0	0	1	0
534	0	0	1	0	580	0	0	1	0
535	0	0	1	0	581	0	0	1	0
536	0	0	1	0	582	0	0	1	0
537	0	0	1	0	583	0	0	1	0
538	0	0	1	0	584	0	0	1	0
539	0	0	1	0	585	0	0	1	0
540	0	0	1	0	586	0	0	1	0
541	0	0	1	0	587	0	0	1	0
542	0	0	1	0	588	0	0	1	0
543	0	0	1	0	589	0	0	1	0
544	0	0	1	0	590	0	0	1	0
545	0	0	1	0	591	0	0	1	0
546	0	0	1	0	592	0	0	1	0
547	0	0	1	0	593	0	0	1	0
548	0	0	1	0	594	0	0	1	0
549	0	0	1	0	595	0	0	1	0
550	0	0	1	0	596	0	0	1	0
551	0	0	1	0	597	0	0	1	0
552	0	0	1	0	598	0	0	1	0
553	0	0	1	0	599	0	0	1	0
554	0	0	1	0	600	0	0	1	0
555	0	0	1	0	601	0	0	1	0
556	0	0	1	0	602	0	0	1	0
557	0	0	1	0	603	0	0	1	0
558	0	0	1	0	604	0	0	1	0
559	0	0	1	0	605	0	0	1	0
560	0	0	1	0	606	0	0	1	0
561	0	0	1	0	607	0	0	1	0
562	0	0	1	0	608	0	0	1	0
563	0	0	1	0	609	0	0	1	0
564	0	0	1	0	610	0	0	1	0
565	0	0	1	0	611	0	0	1	0
566	0	0	1	0	612	0	0	1	0
567	0	0	1	0	613	0	0	1	0
568	0	0	1	0	614	0	0	1	0
569	0	0	1	0	615	0	0	1	0
570	0	0	1	0	616	0	0	1	0

617	0	0	1	0
618	0	0	1	0
619	0	0	1	0
620	0	0	1	0
621	0	0	1	0
622	0	0	1	0
623	0	0	1	0
624	0	0	1	0
625	0	0	1	0
626	0	0	1	0
627	0	0	1	0
628	0	0	1	0
629	0	0	1	0
630	0	0	1	0
631	0	0	1	0
632	0	0	1	0
633	0	0	1	0
634	0	0	1	0
635	0	0	1	0
636	0	0	1	0
637	0	0	1	0
638	0	0	1	0
639	0	0	1	0
640	0	0	1	0
641	0	0	1	0
642	0	0	1	0
643	0	0	1	0
644	0	0	1	0
645	0	0	1	0
646	0	0	1	0
647	0	0	1	0
648	0	0	1	0
649	0	0	1	0
650	0	0	1	0
651	0	0	1	0
652	0	0	1	0
653	0	0	1	0
654	0	0	1	0
655	0	0	1	0
656	0	0	1	0
657	0	0	1	0
658	0	0	1	0
659	0	0	1	0
660	0	0	1	0
661	0	0	1	0
662	0	0	1	0
663	0	0	1	0
664	0	0	1	0
665	0	0	1	0
666	0	0	1	0
667	0	0	1	0
668	0	0	1	0
669	0	0	1	0
670	0	0	1	0
671	0	0	1	0
672	0	0	1	0
673	0	0	1	0
674	0	0	1	0
675	0	0	1	0
676	0	0	1	0
677	0	0	1	0
678	0	0	1	0
679	0	0	1	0
680	0	0	1	0
681	0	0	1	0
682	0	0	1	0
683	0	0	1	0
684	0	0	1	0
685	0	0	1	0
686	0	0	1	0
687	0	0	1	0
688	0	0	1	0
689	0	0	1	0
690	0	0	1	0
691	0	0	1	0
692	0	0	1	0
693	0	0	1	0
694	0	0	1	0
695	0	0	1	0
696	0	0	1	0
697	0	0	1	0
698	0	0	1	0
699	0	0	1	0
700	0	0	1	0
701	0	0	1	0
702	0	0	1	0
703	0	0	1	0
704	0	0	1	0
705	0	0	1	0
706	0	0	1	0
707	0	0	1	0
708	0	0	1	0

709	0	0	1	0	755	0	0	1	0
710	0	0	1	0	756	0	0	1	0
711	0	0	1	0	757	0	0	1	0
712	0	0	1	0	758	0	0	1	0
713	0	0	1	0	759	0	0	1	0
714	0	0	1	0	760	0	0	1	0
715	0	0	1	0	761	0	0	1	0
716	0	0	1	0	762	0	0	1	0
717	0	0	1	0	763	0	0	1	0
718	0	0	1	0	764	0	0	1	0
719	0	0	1	0	765	0	0	1	0
720	0	0	1	0	766	0	0	1	0
721	0	0	1	0	767	0	0	1	0
722	0	0	1	0	768	0	0	1	0
723	0	0	1	0	769	0	0	1	0
724	0	0	1	0	770	0	0	1	0
725	0	0	1	0	771	0	0	1	0
726	0	0	1	0	772	0	0	1	0
727	0	0	1	0	773	0	0	1	0
728	0	0	1	0	774	0	0	1	0
729	0	0	1	0	775	0	0	1	0
730	0	0	1	0	776	0	0	1	0
731	0	0	1	0	777	0	0	1	0
732	0	0	1	0	778	0	0	1	0
733	0	0	1	0	779	0	0	1	0
734	0	0	1	0	780	0	0	1	0
735	0	0	1	0	781	0	0	1	0
736	0	0	1	0	782	0	0	1	0
737	0	0	1	0	783	0	0	1	0
738	0	0	1	0	784	0	0	1	0
739	0	0	1	0	785	0	0	1	0
740	0	0	1	0	786	0	0	1	0
741	0	0	1	0	787	0	0	1	0
742	0	0	1	0	788	0	0	1	0
743	0	0	1	0	789	0	0	1	0
744	0	0	1	0	790	0	0	1	0
745	0	0	1	0	791	0	0	1	0
746	0	0	1	0	792	0	0	1	0
747	0	0	1	0	793	0	0	1	0
748	0	0	1	0	794	0	0	1	0
749	0	0	1	0	795	0	0	1	0
750	0	0	1	0	796	0	0	1	0
751	0	0	1	0	797	0	0	1	0
752	0	0	1	0	798	0	0	1	0
753	0	0	1	0	799	0	0	1	0
754	0	0	1	0	800	0	0	1	0

801	0	0	1	0	811	0	0	1	1
802	0	0	1	0	812	0	0	1	1
803	0	0	1	0	813	0	0	1	1
804	0	0	1	0	814	0	0	1	1
805	0	0	1	0	815	0	0	1	1
806	0	0	1	0	816	0	0	1	1
807	0	0	1	0	817	0	0	1	1
808	0	0	1	0	818	0	0	1	1
809	0	0	1	0	819	0	0	1	1
810	0	0	1	0	820	0	0	1	1

! DISPlacement nodal boundary displacements
! node1 ngen1 (d(i, node1), i = 1...NDF) (pg. 265)
! where d(j,node) Ð Value of displacement for j-dof
DISPlacement

1 0 0 0 0	32 0 0 0 0	63 0 0 0 0
2 0 0 0 0	33 0 0 0 0	64 0 0 0 0
3 0 0 0 0	34 0 0 0 0	65 0 0 0 0
4 0 0 0 0	35 0 0 0 0	66 0 0 0 0
5 0 0 0 0	36 0 0 0 0	67 0 0 0 0
6 0 0 0 0	37 0 0 0 0	68 0 0 0 0
7 0 0 0 0	38 0 0 0 0	69 0 0 0 0
8 0 0 0 0	39 0 0 0 0	70 0 0 0 0
9 0 0 0 0	40 0 0 0 0	71 0 0 0 0
10 0 0 0 0	41 0 0 0 0	72 0 0 0 0
11 0 0 0 0	42 0 0 0 0	73 0 0 0 0
12 0 0 0 0	43 0 0 0 0	74 0 0 0 0
13 0 0 0 0	44 0 0 0 0	75 0 0 0 0
14 0 0 0 0	45 0 0 0 0	76 0 0 0 0
15 0 0 0 0	46 0 0 0 0	77 0 0 0 0
16 0 0 0 0	47 0 0 0 0	78 0 0 0 0
17 0 0 0 0	48 0 0 0 0	79 0 0 0 0
18 0 0 0 0	49 0 0 0 0	80 0 0 0 0
19 0 0 0 0	50 0 0 0 0	81 0 0 0 0
20 0 0 0 0	51 0 0 0 0	82 0 0 0 0
21 0 0 0 0	52 0 0 0 0	83 0 0 0 0
22 0 0 0 0	53 0 0 0 0	84 0 0 0 0
23 0 0 0 0	54 0 0 0 0	85 0 0 0 0
24 0 0 0 0	55 0 0 0 0	86 0 0 0 0
25 0 0 0 0	56 0 0 0 0	87 0 0 0 0
26 0 0 0 0	57 0 0 0 0	88 0 0 0 0
27 0 0 0 0	58 0 0 0 0	89 0 0 0 0
28 0 0 0 0	59 0 0 0 0	90 0 0 0 0
29 0 0 0 0	60 0 0 0 0	91 0 0 0 0
30 0 0 0 0	61 0 0 0 0	92 0 0 0 0
31 0 0 0 0	62 0 0 0 0	93 0 0 0 0

94 0 0 0 0
95 0 0 0 0
96 0 0 0 0
97 0 0 0 0
98 0 0 0 0
99 0 0 0 0
100 0 0 0 0
101 0 0 0 0
102 0 0 0 0
103 0 0 0 0
104 0 0 0 0
105 0 0 0 0
106 0 0 0 0
107 0 0 0 0
108 0 0 0 0
109 0 0 0 0
110 0 0 0 0
111 0 0 0 0
112 0 0 0 0
113 0 0 0 0
114 0 0 0 0
115 0 0 0 0
116 0 0 0 0
117 0 0 0 0
118 0 0 0 0
119 0 0 0 0
120 0 0 0 0
121 0 0 0 0
122 0 0 0 0
123 0 0 0 0
124 0 0 0 0
125 0 0 0 0
126 0 0 0 0
127 0 0 0 0
128 0 0 0 0
129 0 0 0 0
130 0 0 0 0
131 0 0 0 0
132 0 0 0 0
133 0 0 0 0
134 0 0 0 0
135 0 0 0 0
136 0 0 0 0
137 0 0 0 0
138 0 0 0 0
139 0 0 0 0
140 0 0 0 0
141 0 0 0 0
142 0 0 0 0
143 0 0 0 0
144 0 0 0 0
145 0 0 0 0
146 0 0 0 0
147 0 0 0 0
148 0 0 0 0
149 0 0 0 0
150 0 0 0 0
151 0 0 0 0
152 0 0 0 0
153 0 0 0 0
154 0 0 0 0
155 0 0 0 0
156 0 0 0 0
157 0 0 0 0
158 0 0 0 0
159 0 0 0 0
160 0 0 0 0
161 0 0 0 0
162 0 0 0 0
163 0 0 0 0
164 0 0 0 0
165 0 0 0 0
166 0 0 0 0
167 0 0 0 0
168 0 0 0 0
169 0 0 0 0
170 0 0 0 0
171 0 0 0 0
172 0 0 0 0
173 0 0 0 0
174 0 0 0 0
175 0 0 0 0
176 0 0 0 0
177 0 0 0 0
178 0 0 0 0
179 0 0 0 0
180 0 0 0 0
181 0 0 0 0
182 0 0 0 0
183 0 0 0 0
184 0 0 0 0
185 0 0 0 0
186 0 0 0 0
187 0 0 0 0
188 0 0 0 0
189 0 0 0 0
190 0 0 0 0
191 0 0 0 0
192 0 0 0 0
193 0 0 0 0
194 0 0 0 0
195 0 0 0 0
196 0 0 0 0
197 0 0 0 0
198 0 0 0 0
199 0 0 0 0
200 0 0 0 0
201 0 0 0 0
202 0 0 0 0
203 0 0 0 0
204 0 0 0 0
205 0 0 0 0
206 0 0 0 0
207 0 0 0 0
208 0 0 0 0
209 0 0 0 0
210 0 0 0 0
211 0 0 0 0
212 0 0 0 0
213 0 0 0 0
214 0 0 0 0
215 0 0 0 0
216 0 0 0 0
217 0 0 0 0
218 0 0 0 0
219 0 0 0 0
220 0 0 0 0
221 0 0 0 0
222 0 0 0 0
223 0 0 0 0
224 0 0 0 0
225 0 0 0 0
226 0 0 0 0
227 0 0 0 0
228 0 0 0 0
229 0 0 0 0
230 0 0 0 0
231 0 0 0 0

232 0 0 0 0
233 0 0 0 0
234 0 0 0 0
235 0 0 0 0
236 0 0 0 0
237 0 0 0 0
238 0 0 0 0
239 0 0 0 0
240 0 0 0 0
241 0 0 0 0
242 0 0 0 0
243 0 0 0 0
244 0 0 0 0
245 0 0 0 0
246 0 0 0 0
247 0 0 0 0
248 0 0 0 0
249 0 0 0 0
250 0 0 0 0
251 0 0 0 0
252 0 0 0 0
253 0 0 0 0
254 0 0 0 0
255 0 0 0 0
256 0 0 0 0
257 0 0 0 0
258 0 0 0 0
259 0 0 0 0
260 0 0 0 0
261 0 0 0 0
262 0 0 0 0
263 0 0 0 0
264 0 0 0 0
265 0 0 0 0
266 0 0 0 0
267 0 0 0 0
268 0 0 0 0
269 0 0 0 0
270 0 0 0 0
271 0 0 0 0
272 0 0 0 0
273 0 0 0 0
274 0 0 0 0
275 0 0 0 0
276 0 0 0 0
277 0 0 0 0
278 0 0 0 0
279 0 0 0 0
280 0 0 0 0
281 0 0 0 0
282 0 0 0 0
283 0 0 0 0
284 0 0 0 0
285 0 0 0 0
286 0 0 0 0
287 0 0 0 0
288 0 0 0 0
289 0 0 0 0
290 0 0 0 0
291 0 0 0 0
292 0 0 0 0
293 0 0 0 0
294 0 0 0 0
295 0 0 0 0
296 0 0 0 0
297 0 0 0 0
298 0 0 0 0
299 0 0 0 0
300 0 0 0 0
301 0 0 0 0
302 0 0 0 0
303 0 0 0 0
304 0 0 0 0
305 0 0 0 0
306 0 0 0 0
307 0 0 0 0
308 0 0 0 0
309 0 0 0 0
310 0 0 0 0
311 0 0 0 0
312 0 0 0 0
313 0 0 0 0
314 0 0 0 0
315 0 0 0 0
316 0 0 0 0
317 0 0 0 0
318 0 0 0 0
319 0 0 0 0
320 0 0 0 0
321 0 0 0 0
322 0 0 0 0
323 0 0 0 0
324 0 0 0 0
325 0 0 0 0
326 0 0 0 0
327 0 0 0 0
328 0 0 0 0
329 0 0 0 0
330 0 0 0 0
331 0 0 0 0
332 0 0 0 0
333 0 0 0 0
334 0 0 0 0
335 0 0 0 0
336 0 0 0 0
337 0 0 0 0
338 0 0 0 0
339 0 0 0 0
340 0 0 0 0
341 0 0 0 0
342 0 0 0 0
343 0 0 0 0
344 0 0 0 0
345 0 0 0 0
346 0 0 0 0
347 0 0 0 0
348 0 0 0 0
349 0 0 0 0
350 0 0 0 0
351 0 0 0 0
352 0 0 0 0
353 0 0 0 0
354 0 0 0 0
355 0 0 0 0
356 0 0 0 0
357 0 0 0 0
358 0 0 0 0
359 0 0 0 0
360 0 0 0 0
361 0 0 0 0
362 0 0 0 0
363 0 0 0 0
364 0 0 0 0
365 0 0 0 0
366 0 0 0 0
367 0 0 0 0
368 0 0 0 0
369 0 0 0 0

370 0 0 0 0
371 0 0 0 0
372 0 0 0 0
373 0 0 0 0
374 0 0 0 0
375 0 0 0 0
376 0 0 0 0
377 0 0 0 0
378 0 0 0 0
379 0 0 0 0
380 0 0 0 0
381 0 0 0 0
382 0 0 0 0
383 0 0 0 0
384 0 0 0 0
385 0 0 0 0
386 0 0 0 0
387 0 0 0 0
388 0 0 0 0
389 0 0 0 0
390 0 0 0 0
391 0 0 0 0
392 0 0 0 0
393 0 0 0 0
394 0 0 0 0
395 0 0 0 0
396 0 0 0 0
397 0 0 0 0
398 0 0 0 0
399 0 0 0 0
400 0 0 0 0
401 0 0 0 0
402 0 0 0 0
403 0 0 0 0
404 0 0 0 0
405 0 0 0 0
406 0 0 0 0
407 0 0 0 0
408 0 0 0 0
409 0 0 0 0
410 0 0 0 0
411 0 0 0 0
412 0 0 0 0
413 0 0 0 0
414 0 0 0 0
415 0 0 0 0
416 0 0 0 0
417 0 0 0 0
418 0 0 0 0
419 0 0 0 0
420 0 0 0 0
421 0 0 0 0
422 0 0 0 0
423 0 0 0 0
424 0 0 0 0
425 0 0 0 0
426 0 0 0 0
427 0 0 0 0
428 0 0 0 0
429 0 0 0 0
430 0 0 0 0
431 0 0 0 0
432 0 0 0 0
433 0 0 0 0
434 0 0 0 0
435 0 0 0 0
436 0 0 0 0
437 0 0 0 0
438 0 0 0 0
439 0 0 0 0
440 0 0 0 0
441 0 0 0 0
442 0 0 0 0
443 0 0 0 0
444 0 0 0 0
445 0 0 0 0
446 0 0 0 0
447 0 0 0 0
448 0 0 0 0
449 0 0 0 0
450 0 0 0 0
451 0 0 0 0
452 0 0 0 0
453 0 0 0 0
454 0 0 0 0
455 0 0 0 0
456 0 0 0 0
457 0 0 0 0
458 0 0 0 0
459 0 0 0 0
460 0 0 0 0
461 0 0 0 0
462 0 0 0 0
463 0 0 0 0
464 0 0 0 0
465 0 0 0 0
466 0 0 0 0
467 0 0 0 0
468 0 0 0 0
469 0 0 0 0
470 0 0 0 0
471 0 0 0 0
472 0 0 0 0
473 0 0 0 0
474 0 0 0 0
475 0 0 0 0
476 0 0 0 0
477 0 0 0 0
478 0 0 0 0
479 0 0 0 0
480 0 0 0 0
481 0 0 0 0
482 0 0 0 0
483 0 0 0 0
484 0 0 0 0
485 0 0 0 0
486 0 0 0 0
487 0 0 0 0
488 0 0 0 0
489 0 0 0 0
490 0 0 0 0
491 0 0 0 0
492 0 0 0 0
493 0 0 0 0
494 0 0 0 0
495 0 0 0 0
496 0 0 0 0
497 0 0 0 0
498 0 0 0 0
499 0 0 0 0
500 0 0 0 0
501 0 0 0 0
502 0 0 0 0
503 0 0 0 0
504 0 0 0 0
505 0 0 0 0
506 0 0 0 0
507 0 0 0 0

508 0 0 0 0
509 0 0 0 0
510 0 0 0 0
511 0 0 0 0
512 0 0 0 0
513 0 0 0 0
514 0 0 0 0
515 0 0 0 0
516 0 0 0 0
517 0 0 0 0
518 0 0 0 0
519 0 0 0 0
520 0 0 0 0
521 0 0 0 0
522 0 0 0 0
523 0 0 0 0
524 0 0 0 0
525 0 0 0 0
526 0 0 0 0
527 0 0 0 0
528 0 0 0 0
529 0 0 0 0
530 0 0 0 0
531 0 0 0 0
532 0 0 0 0
533 0 0 0 0
534 0 0 0 0
535 0 0 0 0
536 0 0 0 0
537 0 0 0 0
538 0 0 0 0
539 0 0 0 0
540 0 0 0 0
541 0 0 0 0
542 0 0 0 0
543 0 0 0 0
544 0 0 0 0
545 0 0 0 0
546 0 0 0 0
547 0 0 0 0
548 0 0 0 0
549 0 0 0 0
550 0 0 0 0
551 0 0 0 0
552 0 0 0 0
553 0 0 0 0
554 0 0 0 0
555 0 0 0 0
556 0 0 0 0
557 0 0 0 0
558 0 0 0 0
559 0 0 0 0
560 0 0 0 0
561 0 0 0 0
562 0 0 0 0
563 0 0 0 0
564 0 0 0 0
565 0 0 0 0
566 0 0 0 0
567 0 0 0 0
568 0 0 0 0
569 0 0 0 0
570 0 0 0 0
571 0 0 0 0
572 0 0 0 0
573 0 0 0 0
574 0 0 0 0
575 0 0 0 0
576 0 0 0 0
577 0 0 0 0
578 0 0 0 0
579 0 0 0 0
580 0 0 0 0
581 0 0 0 0
582 0 0 0 0
583 0 0 0 0
584 0 0 0 0
585 0 0 0 0
586 0 0 0 0
587 0 0 0 0
588 0 0 0 0
589 0 0 0 0
590 0 0 0 0
591 0 0 0 0
592 0 0 0 0
593 0 0 0 0
594 0 0 0 0
595 0 0 0 0
596 0 0 0 0
597 0 0 0 0
598 0 0 0 0
599 0 0 0 0
600 0 0 0 0
601 0 0 0 0
602 0 0 0 0
603 0 0 0 0
604 0 0 0 0
605 0 0 0 0
606 0 0 0 0
607 0 0 0 0
608 0 0 0 0
609 0 0 0 0
610 0 0 0 0
611 0 0 0 0
612 0 0 0 0
613 0 0 0 0
614 0 0 0 0
615 0 0 0 0
616 0 0 0 0
617 0 0 0 0
618 0 0 0 0
619 0 0 0 0
620 0 0 0 0
621 0 0 0 0
622 0 0 0 0
623 0 0 0 0
624 0 0 0 0
625 0 0 0 0
626 0 0 0 0
627 0 0 0 0
628 0 0 0 0
629 0 0 0 0
630 0 0 0 0
631 0 0 0 0
632 0 0 0 0
633 0 0 0 0
634 0 0 0 0
635 0 0 0 0
636 0 0 0 0
637 0 0 0 0
638 0 0 0 0
639 0 0 0 0
640 0 0 0 0
641 0 0 0 0
642 0 0 0 0
643 0 0 0 0
644 0 0 0 0
645 0 0 0 0

646 0 0 0 0
647 0 0 0 0
648 0 0 0 0
649 0 0 0 0
650 0 0 0 0
651 0 0 0 0
652 0 0 0 0
653 0 0 0 0
654 0 0 0 0
655 0 0 0 0
656 0 0 0 0
657 0 0 0 0
658 0 0 0 0
659 0 0 0 0
660 0 0 0 0
661 0 0 0 0
662 0 0 0 0
663 0 0 0 0
664 0 0 0 0
665 0 0 0 0
666 0 0 0 0
667 0 0 0 0
668 0 0 0 0
669 0 0 0 0
670 0 0 0 0
671 0 0 0 0
672 0 0 0 0
673 0 0 0 0
674 0 0 0 0
675 0 0 0 0
676 0 0 0 0
677 0 0 0 0
678 0 0 0 0
679 0 0 0 0
680 0 0 0 0
681 0 0 0 0
682 0 0 0 0
683 0 0 0 0
684 0 0 0 0
685 0 0 0 0
686 0 0 0 0
687 0 0 0 0
688 0 0 0 0
689 0 0 0 0
690 0 0 0 0
691 0 0 0 0
692 0 0 0 0
693 0 0 0 0
694 0 0 0 0
695 0 0 0 0
696 0 0 0 0
697 0 0 0 0
698 0 0 0 0
699 0 0 0 0
700 0 0 0 0
701 0 0 0 0
702 0 0 0 0
703 0 0 0 0
704 0 0 0 0
705 0 0 0 0
706 0 0 0 0
707 0 0 0 0
708 0 0 0 0
709 0 0 0 0
710 0 0 0 0
711 0 0 0 0
712 0 0 0 0
713 0 0 0 0
714 0 0 0 0
715 0 0 0 0
716 0 0 0 0
717 0 0 0 0
718 0 0 0 0
719 0 0 0 0
720 0 0 0 0
721 0 0 0 0
722 0 0 0 0
723 0 0 0 0
724 0 0 0 0
725 0 0 0 0
726 0 0 0 0
727 0 0 0 0
728 0 0 0 0
729 0 0 0 0
730 0 0 0 0
731 0 0 0 0
732 0 0 0 0
733 0 0 0 0
734 0 0 0 0
735 0 0 0 0
736 0 0 0 0
737 0 0 0 0
738 0 0 0 0
739 0 0 0 0
740 0 0 0 0
741 0 0 0 0
742 0 0 0 0
743 0 0 0 0
744 0 0 0 0
745 0 0 0 0
746 0 0 0 0
747 0 0 0 0
748 0 0 0 0
749 0 0 0 0
750 0 0 0 0
751 0 0 0 0
752 0 0 0 0
753 0 0 0 0
754 0 0 0 0
755 0 0 0 0
756 0 0 0 0
757 0 0 0 0
758 0 0 0 0
759 0 0 0 0
760 0 0 0 0
761 0 0 0 0
762 0 0 0 0
763 0 0 0 0
764 0 0 0 0
765 0 0 0 0
766 0 0 0 0
767 0 0 0 0
768 0 0 0 0
769 0 0 0 0
770 0 0 0 0
771 0 0 0 0
772 0 0 0 0
773 0 0 0 0
774 0 0 0 0
775 0 0 0 0
776 0 0 0 0
777 0 0 0 0
778 0 0 0 0
779 0 0 0 0
780 0 0 0 0
781 0 0 0 0
782 0 0 0 0
783 0 0 0 0

784 0 0 0 0	797 0 0 0 0	810 0 0 0 0
785 0 0 0 0	798 0 0 0 0	811 0 0 0 0
786 0 0 0 0	799 0 0 0 0	812 0 0 0 0
787 0 0 0 0	800 0 0 0 0	813 0 0 0 0
788 0 0 0 0	801 0 0 0 0	814 0 0 0 0
789 0 0 0 0	802 0 0 0 0	815 0 0 0 0
790 0 0 0 0	803 0 0 0 0	816 0 0 0 0
791 0 0 0 0	804 0 0 0 0	817 0 0 0 0
792 0 0 0 0	805 0 0 0 0	818 0 0 0 0
793 0 0 0 0	806 0 0 0 0	819 0 0 0 0
794 0 0 0 0	807 0 0 0 0	820 0 0 0 0
795 0 0 0 0	808 0 0 0 0	
796 0 0 0 0	809 0 0 0 0	

! ANGLe nodal boundary conditions.
! see pp 44, 213, 219.
ANGLe

1	0	9.00E+01	30	0	9.00E+01	59	0	9.00E+01
2	0	9.00E+01	31	0	9.00E+01	60	0	9.00E+01
3	0	9.00E+01	32	0	9.00E+01	61	0	9.00E+01
4	0	9.00E+01	33	0	9.00E+01	62	0	9.00E+01
5	0	9.00E+01	34	0	9.00E+01	63	0	9.00E+01
6	0	9.00E+01	35	0	9.00E+01	64	0	9.00E+01
7	0	9.00E+01	36	0	9.00E+01	65	0	9.00E+01
8	0	9.00E+01	37	0	9.00E+01	66	0	9.00E+01
9	0	9.00E+01	38	0	9.00E+01	67	0	9.00E+01
10	0	9.00E+01	39	0	9.00E+01	68	0	9.00E+01
11	0	9.00E+01	40	0	9.00E+01	69	0	9.00E+01
12	0	9.00E+01	41	0	9.00E+01	70	0	9.00E+01
13	0	9.00E+01	42	0	9.00E+01	71	0	9.00E+01
14	0	9.00E+01	43	0	9.00E+01	72	0	9.00E+01
15	0	9.00E+01	44	0	9.00E+01	73	0	9.00E+01
16	0	9.00E+01	45	0	9.00E+01	74	0	9.00E+01
17	0	9.00E+01	46	0	9.00E+01	75	0	9.00E+01
18	0	9.00E+01	47	0	9.00E+01	76	0	9.00E+01
19	0	9.00E+01	48	0	9.00E+01	77	0	9.00E+01
20	0	9.00E+01	49	0	9.00E+01	78	0	9.00E+01
21	0	9.00E+01	50	0	9.00E+01	79	0	9.00E+01
22	0	9.00E+01	51	0	9.00E+01	80	0	9.00E+01
23	0	9.00E+01	52	0	9.00E+01	81	0	9.00E+01
24	0	9.00E+01	53	0	9.00E+01	82	0	9.00E+01
25	0	9.00E+01	54	0	9.00E+01	83	0	9.00E+01
26	0	9.00E+01	55	0	9.00E+01	84	0	9.00E+01
27	0	9.00E+01	56	0	9.00E+01	85	0	9.00E+01
28	0	9.00E+01	57	0	9.00E+01	86	0	9.00E+01
29	0	9.00E+01	58	0	9.00E+01	87	0	9.00E+01

88	0	9.00E+01	134	0	9.00E+01	180	0	9.00E+01
89	0	9.00E+01	135	0	9.00E+01	181	0	9.00E+01
90	0	9.00E+01	136	0	9.00E+01	182	0	9.00E+01
91	0	9.00E+01	137	0	9.00E+01	183	0	9.00E+01
92	0	9.00E+01	138	0	9.00E+01	184	0	9.00E+01
93	0	9.00E+01	139	0	9.00E+01	185	0	9.00E+01
94	0	9.00E+01	140	0	9.00E+01	186	0	9.00E+01
95	0	9.00E+01	141	0	9.00E+01	187	0	9.00E+01
96	0	9.00E+01	142	0	9.00E+01	188	0	9.00E+01
97	0	9.00E+01	143	0	9.00E+01	189	0	9.00E+01
98	0	9.00E+01	144	0	9.00E+01	190	0	9.00E+01
99	0	9.00E+01	145	0	9.00E+01	191	0	9.00E+01
100	0	9.00E+01	146	0	9.00E+01	192	0	9.00E+01
101	0	9.00E+01	147	0	9.00E+01	193	0	9.00E+01
102	0	9.00E+01	148	0	9.00E+01	194	0	9.00E+01
103	0	9.00E+01	149	0	9.00E+01	195	0	9.00E+01
104	0	9.00E+01	150	0	9.00E+01	196	0	9.00E+01
105	0	9.00E+01	151	0	9.00E+01	197	0	9.00E+01
106	0	9.00E+01	152	0	9.00E+01	198	0	9.00E+01
107	0	9.00E+01	153	0	9.00E+01	199	0	9.00E+01
108	0	9.00E+01	154	0	9.00E+01	200	0	9.00E+01
109	0	9.00E+01	155	0	9.00E+01	201	0	9.00E+01
110	0	9.00E+01	156	0	9.00E+01	202	0	9.00E+01
111	0	9.00E+01	157	0	9.00E+01	203	0	9.00E+01
112	0	9.00E+01	158	0	9.00E+01	204	0	9.00E+01
113	0	9.00E+01	159	0	9.00E+01	205	0	9.00E+01
114	0	9.00E+01	160	0	9.00E+01	206	0	9.00E+01
115	0	9.00E+01	161	0	9.00E+01	207	0	9.00E+01
116	0	9.00E+01	162	0	9.00E+01	208	0	9.00E+01
117	0	9.00E+01	163	0	9.00E+01	209	0	9.00E+01
118	0	9.00E+01	164	0	9.00E+01	210	0	9.00E+01
119	0	9.00E+01	165	0	9.00E+01	211	0	9.00E+01
120	0	9.00E+01	166	0	9.00E+01	212	0	9.00E+01
121	0	9.00E+01	167	0	9.00E+01	213	0	9.00E+01
122	0	9.00E+01	168	0	9.00E+01	214	0	9.00E+01
123	0	9.00E+01	169	0	9.00E+01	215	0	9.00E+01
124	0	9.00E+01	170	0	9.00E+01	216	0	9.00E+01
125	0	9.00E+01	171	0	9.00E+01	217	0	9.00E+01
126	0	9.00E+01	172	0	9.00E+01	218	0	9.00E+01
127	0	9.00E+01	173	0	9.00E+01	219	0	9.00E+01
128	0	9.00E+01	174	0	9.00E+01	220	0	9.00E+01
129	0	9.00E+01	175	0	9.00E+01	221	0	9.00E+01
130	0	9.00E+01	176	0	9.00E+01	222	0	9.00E+01
131	0	9.00E+01	177	0	9.00E+01	223	0	9.00E+01
132	0	9.00E+01	178	0	9.00E+01	224	0	9.00E+01
133	0	9.00E+01	179	0	9.00E+01	225	0	9.00E+01

226	0	9.00E+01	272	0	9.00E+01	318	0	9.00E+01
227	0	9.00E+01	273	0	9.00E+01	319	0	9.00E+01
228	0	9.00E+01	274	0	9.00E+01	320	0	9.00E+01
229	0	9.00E+01	275	0	9.00E+01	321	0	9.00E+01
230	0	9.00E+01	276	0	9.00E+01	322	0	9.00E+01
231	0	9.00E+01	277	0	9.00E+01	323	0	9.00E+01
232	0	9.00E+01	278	0	9.00E+01	324	0	9.00E+01
233	0	9.00E+01	279	0	9.00E+01	325	0	9.00E+01
234	0	9.00E+01	280	0	9.00E+01	326	0	9.00E+01
235	0	9.00E+01	281	0	9.00E+01	327	0	9.00E+01
236	0	9.00E+01	282	0	9.00E+01	328	0	9.00E+01
237	0	9.00E+01	283	0	9.00E+01	329	0	9.00E+01
238	0	9.00E+01	284	0	9.00E+01	330	0	9.00E+01
239	0	9.00E+01	285	0	9.00E+01	331	0	9.00E+01
240	0	9.00E+01	286	0	9.00E+01	332	0	9.00E+01
241	0	9.00E+01	287	0	9.00E+01	333	0	9.00E+01
242	0	9.00E+01	288	0	9.00E+01	334	0	9.00E+01
243	0	9.00E+01	289	0	9.00E+01	335	0	9.00E+01
244	0	9.00E+01	290	0	9.00E+01	336	0	9.00E+01
245	0	9.00E+01	291	0	9.00E+01	337	0	9.00E+01
246	0	9.00E+01	292	0	9.00E+01	338	0	9.00E+01
247	0	9.00E+01	293	0	9.00E+01	339	0	9.00E+01
248	0	9.00E+01	294	0	9.00E+01	340	0	9.00E+01
249	0	9.00E+01	295	0	9.00E+01	341	0	9.00E+01
250	0	9.00E+01	296	0	9.00E+01	342	0	9.00E+01
251	0	9.00E+01	297	0	9.00E+01	343	0	9.00E+01
252	0	9.00E+01	298	0	9.00E+01	344	0	9.00E+01
253	0	9.00E+01	299	0	9.00E+01	345	0	9.00E+01
254	0	9.00E+01	300	0	9.00E+01	346	0	9.00E+01
255	0	9.00E+01	301	0	9.00E+01	347	0	9.00E+01
256	0	9.00E+01	302	0	9.00E+01	348	0	9.00E+01
257	0	9.00E+01	303	0	9.00E+01	349	0	9.00E+01
258	0	9.00E+01	304	0	9.00E+01	350	0	9.00E+01
259	0	9.00E+01	305	0	9.00E+01	351	0	9.00E+01
260	0	9.00E+01	306	0	9.00E+01	352	0	9.00E+01
261	0	9.00E+01	307	0	9.00E+01	353	0	9.00E+01
262	0	9.00E+01	308	0	9.00E+01	354	0	9.00E+01
263	0	9.00E+01	309	0	9.00E+01	355	0	9.00E+01
264	0	9.00E+01	310	0	9.00E+01	356	0	9.00E+01
265	0	9.00E+01	311	0	9.00E+01	357	0	9.00E+01
266	0	9.00E+01	312	0	9.00E+01	358	0	9.00E+01
267	0	9.00E+01	313	0	9.00E+01	359	0	9.00E+01
268	0	9.00E+01	314	0	9.00E+01	360	0	9.00E+01
269	0	9.00E+01	315	0	9.00E+01	361	0	9.00E+01
270	0	9.00E+01	316	0	9.00E+01	362	0	9.00E+01
271	0	9.00E+01	317	0	9.00E+01	363	0	9.00E+01

364	0	9.00E+01	410	0	9.00E+01	456	0	8.64E+01
365	0	9.00E+01	411	0	8.64E+01	457	0	8.64E+01
366	0	9.00E+01	412	0	8.64E+01	458	0	8.64E+01
367	0	9.00E+01	413	0	8.64E+01	459	0	8.64E+01
368	0	9.00E+01	414	0	8.64E+01	460	0	8.64E+01
369	0	9.00E+01	415	0	8.64E+01	461	0	8.64E+01
370	0	9.00E+01	416	0	8.64E+01	462	0	8.64E+01
371	0	9.00E+01	417	0	8.64E+01	463	0	8.64E+01
372	0	9.00E+01	418	0	8.64E+01	464	0	8.64E+01
373	0	9.00E+01	419	0	8.64E+01	465	0	8.64E+01
374	0	9.00E+01	420	0	8.64E+01	466	0	8.64E+01
375	0	9.00E+01	421	0	8.64E+01	467	0	8.64E+01
376	0	9.00E+01	422	0	8.64E+01	468	0	8.64E+01
377	0	9.00E+01	423	0	8.64E+01	469	0	8.64E+01
378	0	9.00E+01	424	0	8.64E+01	470	0	8.64E+01
379	0	9.00E+01	425	0	8.64E+01	471	0	8.64E+01
380	0	9.00E+01	426	0	8.64E+01	472	0	8.64E+01
381	0	9.00E+01	427	0	8.64E+01	473	0	8.64E+01
382	0	9.00E+01	428	0	8.64E+01	474	0	8.64E+01
383	0	9.00E+01	429	0	8.64E+01	475	0	8.64E+01
384	0	9.00E+01	430	0	8.64E+01	476	0	8.64E+01
385	0	9.00E+01	431	0	8.64E+01	477	0	8.64E+01
386	0	9.00E+01	432	0	8.64E+01	478	0	8.64E+01
387	0	9.00E+01	433	0	8.64E+01	479	0	8.64E+01
388	0	9.00E+01	434	0	8.64E+01	480	0	8.64E+01
389	0	9.00E+01	435	0	8.64E+01	481	0	8.64E+01
390	0	9.00E+01	436	0	8.64E+01	482	0	8.64E+01
391	0	9.00E+01	437	0	8.64E+01	483	0	8.64E+01
392	0	9.00E+01	438	0	8.64E+01	484	0	8.64E+01
393	0	9.00E+01	439	0	8.64E+01	485	0	8.64E+01
394	0	9.00E+01	440	0	8.64E+01	486	0	8.64E+01
395	0	9.00E+01	441	0	8.64E+01	487	0	8.64E+01
396	0	9.00E+01	442	0	8.64E+01	488	0	8.64E+01
397	0	9.00E+01	443	0	8.64E+01	489	0	8.64E+01
398	0	9.00E+01	444	0	8.64E+01	490	0	8.64E+01
399	0	9.00E+01	445	0	8.64E+01	491	0	8.64E+01
400	0	9.00E+01	446	0	8.64E+01	492	0	8.64E+01
401	0	9.00E+01	447	0	8.64E+01	493	0	8.64E+01
402	0	9.00E+01	448	0	8.64E+01	494	0	8.64E+01
403	0	9.00E+01	449	0	8.64E+01	495	0	8.64E+01
404	0	9.00E+01	450	0	8.64E+01	496	0	8.64E+01
405	0	9.00E+01	451	0	8.64E+01	497	0	8.64E+01
406	0	9.00E+01	452	0	8.64E+01	498	0	8.64E+01
407	0	9.00E+01	453	0	8.64E+01	499	0	8.64E+01
408	0	9.00E+01	454	0	8.64E+01	500	0	8.64E+01
409	0	9.00E+01	455	0	8.64E+01	501	0	8.64E+01

502	0	8.64E+01	548	0	8.64E+01	594	0	8.64E+01
503	0	8.64E+01	549	0	8.64E+01	595	0	8.64E+01
504	0	8.64E+01	550	0	8.64E+01	596	0	8.64E+01
505	0	8.64E+01	551	0	8.64E+01	597	0	8.64E+01
506	0	8.64E+01	552	0	8.64E+01	598	0	8.64E+01
507	0	8.64E+01	553	0	8.64E+01	599	0	8.64E+01
508	0	8.64E+01	554	0	8.64E+01	600	0	8.64E+01
509	0	8.64E+01	555	0	8.64E+01	601	0	8.64E+01
510	0	8.64E+01	556	0	8.64E+01	602	0	8.64E+01
511	0	8.64E+01	557	0	8.64E+01	603	0	8.64E+01
512	0	8.64E+01	558	0	8.64E+01	604	0	8.64E+01
513	0	8.64E+01	559	0	8.64E+01	605	0	8.64E+01
514	0	8.64E+01	560	0	8.64E+01	606	0	8.64E+01
515	0	8.64E+01	561	0	8.64E+01	607	0	8.64E+01
516	0	8.64E+01	562	0	8.64E+01	608	0	8.64E+01
517	0	8.64E+01	563	0	8.64E+01	609	0	8.64E+01
518	0	8.64E+01	564	0	8.64E+01	610	0	8.64E+01
519	0	8.64E+01	565	0	8.64E+01	611	0	8.64E+01
520	0	8.64E+01	566	0	8.64E+01	612	0	8.64E+01
521	0	8.64E+01	567	0	8.64E+01	613	0	8.64E+01
522	0	8.64E+01	568	0	8.64E+01	614	0	8.64E+01
523	0	8.64E+01	569	0	8.64E+01	615	0	8.64E+01
524	0	8.64E+01	570	0	8.64E+01	616	0	8.64E+01
525	0	8.64E+01	571	0	8.64E+01	617	0	8.64E+01
526	0	8.64E+01	572	0	8.64E+01	618	0	8.64E+01
527	0	8.64E+01	573	0	8.64E+01	619	0	8.64E+01
528	0	8.64E+01	574	0	8.64E+01	620	0	8.64E+01
529	0	8.64E+01	575	0	8.64E+01	621	0	8.64E+01
530	0	8.64E+01	576	0	8.64E+01	622	0	8.64E+01
531	0	8.64E+01	577	0	8.64E+01	623	0	8.64E+01
532	0	8.64E+01	578	0	8.64E+01	624	0	8.64E+01
533	0	8.64E+01	579	0	8.64E+01	625	0	8.64E+01
534	0	8.64E+01	580	0	8.64E+01	626	0	8.64E+01
535	0	8.64E+01	581	0	8.64E+01	627	0	8.64E+01
536	0	8.64E+01	582	0	8.64E+01	628	0	8.64E+01
537	0	8.64E+01	583	0	8.64E+01	629	0	8.64E+01
538	0	8.64E+01	584	0	8.64E+01	630	0	8.64E+01
539	0	8.64E+01	585	0	8.64E+01	631	0	8.64E+01
540	0	8.64E+01	586	0	8.64E+01	632	0	8.64E+01
541	0	8.64E+01	587	0	8.64E+01	633	0	8.64E+01
542	0	8.64E+01	588	0	8.64E+01	634	0	8.64E+01
543	0	8.64E+01	589	0	8.64E+01	635	0	8.64E+01
544	0	8.64E+01	590	0	8.64E+01	636	0	8.64E+01
545	0	8.64E+01	591	0	8.64E+01	637	0	8.64E+01
546	0	8.64E+01	592	0	8.64E+01	638	0	8.64E+01
547	0	8.64E+01	593	0	8.64E+01	639	0	8.64E+01

640	0	8.64E+01	686	0	8.64E+01	732	0	8.64E+01
641	0	8.64E+01	687	0	8.64E+01	733	0	8.64E+01
642	0	8.64E+01	688	0	8.64E+01	734	0	8.64E+01
643	0	8.64E+01	689	0	8.64E+01	735	0	8.64E+01
644	0	8.64E+01	690	0	8.64E+01	736	0	8.64E+01
645	0	8.64E+01	691	0	8.64E+01	737	0	8.64E+01
646	0	8.64E+01	692	0	8.64E+01	738	0	8.64E+01
647	0	8.64E+01	693	0	8.64E+01	739	0	8.64E+01
648	0	8.64E+01	694	0	8.64E+01	740	0	8.64E+01
649	0	8.64E+01	695	0	8.64E+01	741	0	8.64E+01
650	0	8.64E+01	696	0	8.64E+01	742	0	8.64E+01
651	0	8.64E+01	697	0	8.64E+01	743	0	8.64E+01
652	0	8.64E+01	698	0	8.64E+01	744	0	8.64E+01
653	0	8.64E+01	699	0	8.64E+01	745	0	8.64E+01
654	0	8.64E+01	700	0	8.64E+01	746	0	8.64E+01
655	0	8.64E+01	701	0	8.64E+01	747	0	8.64E+01
656	0	8.64E+01	702	0	8.64E+01	748	0	8.64E+01
657	0	8.64E+01	703	0	8.64E+01	749	0	8.64E+01
658	0	8.64E+01	704	0	8.64E+01	750	0	8.64E+01
659	0	8.64E+01	705	0	8.64E+01	751	0	8.64E+01
660	0	8.64E+01	706	0	8.64E+01	752	0	8.64E+01
661	0	8.64E+01	707	0	8.64E+01	753	0	8.64E+01
662	0	8.64E+01	708	0	8.64E+01	754	0	8.64E+01
663	0	8.64E+01	709	0	8.64E+01	755	0	8.64E+01
664	0	8.64E+01	710	0	8.64E+01	756	0	8.64E+01
665	0	8.64E+01	711	0	8.64E+01	757	0	8.64E+01
666	0	8.64E+01	712	0	8.64E+01	758	0	8.64E+01
667	0	8.64E+01	713	0	8.64E+01	759	0	8.64E+01
668	0	8.64E+01	714	0	8.64E+01	760	0	8.64E+01
669	0	8.64E+01	715	0	8.64E+01	761	0	8.64E+01
670	0	8.64E+01	716	0	8.64E+01	762	0	8.64E+01
671	0	8.64E+01	717	0	8.64E+01	763	0	8.64E+01
672	0	8.64E+01	718	0	8.64E+01	764	0	8.64E+01
673	0	8.64E+01	719	0	8.64E+01	765	0	8.64E+01
674	0	8.64E+01	720	0	8.64E+01	766	0	8.64E+01
675	0	8.64E+01	721	0	8.64E+01	767	0	8.64E+01
676	0	8.64E+01	722	0	8.64E+01	768	0	8.64E+01
677	0	8.64E+01	723	0	8.64E+01	769	0	8.64E+01
678	0	8.64E+01	724	0	8.64E+01	770	0	8.64E+01
679	0	8.64E+01	725	0	8.64E+01	771	0	8.64E+01
680	0	8.64E+01	726	0	8.64E+01	772	0	8.64E+01
681	0	8.64E+01	727	0	8.64E+01	773	0	8.64E+01
682	0	8.64E+01	728	0	8.64E+01	774	0	8.64E+01
683	0	8.64E+01	729	0	8.64E+01	775	0	8.64E+01
684	0	8.64E+01	730	0	8.64E+01	776	0	8.64E+01
685	0	8.64E+01	731	0	8.64E+01	777	0	8.64E+01

```
778     0       8.64E+01        793     0       8.64E+01        808     0       8.64E+01
779     0       8.64E+01        794     0       8.64E+01        809     0       8.64E+01
780     0       8.64E+01        795     0       8.64E+01        810     0       8.64E+01
781     0       8.64E+01        796     0       8.64E+01        811     0       8.64E+01
782     0       8.64E+01        797     0       8.64E+01        812     0       8.64E+01
783     0       8.64E+01        798     0       8.64E+01        813     0       8.64E+01
784     0       8.64E+01        799     0       8.64E+01        814     0       8.64E+01
785     0       8.64E+01        800     0       8.64E+01        815     0       8.64E+01
786     0       8.64E+01        801     0       8.64E+01        816     0       8.64E+01
787     0       8.64E+01        802     0       8.64E+01        817     0       8.64E+01
788     0       8.64E+01        803     0       8.64E+01        818     0       8.64E+01
789     0       8.64E+01        804     0       8.64E+01        819     0       8.64E+01
790     0       8.64E+01        805     0       8.64E+01        820     0       8.64E+01
791     0       8.64E+01        806     0       8.64E+01
792     0       8.64E+01        807     0       8.64E+01

end

!INTER
BATCh
        LIST,,1
END
1,10,401,410

! BATCh specify some solution  steps (pg. 137)
BATCh

!       ! PLOT deformations  in the x_i direction  where i = 1.
!       plot,defo,1
!
!       ! PLOT using 3D PERSpective view with inew  = 1 for use of old parameters (pg. 496).
!       plot,pers,1

        ! PROPortional load command (pg. 148)
        ! Input a proportional  load with ramp loading.
        ! NOT BEING USED FOR ARTERY
        !prop,,1

        ! The value for a time increment (pg. 141)
        dt,,1.0

        ! Perform check of mesh correctness (pg. 139)
        check

        ! Repeated execution of solution  commands (pg. 144)
        !
```

```
loop time 600

        ! We can have it continue to solve for as long as we want (pg. 154)
        time,,0.0

        ! Set the convergence tolerace (pg. 155)
        tol,,1.0e-5

        ! Use this many Newton-Raphson iterations
        loop newton 100

                ! UTANgent matrix command (pg. 159)
                ! Permits a non-symmetric tanget array
                ! results in the computation of a tangent array
                utan,,1

!               ! Clear the PLOT screen (pg. 198)
!               plot,wipe
!
!               ! Hides interior surfaces (pg. 204)
!               plot,hide
!
!               ! PLOT deformations
!               plot,defo
!
!               ! PLOT mesh
!               plot,mesh
!
!               ! Show filled plots
!               plot,fill
!
!               ! Show axes
!               plot,axis
!
!               ! Plot CONTours for dof 3
!               plot,cont,1
        next newton

        ! Output all displacements and stresses.
        disp,LIST,1
        !stre,all
        !stre,node,1,10660
        !grdt
next

! End the time loop
```

```
        end
! End the batch job
END

Stop
```

APPENDIX B

COMPARISON OF MODEL OUTPUTS FOR HOMEOSTATIC, BASELINE, AND 2X ELASTIN PRODUCTION MODELS

The following describes the changes in mass and mass production rates of the constituents of the AAA G&R models (elastin, collagen, and smooth muscle) used in **Figures 44-48**. All constituent and active stress time history plots are shown for the medial layer as the adventitial layer contains no smooth muscle and a small amount of elastin.

The amount of each constituent depends on the survival of the original and any subsequently produced material and how much material is produced. The decay constant for collagen and smooth muscle scales with deviations of tension with respect to the tension of the constituent at its depositional prestretch (i.e. the removal is faster at higher tensions and lower and slower at lower tensions). The production rate for collagen and smooth muscle scales with deviations from a homeostatic stress (i.e. larger stresses lead to a net production of material and smaller stresses lead to a net removal of material). Active stress scales with both the relative amount of smooth muscle compared to the total amount of material and the stretch of the smooth muscle (i.e. larger stretches produces higher active stresses). Elastin decays at a constant rate unless noted otherwise.

Homeostasis model: This model has no step loss in elastin, collagen, or smooth muscle. The net mass production rates for collagen and smooth muscle follow the stress based mass

production rules. The net mass production for elastin is modeled by exponential decay with a 40 year half-life.

Baseline model: This model has a step loss in elastin (~65%), collagen (~3.5%), and smooth muscle (~3.5%) at the start of the model. After this step loss, the net mass production rates for collagen and smooth muscle follow the stress based mass production rules, and the net mass production for elastin is modeled by exponential decay with a 40 year half-life.

2x elastin production model: This model has a step loss in elastin (~65%), collagen (~3.5%), and smooth muscle (~3.5%) at the start of the model. After this step loss, the net mass production rates for collagen and smooth muscle follow the stress based mass production rules, and the net mass production for elastin is modeled by exponential decay with a 40 year half-life up until a 30% increase in the outer diameter of the vessel (~8.6 years simulation time). Up until this intervention point, this model is exactly the same as the baseline model. At the intervention time point, elastin decay goes to zero, and new elastin is added to the remaining elastin at a rate of 1.350 $\mu g/mm^3/2$ weeks.

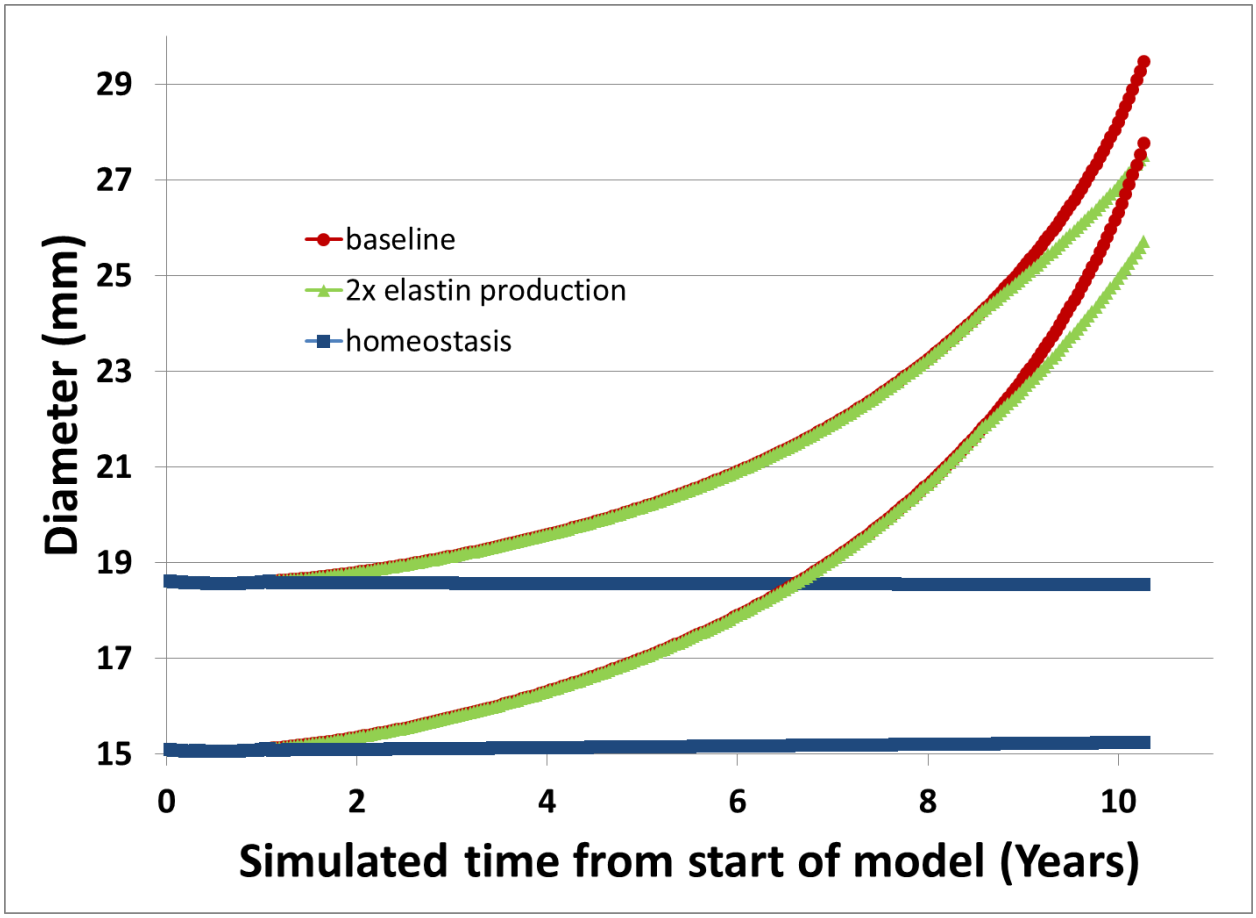

Figure 44. Diameters of computation models of AAA G&R. A homeostatic model was created that shows little change in inner and outer aortic diameters (blue). The baseline model of AAA G&R is shown in red. The model of AAA G&R with 2x elastin production at 30% increase in baseline outer diameter is shown in green. Diameter (mm) is on the y-axis. Model simulation time is shown on the x-axis.

Description of diameter plot (Figure 44):

The homeostasis model (shown in blue) maintains the vessel geometry while experiencing the gradual loss in elastin. This is likely due to increases in the amount of collagen, smooth muscle, and the active generation of stress.

In the baseline (shown in red) and 2x elastin production (shown in green) models prior to the elastogenic intervention, the large decrease in elastin and small decreases in collagen and smooth muscle do not initially change the diameter. This can be attributed to the stiffness of the remaining collagen (in both the media and adventitia) and active stress generated by smooth muscle. The luminal expansion starts at approximately one year (after approximately 5 collagen half-lives when only about ~3% of the original collagen has survived from the start of the model) when the continued loss of highly prestretched elastin, coupled with continued small losses in collagen and smooth muscle have diminished the ability to actively maintain inner radius due to substantial increased circumferential passive stiffening. In the baseline model, the diameter continues to increase.

Once we introduce the elastogenic intervention, this addition of prestretched elastin immediately begins to change the rate of growth of the AAA in part because of the prestretch and in part due to the increases in mass in all of the wall constituents.

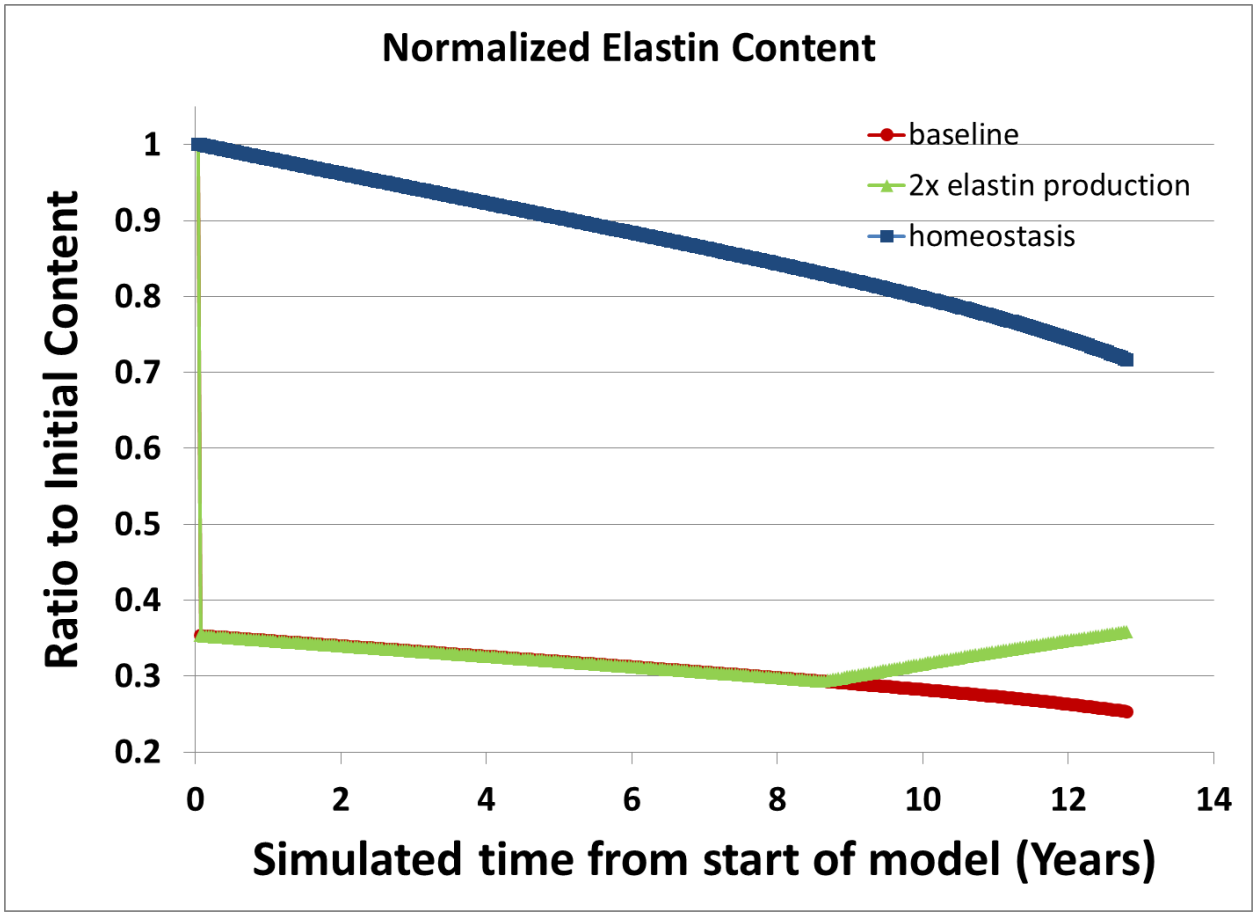

Figure 45. Medial ratio of remaining elastin to initial elastin within computation models of AAA G&R. The homeostatic model is shown in blue. The baseline model of AAA G&R is shown in red. The model of AAA G&R with 2x elastin production at 30% increase in baseline outer diameter is shown in green. Ratio of elastin to initial elastin is on the y-axis. Model simulation time is shown on the x-axis.

Description of elastin plot (Figure 45):

The homeostasis model (shown in blue) loses elastin at a rate modeled by exponential decay with a 40 year half-life.

In the baseline (shown in red) and 2x elastin production (shown in green) models prior to the elastogenic intervention, there is a step loss of elastin at the beginning of the model of ~65%. After the initial step loss, the remaining elastin is lost at a rate modeled by exponential decay with a 40 year half-life).

In the 2x elastin production model at the intervention time point, elastin decay goes to zero and new elastin is added to the remaining elastin at a rate of 1.350 $\mu g/mm^3/2$ weeks.

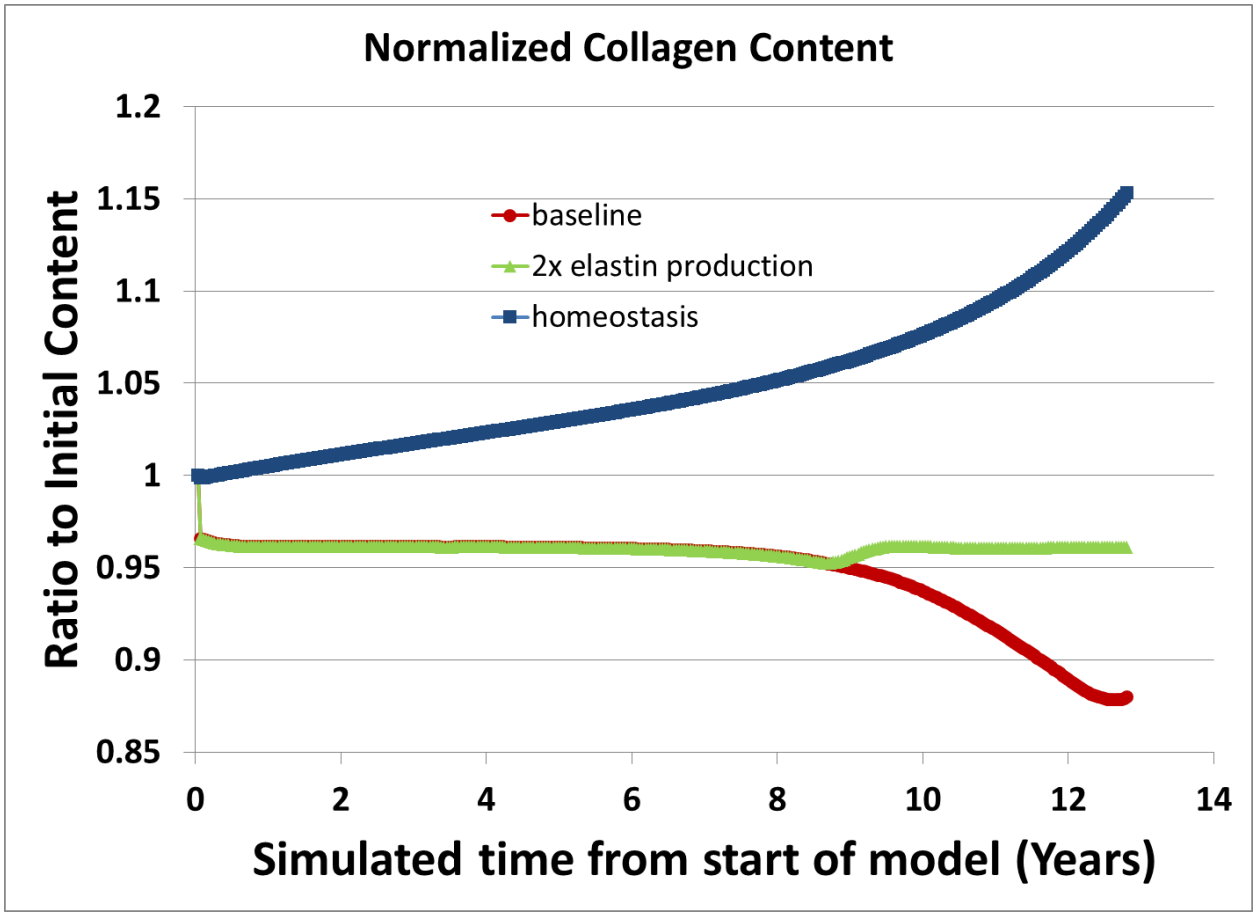

Figure 46. Medial ratio of remaining collagen to initial collagen within computation models of AAA G&R. The homeostatic model is shown in blue. The baseline model of AAA G&R is shown in red. The model of AAA G&R with 2x elastin production at 30% increase in baseline outer diameter is shown in green. Ratio of collagen to initial collagen is on the y-axis. Model simulation time is shown on the x-axis.

Description of collagen plot (Figure 46):

The homeostasis model (shown in blue) slowly adds collagen as elastin is slowly degraded. This addition helps to maintain the vessel geometry.

In the baseline (shown in red) and 2x elastin production (shown in green) models prior to the elastogenic intervention, there is a small step loss of collagen at the beginning of the model of ~3.5%. After the initial step loss, collagen continues to decrease in the media (due to a shift of stress from the media to the adventitia) before maintaining a constant level until approximately 8 years simulation time where accelerated removal due to higher tensions is balancing higher production rates due to higher stresses. After this point in the baseline model the increase in tension has become so large that collagen production is unable to compensate, and the collagen is removed again until the end of the simulation.

In the 2x elastin production model at the intervention time point, increasing elastin is associated with an increase in the amount of collagen produced. This is due to the elastin lowering the tension on the collagen and thus reducing the collagen decay constant. The system then returns to a balance between the removal of old collagen and the production of new collagen.

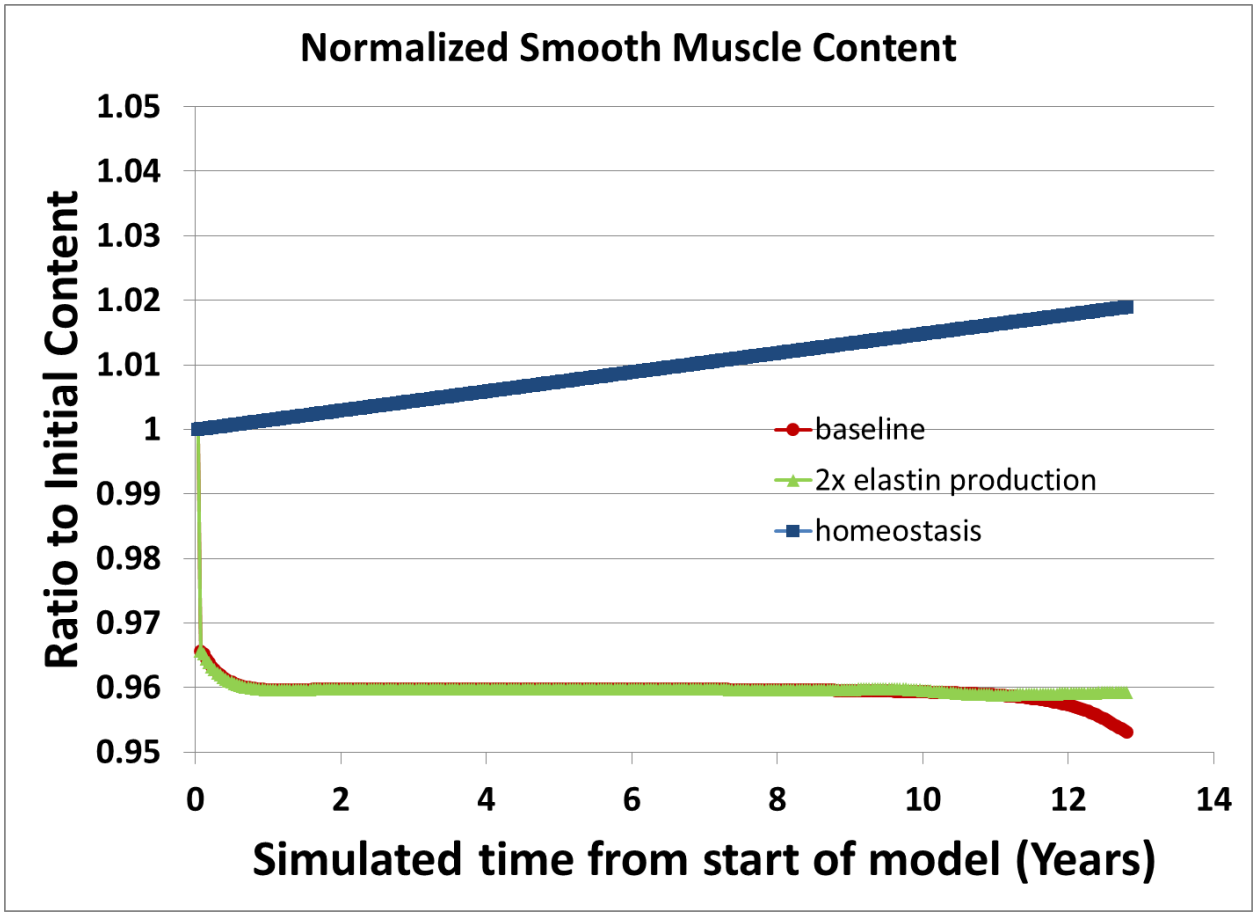

Figure 47. Medial ratio of remaining smooth muscle to initial smooth muscle within computation models of AAA G&R. The homeostatic model is shown in blue. The baseline model of AAA G&R is shown in red. The model of AAA G&R with 2x elastin production at 30% increase in baseline outer diameter is shown in green. Ratio of smooth muscle to initial smooth muscle is on the y-axis. Model simulation time is shown on the x-axis.

Description of smooth muscle plot (Figure 47):

The homeostasis model (shown in blue) slowly adds smooth muscle as elastin is slowly degraded. This addition helps to maintain the vessel geometry.

In the baseline (shown in red) and 2x elastin production (shown in green) models prior to the elastogenic intervention, there is a small step loss of smooth muscle at the beginning of the model of ~3.5%. After the initial step loss, smooth muscle continues to decrease in the media (due to a shift of stress from the media to the adventitia) before maintaining a constant level until approximately 10 years simulation time where accelerated removal due to higher tensions is balancing higher production rates due to higher stresses. After this point in the baseline model the increase in tension has become so large that smooth muscle production is unable to compensate, and the smooth muscle is removed again until the end of the simulation.

In the 2x elastin production model at the intervention time point, increasing elastin is associated with maintenance of the amount of smooth muscle. This is due to the elastin lowering the tension on the smooth muscle and thus reducing the smooth muscle decay constant. The system then returns to a balance between the removal of old smooth muscle and the production of new smooth muscle.

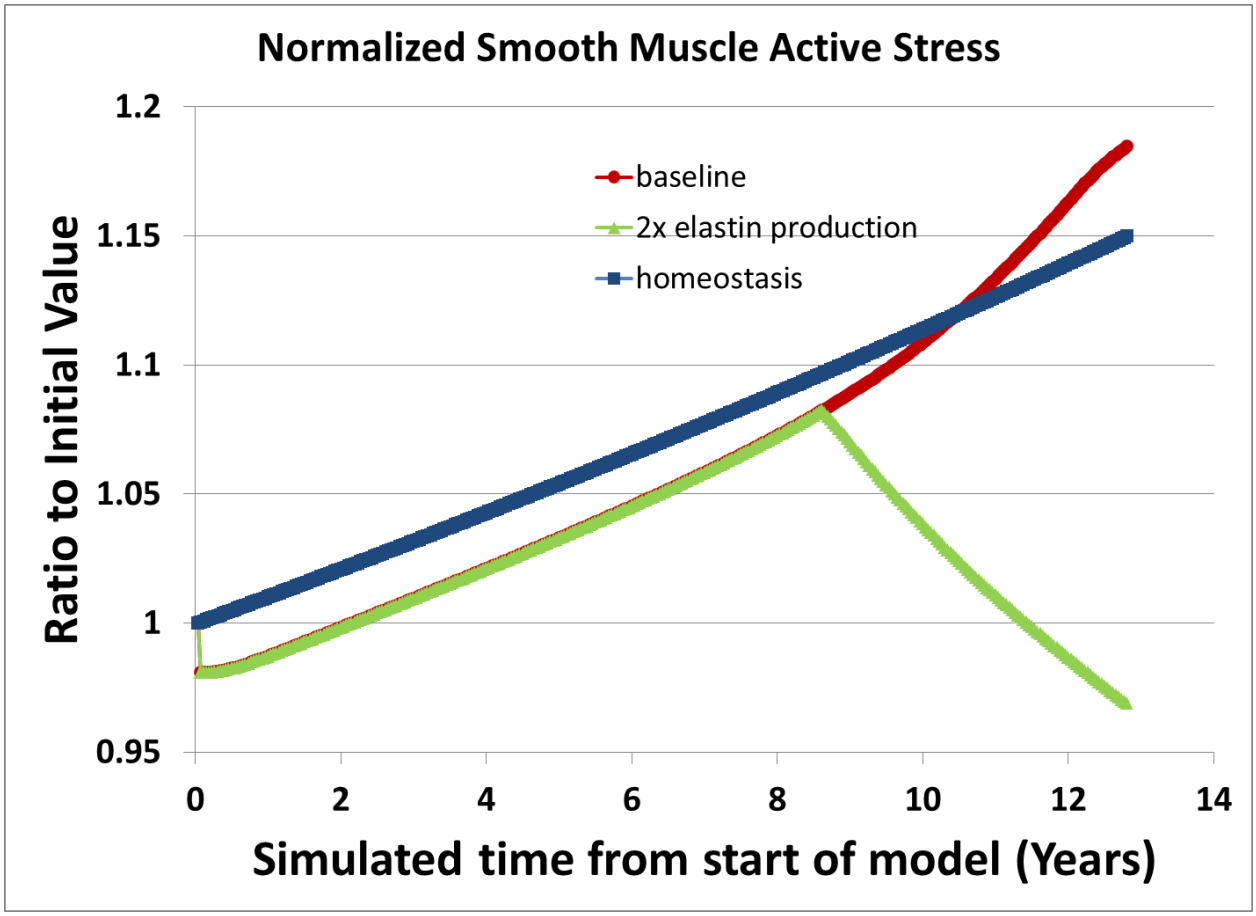

Figure 48. Medial ratio of smooth muscle active stress to initial smooth muscle active stress within computation models of AAA G&R. The homeostatic model is shown in blue. The baseline model of AAA G&R is shown in red. The model of AAA G&R with 2x elastin production at 30% increase in baseline outer diameter is shown in green. Ratio of smooth muscle active stress to initial smooth muscle active is on the y-axis. Model simulation time is shown on the x-axis.

Description of active stress plot (Figure 48):

The homeostasis model (shown in blue) shows slow increases in the level of active stress as elastin is slowly degraded, helping to maintain vessel geometry. The small loses of elastin at each time step within the model would normally result in a small increase in vessel diameter. Active stress is generated due to this small increase in vessel diameter which then works to decrease the diameter of the vessel. These small oscillations ultimately maintain that diameter for the model history.

In the baseline (shown in red) and 2x elastin production (shown in green) models prior to the elastogenic intervention, there is a small step loss in the level of active stress at the beginning of the model of which directly scales with the decrease in amount of smooth muscle. After the initial step loss, the level of active stress continues to slowly increase as elastin is slowly degraded. This increase is likely due to a shift in the relative proportion of smooth muscle in the system as the total elastin is decreasing in the system. In the later stages of the model, the active stress continues to rise as the diameter increases even though the amount of smooth muscle is decreasing.

In the 2x elastin production model at the intervention time point, increasing elastin is associated with a decrease in the amount of active stress. This decrease is due to the lower relative proportion of smooth muscle to the total amount of material in the system.

Discussion:

The G&R models represent a balance between competing biomechanical forces. Within the AAA G&R baseline model, we have the competition of accelerated removal of constituents due to higher tensions, the production of constituents due to the higher stresses, and the generation of active stress from smooth muscle. The loss of elastin initiates a complex G&R sequence, resulting in luminal expansion and wall thinning. This is due to the loss of highly prestretched elastin, coupled with a diminished ability to actively maintain inner radius. The accelerated constituent removal due to ever increasing tensions ultimately overcomes the constituent production due to higher stresses.

In the experimental 2x elastin production model, adding back highly prestretched elastin lowers the tension that the collagen and smooth muscle are under while also lowering the stress which increases the amount of both collagen and smooth muscle in the system while lowering the active stress generated by smooth muscle. The macroscopic result of introducing new elastin is a lower luminal expansion rate.

APPENDIX C

QUALITATIVE FIBRIN GEL MIXER ASSESMENT

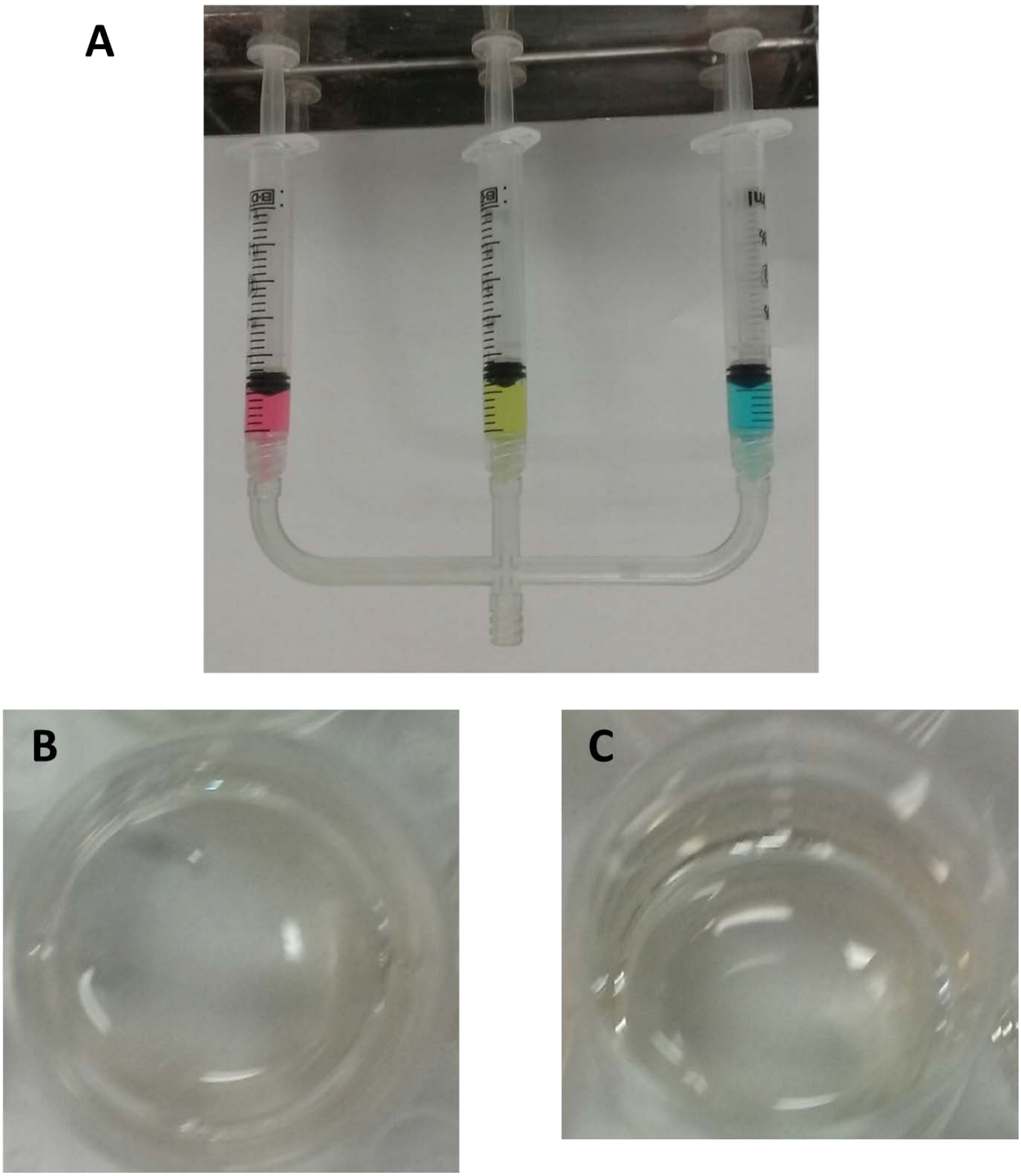

Figure 49. Mixing colored fibrin gel constituent solutions through the fibrin gel mixer produces gels that appear similar in color to a gel mixed by manual pipetting. A) Fibrin gel constituent components loaded into a syringe and locked in the fibrin gel mixer. From left to right, the constituents are fibrinogen solution (pink), cell suspension (yellow), and thrombin solution (blue). B) Photo of a gel mixed with manual pipetting. C) Photo of gel that came out of the fibrin gel mixer.

BIBLIOGRAPHY

1. Boddy AM, Lenk GM, Lillvis JH, Nischan J, Kyo Y, Kuivaniemi H. Basic research studies to understand aneurysm disease. Drug News and Perspectives. 2008;21(3):142-8.

2. Bashur CA, Rao RR, Ramamurthi A. Perspectives on Stem Cell-Based Elastic Matrix Regenerative Therapies for Abdominal Aortic Aneurysms. Stem cells translational medicine. 2013;2(6):401-8.

3. McGregor J, Pollock J, Anton H. The value of ultrasonography in the diagnosis of abdominal aortic aneurysm. Scottish medical journal. 1975;20(3):133-7.

4. Johnston KW, Rutherford RB, Tilson MD, Shah DM, Hollier L, Stanley JC. Suggested standards for reporting on arterial aneurysms. Journal of vascular surgery. 1991;13(3):452-8.

5. Ernst CB. Abdominal aortic aneurysm. New England Journal of Medicine. 1993;328(16):1167-72.

6. Sakalihasan N, Limet R, Defawe O. Abdominal aortic aneurysm. The Lancet. 2005;365(9470):1577-89.

7. Nevitt MP, Ballard DJ, Hallett Jr JW. Prognosis of abdominal aortic aneurysms. New England Journal of Medicine. 1989;321(15):1009-14.

8. Alcorn HG, Wolfson SK, Sutton-Tyrrell K, Kuller LH, O'Leary D. Risk factors for abdominal aortic aneurysms in older adults enrolled in The Cardiovascular Health Study. Arteriosclerosis, thrombosis, and vascular biology. 1996;16(8):963-70.

9. Brady AR, Thompson SG, Fowkes FGR, Greenhalgh RM, Powell JT. Abdominal aortic aneurysm expansion risk factors and time intervals for surveillance. Circulation. 2004;110(1):16-21.

10. Judge DP, Dietz HC. Marfan's syndrome. The Lancet. 2005;366(9501):1965-76.

11. Loeys BL, Schwarze U, Holm T, Callewaert BL, Thomas GH, Pannu H, et al. Aneurysm syndromes caused by mutations in the TGF-β receptor. New England Journal of Medicine. 2006;355(8):788-98.

12. Pepin M, Schwarze U, Superti-Furga A, Byers PH. Clinical and genetic features of Ehlers–Danlos syndrome type IV, the vascular type. New England Journal of Medicine. 2000;342(10):673-80.

13. Lin AE, Lippe BM, Geffner ME, Gomes A, Lois JF, Barton CW, et al. Aortic dilation, dissection, and rupture in patients with Turner syndrome. The Journal of pediatrics. 1986;109(5):820-6.

14. Edwards W, Leaf D, Edwards J. Dissecting aortic aneurysm associated with congenital bicuspid aortic valve. Circulation. 1978;57(5):1022-5.

15. Jarrett F, Darling RC, Mundth ED, Austen WG. Experience with infected aneurysms of the abdominal aorta. Archives of Surgery. 1975;110(11):1281-6.

16. Hellmann DB, Grand DJ, Freischlag JA. Inflammatory abdominal aortic aneurysm. Jama. 2007;297(4):395-400.

17. Shimizu K, Mitchell RN, Libby P. Inflammation and cellular immune responses in abdominal aortic aneurysms. Arteriosclerosis, thrombosis, and vascular biology. 2006;26(5):987-94.

18. PARMLEY LF, MATTINGLY TW, MANION WC, JAHNKE EJ. Nonpenetrating traumatic injury of the aorta. Circulation. 1958;17(6):1086-101.

19. Standring S. Gray\'s Anatomy: The Anatomical Basis of Clinical Practice2008.

20. Lacolley P, Regnault V, Nicoletti A, Li Z, Michel J-B. The vascular smooth muscle cell in arterial pathology: a cell that can take on multiple roles. Cardiovascular research. 2012;95(2):194-204.

21. Owens GK, Kumar MS, Wamhoff BR. Molecular regulation of vascular smooth muscle cell differentiation in development and disease. Physiological Reviews. 2004;84(3):767-801.

22. Valentin A, Humphrey J. Evaluation of fundamental hypotheses underlying constrained mixture models of arterial growth and remodelling. Philosophical Transactions of the Royal Society of London A: Mathematical, Physical and Engineering Sciences. 2009;367(1902):3585-606.

23. Valentín A, Humphrey J. Parameter sensitivity study of a constrained mixture model of arterial growth and remodeling. Journal of biomechanical engineering. 2009;131(10):101006.

24. Valentín A, Humphrey J, Holzapfel GA. A multi-layered computational model of coupled elastin degradation, vasoactive dysfunction, and collagenous stiffening in aortic aging. Annals of Biomedical Engineering. 2011;39(7):2027-45.

25. Valentín A, Humphrey J, Holzapfel GA. A finite element-based constrained mixture implementation for arterial growth, remodeling, and adaptation: Theory and numerical

verification. International journal for numerical methods in biomedical engineering. 2013;29(8):822-49.

26. Ailawadi G, Moehle CW, Pei H, Walton SP, Yang Z, Kron IL, et al. Smooth muscle phenotypic modulation is an early event in aortic aneurysms. The Journal of thoracic and cardiovascular surgery. 2009;138(6):1392-9.

27. Bunton TE, Biery NJ, Myers L, Gayraud B, Ramirez F, Dietz HC. Phenotypic alteration of vascular smooth muscle cells precedes elastolysis in a mouse model of Marfan syndrome. Circulation research. 2001;88(1):37-43.

28. Liao S, Curci JA, Kelley BJ, Sicard GA, Thompson RW. Accelerated replicative senescence of medial smooth muscle cells derived from abdominal aortic aneurysms compared to the adjacent inferior mesenteric artery. J Surg Res. 2000;92(1):85-95. Epub 2000/06/23. doi: 10.1006/jsre.2000.5878. PubMed PMID: 10864487.

29. Starke RM, Chalouhi N, Ding D, Raper DM, Mckisic MS, Owens GK, et al. Vascular smooth muscle cells in cerebral aneurysm pathogenesis. Translational stroke research. 2014;5(3):338-46.

30. Rzucidlo EM, Martin KA, Powell RJ. Regulation of vascular smooth muscle cell differentiation. Journal of Vascular Surgery. 2007;45(6):A25-A32.

31. Rudijanto A. The role of vascular smooth muscle cells on the pathogenesis of atherosclerosis. Acta Med Indones. 2007;39(2):86-93.

32. Gomez D, Owens GK. Smooth muscle cell phenotypic switching in atherosclerosis. Cardiovascular research. 2012:cvs115.

33. Herring BP, Hoggatt AM, Burlak C, Offermanns S. Previously differentiated medial vascular smooth muscle cells contribute to neointima formation following vascular injury. Vascular cell. 2014;6(1):1-14.

34. Nguyen AT, Gomez D, Bell RD, Campbell JH, Clowes AW, Gabbiani G, et al. Smooth Muscle Cell Plasticity Fact or Fiction? Circulation Research. 2013;112(1):17-22.

35. Rensen S, Doevendans P, Van Eys G. Regulation and characteristics of vascular smooth muscle cell phenotypic diversity. Netherlands Heart Journal. 2007;15(3):100-8.

36. Beamish JA, He P, Kottke-Marchant K, Marchant RE. Molecular regulation of contractile smooth muscle cell phenotype: implications for vascular tissue engineering. Tissue Engineering Part B: Reviews. 2010;16(5):467-91.

37. McDaniel DP, Shaw GA, Elliott JT, Bhadriraju K, Meuse C, Chung K-H, et al. The stiffness of collagen fibrils influences vascular smooth muscle cell phenotype. Biophysical Journal. 2007;92(5):1759-69.

38. Henderson EL, Geng YJ, Sukhova GK, Whittemore AD, Knox J, Libby P. Death of smooth muscle cells and expression of mediators of apoptosis by T lymphocytes in human abdominal aortic aneurysms. Circulation. 1999;99(1):96-104. Epub 1999/01/13. PubMed PMID: 9884385.

39. Holmes DR, Lopez-Candales A, Liao S, Thompson RW. Smooth muscle cell apoptosis and p53 expression in human abdominal aortic aneurysms. Ann N Y Acad Sci. 1996;800:286-7. Epub 1996/11/18. PubMed PMID: 8959016.

40. Jacob T, Hingorani A, Ascher E. Examination of the apoptotic pathway and proteolysis in the pathogenesis of popliteal artery aneurysms. European journal of vascular and endovascular surgery : the official journal of the European Society for Vascular Surgery. 2001;22(1):77-85. Epub 2001/07/20. doi: 10.1053/ejvs.2001.1344. PubMed PMID: 11461108.

41. Lopez-Candales A, Holmes DR, Liao S, Scott MJ, Wickline SA, Thompson RW. Decreased vascular smooth muscle cell density in medial degeneration of human abdominal aortic aneurysms. The American journal of pathology. 1997;150(3):993-1007. Epub 1997/03/01. PubMed PMID: 9060837; PubMed Central PMCID: PMC1857880.

42. Thompson RW, Liao S, Curci JA. Vascular smooth muscle cell apoptosis in abdominal aortic aneurysms. Coronary artery disease. 1997;8(10):623-31. Epub 1998/02/11. PubMed PMID: 9457444.

43. Mao D, Lee JK, VanVickle SJ, Thompson RW. Expression of collagenase-3 (MMP-13) in human abdominal aortic aneurysms and vascular smooth muscle cells in culture. Biochemical and biophysical research communications. 1999;261(3):904-10.

44. Airhart N, Brownstein BH, Cobb JP, Schierding W, Arif B, Ennis TL, et al. Smooth muscle cells from abdominal aortic aneurysms are unique and can independently and synergistically degrade insoluble elastin. J Vasc Surg. 2013.

45. Nivison-Smith L, Weiss A. Elastin based constructs: INTECH Open Access Publisher; 2011.

46. Kielty CM, Sherratt MJ, Shuttleworth CA. Elastic fibres. Journal of Cell Science. 2002;115(14):2817-28.

47. Kelleher CM, McLean SE, Mecham RP. Vascular extracellular matrix and aortic development. Current Topics in Developmental Biology. 2004;62:153-88.

48. Wagenseil JE, Mecham RP. Vascular extracellular matrix and arterial mechanics. Physiological Reviews. 2009;89(3):957-89.

49. Humphrey J, Holzapfel GA. Mechanics, mechanobiology, and modeling of human abdominal aorta and aneurysms. Journal of biomechanics. 2012;45(5):805-14.

50. Davis EC. Stability of elastin in the developing mouse aorta: a quantitative radioautographic study. Histochemistry. 1993;100(1):17-26.

51. Mithieux SM, Weiss AS. In Vivo Synthesis of Elastic Fiber. Google Patents; 2012.

52. Baxter BT, McGee GS, Shively VP, Drummond IA, Dixit SN, Yamauchi M, et al. Elastin content, cross-links, and mRNA in normal and aneurysmal human aorta. Journal of vascular surgery. 1992;16(2):192-200.

53. Campa J, Greenhalgh R, Powell JT. Elastin degradation in abdominal aortic aneurysms. Atherosclerosis. 1987;65(1):13-21.

54. Shapiro SD, Endicott SK, Province MA, Pierce JA, Campbell EJ. Marked longevity of human lung parenchymal elastic fibers deduced from prevalence of D-aspartate and nuclear weapons-related radiocarbon. The Journal of clinical investigation. 1991;87(5):1828-34. Epub 1991/05/01. doi: 10.1172/JCI115204. PubMed PMID: 2022748; PubMed Central PMCID: PMC295305.

55. Tamarina NA, McMillan WD, Shively VP, Pearce WH. Expression of matrix metalloproteinases and their inhibitors in aneurysms and normal aorta. Surgery. 1997;122(2):264-72.

56. Wilson WRW, Anderton M, Schwalbe EC, Jones JL, Furness PN, Bell PR, et al. Matrix metalloproteinase-8 and-9 are increased at the site of abdominal aortic aneurysm rupture. Circulation. 2006;113(3):438-45.

57. Annabi B, Shedid D, Ghosn P, Kenigsberg RL, Desrosiers RR, Bojanowski MW, et al. Differential regulation of matrix metalloproteinase activities in abdominal aortic aneurysms. J Vasc Surg. 2002;35(3):539-46. Epub 2002/03/06. PubMed PMID: 11877705.

58. Carrell TW, Burnand KG, Wells GM, Clements JM, Smith A. Stromelysin-1 (matrix metalloproteinase-3) and tissue inhibitor of metalloproteinase-3 are overexpressed in the wall of abdominal aortic aneurysms. Circulation. 2002;105(4):477-82. Epub 2002/01/30. PubMed PMID: 11815431.

59. Curci JA, Liao S, Huffman MD, Shapiro SD, Thompson RW. Expression and localization of macrophage elastase (matrix metalloproteinase-12) in abdominal aortic aneurysms. The Journal of clinical investigation. 1998;102(11):1900-10. Epub 1998/12/03. doi: 10.1172/JCI2182. PubMed PMID: 9835614; PubMed Central PMCID: PMC509141.

60. Elmore JR, Keister BF, Franklin DP, Youkey JR, Carey DJ. Expression of matrix metalloproteinases and TIMPs in human abdominal aortic aneurysms. Annals of vascular surgery. 1998;12(3):221-8. Epub 1998/05/20. PubMed PMID: 9588507.

61. Fontaine V, Jacob MP, Houard X, Rossignol P, Plissonnier D, Angles-Cano E, et al. Involvement of the mural thrombus as a site of protease release and activation in human aortic aneurysms. The American journal of pathology. 2002;161(5):1701-10. Epub 2002/11/05. doi: 10.1016/S0002-9440(10)64447-1. PubMed PMID: 12414517; PubMed Central PMCID: PMC1850780.

62. Higashikata T, Yamagishi M, Sasaki H, Minatoya K, Ogino H, Ishibashi-Ueda H, et al. Application of real-time RT-PCR to quantifying gene expression of matrix metalloproteinases and tissue inhibitors of metalloproteinases in human abdominal aortic aneurysm. Atherosclerosis. 2004;177(2):353-60. Epub 2004/11/09. doi: 10.1016/j.atherosclerosis.2004.07.013. PubMed PMID: 15530910.

63. Hovsepian DM, Ziporin SJ, Sakurai MK, Lee JK, Curci JA, Thompson RW. Elevated plasma levels of matrix metalloproteinase-9 in patients with abdominal aortic aneurysms: a circulating marker of degenerative aneurysm disease. Journal of vascular and interventional radiology : JVIR. 2000;11(10):1345-52. Epub 2000/12/01. PubMed PMID: 11099248.

64. McMillan WD, Patterson BK, Keen RR, Pearce WH. In situ localization and quantification of seventy-two-kilodalton type IV collagenase in aneurysmal, occlusive, and normal aorta. J Vasc Surg. 1995;22(3):295-305. Epub 1995/09/01. PubMed PMID: 7674473.

65. McMillan WD, Patterson BK, Keen RR, Shively VP, Cipollone M, Pearce WH. In situ localization and quantification of mRNA for 92-kD type IV collagenase and its inhibitor in aneurysmal, occlusive, and normal aorta. Arterioscler Thromb Vasc Biol. 1995;15(8):1139-44. Epub 1995/08/01. PubMed PMID: 7627707.

66. Thompson R, Holmes D, Mertens R, Liao S, Botney M, Mecham R, et al. Production and localization of 92-kilodalton gelatinase in abdominal aortic aneurysms. An elastolytic metalloproteinase expressed by aneurysm-infiltrating macrophages. Journal of Clinical Investigation. 1995;96(1):318.

67. Gacko M, Glowinski S. Cathepsin D and cathepsin L activities in aortic aneurysm wall and parietal thrombus. Clinical chemistry and laboratory medicine : CCLM / FESCC. 1998;36(7):449-52. Epub 1998/09/24. doi: 10.1515/CCLM.1998.075. PubMed PMID: 9746268.

68. Sukhova GK, Shi GP. Do cathepsins play a role in abdominal aortic aneurysm pathogenesis? Ann N Y Acad Sci. 2006;1085:161-9. Epub 2006/12/22. doi: 10.1196/annals.1383.028. PubMed PMID: 17182932.

69. Colonnello JS, Hance KA, Shames ML, Wyble CW, Ziporin SJ, Leidenfrost JE, et al. Transient exposure to elastase induces mouse aortic wall smooth muscle cell production of MCP-1 and RANTES during development of experimental aortic aneurysm. J Vasc Surg. 2003;38(1):138-46. Epub 2003/07/05. PubMed PMID: 12844103.

70. Houard X, Touat Z, Ollivier V, Louedec L, Philippe M, Sebbag U, et al. Mediators of neutrophil recruitment in human abdominal aortic aneurysms. Cardiovascular research. 2009;82(3):532-41. Epub 2009/02/10. doi: 10.1093/cvr/cvp048. PubMed PMID: 19201759; PubMed Central PMCID: PMC2682614.

71. Lindeman JH, Abdul-Hussien H, van Bockel JH, Wolterbeek R, Kleemann R. Clinical trial of doxycycline for matrix metalloproteinase-9 inhibition in patients with an abdominal aneurysm: doxycycline selectively depletes aortic wall neutrophils and cytotoxic T cells. Circulation. 2009;119(16):2209-16. Epub 2009/04/15. doi: 10.1161/CIRCULATIONAHA.108.806505. PubMed PMID: 19364980.

72. Lindholt JS, Erlandsen EJ, Henneberg EW. Cystatin C deficiency is associated with the progression of small abdominal aortic aneurysms. The British journal of surgery. 2001;88(11):1472-5. Epub 2001/10/31. doi: 10.1046/j.0007-1323.2001.01911.x. PubMed PMID: 11683743.

73. Longo GM, Xiong W, Greiner TC, Zhao Y, Fiotti N, Baxter BT. Matrix metalloproteinases 2 and 9 work in concert to produce aortic aneurysms. The Journal of clinical investigation. 2002;110(5):625-32. Epub 2002/09/05. doi: 10.1172/JCI15334. PubMed PMID: 12208863; PubMed Central PMCID: PMC151106.

74. Pagano MB, Bartoli MA, Ennis TL, Mao D, Simmons PM, Thompson RW, et al. Critical role of dipeptidyl peptidase I in neutrophil recruitment during the development of experimental abdominal aortic aneurysms. Proceedings of the National Academy of Sciences of the United States of America. 2007;104(8):2855-60. Epub 2007/02/16. doi: 10.1073/pnas.0606091104. PubMed PMID: 17301245; PubMed Central PMCID: PMC1797622.

75. Pagano MB, Zhou HF, Ennis TL, Wu X, Lambris JD, Atkinson JP, et al. Complement-dependent neutrophil recruitment is critical for the development of elastase-induced abdominal aortic aneurysm. Circulation. 2009;119(13):1805-13. Epub 2009/03/25. doi: 10.1161/CIRCULATIONAHA.108.832972. PubMed PMID: 19307471; PubMed Central PMCID: PMC2758616.

76. Pyo R, Lee JK, Shipley JM, Curci JA, Mao D, Ziporin SJ, et al. Targeted gene disruption of matrix metalloproteinase-9 (gelatinase B) suppresses development of experimental abdominal aortic aneurysms. Journal of Clinical Investigation. 2000;105(11):1641-9.

77. Shi GP, Sukhova GK, Grubb A, Ducharme A, Rhode LH, Lee RT, et al. Cystatin C deficiency in human atherosclerosis and aortic aneurysms. The Journal of clinical investigation. 1999;104(9):1191-7. Epub 1999/11/05. doi: 10.1172/JCI7709. PubMed PMID: 10545518; PubMed Central PMCID: PMC409823.

78. Cohen J, Sarfati I, Danna D, Wise L. Smooth muscle cell elastase, atherosclerosis, and abdominal aortic aneurysms. Annals of surgery. 1992;216(3):327.

79. Sinha A, Vyavahare NR. High-glucose levels and elastin degradation products accelerate osteogenesis in vascular smooth muscle cells. Diabetes and Vascular Disease Research. 2013:1479164113485101.

80. Di Lullo GA, Sweeney SM, Körkkö J, Ala-Kokko L, San Antonio JD. Mapping the ligand-binding sites and disease-associated mutations on the most abundant protein in the human, type I collagen. Journal of Biological Chemistry. 2002;277(6):4223-31.

81. Menashi S, Campa JS, Greenhalgh RM, Powell JT. Collagen in abdominal aortic aneurysm: typing, content, and degradation. Journal of vascular surgery. 1987;6(6):578-82.

82. Shingleton W, Cawston T, Hodges D, Brick P. Collagenase: a key enzyme in collagen turnover. Biochemistry and cell biology. 1996;74(6):759-75.

83. Abdul-Hussien H, Soekhoe RG, Weber E, Jan H, Kleemann R, Mulder A, et al. Collagen degradation in the abdominal aneurysm: a conspiracy of matrix metalloproteinase and cysteine collagenases. The American journal of pathology. 2007;170(3):809-17.

84. He CM, Roach MR. The composition and mechanical properties of abdominal aortic aneurysms. Journal of vascular surgery. 1994;20(1):6-13.

85. Rizzo RJ, McCarthy WJ, Dixit SN, Lilly MP, Shively VP, Flinn WR, et al. Collagen types and matrix protein content in human abdominal aortic aneurysms. Journal of vascular surgery. 1989;10(4):365-73.

86. Satta J, Juvonen T, Haukipuro K, Juvonen M, Kairaluoma MI. Increased turnover of collagen in abdominal aortic aneurysms, demonstrated by measuring the concentration of the aminoterminal propeptide of type III procollagen in peripheral and aortal blood samples. Journal of vascular surgery. 1995;22(2):155-60.

87. Carmo M, Colombo L, Bruno A, Corsi F, Roncoroni L, Cuttin M, et al. Alteration of elastin, collagen and their cross-links in abdominal aortic aneurysms. European journal of vascular and endovascular surgery. 2002;23(6):543-9.

88. Dorbin P. Pathophysiology and pathogenesis of aortic aneurysms. Surg Clin of N Amer. 1989;69:689-703.

89. Vorp DA, Raghavan M, Muluk SC, Makaroun MS, Steed DL, Shapiro R, et al. Wall strength and stiffness of aneurysmal and nonaneurysmal abdominal aorta. Annals of the New York Academy of Sciences. 1996;800(1):274-6.

90. Raghavan M, Vorp DA, Federle MP, Makaroun MS, Webster MW. Wall stress distribution on three-dimensionally reconstructed models of human abdominal aortic aneurysm. Journal of vascular surgery. 2000;31(4):760-9.

91. Vorp DA, Raghavan M, Webster MW. Mechanical wall stress in abdominal aortic aneurysm: influence of diameter and asymmetry. Journal of Vascular Surgery. 1998;27(4):632-9.

92. Vande Geest JP, Sacks MS, Vorp DA. The effects of aneurysm on the biaxial mechanical behavior of human abdominal aorta. Journal of biomechanics. 2006;39(7):1324-34.

93. Di Martino ES, Bohra A, Geest JPV, Gupta N, Makaroun MS, Vorp DA. Biomechanical properties of ruptured versus electively repaired abdominal aortic aneurysm wall tissue. Journal of Vascular Surgery. 2006;43(3):570-6.

94. Vorp DA, Geest JPV. Biomechanical determinants of abdominal aortic aneurysm rupture. Arteriosclerosis, thrombosis, and vascular biology. 2005;25(8):1558-66.

95. Wang DH, Makaroun MS, Webster MW, Vorp DA. Effect of intraluminal thrombus on wall stress in patient-specific models of abdominal aortic aneurysm. Journal of Vascular Surgery. 2002;36(3):598-604.

96. Virag L, Wilson JS, Humphrey JD, Karšaj I. A Computational Model of Biochemomechanical Effects of Intraluminal Thrombus on the Enlargement of Abdominal Aortic Aneurysms. Annals of biomedical engineering. 2015;43(12):2852-67.

97. Vorp D, Mandarino W, Webster M, Gorcsan J. Potential influence of intraluminal thrombus on abdominal aortic aneurysm as assessed by a new non-invasive method. Vascular. 1996;4(6):732-9.

98. Vorp D, Wang D, Webster M, Federspiel W. Effect of intraluminal thrombus thickness and bulge diameter on the oxygen diffusion in abdominal aortic aneurysm. Journal of biomechanical engineering. 1998;120(5):579-83.

99. VANDE GEEST JP, Di Martino ES, Bohra A, Makaroun MS, Vorp DA. A Biomechanics-Based Rupture Potential Index for Abdominal Aortic Aneurysm Risk Assessment. Annals of the New York Academy of Sciences. 2006;1085(1):11-21.

100. Dooley A, Gao B, Shi-Wen X, Abraham DJ, Black CM, Jacobs M, et al. Effect of nitric oxide and peroxynitrite on type I collagen synthesis in normal and scleroderma dermal fibroblasts. Free Radical Biology and Medicine. 2007;43(2):253-64.

101. Leung D, Glagov S, Mathews MB. Cyclic stretching stimulates synthesis of matrix components by arterial smooth muscle cells in vitro. Science. 1976;191(4226):475-7.

102. Li Q, Muragaki Y, Hatamura I, Ueno H, Ooshima A. Stretch-induced collagen synthesis in cultured smooth muscle cells from rabbit aortic media and a possible involvement of angiotensin II and transforming growth factor-β. Journal of vascular research. 1998;35(2):93-103.

103. Rizvi MA, Myers PR. Nitric oxide modulates basal and endothelin-induced coronary artery vascular smooth muscle cell proliferation and collagen levels. Journal of molecular and cellular cardiology. 1997;29(7):1779-89.

104. Fung Y. What are the residual stresses doing in our blood vessels? Annals of biomedical engineering. 1991;19(3):237-49.

105. Thoma R. Untersuchungen über die Histogenese und Histomechanik des Gefäßsystems: Enke; 1893.

106. Driessen N, Wilson W, Bouten C, Baaijens F. A computational model for collagen fibre remodelling in the arterial wall. Journal of theoretical biology. 2004;226(1):53-64.

107. Hariton I, Gasser T, Holzapfel G. Stress-driven collagen fiber remodeling in arterial walls. Biomech Model Mechanobiol. 2007;6(3):163-75.

108. Wolinsky H, Glagov S. Comparison of abdominal and thoracic aortic medial structure in mammals. Circulation Research. 1969;25(6):677-86.

109. Crowther M, Goodall S, Jones J, Bell P, Thompson M. Localization of matrix metalloproteinase 2 within the aneurysmal and normal aortic wall. British journal of surgery. 2000;87(10):1391-400.

110. Herron GS, Unemori E, Wong M, Rapp JH, Hibbs MH, Stoney RJ. Connective tissue proteinases and inhibitors in abdominal aortic aneurysms. Involvement of the vasa vasorum in the pathogenesis of aortic aneurysms. Arteriosclerosis, Thrombosis, and Vascular Biology. 1991;11(6):1667-77.

111. Saito S, Zempo N, Yamashita A, Takenaka H, Fujioka K, Esato K. Matrix metalloproteinase expressions in arteriosclerotic aneurysmal disease. Vascular and endovascular surgery. 2002;36(1):1-7.

112. Holmes DR, Liao S, Parks WC, Hompson RW. Medial neovascularization in abdominal aortic aneurysms: a histopathologic marker of aneurysmal degeneration with pathophysiologic implications. Journal of vascular surgery. 1995;21(5):761-72.

113. Harter L, Gross B, Callen P, Barth R. Ultrasonic evaluation of abdominal aortic thrombus. Journal of Ultrasound in Medicine. 1982;1(8):315-8.

114. Phillippi JA, Pasta S, Vorp DA. Biomechanics and pathobiology of aortic aneurysms. Biomechanics and Mechanobiology of Aneurysms: Springer; 2011. p. 67-118.

115. Brophy CM, Marks WH, Reilly JM, Tilson MD. Decreased tissue inhibitor of metalloproteinases (TIMP) in abdominal aortic aneurysm tissue: a preliminary report. Journal of Surgical Research. 1991;50(6):653-7.

116. Mozaffarian D, Benjamin EJ, Go AS, Arnett DK, Blaha MJ, Cushman M, et al. Heart disease and stroke statistics--2015 update: A report from the American Heart Association. Circulation. 2015;131(4):e29.

117. De Bruin JL, Baas AF, Buth J, Prinssen M, Verhoeven EL, Cuypers PW, et al. Long-term outcome of open or endovascular repair of abdominal aortic aneurysm. New England Journal of Medicine. 2010;362(20):1881-9.

118. Greenhalgh RM, Forbes JF, Fowkes FG, Powel JT, Ruckley CV, Brady AR, et al. Early elective open surgical repair of small abdominal aortic aneurysms is not recommended: results of the UK Small Aneurysm Trial. Steering Committee. European journal of vascular and endovascular surgery : the official journal of the European Society for Vascular Surgery. 1998;16(6):462-4. Epub 1999/01/23. PubMed PMID: 9894483.

119. Lederle F, Stroupe K, Group OVERVACS. Cost–effectiveness at two years in the VA open versus endovascular repair trial. European Journal of Vascular and Endovascular Surgery. 2012;44(6):543-8.

120. Bartoli MA, Parodi FE, Chu J, Pagano MB, Mao D, Baxter BT, et al. Localized administration of doxycycline suppresses aortic dilatation in an experimental mouse model of

abdominal aortic aneurysm. Annals of vascular surgery. 2006;20(2):228-36. Epub 2006/03/31. doi: 10.1007/s10016-006-9017-z. PubMed PMID: 16572291.

121. Curci JA, Petrinec D, Liao S, Golub LM, Thompson RW. Pharmacologic suppression of experimental abdominal aortic aneurysms: a comparison of doxycycline and four chemically modified tetracyclines. J Vasc Surg. 1998;28(6):1082-93.

122. Holmes DR, Petrinec D, Wester W, Thompson RW, Reilly JM. Indomethacin prevents elastase-induced abdominal aortic aneurysms in the rat. Journal of Surgical Research. 1996;63(1):305-9.

123. Petrinec D, Liao S, Holmes DR, Reilly JM, Parks WC, Thompson RW. Doxycycline inhibition of aneurysmal degeneration in an elastase-induced rat model of abdominal aortic aneurysm: preservation of aortic elastin associated with suppressed production of 92 kD gelatinase. Journal of vascular surgery. 1996;23(2):336-46.

124. Ricci MA, Strindberg G, Slaiby JM, Guibord R, Bergersen LJ, Nichols P, et al. Anti-CD 18 monoclonal antibody slows experimental aortic aneurysm expansion. Journal of vascular surgery. 1996;23(2):301-7.

125. Shah PK. Inflammation, Metalloproteinases, and Increased Proteolysis An Emerging Pathophysiological Paradigm in Aortic Aneurysm. Circulation. 1997;96(7):2115-7.

126. Baxter BT, Matsumura J, Curci J, McBride R, Blackwelder WC, Liu X, et al. Non-invasive Treatment of Abdominal Aortic Aneurysm Clinical Trial (N-TA 3 CT): Design of a Phase IIb, placebo-controlled, double-blind, randomized clinical trial of doxycycline for the reduction of growth of small abdominal aortic aneurysm. Contemporary clinical trials. 2016;48:91-8.

127. Hallisey MJ. A transluminally created abdominal aortic aneurysm model. Journal of vascular and interventional radiology. 1997;8(3):305-12.

128. Strindberg G, Nichols P, Ricci MA, Marinov G, Marois Y, Roby P, et al. Experimental modifications to a canine infrarenal aortic aneurysm model for the validation of endovascular stent-grafts: an exploratory study. Investigative Surgery. 1998;11(3):185-97.

129. Chen M, Murphy EA, Levison J, Cohen JR. Laparoscopic aortic replacement in the porcine model: a feasibility study in preparation for laparoscopically assisted abdominal aortic aneurysm repair in humans. Journal of the American College of Surgeons. 1996;183(2):126-32.

130. Jordan Jr WD, Sampson LK, Iyer S, Anderson PG. Abdominal aortic aneurysm repair via percutaneous endovascular stenting in the swine model. The American Surgeon. 1998;64(11):1070.

131. Milner R, Ruurda JP, Blankensteijn JD. Durability and validity of a remote, miniaturized pressure sensor in an animal model of abdominal aortic aneurysm. Journal of Endovascular Therapy. 2004;11(4):372-7.

132. Ruiz CE, Zhang HP, Butt AI, Whittaker P. Percutaneous Treatment of Abdominal Aortic Aneurysm in a Swine Model Understanding the Behavior of Aortic Aneurysm Closure Through a Serial Histopathological Analysis. Circulation. 1997;96(7):2438-48.

133. Turnbull IC, Hadri L, Rapti K, Sadek M, Liang L, Shin HJ, et al. Aortic implantation of mesenchymal stem cells after aneurysm injury in a porcine model. The Journal of surgical research. 2011;170(1):e179.

134. Uflacker R, Brothers T. Filling of the aneurysmal sac with DEAC-glucosamine in an animal model of abdominal aortic aneurysm following stent-graft repair. Journal of Cardiovascular Surgery. 2006;47(4):425.

135. Beygui RE, Kinney EV, Pelc LR, Krievins D, Whittemore J, Fogarty TJ, et al. Prevention of spinal cord ischemia in an ovine model of abdominal aortic aneurysm treated with a self-expanding stent-graft. Journal of Endovascular Therapy. 1999;6(3):278-84.

136. Schoder M, Pavcnik D, Uchida BT, Corless C, Timmermans HA, Yin Q, et al. Small intestinal submucosa aneurysm sac embolization for endoleak prevention after abdominal aortic aneurysm endografting: a pilot study in sheep. Journal of vascular and interventional radiology. 2004;15(1):69-83.

137. Yamada K, Pavcnik D, Uchida BT, Timmermans HA, Corless CL, Yin Q, et al. Endoluminal treatment of ruptured abdominal aortic aneurysm with small intestinal submucosa sandwich endografts: a pilot study in sheep. Cardiovascular and interventional radiology. 2001;24(2):99-105.

138. Gresham G, Howard A. Aortic rupture in the turkey. Journal of atherosclerosis research. 1961;1(1):75-80.

139. Bergoeing MP, Arif B, Hackmann AE, Ennis TL, Thompson RW, Curci JA. Cigarette smoking increases aortic dilatation without affecting matrix metalloproteinase-9 and-12 expression in a modified mouse model of aneurysm formation. Journal of vascular surgery. 2007;45(6):1217-27. e2.

140. Blose KJ, Ennis TL, Arif B, Weinbaum JS, Curci JA, Vorp DA. Periadventitial adipose-derived stem cell treatment halts elastase-induced abdominal aortic aneurysm progression. Regenerative Medicine. 2014;In revision.

141. Jin J, Arif B, Garcia-Fernandez F, Ennis TL, Davis EC, Thompson RW, et al. Novel mechanism of aortic aneurysm development in mice associated with smoking and leukocytes. Arterioscler Thromb Vasc Biol. 2012;32(12):2901-9. Epub 2012/10/09. doi: 10.1161/ATVBAHA.112.300208. PubMed PMID: 23042818; PubMed Central PMCID: PMC3506015.

142. Fujiwara Y, Shiraya S, Miyake T, Yamakawa S, Aoki M, Makino H, et al. Inhibition of experimental abdominal aortic aneurysm in a rat model by the angiotensin receptor blocker valsartan. International journal of molecular medicine. 2008;22(6):703.

143. Nakashima H, Aoki M, Miyake T, Kawasaki T, Iwai M, Jo N, et al. Inhibition of experimental abdominal aortic aneurysm in the rat by use of decoy oligodeoxynucleotides suppressing activity of nuclear factor κB and ets transcription factors. Circulation. 2004;109(1):132-8.

144. Shiraya S, Miyake T, Aoki M, Yoshikazu F, Ohgi S, Nishimura M, et al. Inhibition of development of experimental aortic abdominal aneurysm in rat model by atorvastatin through inhibition of macrophage migration. Atherosclerosis. 2009;202(1):34-40.

145. Gertz SD, Kurgan A, Eisenberg D. Aneurysm of the rabbit common carotid artery induced by periarterial application of calcium chloride in vivo. Journal of Clinical Investigation. 1988;81(3):649.

146. Miyake T, Aoki M, Masaki H, Kawasaki T, Oishi M, Kataoka K, et al. Regression of abdominal aortic aneurysms by simultaneous inhibition of nuclear factor κB and ets in a rabbit model. Circulation research. 2007;101(11):1175-84.

147. Miyake T, Aoki M, Nakashima H, Kawasaki T, Oishi M, Kataoka K, et al. Prevention of abdominal aortic aneurysms by simultaneous inhibition of NFκB and ets using chimeric decoy oligonucleotides in a rabbit model. Gene therapy. 2006;13(8):695-704.

148. Chiou AC, Chiu B, Pearce WH. Murine aortic aneurysm produced by periarterial application of calcium chloride. Journal of Surgical Research. 2001;99(2):371-6.

149. Rush C, Nyara M, Moxon JV, Trollope A, Cullen B, Golledge J. Whole genome expression analysis within the angiotensin II-apolipoprotein E deficient mouse model of abdominal aortic aneurysm. BMC genomics. 2009;10(1):1.

150. Moláček J, Třeška V, Kobr J, Čertík B, Skalický T, Kuntscher V, et al. Optimization of the model of abdominal aortic aneurysm–experiment in an animal model. Journal of vascular research. 2008;46(1):1-5.

151. Allaire E, Forouoh R, Wang T, Clowes M, Clowes AW. Tissue metalloproteinase inhibitor-1 (TIMP-1) overexpression prevents arterial rupture and dilation in a xenograft model. FASEB Journal. 1996;10(6).

152. Allaire E, Guettier C, Bruneval P, Plissonnier D, Michel J-B. Cell-free arterial grafts: morphologic characteristics of aortic isografts, allografts, and xenografts in rats. Journal of vascular surgery. 1994;19(3):446-56.

153. Piedrahita JA, Zhang SH, Hagaman JR, Oliver PM, Maeda N. Generation of mice carrying a mutant apolipoprotein E gene inactivated by gene targeting in embryonic stem cells. Proceedings of the National Academy of Sciences. 1992;89(10):4471-5.

154. Trollope A, Moxon JV, Moran CS, Golledge J. Animal models of abdominal aortic aneurysm and their role in furthering management of human disease. Cardiovascular Pathology. 2011;20(2):114-23.

155. Economou SG, Taylor CB, Beattie Jr E, Davis Jr C. Persistent experimental aortic aneurysms in dogs. Surgery. 1960;47:21-8.

156. Nabseth D, Martin D, Rowe M, Gotlieb L, Deterling Jr R. Enzymatic destruction of aortic elastic tissue and possible relationship to experimental atherosclerosis. The Journal of cardiovascular surgery. 1963;4:11-7.

157. Lee JK, Borhani M, Ennis TL, Upchurch GR, Thompson RW. Experimental abdominal aortic aneurysms in mice lacking expression of inducible nitric oxide synthase. Arteriosclerosis, thrombosis, and vascular biology. 2001;21(9):1393-401.

158. Haskett D, Azhar M, Utzinger U, Geest JV. Progressive alterations in microstructural organization and biomechanical response in the ApoE mouse model of aneurysm. Biomatter. 2013;3(2):e24648.

159. Kuhl E, Holzapfel GA. A continuum model for remodeling in living structures. Journal of Materials Science. 2007;42(21):8811-23.

160. Rachev A, Stergiopulos N, Meister J-J. A model for geometric and mechanical adaptation of arteries to sustained hypertension. Journal of biomechanical engineering. 1998;120(1):9-17.

161. Rodriguez EK, Hoger A, McCulloch AD. Stress-dependent finite growth in soft elastic tissues. Journal of biomechanics. 1994;27(4):455-67.

162. Skalak R, editor. Growth as a finite displacement field. Proceedings of the IUTAM Symposium on Finite Elasticity; 1981: Springer.

163. Taber L. A model for aortic growth based on fluid shear and fiber stresses. Journal of biomechanical engineering. 1998;120(3):348-54.

164. Humphrey J, Rajagopal K. A constrained mixture model for growth and remodeling of soft tissues. Mathematical models and methods in applied sciences. 2002;12(03):407-30.

165. Alford PW, Humphrey JD, Taber LA. Growth and remodeling in a thick-walled artery model: effects of spatial variations in wall constituents. Biomech Model Mechanobiol. 2008;7(4):245-62.

166. Bellini C, Ferruzzi J, Roccabianca S, Di Martino E, Humphrey J. A microstructurally motivated model of arterial wall mechanics with mechanobiological implications. Annals of biomedical engineering. 2014;42(3):488-502.

167. Collins M, Eberth J, Wilson E, Humphrey J. Acute mechanical effects of elastase on the infrarenal mouse aorta: implications for models of aneurysms. Journal of biomechanics. 2012;45(4):660-5.

168. Ferruzzi J, Vorp D, Humphrey J. On constitutive descriptors of the biaxial mechanical behaviour of human abdominal aorta and aneurysms. Journal of the Royal Society Interface. 2010:rsif20100299.

169. Gleason R, Humphrey J. A mixture model of arterial growth and remodeling in hypertension: altered muscle tone and tissue turnover. Journal of vascular research. 2004;41(4):352-63.

170. Gleason R, Humphrey J. Effects of a sustained extension on arterial growth and remodeling: a theoretical study. Journal of biomechanics. 2005;38(6):1255-61.

171. Gleason RL, Humphrey JD. A 2D constrained mixture model for arterial adaptations to large changes in flow, pressure and axial stretch. Mathematical Medicine and Biology. 2005;22(4):347-69.

172. Hayenga HN, Thorne BC, Peirce SM, Humphrey JD. Ensuring congruency in multiscale modeling: towards linking agent based and continuum biomechanical models of arterial adaptation. Annals of biomedical engineering. 2011;39(11):2669-82.

173. Humphrey J, Eberth J, Dye W, Gleason R. Fundamental role of axial stress in compensatory adaptations by arteries. Journal of biomechanics. 2009;42(1):1-8.

174. Humphrey J, Rajagopal K. A constrained mixture model for arterial adaptations to a sustained step change in blood flow. Biomech Model Mechanobiol. 2003;2(2):109-26.

175. Karšaj I, Humphrey JD. A multilayered wall model of arterial growth and remodeling. Mechanics of materials. 2012;44:110-9.

176. Karšaj I, Sorić J, Humphrey JD. A 3-D framework for arterial growth and remodeling in response to altered hemodynamics. International journal of engineering science. 2010;48(11):1357-72.

177. Miller KS, Lee Y-U, Naito Y, Breuer CK, Humphrey JD. Computational model of the in vivo development of a tissue engineered vein from an implanted polymeric construct. Journal of biomechanics. 2014;47(9):2080-7.

178. Sankaran S, Humphrey JD, Marsden AL. An efficient framework for optimization and parameter sensitivity analysis in arterial growth and remodeling computations. Computer methods in applied mechanics and engineering. 2013;256:200-10.

179. Thorne BC, Hayenga HN, Humphrey JD, Peirce SM. Toward a multi-scale computational model of arterial adaptation in hypertension: verification of a multi-cell agent based model. Frontiers in physiology. 2011;2:20.

180. Udelsman BV, Khosravi R, Miller KS, Dean EW, Bersi MR, Rocco K, et al. Characterization of evolving biomechanical properties of tissue engineered vascular grafts in the arterial circulation. Journal of Biomechanics. 2014;47(9):2070-9.

181. Valentín A, Humphrey JD. Modeling effects of axial extension on arterial growth and remodeling. Medical & biological engineering & computing. 2009;47(9):979-87.

182. Watton PN, Ventikos Y, Holzapfel GA. Modelling cerebral aneurysm evolution. Biomechanics and Mechanobiology of Aneurysms: Springer; 2011. p. 373-99.

183. Valentín A, Holzapfel GA. Constrained mixture models as tools for testing competing hypotheses in arterial biomechanics: A brief survey. Mechanics research communications. 2012;42:126-33.

184. Baxter BT, Pearce WH, Waltke EA, Littooy FN, Hallett JW, Kent KC, et al. Prolonged administration of doxycycline in patients with small asymptomatic abdominal aortic aneurysms: report of a prospective (Phase II) multicenter study. Journal of vascular surgery. 2002;36(1):1-12.

185. Isenburg JC, Simionescu DT, Starcher BC, Vyavahare NR. Elastin stabilization for treatment of abdominal aortic aneurysms. Circulation. 2007;115(13):1729-37.

186. Zhang C. MicroRNomics: a newly emerging approach for disease biology. Physiological genomics. 2008;33(2):139-47.

187. Maegdefessel L, Azuma J, Toh R, Deng A, Merk DR, Raiesdana A, et al. MicroRNA-21 blocks abdominal aortic aneurysm development and nicotine-augmented expansion. Science translational medicine. 2012;4(122):122ra22-ra22.

188. Leeper NJ, Raiesdana A, Kojima Y, Chun HJ, Azuma J, Maegdefessel L, et al. MicroRNA-26a is a novel regulator of vascular smooth muscle cell function. Journal of cellular physiology. 2011;226(4):1035-43.

189. Boon RA, Seeger T, Heydt S, Fischer A, Hergenreider E, Horrevoets AJ, et al. MicroRNA-29 in aortic dilation: implications for aneurysm formation. Circulation research. 2011;109(10):1115-9.

190. Maegdefessel L, Azuma J, Toh R, Merk DR, Deng A, Chin JT, et al. Inhibition of microRNA-29b reduces murine abdominal aortic aneurysm development. The Journal of clinical investigation. 2012;122(2):497-506.

191. Kim CW, Kumar S, Son DJ, Jang I-H, Griendling KK, Jo H. Prevention of abdominal aortic aneurysm by Anti–MicroRNA-712 or Anti–MicroRNA-205 in angiotensin II–infused mice. Arteriosclerosis, thrombosis, and vascular biology. 2014;34(7):1412-21.

192. Jones JA, Stroud RE, O'Quinn EC, Black LE, Barth JL, Elefteriades JA, et al. Selective MicroRNA suppression in human thoracic aneurysms relationship of miR-29a to aortic size and proteolytic induction. Circulation: Cardiovascular Genetics. 2011;4(6):605-13.

193. Kinnaird T, Stabile E, Burnett M, Lee C, Barr S, Fuchs S, et al. Marrow-derived stromal cells express genes encoding a broad spectrum of arteriogenic cytokines and promote in vitro and in vivo arteriogenesis through paracrine mechanisms. Circulation research. 2004;94(5):678-85.

194. Rehman J, Traktuev D, Li J, Merfeld-Clauss S, Temm-Grove CJ, Bovenkerk JE, et al. Secretion of angiogenic and antiapoptotic factors by human adipose stromal cells. Circulation. 2004;109(10):1292-8.

195. Sharma AK, Lu G, Jester A, Johnston WF, Zhao Y, Hajzus VA, et al. Experimental abdominal aortic aneurysm formation is mediated by IL-17 and attenuated by mesenchymal stem cell treatment. Circulation. 2012;126(11 Suppl 1):S38-45. Epub 2012/09/22. doi: 10.1161/CIRCULATIONAHA.111.083451. PubMed PMID: 22965992; PubMed Central PMCID: PMC3448933.

196. Fu X-m, Yamawaki-Ogata A, Oshima H, Ueda Y, Usui A, Narita Y. Intravenous administration of mesenchymal stem cells prevents angiotensin II-induced aortic aneurysm formation in apolipoprotein E-deficient mouse. Journal of translational medicine. 2013;11(1):1.

197. Hashizume R, Yamawaki-Ogata A, Ueda Y, Wagner WR, Narita Y. Mesenchymal stem cells attenuate angiotensin II-induced aortic aneurysm growth in apolipoprotein E-deficient mice. Journal of vascular surgery. 2011;54(6):1743-52.

198. Adolph R, Vorp DA, Steed DL, Webster MW, Kameneva MV, Watkins SC. Cellular content and permeability of intraluminal thrombus in abdominal aortic aneurysm. Journal of Vascular Surgery. 1997;25(5):916-26.

199. Cheheltani R, McGoverin CM, Rao J, Vorp DA, Kiani MF, Pleshko N. Fourier transform infrared spectroscopy to quantify collagen and elastin in an in vitro model of extracellular matrix degradation in aorta. Analyst. 2014;139(12):3039-47.

200. Cheheltani R, Rao J, Vorp DA, Pleshko N, Kiani MF. Prediction of Elastin Degradation in Aorta Using a Novel Infrared Spectroscopic Methodology. Circulation. 2013;128(22 Supplement):A18128.

201. Phillippi JA, Green BR, Eskay MA, Kotlarczyk MP, Hill MR, Robertson AM, et al. Mechanism of aortic medial matrix remodeling is distinct in patients with bicuspid aortic valve. The Journal of thoracic and cardiovascular surgery. 2014;147(3):1056-64.

202. Rao J, Brown BN, Weinbaum JS, Ofstun EL, Makaroun MS, Humphrey JD, et al. Distinct macrophage phenotype and collagen organization within the intraluminal thrombus of abdominal aortic aneurysm. Journal of vascular surgery. 2015;62(3):585-93.

203. Speelman L, Bohra A, Bosboom EMH, Schurink GWH, van de Vosse FN, Makaroun MS, et al. Effects of wall calcifications in patient-specific wall stress analyses of abdominal aortic aneurysms. Journal of biomechanical engineering. 2007;129(1):105-9.

204. Vorp DA, Federspiel WJ, Webster MW. Does laminated intraluminal thrombus within abdominal aortic aneurysm cause anoxia of the aortic wall? Journal of vascular surgery. 1996;23(3):540-1.

205. Vorp DA, Lee PC, Wang DH, Makaroun MS, Nemoto EM, Ogawa S, et al. Association of intraluminal thrombus in abdominal aortic aneurysm with local hypoxia and wall weakening. J Vasc Surg. 2001;34(2):291-9.

206. Vorp DA, Xavier AE, Chew DW, Cleary DA, Morgan MA, Shah SR, et al. Differential Gene and Protein Expression is Associated with Hypoxia in the Human Abdominal Aortic Aneurysm (AAA) Wall. The FASEB Journal. 2009;23(1 Supplement):635.6-.6.

207. Di Martino ES, Vorp DA. Effect of variation in intraluminal thrombus constitutive properties on abdominal aortic aneurysm wall stress. Annals of biomedical engineering. 2003;31(7):804-9.

208. Doyle BJ, Cloonan AJ, Walsh MT, Vorp DA, McGloughlin TM. Identification of rupture locations in patient-specific abdominal aortic aneurysms using experimental and computational techniques. Journal of biomechanics. 2010;43(7):1408-16.

209. Doyle BJ, Corbett TJ, Callanan A, Walsh MT, Vorp DA, McGloughlin TM. An experimental and numerical comparison of the rupture locations of an abdominal aortic aneurysm. Journal of Endovascular Therapy. 2009;16(3):322-35.

210. Doyle BJ, Corbett TJ, Cloonan AJ, O'Donnell MR, Walsh MT, Vorp DA, et al. Experimental modelling of aortic aneurysms: novel applications of silicone rubbers. Medical engineering & physics. 2009;31(8):1002-12.

211. Doyle BJ, Morris LG, Callanan A, Kelly P, Vorp DA, McGloughlin TM. 3D reconstruction and manufacture of real abdominal aortic aneurysms: from CT scan to silicone model. Journal of biomechanical engineering. 2008;130(3):034501.

212. Geest JPV, Sacks MS, Vorp DA. Age dependency of the biaxial biomechanical behavior of human abdominal aorta. Journal of biomechanical engineering. 2004;126(6):815-22.

213. Geest JPV, Sacks MS, Vorp DA. The effects of aneurysm on the biaxial mechanical behavior of human abdominal aorta. Journal of biomechanics. 2006;39(7):1324-34.

214. Geest JPV, Sacks MS, Vorp DA. A planar biaxial constitutive relation for the luminal layer of intra-luminal thrombus in abdominal aortic aneurysms. Journal of biomechanics. 2006;39(13):2347-54.

215. Geest JPV, Wang DH, Wisniewski SR, Makaroun MS, Vorp DA. Towards a noninvasive method for determination of patient-specific wall strength distribution in abdominal aortic aneurysms. Annals of biomedical engineering. 2006;34(7):1098-106.

216. Martufi G, Satriano A, Moore RD, Vorp DA, Di Martino ES. Local quantification of wall thickness and intraluminal thrombus offer insight into the mechanical properties of the aneurysmal aorta. Annals of biomedical engineering. 2015;43(8):1759-71.

217. Pal S, Tsamis A, Pasta S, D'Amore A, Gleason TG, Vorp DA, et al. A mechanistic model on the role of "radially-running" collagen fibers on dissection properties of human ascending thoracic aorta. Journal of biomechanics. 2014;47(5):981-8.

218. Pasta S, Cho J-S, Dur O, Pekkan K, Vorp DA. Computer modeling for the prediction of thoracic aortic stent graft collapse. Journal of vascular surgery. 2013;57(5):1353-61.

219. Pasta S, Phillipi JA, Gleason TG, Vorp DA. Mechanical Properties of Ascending Thoracic Aortic Aneurysm (ATAA): Association with Valve Morphology. Computer Models in Biomechanics: Springer; 2013. p. 149-60.

220. Pasta S, Phillippi JA, Gleason TG, Vorp DA. Effect of aneurysm on the mechanical dissection properties of the human ascending thoracic aorta. The Journal of thoracic and cardiovascular surgery. 2012;143(2):460-7.

221. Pichamuthu JE, Phillippi JA, Cleary DA, Chew DW, Hempel J, Vorp DA, et al. Differential tensile strength and collagen composition in ascending aortic aneurysms by aortic valve phenotype. The Annals of thoracic surgery. 2013;96(6):2147-54.

222. Raghavan M, Webster MW, Vorp DA. Ex vivo biomechanical behavior of abdominal aortic aneurysm: assessment using a new mathematical model. Annals of biomedical engineering. 1996;24(5):573-82.

223. Raghavan ML, Vorp DA. Biomechanical Modeling of Aneurysms. Image-Based Computational Modeling of the Human Circulatory and Pulmonary Systems: Springer; 2010. p. 313-41.

224. Sacks MS, Vorp DA, Raghavan M, Federle MP, Webster MW. In vivo three-dimensional surface geometry of abdominal aortic aneurysms. Annals of biomedical engineering. 1999;27(4):469-79.

225. Santelices L, Calano S, Erhart J, Prantil R, Haney J, Vorp D, et al. Experimental system for ex vivo measurement of murine aortic stiffness. Physiological Measurement. 2007;28(8):N39.

226. Santelices LC, Rutman SJ, Prantil-Baun R, Vorp DA, Ahearn JM. Relative contributions of age and atherosclerosis to vascular stiffness. Clinical and translational science. 2008;1(1):62-6. Epub 2008/05/01. doi: 10.1111/j.1752-8062.2008.00014.x. PubMed PMID: 20443820.

227. Smith DB, Sacks MS, Vorp DA, Thornton M. Surface geometric analysis of anatomic structures using biquintic finite element interpolation. Annals of biomedical engineering. 2000;28(6):598-611.

228. Soares JS, Pasta S, Vorp DA, Moore JE. Modeling in cardiovascular biomechanics. International Journal of Engineering Science. 2010;48(11):1563-75.

229. Steinman D, Vorp D, Ethier C. Computational modeling of arterial biomechanics: insights into pathogenesis and treatment of vascular disease. Journal of Vascular Surgery. 2003;37(5):1118-28.

230. Thunes JR, Pal S, Fortunato RN, Phillippi JA, Gleason TG, Vorp DA, et al. A structural finite element model for lamellar unit of aortic media indicates heterogeneous stress field after collagen recruitment. Journal of biomechanics. 2016;49(9):1562-9.

231. VANDE GEEST JP, Dillavou ED, Di Martino ES, Oberdier M, Bohra A, Makaroun MS, et al. Gender-Related Differences in the Tensile Strength of Abdominal Aortic Aneurysm. Annals of the New York Academy of Sciences. 2006;1085(1):400-2.

232. VANDE GEEST JP, Sacks MS, Vorp DA. Age dependency of the biaxial biomechanical behavior of human abdominal aorta. Journal of biomechanical engineering. 2004;126(6):815-22.

233. Volokh K, Vorp D. A model of growth and rupture of abdominal aortic aneurysm. Journal of biomechanics. 2008;41(5):1015-21.

234. Vorp DA. Finite element modelling and analyses of nonlinearly elastic, orthotropic, vascular tissue in distension. Annals of Biomedical Engineering. 1993;21(6):736-7.

235. Vorp DA. Biomechanics of abdominal aortic aneurysm. Journal of biomechanics. 2007;40(9):1887-902.

236. Vorp DA, Raghavan M, Borovetz HS, Greisler HP, Webster MW. Modeling the transmural stress distribution during healing of bioresorbable vascular prostheses. Annals of biomedical engineering. 1995;23(2):178-88.

237. Vorp DA, Schiro BJ, Ehrlich MP, Juvonen TS, Ergin MA, Griffith BP. Effect of aneurysm on the tensile strength and biomechanical behavior of the ascending thoracic aorta. The Annals of thoracic surgery. 2003;75(4):1210-4.

238. Vorp DA, Steinman DA, Ethier CR. Computational modeling of arterial biomechanics. Computing in Science & Engineering. 2001;3(5):51-64.

239. Wang DH, Makaroun M, Webster MW, Vorp DA. Mechanical properties and microstructure of intraluminal thrombus from abdominal aortic aneurysm. Journal of biomechanical engineering. 2001;123(6):536-9.

240. Zeinali-Davarani S, Raguin LG, Vorp DA, Baek S. Identification of in vivo material and geometric parameters of a human aorta: toward patient-specific modeling of abdominal aortic aneurysm. Biomech Model Mechanobiol. 2011;10(5):689-99.

241. Di Martino ES, Bohra A, Scotti C, Finol E, Vorp DA, editors. Wall stresses before and after endovascular repair of abdominal aortic aneurysms. ASME 2004 International Mechanical Engineering Congress and Exposition; 2004: American Society of Mechanical Engineers.

242. Geest JPV, Schmidt DE, Sacks MS, Vorp DA. The effects of anisotropy on the stress analyses of patient-specific abdominal aortic aneurysms. Annals of biomedical engineering. 2008;36(6):921-32.

243. Vorp D, Raghavan M, Webster M. Stress distribution in abdominal aortic aneurysm: influence of diameter and symmetry. J Vasc Surg. 1998;27:632-9.

244. El-Kurdi MS, Vipperman JS, Vorp DA. Design and subspace system identification of an ex vivo vascular perfusion system. Journal of biomechanical engineering. 2009;131(4):041012.

245. VanEpps JS, Vorp DA. Mechanopathobiology of atherogenesis: a review. Journal of Surgical Research. 2007;142(1):202-17.

246. Vorp DA, Severyn DA, Steed DL, Webster MW. A device for the application of cyclic twist and extension on perfused vascular segments. American Journal of Physiology-Heart and Circulatory Physiology. 1996;270(2):H787-H95.

247. Doyle BJ, Callanan A, Burke PE, Grace PA, Walsh MT, Vorp DA, et al. Vessel asymmetry as an additional diagnostic tool in the assessment of abdominal aortic aneurysms. Journal of Vascular Surgery. 2009;49(2):443-54.

248. Raghavan M, Vorp DA. Toward a biomechanical tool to evaluate rupture potential of abdominal aortic aneurysm: identification of a finite strain constitutive model and evaluation of its applicability. Journal of biomechanics. 2000;33(4):475-82.

249. Pasta S, Rinaudo A, Luca A, Pilato M, Scardulla C, Gleason TG, et al. Difference in hemodynamic and wall stress of ascending thoracic aortic aneurysms with bicuspid and tricuspid aortic valve. Journal of biomechanics. 2013;46(10):1729-38.

250. Koch RG, Tsamis A, D'Amore A, Wagner WR, Watkins SC, Gleason TG, et al. A custom image-based analysis tool for quantifying elastin and collagen micro-architecture in the wall of the human aorta from multi-photon microscopy. Journal of biomechanics. 2014;47(5):935-43.

251. Tsamis A, Krawiec JT, Vorp DA. Elastin and collagen fibre microstructure of the human aorta in ageing and disease: a review. Journal of the Royal Society Interface. 2013;10(83):20121004.

252. Tsamis A, Pal S, Phillippi JA, Gleason TG, Maiti S, Vorp DA. Effect of aneurysm on biomechanical properties of “radially-oriented” collagen fibers in human ascending thoracic aortic media. Journal of biomechanics. 2014;47(16):3820-4.

253. Tsamis A, Phillippi JA, Koch RG, Chan PG, Krawiec JT, D'Amore A, et al. Extracellular matrix fiber microarchitecture is region-specific in bicuspid aortic valve-associated ascending aortopathy. The Journal of thoracic and cardiovascular surgery. 2016;151(6):1718-28. e5.

254. Tsamis A, Phillippi JA, Koch RG, Pasta S, D'Amore A, Watkins SC, et al. Fiber micro-architecture in the longitudinal-radial and circumferential-radial planes of ascending thoracic aortic aneurysm media. Journal of biomechanics. 2013;46(16):2787-94.

255. Tsamis A, Phillippi JA, Pasta S, D'Amore A, Watkins SC, Wagner W, et al. Collagen fiber architecture in the longitudinal-radial plane of ascending aorta is distinctly different among bicuspid aortic valve and tricuspid aortic valve patients with ascending aortic aneurysm. Cardiovascular Pathology. 2013;22(3):e34-e5.

256. Blose KJ, Pichamuthu JE, Weinbaum JS, Vorp DA. Design and validation of a vacuum assisted anchorage for the uniaxial tensile testing of soft materials. Soft Materials. 2016;14(2):72-7.

257. Swartz DD, Russell JA, Andreadis ST. Engineering of fibrin-based functional and implantable small-diameter blood vessels. American Journal of Physiology-Heart and Circulatory Physiology. 2005;288(3):H1451-H60.

258. Syedain ZH, Meier LA, Bjork JW, Lee A, Tranquillo RT. Implantable arterial grafts from human fibroblasts and fibrin using a multi-graft pulsed flow-stretch bioreactor with noninvasive strength monitoring. Biomaterials. 2011;32(3):714-22.

259. Syedain ZH, Weinberg JS, Tranquillo RT. Cyclic distension of fibrin-based tissue constructs: evidence of adaptation during growth of engineered connective tissue. Proceedings of the National Academy of Sciences. 2008;105(18):6537-42.

260. Flanagan TC, Cornelissen C, Koch S, Tschoeke B, Sachweh JS, Schmitz-Rode T, et al. The in vitro development of autologous fibrin-based tissue-engineered heart valves through optimised dynamic conditioning. Biomaterials. 2007;28(23):3388-97.

261. Robinson PS, Johnson SL, Evans MC, Barocas VH, Tranquillo RT. Functional tissue-engineered valves from cell-remodeled fibrin with commissural alignment of cell-produced collagen. Tissue Engineering Part A. 2008;14(1):83-95.

262. Garvin J, Qi J, Maloney M, Banes AJ. Novel system for engineering bioartificial tendons and application of mechanical load. Tissue Engineering. 2003;9(5):967-79.

263. Nieponice A, Maul TM, Cumer JM, Soletti L, Vorp DA. Mechanical stimulation induces morphological and phenotypic changes in bone marrow-derived progenitor cells within a three-dimensional fibrin matrix. Journal of Biomedical Materials Research Part A. 2007;81A(3):523-30. doi: 10.1002/jbm.a.31041.

264. Weinbaum JS, Schmidt JB, Tranquillo RT. Combating Adaptation to Cyclic Stretching by Prolonging Activation of Extracellular Signal-Regulated Kinase. Cellular and Molecular Bioengineering. 2013:1-8.

265. Sander E, Barocas V, Tranquillo R. Initial fiber alignment pattern alters extracellular matrix synthesis in fibroblast-populated fibrin gel cruciforms and correlates with predicted tension. Annals of biomedical engineering. 2011;39(2):714-29.

266. Lake SP, Barocas VH. Mechanical and structural contribution of non-fibrillar matrix in uniaxial tension: a collagen-agarose co-gel model. Annals of biomedical engineering. 2011;39(7):1891-903.

267. Cummings CL, Gawlitta D, Nerem RM, Stegemann JP. Properties of engineered vascular constructs made from collagen, fibrin, and collagen–fibrin mixtures. Biomaterials. 2004;25(17):3699-706.

268. Rowe SL, Lee S, Stegemann JP. Influence of thrombin concentration on the mechanical and morphological properties of cell-seeded fibrin hydrogels. Acta Biomaterialia. 2007;3(1):59-67.

269. Rowe SL, Stegemann JP. Interpenetrating collagen-fibrin composite matrices with varying protein contents and ratios. Biomacromolecules. 2006;7(11):2942-8.

270. Davis JR. Tensile testing: ASM international; 2004.

271. Kwok R, Evans E. Thermoelasticity of large lecithin bilayer vesicles. Biophysical Journal. 1981;35(3):637-52.

272. Rivlin RS, Saunders D. Large elastic deformations of isotropic materials. VII. Experiments on the deformation of rubber. Philosophical Transactions of the Royal Society of London Series A, Mathematical and Physical Sciences. 1951;243(865):251-88.

273. Christensen RM. Observations on the definition of yield stress. Acta Mechanica. 2008;196(3-4):239-44.

274. Kirchmajer DM, Watson CA, Ranson M. Gelapin, a degradable genipin cross-linked gelatin hydrogel. RSC Advances. 2013;3(4):1073-81.

275. Bryant SJ, Anseth KS. Hydrogel properties influence ECM production by chondrocytes photoencapsulated in poly (ethylene glycol) hydrogels. Journal of Biomedical Materials Research. 2002;59(1):63-72.

276. Cloyd JM, Malhotra NR, Weng L, Chen W, Mauck RL, Elliott DM. Material properties in unconfined compression of human nucleus pulposus, injectable hyaluronic acid-based hydrogels and tissue engineering scaffolds. European Spine Journal. 2007;16(11):1892-8.

277. Mauck RL, Soltz MA, Wang CC, Wong DD, Chao P-HG, Valhmu WB, et al. Functional tissue engineering of articular cartilage through dynamic loading of chondrocyte-seeded agarose gels. Journal of biomechanical engineering. 2000;122(3):252-60.

278. Smeds KA, Grinstaff MW. Photocrosslinkable polysaccharides for in situ hydrogel formation. Journal of biomedical materials research. 2001;54(1):115-21.

279. Solon J, Levental I, Sengupta K, Georges PC, Janmey PA. Fibroblast Adaptation and Stiffness Matching to Soft Elastic Substrates. Biophysical Journal. 2007;93(12):4453-61. doi: http://dx.doi.org/10.1529/biophysj.106.101386.

280. Ryan EA, Mockros LF, Weisel JW, Lorand L. Structural origins of fibrin clot rheology. Biophysical Journal. 1999;77(5):2813-26.

281. Wagenseil JE, Mecham RP. New insights into elastic fiber assembly. Birth Defects Research Part C: Embryo Today: Reviews. 2007;81(4):229-40.

282. Arribas SM, Hinek A, González MC. Elastic fibres and vascular structure in hypertension. Pharmacology & therapeutics. 2006;111(3):771-91.

283. Hinek A, Mecham RP, Keeley F, Rabinovitch M. Impaired elastin fiber assembly related to reduced 67-kD elastin-binding protein in fetal lamb ductus arteriosus and in cultured aortic smooth muscle cells treated with chondroitin sulfate. Journal of Clinical Investigation. 1991;88(6):2083.

284. Kielty CM, Stephan S, Sherratt MJ, Williamson M, Shuttleworth CA. Applying elastic fibre biology in vascular tissue engineering. Philosophical Transactions of the Royal Society of London B: Biological Sciences. 2007;362(1484):1293-312.

285. Baldwin AK, Simpson A, Steer R, Cain SA, Kielty CM. Elastic fibres in health and disease. Expert reviews in molecular medicine. 2013;15:e8.

286. Vrhovski B, Weiss AS. Biochemistry of tropoelastin. European Journal of Biochemistry. 1998;258(1):1-18.

287. Kagan HM, Li W. Lysyl oxidase: properties, specificity, and biological roles inside and outside of the cell. Journal of cellular biochemistry. 2003;88(4):660-72.

288. Kothapalli CR, Ramamurthi A. Copper nanoparticle cues for biomimetic cellular assembly of crosslinked elastin fibers. Acta biomaterialia. 2009;5(2):541-53.

289. Sherratt MJ. Tissue elasticity and the ageing elastic fibre. Age. 2009;31(4):305-25.

290. Armentano RL, Levenson J, Barra JG, Fischer E, Breitbart GJ, Pichel RH, et al. Assessment of elastin and collagen contribution to aortic elasticity in conscious dogs. American Journal of Physiology-Heart and Circulatory Physiology. 1991;260(6):H1870-H7.

291. Davidson JM, LuValle PA, Zoia O, Quaglino D, Giro M. Ascorbate differentially regulates elastin and collagen biosynthesis in vascular smooth muscle cells and skin fibroblasts by pretranslational mechanisms. Journal of Biological chemistry. 1997;272(1):345-52.

292. Brettell LM, McGowan SE. Basic fibroblast growth factor decreases elastin production by neonatal rat lung fibroblasts. American journal of respiratory cell and molecular biology. 1994;10(3):306-15.

293. Mecham R, Levy B, Morris S, Madaras J, Wrenn D. Increased cyclic GMP levels lead to a stimulation of elastin production in ligament fibroblasts that is reversed by cyclic AMP. Journal of Biological Chemistry. 1985;260(6):3255-8.

294. Davis EC, Mecham RP. Intracellular trafficking of tropoelastin. Matrix biology. 1998;17(4):245-54.

295. Mecham RP, Lange G, Madaras J, Starcher B. Elastin synthesis by ligamentum nuchae fibroblasts: effects of culture conditions and extracellular matrix on elastin production. The Journal of cell biology. 1981;90(2):332-8.

296. Rich C, Goud H, Bashir M, Rosenbloom J, Foster J. Developmental regulation of aortic elastin gene expression involves disruption of an IGF-I sensitive repressor complex. Biochemical and biophysical research communications. 1993;196(3):1316-22.

297. Wolfe BL, Rich CB, Goud HD, Terpstra A, Bashir M, Rosenbloom J, et al. Insulin-like growth factor-I regulates transcription of the elastin gene. Journal of Biological Chemistry. 1993;268(17):12418-26.

298. Sales VL, Engelmayr GC, Mettler BA, Johnson JA, Sacks MS, Mayer JE. Transforming growth factor-β1 modulates extracellular matrix production, proliferation, and apoptosis of endothelial progenitor cells in tissue-engineering scaffolds. Circulation. 2006;114(1 suppl):I-193-I-9.

299. Long JL, Tranquillo RT. Elastic fiber production in cardiovascular tissue-equivalents. Matrix biology : journal of the International Society for Matrix Biology. 2003;22(4):339-50. Epub 2003/08/26. PubMed PMID: 12935818.

300. Starcher B. A ninhydrin-based assay to quantitate the total protein content of tissue samples. Analytical biochemistry. 2001;292(1):125-9. Epub 2001/04/26. doi: 10.1006/abio.2001.5050. PubMed PMID: 11319826.

301. Ailawadi G, Eliason JL, Upchurch GR. Current concepts in the pathogenesis of abdominal aortic aneurysm. Journal of vascular surgery. 2003;38(3):584-8.

302. Brophy CM, Reilly JM, Smith GW, Tilson MD. The role of inflammation in nonspecific abdominal aortic aneurysm disease. Annals of vascular surgery. 1991;5(3):229-33.

303. Hance KA, Tataria M, Ziporin SJ, Lee JK, Thompson RW. Monocyte chemotactic activity in human abdominal aortic aneurysms: Role of elastin degradation peptides and the 67–kD cell surface elastin receptor. Journal of vascular surgery. 2002;35(2):254-61.

304. Dale MA, Xiong W, Carson JS, Suh MK, Karpisek AD, Meisinger TM, et al. Elastin-Derived Peptides Promote Abdominal Aortic Aneurysm Formation by Modulating M1/M2 Macrophage Polarization. The Journal of Immunology. 2016;196(11):4536-43.

305. Krettek A, Sukhova GK, Libby P. Elastogenesis in Human Arterial Disease A Role for Macrophages in Disordered Elastin Synthesis. Arteriosclerosis, thrombosis, and vascular biology. 2003;23(4):582-7.

306. Thie M, Schlumberger W, Semich R, Rauterberg J, Robenek H. Aortic smooth muscle cells in collagen lattice culture: effects on ultrastructure, proliferation and collagen synthesis. European journal of cell biology. 1991;55(2):295-304.

307. Johnson D, Robson P, Hew Y, Keeley F. Decreased elastin synthesis in normal development and in long-term aortic organ and cell cultures is related to rapid and selective destabilization of mRNA for elastin. Circulation research. 1995;77(6):1107-13.

308. Gacchina C, Brothers T, Ramamurthi A. Evaluating smooth muscle cells from CaCl2-induced rat aortal expansions as a surrogate culture model for study of elastogenic induction of human aneurysmal cells. Tissue Engineering Part A. 2011;17(15-16):1945-58.

309. Gacchina CE, Deb P, Barth JL, Ramamurthi A. Elastogenic inductability of smooth muscle cells from a rat model of late stage abdominal aortic aneurysms. Tissue Engineering Part A. 2011;17(13-14):1699-711.

310. Patel A, Fine B, Sandig M, Mequanint K. Elastin biosynthesis: the missing link in tissue-engineered blood vessels. Cardiovascular research. 2006;71(1):40-9.

311. Minion D, Davis V, Wang Y, McManus B, Baxter B. Elastin is increased in abdominal aortic aneurysms. Journal of Surgical Research. 1994;57(4):443-6.

312. Davidson JM, Zoia O, Liu J-M. Modulation of transforming growth factor-beta 1 stimulated elastin and collagen production and proliferation in porcine vascular smooth muscle cells and skin fibroblasts by basic fibroblast growth factor, transforming growth factor-α, and insulin-like growth factor-I. Journal of Cellular Physiology. 1993;155(1):149-56.

313. Lin S, Sandig M, Mequanint K. Three-dimensional topography of synthetic scaffolds induces elastin synthesis by human coronary artery smooth muscle cells. Tissue Engineering Part A. 2011;17(11-12):1561-71.

314. Liu J-m, Davidson JM. The elastogenic effect of recombinant transforming growth factor-beta on porcine aortic smooth muscle cells. Biochemical and biophysical research communications. 1988;154(3):895-901.

315. Swaminathan G, Gadepalli VS, Stoilov I, Mecham RP, Rao RR, Ramamurthi A. Pro-elastogenic effects of bone marrow mesenchymal stem cell-derived smooth muscle cells on cultured aneurysmal smooth muscle cells. Journal of tissue engineering and regenerative medicine. 2014.

316. Shanley CJ, Gharaee-Kermani M, Sarkar R, Welling TH, Kriegel A, Ford JW, et al. Transforming growth factor-β 1 increases lysyl oxidase enzyme activity and mRNA in rat aortic smooth muscle cells. Journal of vascular surgery. 1997;25(3):446-52.

317. Dai J, Losy F, Guinault A-M, Pages C, Anegon I, Desgranges P, et al. Overexpression of transforming growth factor-β1 stabilizes already-formed aortic aneurysms a first approach to induction of functional healing by endovascular gene therapy. Circulation. 2005;112(7):1008-15.

318. Losy F, Dai J, Pages C, Ginat M, Muscatelli-Groux B, Guinault A-M, et al. Paracrine secretion of transforming growth factor-β 1 in aneurysm healing and stabilization with endovascular smooth muscle cell therapy. Journal of vascular surgery. 2003;37(6):1301-9.

319. Kothapalli CR, Ramamurthi A. Benefits of concurrent delivery of hyaluronan and IGF-1 cues to regeneration of crosslinked elastin matrices by adult rat vascular cells. Journal of tissue engineering and regenerative medicine. 2008;2(2-3):106-16.

320. Kothapalli CR, Taylor PM, Smolenski RT, Yacoub MH, Ramamurthi A. Transforming growth factor beta 1 and hyaluronan oligomers synergistically enhance elastin matrix regeneration by vascular smooth muscle cells. Tissue Engineering Part A. 2009;15(3):501-11.

321. Kothapalli CR, Ramamurthi A. Lysyl oxidase enhances elastin synthesis and matrix formation by vascular smooth muscle cells. Journal of tissue engineering and regenerative medicine. 2009;3(8):655-61.

322. Cantinieaux D, Quertainmont R, Blacher S, Rossi L, Wanet T, Noël A, et al. Conditioned medium from bone marrow-derived mesenchymal stem cells improves recovery after spinal cord injury in rats: an original strategy to avoid cell transplantation. PLoS One. 2013;8(8):e69515.

323. Song M, Heo J, Chun J-Y, Bae HS, Kang JW, Kang H, et al. The paracrine effects of mesenchymal stem cells stimulate the regeneration capacity of endogenous stem cells in the repair of a bladder-outlet-obstruction-induced overactive bladder. Stem cells and development. 2013;23(6):654-63.

324. Fitzpatrick E, Wu Y, Dhadda P, Hughes RD, Mitry RR, Qin H, et al. Coculture with mesenchymal stem cells results in improved viability and function of human hepatocytes. Cell transplantation. 2015;24(1):73-83.

325. Rubach M, Adelmann R, Haustein M, Drey F, Pfannkuche K, Xiao B, et al. Mesenchymal Stem Cells and Their Conditioned Medium Improve Integration of Purified Induced Pluripotent Stem Cell–Derived Cardiomyocyte Clusters into Myocardial Tissue. Stem cells and development. 2013;23(6):643-53.

326. Krawiec JT, Weinbaum JS, Liao H-T, Ramaswamy AK, Pezzone DJ, Josowitz AD, et al. In Vivo Functional Evaluation of Tissue-Engineered Vascular Grafts Fabricated Using Human Adipose-Derived Stem Cells from High Cardiovascular Risk Populations. Tissue Engineering Part A. 2016;22(9-10):765-75.

327. Krawiec JT, Weinbaum JS, St. Croix CM, Phillippi JA, Watkins SC, Rubin JP, et al. A Cautionary Tale for Autologous Vascular Tissue Engineering: Impact of Human Demographics on the Ability of Adipose-Derived Mesenchymal Stem Cells to Recruit and Differentiate into Smooth Muscle Cells. Tissue Engineering Part A. 2014. doi: 10.1089/ten.tea.2014.0208.

328. Davis JP, Salmon M, Pope NH, Lu G, Su G, Sharma AK, et al. Attenuation of aortic aneurysms with stem cells from different genders. Journal of Surgical Research. 2015;199(1):249-58.

329. Gimble JM, Wu X. Non-Enzymatic Method for Isolating Human Adipose-Derived Stromal Stem Cells. Google Patents; 2012.

330. Mizuno H. Adipose-derived stem cells for tissue repair and regeneration: ten years of research and a literature review. Journal of Nippon Medical School. 2009;76(2):56-66.

331. Wei H-J, Chen C-H, Lee W-Y, Chiu I, Hwang S-M, Lin W-W, et al. Bioengineered cardiac patch constructed from multilayered mesenchymal stem cells for myocardial repair. Biomaterials. 2008;29(26):3547-56.

332. Schoen FJ. Heart valve tissue engineering: quo vadis? Current opinion in biotechnology. 2011;22(5):698-705.

333. Tedder ME, Simionescu A, Chen J, Liao J, Simionescu DT. Assembly and testing of stem cell-seeded layered collagen constructs for heart valve tissue engineering. Tissue Engineering Part A. 2010;17(1-2):25-36.

334. Steinert AF, Rackwitz L, Gilbert F, Nöth U, Tuan RS. Concise review: the clinical application of mesenchymal stem cells for musculoskeletal regeneration: current status and perspectives. Stem cells translational medicine. 2012;1(3):237-47.

335. Kokai LE, Marra K, Rubin JP. Adipose stem cells: biology and clinical applications for tissue repair and regeneration. Translational Research. 2014;163(4):399-408.

336. Du Y, Roh DS, Funderburgh ML, Mann MM, Marra KG, Rubin JP, et al. Adipose-derived stem cells differentiate to keratocytes in vitro. Molecular Vision. 2010;16:2680.

337. Dudas JR, Marra KG, Cooper GM, Penascino VM, Mooney MP, Jiang S, et al. The Osteogenic Potential of Adipose-Derived Stem Cells for the Repair of Rabbit Calvarial Defects. Annals of Plastic Surgery. 2006;56(5):543-8.

338. Gerlach JC, Lin Y-C, Brayfield CA, Minteer DM, Li H, Rubin JP, et al. Adipogenesis of human adipose-derived stem cells within three-dimensional hollow fiber-based bioreactors. Tissue Engineering Part C: Methods. 2011;18(1):54-61.

339. Santiago LYC-A, Julio; Brayfield, Candace; Rubin, J. Peter; Marra, Kacey G. Delivery of Adipose-Derived Precursor Cells for Peripheral Nerve Repair. Cell Transplantation. 2009;18:145-58.

340. Zimmerlin L, Donnenberg VS, Pfeifer ME, Meyer EM, Péault B, Rubin JP, et al. Stromal vascular progenitors in adult human adipose tissue. Cytometry Part A. 2010;77(1):22-30.

341. Aksu AE, Rubin JP, Dudas JR, Marra KG. Role of Gender and Anatomical Region on Induction of Osteogenic Differentiation of Human Adipose-Derived Stem Cells. Annals of Plastic Surgery. 2008;60(3):306-22. Epub 2008/04/30. doi: 10.1097/SAP.0b013e3180621ff0

00000637-200803000-00016 [pii]. PubMed PMID: 18443514.

342. Bellas E, Panilaitis BJ, Glettig DL, Kirker-Head CA, Yoo JJ, Marra KG, et al. Sustained volume retention in vivo with adipocyte and lipoaspirate seeded silk scaffolds. Biomaterials. 2013;34(12):2960-8.

343. Djian P, Roncari A, Hollenberg C. Influence of anatomic site and age on the replication and differentiation of rat adipocyte precursors in culture. Journal of Clinical Investigation. 1983;72(4):1200.

344. Djian P, Roncari D, Hollenberg C. Adipocyte precursor clones vary in capacity for differentiation. Metabolism: Clinical and Experimental. 1985;34(9):880-3.

345. Dudas JR, Losee JE, Penascino VM, Smith DM, Cooper GM, Mooney MP, et al. Leporine-Derived Adipose Precursor Cells Exhibit In Vitro Osteogenic Potential. Journal of Craniofacial Surgery. 2008;19(2):360-8.

346. Kirkland JL, Hollenberg CH, Gillon WS. Age, anatomic site, and the replication and differentiation of adipocyte precursors. American Journal of Physiology-Cell Physiology. 1990;258(2):C206-C10.

347. Schipper BM, Marra KG, Zhang W, Donnenberg AD, Rubin JP. Regional anatomic and age effects on cell function of human adipose-derived stem cells. Ann Plast Surg. 2008;60(5):538-44. Epub 2008/04/25. doi: 10.1097/SAP.0b013e3181723bbe

00000637-200805000-00014 [pii]. PubMed PMID: 18434829.

348. Sorisky A. From preadipocyte to adipocyte: differentiation-directed signals of insulin from the cell surface to the nucleus. Critical Reviews in Clinical Laboratory Sciences. 1999;36(1):1-34.

349. Tsuji W, Rubin JP, Marra KG. Adipose-derived stem cells: Implications in tissue regeneration. World journal of stem cells. 2014;6(3):312.

350. Zimmerlin L, Rubin JP, Pfeifer ME, Moore LR, Donnenberg VS, Donnenberg AD. Human adipose stromal vascular cell delivery in a fibrin spray. Cytotherapy. 2013;15(1):102-8.

351. Zuk PA, Zhu M, Mizuno H, Huang J, Futrell JW, Katz AJ, et al. Multilineage cells from human adipose tissue: implications for cell-based therapies. Tissue Engineering. 2001;7(2):211-28. PubMed PMID: ISI:000168274200010.

352. Kokai L, Rubin JP. Whitening Effects of Adipose-Derived Stem Cells: An In Vivo Study. Aesthetic Plastic Surgery. 2014;38(1):234.

353. Zhang P, Kling RE, Ravuri SK, Kokai LE, Rubin JP, Chai J-k, et al. A review of adipocyte lineage cells and dermal papilla cells in hair follicle regeneration. Journal of Tissue Engineering. 2014;5:2041731414556850.

354. Zimmerlin L, Donnenberg AD, Rubin JP, Basse P, Landreneau RJ, Donnenberg VS. Regenerative Therapy and Cancer: In Vitro and In Vivo Studies of the Interaction Between

Adipose-Derived Stem Cells and Breast Cancer Cells from Clinical Isolates. Tissue Engineering Part A. 2011;17(1-2):93-106. doi: DOI 10.1089/ten.tea.2010.0248. PubMed PMID: ISI:000285995800010.

355. Deyl Z, Macek K, Adam M. Studies on the chemical nature of elastin fluorescence. Biochimica et Biophysica Acta (BBA)-Protein Structure. 1980;625(2):248-54.

356. Sommer N, Sattler M, Weise JM, Wenck H, Gallinat S, Fischer F. A tissue-engineered human dermal construct utilizing fibroblasts and transforming growth factor β1 to promote elastogenesis. Biotechnology journal. 2013;8(3):317-26.

357. Mansfield J, Yu J, Attenburrow D, Moger J, Tirlapur U, Urban J, et al. The elastin network: its relationship with collagen and cells in articular cartilage as visualized by multiphoton microscopy. Journal of anatomy. 2009;215(6):682-91.

358. Boulesteix T, Pena AM, Godeau G, Sauviat MP, Beaurepaire E, Schanne-Klein MC. Micrometer scale ex vivo multiphoton imaging of unstained arterial wall structure. Cytometry Part A. 2006;69(1):20-6.

359. Zoumi A, Lu X, Kassab GS, Tromberg BJ. Imaging coronary artery microstructure using second-harmonic and two-photon fluorescence microscopy. Biophysical journal. 2004;87(4):2778-86.

360. König K, Schenke-Layland K, Riemann I, Stock U. Multiphoton autofluorescence imaging of intratissue elastic fibers. Biomaterials. 2005;26(5):495-500.

361. Schenke-Layland K, Riemann I, Opitz F, König K, Halbhuber K, Stock U. Comparative study of cellular and extracellular matrix composition of native and tissue engineered heart valves. Matrix biology. 2004;23(2):113-25.

362. Brockbank KG, MacLellan WR, Xie J, Hamm-Alvarez SF, Chen ZZ, Schenke-Layland K. Quantitative second harmonic generation imaging of cartilage damage. Cell and tissue banking. 2008;9(4):299-307.

363. Ross J, Tranquillo R. ECM gene expression correlates with in vitro tissue growth and development in fibrin gel remodeled by neonatal smooth muscle cells. Matrix biology. 2003;22(6):477-90.

364. Kozel BA, Rongish BJ, Czirok A, Zach J, Little CD, Davis EC, et al. Elastic fiber formation: a dynamic view of extracellular matrix assembly using timer reporters. Journal of cellular physiology. 2006;207(1):87-96.

365. Meshel AS, Wei Q, Adelstein RS, Sheetz MP. Basic mechanism of three-dimensional collagen fibre transport by fibroblasts. Nature Cell Biology. 2005;7(2):157-64.

366. Cardamone L, Valentin A, Eberth J, Humphrey J. Origin of axial prestretch and residual stress in arteries. Biomech Model Mechanobiol. 2009;8(6):431-46.

367. Langille BL. Arterial remodeling: relation to hemodynamics. Canadian journal of physiology and pharmacology. 1996;74(7):834-41.

368. Stenmark K, Mecham R. Cellular and molecular mechanisms of pulmonary vascular remodeling. Annual review of physiology. 1997;59(1):89-144.

369. Dobrin P, Canfield T, Sinha S. Development of longitudina retraction of carotid arteries in neonatal dogs. Experientia. 1975;31(11):1295-6.

370. Dobrin PB, Schwarcz TH, Mrkvicka R. Longitudinal retractive force in pressurized dog and human arteries. Journal of Surgical Research. 1990;48(2):116-20.

371. Murray CD. The physiological principle of minimum work I. The vascular system and the cost of blood volume. Proceedings of the National Academy of Sciences. 1926;12(3):207-14.

372. Rodbard S. Vascular caliber. Cardiology. 1975;60(1):4-49.

373. Zamir M. Shear forces and blood vessel radii in the cardiovascular system. The Journal of general physiology. 1977;69(4):449-61.

374. Price JM, Davis D, Knauss E. Length-dependent sensitivity in vascular smooth muscle. American Journal of Physiology-Heart and Circulatory Physiology. 1981;241(4):H557-H63.

375. Guyton AC. Human physiology and mechanisms of disease1987.

376. Bai TR, Bates JH, Brusasco V, Camoretti-Mercado B, Chitano P, Deng LH, et al. On the terminology for describing the length-force relationship and its changes in airway smooth muscle. Journal of Applied Physiology. 2004;97(6):2029-34.

377. Dajnowiec D, Langille BL. Arterial adaptations to chronic changes in haemodynamic function: coupling vasomotor tone to structural remodelling. Clinical Science. 2007;113(1):15-23.

378. Taylor L. A finite element analysis program (FEAP) v8. 2. Department of Civil and Environmental Engineering, University of California at Berkeley, Berkeley CA. 2008.

379. Holzapfel G. Nonlinear solid mechanics. A continuum approach for engineering. West Sussex, England: John Wiley & Sons, Ltd.

380. Holzapfel GA, Ogden RW. Biomechanics of soft tissue in cardiovascular systems: Springer; 2014.

381. Wriggers P. Nonlinear finite element methods: Springer Science & Business Media; 2008.

382. Anderson E, Bai Z, Bischof C, Blackford S, Dongarra J, Du Croz J, et al. LAPACK Users' guide: Siam; 1999.

383. Kazi M, Thyberg J, Religa P, Roy J, Eriksson P, Hedin U, et al. Influence of intraluminal thrombus on structural and cellular composition of abdominal aortic aneurysm wall. Journal of vascular surgery. 2003;38(6):1283-92.

384. Sakalihasan N, Heyeres A, Nusgens BV, Limet R, Lapiére CM. Modifications of the extracellular matrix of aneurysmal abdominal aortas as a function of their size. European journal of vascular surgery. 1993;7(6):633-7.

385. Klink A, Hyafil F, Rudd J, Faries P, Fuster V, Mallat Z, et al. Diagnostic and therapeutic strategies for small abdominal aortic aneurysms. Nature Reviews Cardiology. 2011;8(6):338-47.

386. Watton P, Hill N, Heil M. A mathematical model for the growth of the abdominal aortic aneurysm. Biomech Model Mechanobiol. 2004;3(2):98-113.

387. Schmid H, Grytsan A, Poshtan E, Watton PN, Itskov M. Influence of differing material properties in media and adventitia on arterial adaptation—application to aneurysm formation and rupture. Computer methods in biomechanics and biomedical engineering. 2013;16(1):33-53.

388. Schmid H, Watton P, Maurer M, Wimmer J, Winkler P, Wang Y, et al. Impact of transmural heterogeneities on arterial adaptation. Biomech Model Mechanobiol. 2010;9(3):295-315.

389. Baxter BT. Could medical intervention work for aortic aneurysms? American Journal of Surgery. 2004;188(6):628-32.

390. Mosorin M, Juvonen J, Biancari F, Satta J, Surcel HM, Leinonen M, et al. Use of doxycycline to decrease the growth rate of abdominal aortic aneurysms: a randomized, double-blind, placebo-controlled pilot study. J Vasc Surg. 2001;34(4):606-10. Epub 2001/10/23. doi: 10.1067/mva.2001.117891. PubMed PMID: 11668312.

391. Thompson R, Liao S, Curci J. Therapeutic potential of tetracycline derivatives to suppress the growth of abdominal aortic aneurysms. Advances in Dental Research. 1998;12(1):159-65.

392. Kozel BA, Ciliberto CH, Mecham RP. Deposition of tropoelastin into the extracellular matrix requires a competent elastic fiber scaffold but not live cells. Matrix biology. 2004;23(1):23-34.

393. Curci JA, Thompson RW. "Variable induction of experimental abdominal aortic aneurysms with different preparations of porcine pancreatic elastase". J Vasc Surg. 1999;29(2):385. Epub 1999/02/10. PubMed PMID: 9950998.

394. Cohen JR, Keegan L, Sarfati I, Danna D, Ilardi C, Wise L. Neutrophil chemotaxis and neutrophil elastase in the aortic wall in patients with abdominal aortic aneurysms. Journal of Investigative Surgery. 2009.

395. Lederle F, Johnson G, Wilson S, Chute E, Littooy F, Bandyk D, et al. Aneurysm Detection and Management (ADAM) Veterans Affairs Cooperative Study Group. Prevalence

and associations of abdominal aortic aneurysm detected through screening. Ann Intern Med. 1997;126(6):441-9.

396. Gronthos S, Franklin DM, Leddy HA, Robey PG, Storms RW, Gimble JM. Surface protein characterization of human adipose tissue-derived stromal cells. Journal of cellular physiology. 2001;189(1):54-63.

397. Hashemi SM, Hassan ZM, Pourfathollah AA, Soudi S, Shafiee A, Soleimani M. Comparative immunomodulatory properties of adipose-derived mesenchymal stem cells conditioned media from BALB/c, C57BL/6, and DBA mouse strains. Journal of cellular biochemistry. 2013;114(4):955-65.

398. Karp JM, Teo GSL. Mesenchymal stem cell homing: the devil is in the details. Cell stem cell. 2009;4(3):206-16.

399. Arbab AS, Wilson LB, Ashari P, Jordan EK, Lewis BK, Frank JA. A model of lysosomal metabolism of dextran coated superparamagnetic iron oxide (SPIO) nanoparticles: implications for cellular magnetic resonance imaging. NMR in Biomedicine. 2005;18(6):383-9.

400. Kim EH, Lee HS, Kwak BK, Kim B-K. Synthesis of ferrofluid with magnetic nanoparticles by sonochemical method for MRI contrast agent. Journal of Magnetism and Magnetic Materials. 2005;289:328-30.

401. Nasongkla N, Bey E, Ren J, Ai H, Khemtong C, Guthi JS, et al. Multifunctional polymeric micelles as cancer-targeted, MRI-ultrasensitive drug delivery systems. Nano letters. 2006;6(11):2427-30.

402. Cheng K, Shen D, Hensley MT, Middleton R, Sun B, Liu W, et al. Magnetic antibody-linked nanomatchmakers for therapeutic cell targeting. Nat Commun. 2014;5. doi: 10.1038/ncomms5880.

403. Yanai A, Häfeli UO, Metcalfe AL, Soema P, Addo L, Gregory-Evans CY, et al. Focused Magnetic Stem Cell Targeting to the Retina Using Superparamagnetic Iron Oxide Nanoparticles. Cell Transplantation. 2012;21(6):1137-48. doi: 10.3727/096368911x627435.

404. Wolf YG, Tillich M, Lee WA, Rubin GD, Fogarty TJ, Zarins CK. Impact of aortoiliac tortuosity on endovascular repair of abdominal aortic aneurysms: evaluation of 3D computer-based assessment. Journal of vascular surgery. 2001;34(4):594-9.

405. Chuter T. Bifurcated endovascular graft insertion for abdominal aortic aneurysm. from Greenhalgh, Vascular and Endovascular Surgical Techniques. 1994:92-9.

406. Laborde J, Parodi J, Clem M, Tio F, Barone H, Rivera F, et al. Intraluminal bypass of abdominal aortic aneurysm: feasibility study. Radiology. 1992;184(1):185-90.

407. Marin ML, Veith FJ, Panetta TF, Cynamon J, Sanchez LA, Schwartz ML, et al. Transluminally placed endovascular stented graft repair for arterial trauma. Journal of vascular surgery. 1994;20(3):466-73.

408. Parodi JC, Palmaz J, Barone H. Transfemoral intraluminal graft implantation for abdominal aortic aneurysms. Annals of vascular surgery. 1991;5(6):491-9.

409. Rockman C, editor. Reducing complications by better case selection: anatomic considerations. Seminars in vascular surgery; 2004: Elsevier.

410. Parodi JC. Endovascular repair of abdominal aortic aneurysms and other arterial lesions. Journal of Vascular Surgery. 1995;21(4):549-57.

411. Ahmann KA, Weinbaum JS, Johnson SL, Tranquillo RT. Fibrin degradation enhances vascular smooth muscle cell proliferation and matrix deposition in fibrin-based tissue constructs fabricated in vitro. Tissue engineering Part A. 2010;16(10):3261-70. Epub 2010/06/12. doi: 10.1089/ten.TEA.2009.0708. PubMed PMID: 20536358; PubMed Central PMCID: PMC2947425.

412. Black III LD, Meyers JD, Weinbaum JS, Shvelidze YA, Tranquillo RT. Cell-induced alignment augments twitch force in fibrin gel–based engineered myocardium via gap junction modification. Tissue Engineering Part A. 2009;15(10):3099-108.

413. Nieponice A, Maul TM, Cumer JM, Soletti L, Vorp DA. Mechanical stimulation induces morphological and phenotypic changes in bone marrow-derived progenitor cells within a three-dimensional fibrin matrix. Journal of biomedical materials research Part A. 2007;81(3):523-30. Epub 2006/11/30. doi: 10.1002/jbm.a.31041. PubMed PMID: 17133453.

414. Weinbaum JS, Qi J, Tranquillo RT. Monitoring collagen transcription by vascular smooth muscle cells in fibrin-based tissue constructs. Tissue engineering Part C, Methods. 2010;16(3):459-67. Epub 2009/07/29. doi: 10.1089/ten.TEC.2009.0112. PubMed PMID: 19635030; PubMed Central PMCID: PMC2945866.

415. (FDA) UFaDA. Early Development Considerations for Innovative Combination Products http://www.fda.gov/RegulatoryInformation/Guidances/ucm126050.htm2015 [May 2015]. Available from: http://www.fda.gov/RegulatoryInformation/Guidances/ucm126050.htm.

416. Amariglio N, Hirshberg A, Scheithauer BW, Cohen Y, Loewenthal R, Trakhtenbrot L, et al. Donor-derived brain tumor following neural stem cell transplantation in an ataxia telangiectasia patient. PLoS Med. 2009;6(2):e1000029.

417. Banas A, Teratani T, Yamamoto Y, Tokuhara M, Takeshita F, Osaki M, et al. IFATS collection: in vivo therapeutic potential of human adipose tissue mesenchymal stem cells after transplantation into mice with liver injury. Stem cells. 2008;26(10):2705-12.

418. Zhang YM, Hartzell C, Narlow M, Dudley SC. Stem cell-derived cardiomyocytes demonstrate arrhythmic potential. Circulation. 2002;106(10):1294-9.

419. Loebinger MR, Kyrtatos PG, Turmaine M, Price AN, Pankhurst Q, Lythgoe MF, et al. Magnetic Resonance Imaging of Mesenchymal Stem Cells Homing to Pulmonary Metastases Using Biocompatible Magnetic Nanoparticles. Cancer Research. 2009;69(23):8862-7. doi: 10.1158/0008-5472.can-09-1912.

420. Riegler J, Wells JA, Kyrtatos PG, Price AN, Pankhurst QA, Lythgoe MF. Targeted magnetic delivery and tracking of cells using a magnetic resonance imaging system. Biomaterials. 2010;31(20):5366-71. doi: http://dx.doi.org/10.1016/j.biomaterials.2010.03.032.

421. Wang J, Xiang B, Deng J, Lin H-Y, Zheng D, Freed DH, et al. Externally Applied Static Magnetic Field Enhances Cardiac Retention and Functional Benefit of Magnetically Iron-Labeled Adipose-Derived Stem Cells in Infarcted Hearts. Stem Cells Translational Medicine. 2016:sctm. 2015-0220.

422. Dubey N, Letourneau P, Tranquillo R. Guided neurite elongation and Schwann cell invasion into magnetically aligned collagen in simulated peripheral nerve regeneration. Experimental neurology. 1999;158(2):338-50.

423. Dubey N, Letourneau P, Tranquillo R. Neuronal contact guidance in magnetically aligned fibrin gels: effect of variation in gel mechano-structural properties. Biomaterials. 2001;22(10):1065-75.

424. Morin KT, Tranquillo RT. Guided sprouting from endothelial spheroids in fibrin gels aligned by magnetic fields and cell-induced gel compaction. Biomaterials. 2011;32(26):6111-8.

425. (FDA) UFaDA. Cellular & Gene Therapy Guidances http://www.fda.gov/BiologicsBloodVaccines/GuidanceComplianceRegulatoryInformation/Guidances/CellularandGeneTherapy/2015 [May 2015]. Available from: http://www.fda.gov/BiologicsBloodVaccines/GuidanceComplianceRegulatoryInformation/Guidances/CellularandGeneTherapy/.

426. Gu E, Chen W-Y, Gu J, Burridge P, Wu JC. Molecular imaging of stem cells: tracking survival, biodistribution, tumorigenicity, and immunogenicity. Theranostics. 2012;2(4):335-45.

427. Schipper BM, Marra KG, Zhang W, Donnenberg AD, Rubin JP. Regional anatomic and age effects on cell function of human adipose-derived stem cells. Annals of plastic surgery. 2008;60(5):538.